

**INVESTIGATION INTO GAS FLARING
REDUCTION IN THE OIL AND GAS
INDUSTRY**

MUSA BASHIR ABUHESA

Ph.D. Thesis

2010

SRG



Spray Research Group



**INVESTIGATION INTO GAS FLARING
REDUCTION IN THE OIL AND GAS
INDUSTRY**

Musa Bashir ABUHESA

BSc, MRes.

School of Computing, Sciences and Engineering
University of Salford, Manchester, UK

Submitted in Partial Fulfilment of the Requirements of the
Degree of Doctor of Philosophy, December 2010

DEDICTED TO MY MOTHER FOR HER SUPPORT, MY WIFE, MY
SONS; AMMAR, MOHAMED, BASHIR AND NASER AND MY
DAUGHTERS; SUHAILA, SUZAN AND SUNDESS

CONTENTS

CONTENTS	i
LIST OF TABLES	ix
LIST OF FIGURES	x
ACKNOWLEDGMENTS	xix
DECLARATION	xx
NOMENCLATURE	xxi
ABSTRACT	xxiii
CHAPTER-1: INTRODUCTION	2
1.1 Overview of the Topic	2
1.2 Aims.....	4
1.3 Objectives	4
1.4 Thesis Structure	5
CHAPTER-2: GENERAL BACKGROUND	7
2.1 Introduction.....	7
2.2 Problem Definition	9
2.3 Gas Flaring Emission.....	11
2.4 Sources of Gas Flaring.....	13
2.5 Typical Composition of Natural Gas	14
2.6 Flare Stack	15
2.7 Barriers to Gas Utilisation	15
2.8 Natural Gas Utilisation Options.....	16

2.8.1 Re-injection of Natural Gas	17
2.8.2 Gas Transportation.....	18
2.8.2.1 Gas to Pipelines	18
2.8.2.2 Power Generation	19
2.8.3 Liquefied Natural Gas.....	20
2.8.4 Hydrogen Production.....	21
2.8.5 Gas to Liquid Technology	21
2.8.5.1 Methane Steam Reforming.....	24
2.8.5.2 Autothermal Reforming	27
2.8.5.3 Partial Oxidation of Methane	28
2.8.5.4 Comparison Between Steam Reforming and Partial Oxidation of Methane	28
2.9 Synthesis Gas Production	29
2.10 Carbon Nanotubes.....	30
2.10.1 Carbon Nanotubes Synthesis	32
2.10.1.1 Laser Vaporisation Method.....	32
2.10.1.2 Chemical Vapour Deposition	33
2.10.1.3 Arc Discharge.....	33
2.10.2 CNTs Generation Using Sprays and Atomisation Techniques	34
CHAPTER-3: MEMBRANES' OVERVIEW	36
3.1 Introduction.....	36
3.2 What are Membranes?	36
3.2.1 Organic Membranes.....	38

3.2.2 Inorganic Membranes	39
3.2.2.1 Porous Membranes	39
3.2.2.2 Non-porous Membranes	42
3.3 Synthesis of Ceramic Membrane Powders	44
3.3.1 Sol-gel Method	44
3.3.2 Solid-state Method.....	45
3.3.3 Combustion Spray Pyrolysis Method	45
3.4 Membrane Reactors	45
3.5 Ceramic Membrane Reactors.....	49
3.5.1 Natural Gas Conversion into Syngas by Partial Oxidation ..	49
3.5.1.1 Oxygen Permeation in Perovskite Membranes	50
CHAPTER-4: SYNGAS PRODUCTION INVESTIGATION	54
4.1 Introduction.....	54
4.2 Feasibility Study for POM using Perovskite Membranes	54
4.2.1 Introduction.....	54
4.2.2 Consideration of LSCF Membrane	57
4.2.3 Thin Layer Membranes on a Porous Substrate.....	58
4.2.4 Assumptions and Calculation Procedures	61
4.2.4.1 Number of Tubes Required Calculation.....	63
4.2.4.2 Amount of LSCF (6428) and Cost	65
4.3 Analysis	66
CHAPTER-5: THE BACKGROUND TO SPRAYS AND ATOMISATION	72
5.1 Introduction.....	72
5.2 Definition of an Atomisation	72

5.2.1 Basic Mechanisms of Atomisation	73
5.2.1.1 Break-up of Liquid Jets	74
5.2.1.2 Break-up of Liquid Sheets.....	75
5.2.1.3 Break-up of Droplets	76
5.3 Characterisation of Sprays	77
5.3.1 Factors Affecting a Spray	80
5.3.1.1 Fluid Properties	80
5.3.1.2 Pressure	81
5.3.1.3 Temperature	81
5.3.1.4 Flow Rate	81
5.3.2 Drop Size Distribution	82
5.3.2.1 Settling Velocity.....	88
5.3.3 Drop Size Measurements	91
5.3.3.1 The Malvern Mastersizer-X	92
5.3.3.2 Operating Procedure of Malvern Mastersizer-X.....	94
5.3.3.3 Limitations of Mastersizer-X and Measurement Errors	95
5.4 Atomiser Types	95
5.4.1 Twin Fluid Atomisers	96
5.4.2 Single Fluid Atomisers	98
5.4.2.1 Rotary Atomiser	98
5.4.2.2 Ultrasonic Atomiser	99
5.4.2.3 Electrostatic Atomiser	100
5.4.2.4 Pressure Atomisers	101

CHAPTER - 6: DESIGN OF A FINE SPRAY ATOMISER DEVICE,

EXPERIMENTAL SET-UP AND PROCEDURE.....	108
6.1 Introduction.....	108
6.2 Design Philosophy and Procedure	109
6.2.1 Atomiser Device Design Specification: B1	110
6.2.2 Design of Fine Spray Atomiser Device	111
6.2.2.1 The Investigation and Gathering of Information (IGI): B2	111
6.2.2.2 Generation of Ideas and Evaluation (GIE): B3 - B5	116
6.2.2.3 Atomiser Device Development and Testing (D and T): B6.....	116
6.2.2.4 Estimation of Settling Velocity (D and T): B6	122
6.3 Experimental Apparatus Set-up	124
6.3.1 Overview.....	124
6.3.2 Apparatus Set-up	124
6.3.2.1 Reservoir Tank and Water Pump	126
6.3.2.2 Air Supply and Flow Metering.....	127
6.3.2.3 Atomiser Holding and Positioning Assembly	129
6.3.2.4 Malvern Mastersizer-X Set-up	129
6.3.2.5 Still Camera.....	131
6.3.3 Experimental Procedure.....	132
6.3.3.1 Phase I: Spraying and Atomisation Experimental Procedure	132

6.3.3.2 Phase II: Proposed Prototype and Testing (PP and T): B8.....	133
CHAPTER-7: RESULTS, ANALYSIS AND DISCUSSION.....	136
7.1 Introduction.....	136
7.2 Results and Discussion: Feasibility Study of the Partial Oxidation of Methane to Syngas.....	136
7.2.1 Oxygen Permeation through Membrane Tubes.....	137
7.2.2 Effect of Oxygen Partial Pressure on Oxygen Permeation.	139
7.2.3 Modelling of Partial Oxidation of Natural Gas	141
7.3 Results and Discussion: Single-Walled Carbon Nanotubes (SWCNT) Production	149
7.3.1 Overview	149
7.3.2 <i>Phase I</i> : Spray Characterisation.....	150
7.3.2.1 Inverted Atomiser Device Position	151
7.3.2.2 Horizontal Atomiser Device Position	151
7.3.2.3 Vertical Atomiser Device Position.....	154
7.3.2.4 Summary	182
7.3.3 <i>Phase II</i> : Single-Walled Carbon Nanotubes Generation: Highlight of the Results and Discussion	183
CHAPTER-8: CONSIDRATION OF ECONOMIC ANALYSIS	189
8.1 Introduction.....	189
8.2 Concept of a Visual Basic Programme	190
8.2.1 Programming Fundamentals and Overview of the Economic Analysis	191

8.2.2 Feasibility Study	192
8.2.2.1 Software Identification	193
8.2.2.2 Analysis Stage	193
8.2.2.3 Functional and Non-functional Requirements	195
8.2.2.4 Entities and Attributes	196
8.2.2.5 Entities Relationship Diagram	198
8.2.2.6 Context Diagram and Level 1 Data flow Diagram	199
8.2.3 Design Stage	200
8.2.3.1 Interface Structure	200
8.2.3.2 Database Structure.....	202
8.2.3.3 Links Between VB Interface and the Database.....	203
8.2.4 Implementation Stage	203
8.2.4.1 VB scripts	203
8.2.4.2 Testing.....	204
8.2.4.3 User Guide.....	204
8.3 Economic Analysis and Comparison	205
8.3.1 Assumption	205
8.3.1.1 Scenario 1: Gas is Flared.....	205
8.3.1.2 Scenario 2: Gas is Recycled	206
CHAPTER-9: CONCLUSIONS AND RECOMMENDATIONS.....	211
9.1 Conclusions.....	211
9.2 Recommendations for Future Work	213
APPENDICES	215

Appendix A: Tabulated Results of Chapter 4 and Chapter 7 (Section 7.2) Analysis.....	216
Appendix B: Experimental Design and Experimental Results.....	222
Appendix C: Normalisation Table.....	257
Appendix D: Visual Basic Scripts.....	258
Appendix E: VB programme Testing Results.....	265
Appendix F: User Guide for CCS System.....	268
Appendix G: Comparison and Economic Analysis Results.....	279
REFERENCES.....	283

LIST OF TABLES

Table 2.1:	Worldwide top twenty gas flarer countries in 2008	12
Table 2.1:	General typical composition of natural gas	14
Table 2.2:	Pipeline gas quality specifications	19
Table 3.1:	Classification of porous membranes	40
Table 4 1:	Oxygen flux summary for some work on LSCF membrane	60
Table 5.1:	Mean diameters and their applications	87
Table 6.1:	Performance specification, 121 hollow-cone spray atomisers.....	115
Table 7.7:	Operating parameters	150
Table 7.1:	Summary of horizontal position results of the atomiser device	153
Table 7.2:	Initial experimental results of atomiser device vertical position at baffle plate position of 110 mm and aerosol tube position of 100 mm from the base cover	161
Table 7.3:	Typical experimental data obtained for the optimum baffle plate and aersol tube positions	166
Table 7.4:	Results of various tests showing the effect of water supply pressure and water flow rate on droplet sizes	169
Table 7.5:	Typical results of air flow rates and water s supply pressures on droplet sizes	172
Table 7.6:	Typical results showing the effect of downstream distance of atomiser exit on droplet sizes	177
Table 8.1:	List of entities and relevant attributes	197
Table 8.2:	Economic analysis results	208

LIST OF FIGURES

Figure 2.1:	Typical processes flow diagram of oil and gas production.....	10
Figure 2.2:	Carbon nanotubes molecular representations.....	30
Figure 3.1:	A membrane separation principle	37
Figure 3.2:	The main membrane functions in the membrane reactor.....	47
Figure 4.1:	Dense membrane reactor mechanisms	62
Figure 4.2:	Effect of oxygen permeation on a number of tubes (O_2 flow rate = 10,000 m^3/day , tube outer diameter, 0.015 m, tube thickness= 0.002 m and tube length = 1.50 m)	67
Figure 4.3:	Effect of tube relative length on a number of tubes (O_2 flow rate = 10,000 m^3/day , tube outer diameter, 0.015 m and tube = 0.002 m thickness)	68
Figure 4.4:	Effect of oxygen flow rate on a number of tubes (tube outer diameter = 0.015 m, tube thickness = 0.002 m, tube length = 1.50 m, O_2 flux = 10 $ml/(cm^2 \cdot min)$).....	68
Figure 4.5:	Effect of tube thickness on the price of tubes (tube outer diameter = 0.015 m, tube length = 1.50 m, O_2 flux = 10 $ml/(cm^2 \cdot min)$).....	69
Figure 5.1:	General atomisation mechanisms.....	73
Figure 5.2:	Liquid column break-up at different velocities.....	75
Figure 5.3:	Break-up mechanism of a liquid sheet into ligaments and droplets.....	76
Figure 5.4:	Drop break-up mechanism in low and high Weber numbers.....	77
Figure 5.5:	Spray cone angle defination	78
Figure 5.6:	Various spray patternations.....	80

Figure 5.7:	Typical drop size distribution	82
Figure 5.8:	Drop size histograms based on number and volume.....	83
Figure 5.9:	Typical drop size frequency distribution curves	84
Figure 5.10:	Typical shape of cumulative drop size.....	84
Figure 5.11:	Creeping flow past a spherical particle	88
Figure 5.12:	Optical arrangement employed in Malvern Mastersizer-X.....	93
Figure 5.13:	Two-fluid atomiser design	97
Figure 5.14:	Schematic diagram of rotary atomiser	98
Figure 5.15:	Schematic diagram of ultrasonic atomiser	99
Figure 5.16:	Schematic diagram of electrostatic atomiser.....	100
Figure 5.17:	Typical plain orifice pressure atomiser	102
Figure 5.18:	Fan (Vee) Jet atomiser	102
Figure 5.19:	Various designs of pressure swirl atomiser.....	103
Figure 5.20:	Spray development stages with fluid pressure increase.....	106
Figure 6.1:	General design decision tree process	109
Figure 6.2:	The design process for the atomiser device for carbon nanotubes production	111
Figure 6.3:	Schematic diagram of typical cascade impactor	112
Figure 6.4:	Schlick hollow-cone atomiser, type 121 (dimensions are in mm).....	114
Figure 6.5:	The variations of mean volume droplet size with orifice diameter for different liquid supply pressure **	114
Figure 6.6:	Proposed diagram of atomiser manifold	117
Figure 6.7:	Proposed diagram of atomiser device (inverted)	117
Figure 6.8:	Proposed diagram of atomiser device (horizontal)	118

Figure 6.9:	Proposed final diagram of atomiser device (vertical)	118
Figure 6.10:	Illustration of atomiser device set-up	119
Figure 6.11:	Confinement tube with top cover and bottom cover	120
Figure 6.12:	Liquid spraying atomisers and holding block	120
Figure 6.13:	Schematic flow diagram of experimental set up (phase-I)	125
Figure 6.14:	Speck Kolben water pump	127
Figure 6.15:	Air flow rate standard calibration charts	128
Figure 6.16:	Atomiser device connected to air flow meters	129
Figure 6.17:	Malvern Mastersizer-X	130
Figure 6.18:	Malvern Mastersizer-X schematic diagram and the spray device set-up	130
Figure 6.19:	Experimental apparatus of single-walled carbon nanotubes generation	134
Figure 7.1:	Effect of temperature on O ₂ permeation in LSCF 6482 membranes reactor, for different membrane thicknesses (O ₂ partial pressure 0.21/1x10 ⁻³ atm)	138
Figure 7.2:	Variation of O ₂ permeation for different membrane wall thicknesses and different temperatures (O ₂ partial pressure 0.21/1x10 ⁻³ atm)	139
Figure 7.3:	O ₂ permeation flux at various permeate side partial pressures and at different temperatures (O ₂ feed side partial pressure = 0.21 atm, tube thickness = 0.20 cm)	140
Figure 7.4:	O ₂ permeation flux at various feed side partial pressures and at different temperatures (O ₂ permeate side partial pressure = 0.005 atm, tube thickness = 0.20 cm)	141

Figure 7.5:	Schematic diagram of dense membrane reactor.....	142
Figure 7.6:	Predicted molar flow rate profiles for each species as a function of reactor length, (Fixed bed reactor), O ₂ inlet 0.65 mol/s, CH ₄ inlet =1.33, T = 873 K.....	147
Figure 7.7:	Predicted molar flow rate profiles for each species as a function of reactor length, (Fixed bed reactor), O ₂ inlet 0.65 mol/s, CH ₄ inlet =1.33 mol/s, T = 1073 K.....	148
Figure 7.8:	Sketch diagram of horizontal position of the atomiser device.....	152
Figure 7.9:	No aerosol stream crossing the laser beam during the measurement..	156
Figure 7.10:	Positions of baffle plate (at 110 mm) and aerosol tube (at 100 mm).	157
Figure 7.11:	Fine spray stream crossing the laser beam during measurement, (Test AS-12: Baffle plate position = 110 mm, aerosol tube position =100 mm based on the base cover)	158
Figure 7.12:	Typical particle diameter (μm) distributions for tests AS-12 (a) and AS-13 (b), based on $D_{n0.50}$	159
Figure 7.13:	Typical particle diameter (μm) distributions for tests AS-12 (a) and AS-13 (b), based on D_{32}	160
Figure 7.14:	Optimum baffle plate (80 mm) and aerosol tube (77 mm) positions...	162
Figure 7.15:	Fine spray stream crossing the laser beam during measurement (Test AS-15)	163
Figure 7.16:	Typical particle diameter (μm) distributions for tests AS-15 (a) and AS-16 (b), based on $D_{n0.50}$	164
Figure 7.17:	Typical particle diameter (μm) distributions for tests AS-15 (a) and AS-16 (b), based on D_{32}	165

Figure 7.18:	Typical particle diameter (μm) distributions for tests AS-20 (a) and AS-27 (b), based on $D_{n0.50}$	167
Figure 7.19:	Typical particle diameter (μm) distributions for tests AS-20 (a) and AS-27 (b), based on D_{32}	168
Figure 7.20:	Variation of drop size ($D_{n0.50}$) with water supply pressure for different water flow rates	170
Figure 7.21:	$D_{n0.50}$ (μm) “iso-contours” plots for different water flow rates (0.01-0.05) l/min and different water supply pressures (6 -11) MPa, for tests (AS-18 to AS-29).....	171
Figure 7.22:	Typical particle diameter (μm) distributions for tests AS-30 (a) and AS-41 (b), based on $D_{n0.5}$	173
Figure 7.23:	Typical particle diameter (μm) distributions for tests AS-30 (a) and AS-41 (b), based on D_{32}	174
Figure 7.24:	Variation of drop size ($D_{n0.50}$) with water supply pressure for different air flow rates.....	175
Figure 7.25:	$D_{n0.50}$ (μm) “iso-contours” plots for different air flow rates (0.3 - 0.4) l/min and different water supply pressures (6 to11) MPa, (Tests AS-30 to AS-41).....	176
Figure 7.26:	Spray device positions with respect to the laser beam.....	177
Figure 7.27:	Typical particle diameter (μm) distributions for tests AS-44 (a) and AS-47 (b), based on $D_{n0.5}$	178
Figure 7.28:	Typical particle diameter (μm) distributions for tests AS-44 (a) and AS-47 (b), based on D_{32}	179

Figure 7.29:	Droplet size ($D_{n0.50}$) as a function of downstream distance for 0.3 and 0.4 l/min air flow rates	180
Figure 7.30:	$D_{n0.50}$ (μm) “iso-contours” plots for different air flow rates (0.3-0.4) l/min and different downstream distance (40-100 mm) (Tests AS-41 to AS-49).....	181
Figure 7.31:	The atomiser device and the furnace connection overview	184
Figure 7.32:	Radiator in a bucket with running water	185
Figure 7.33:	Illustration of laser beam on the product particles	186
Figure 7.34:	TEM image of the products of <i>Phase II</i> experiments (oxygen and Fe liquid catalyst).....	187
Figure 7.35:	TEM image of the products of <i>Phase II</i> experiments (methane and Fe liquid catalyst).....	187
Figure 8.1:	Diagram of cost comparison request.....	192
Figure 8.2:	Process flow diagram	194
Figure 8.3:	Entities relationship diagram.....	198
Figure 8.4:	Context diagram	200
Figure 8.5:	Level 1 data flow diagram.....	201
Figure 8.6:	Typical cost analysis when comparing syngas and SWCNT generation with flare gas system	209
Figure B4-1:	Typical spray characteristics; Number (%), particle diameter (μm) and analysis table for test SA -14.....	229
Figure B4-2:	Typical spray characteristics; Number (%), particle diameter (μm) and analysis table for test SA -17.....	230

Figure B4-3:	Typical spray characteristics; Number (%), particle diameter (μm) and analysis table for test SA -18.....	231
Figure B4-4:	Typical spray characteristics; Number (%), particle diameter (μm) and analysis table for test SA -19.....	232
Figure B4-5:	Typical spray characteristics; Number (%), particle diameter (μm) and analysis table for test SA -21.....	233
Figure B4-6:	Typical spray characteristics; Number (%), particle diameter (μm) and analysis table for test SA -22.....	234
Figure B4-7:	Typical spray characteristics; Number (%), particle diameter (μm) and analysis table for test SA -23.....	235
Figure B4-8:	Typical spray characteristics; Number (%), particle diameter (μm) and analysis table for test SA -24.....	236
Figure B4-9:	Typical spray characteristics; Number (%), particle diameter (μm) and analysis table for test SA -25.....	237
Figure B4-10:	Typical spray characteristics; Number (%), particle diameter (μm) and analysis table for test SA-26.....	238
Figure B4-11:	Typical spray characteristics; Number (%), particle diameter (μm) and analysis table for test SA-28.....	239
Figure B4-12:	Typical spray characteristics; Number (%), particle diameter (μm) and analysis table for test SA-29.....	240
Figure B4-13:	Typical spray characteristics; Number (%), particle diameter (μm) and analysis table for test SA-31.....	241
Figure B4-14:	Typical spray characteristics; Number (%), particle diameter (μm) and analysis table for test SA-32.....	242

Figure B4-15: Typical spray characteristics; Number (%), particle diameter (μm) and analysis table for test SA-33.....	243
Figure B4-16: Typical spray characteristics; Number (%), particle diameter (μm) and analysis table for test SA-34.....	244
Figure B4-17: Typical spray characteristics; Number (%), particle diameter (μm) and analysis table for test SA-35.....	245
Figure B4-18: Typical spray characteristics; Number (%), particle diameter (μm) and analysis table for test SA-36.....	246
Figure B4-19: Typical spray characteristics; Number (%), particle diameter (μm) and analysis table for test SA-37.....	247
Figure B4-20: Typical spray characteristics; Number (%), particle diameter (μm) and analysis table for test SA-38.....	248
Figure B4-21: Typical spray characteristics; Number (%), particle diameter (μm) and analysis table for test SA-39.....	249
Figure B4-22: Typical spray characteristics; Number (%), particle diameter (μm) and analysis table for test SA-40.....	250
Figure B4-23: Typical spray characteristics; Number (%), particle diameter (μm) and analysis table for test SA-42.....	251
Figure B4-24: Typical spray characteristics; Number (%), particle diameter (μm) and analysis table for test SA-43.....	252
Figure B4-25: Typical spray characteristics; Number (%), particle diameter (μm) and analysis table for test SA-45.....	253
Figure B4-26: Typical spray characteristics; Number (%), particle diameter (μm) and analysis table for test SA-46.....	254

Figure B4-27: Typical spray characteristics; Number (%), particle diameter (μm)
and analysis table for test SA-48..... 255

Figure B4-28: Typical spray characteristics; Number (%), particle diameter (μm)
and analysis table for test SA-49..... 256

ACKNOWLEDGMENTS

First of all, I wish to express my sincere appreciation and deepest gratitude to my supervisors, Professor Ghasem G. Nasr and Professor Ron Hughes, for their endless support, helpful guidance, advice and great patience.

I wish to express my gratitude to the University of Salford and all those who directly, or indirectly, were involved in this research.

Special thanks are given to Mr David Stevens for his help during the course of the experimental work and, above all, for his craftsmanship in setting up the test facility.

Many thanks to all my colleagues at the Spray Research Group (SRG) laboratory at the University of Salford, A. Nourian, M. El Kamkhi, N. Asmuin, G. Enyi and I. Ugbogu with whom I have had the pleasure to work. They have provided me with a great research environment and a relaxed atmosphere.

I would like to thank my wonderful family for their sincere moral support and for being with me through both the good and the hard times.

Last, but not least, I would like to express my thanks to the Libyan Ministry of Higher Education and to the Libyan Embassy staff in London for their financial support.

DECLARATION

Unless otherwise stated, the work in this thesis is that of the author, and has not previously submitted in part or in whole, at this or any other establishment.

Author:

Musa Abuhesa -----

Supervisors:

Prof. G. G. Nasr-----

Prof. R. Hughes-----

NOMENCLATURE

$\pounds M/\text{year}$	£Million per year
AIChE	American Institute of Chemical Engineers
AIAA	Aerospace Sciences Meeting and Exhibition
ATR	Autothermal reforming
ASME	American Society of Mechanical Engineers
BASF	The largest chemical company in the world and is head quartered in Germany. Originally stood for (Baden Aniline and Soda Factory)
Bcm	Billion Cubic Metres
CAPP	Canadian Association of Petroleum Producers
CCS	Cost Comparison System
CDM	Clean Development Mechanism
CER	Certified Emission Reduction
CH ₄	Methane
CO	Carbon monoxide
CO ₂	Carbon dioxide
O ₂	Oxygen
D	Droplet diameter (μm)
$D_{n0.50}$	Number Mean Diameter
$D_{v0.50}$	Volume Mean Diameter
D_{32}	Sauter Mean Diameter
EIA	Energy Information Administration (USA)
FT	Fischer-Tropsch

GGFR	Global Gas Flaring Reduction
GHGs	Greenhouse Gases
GTL	Gas to Liquid
HP	High Pressure
IPCC	Inter-governmental Panel on Climate Change
K£	Thousand £
<i>l</i> /min	Litres per minute
LNG	Liquefied Natural Gas
LP	Low Pressure
LPG	Liquefied Petroleum Gas
LSCF	Lanthanum Strontium Cobalt Ferrite
MWCNT	Multi-Walled Carbon Nanotubes
N_i	Number of droplets
OGP	Association of Oil and Gas Producers
P	Pressure (MPa)
POM	Partial Oxidation of Methane
Q	Flow rate (<i>l</i> /min)
SA-1, SA-2 ...	Test Number
SWCNT	Single-Walled Carbon Nanotubes
SMR	Steam Reforming
T	Temperature (°C)

ABSTRACT

Gas flaring is the burning of unwanted produced natural gas, which cannot be processed or sold during oil and gas production and processing operations. In past decades, gas flaring was believed to be environmentally tolerable. However, scientists have found that the flaring of gas is an impediment to the environment; this has led to attempting to tackle the problem of gas flaring to advance it to an acceptable level worldwide.

In this study, two options were investigated for the utilisation of natural gas that was previously flared. The *first* option was a theoretical investigation of the use of ceramic perovskite membranes in a tubular reactor for the partial oxidation of methane (flare gas) to syngas. The H₂/C product ratio of partial oxidation of methane is 2:1, which is suitable for Fischer-Tropch technology or methanol synthesis. It was found that this option is ideal for converting natural gas into synthesis gas (CO + H₂), and it reduces capital and running costs, as these membranes are able to separate oxygen from the air stream with no need for an oxygen separation plant. The novelty of this approach is that the production of syngas using oxygen selective membranes can be achieved at the “Wellhead” with no requirement for the gas to be transported and a consequent reduction in transport costs.

The *second* option was an experimental investigation in using spraying and atomisation techniques for the generation of carbon nanotubes, by spraying simulated catalyst solution droplets into a hydrocarbon gas stream (*methane as a carbon source*) using a novel “atomiser device” incorporating pressure swirl atomisers.

The second part of the investigation was divided into two phases: *Phase-I*, which was implemented at the Spray Research Group laboratory at the University of Salford, involved a series of experiments which were undertaken to produce fine aerosol droplets that have a number mean diameter of less than or equal to 5 μm , which was successfully achieved. In this *phase*, water and air were used to simulate the metal catalyst and methane, respectively, which were used in *Phase-II*.

Phase-II trials were implemented at the University of Oxford on a collaborative basis. A furnace was installed underneath of the *Phase-I* “atomiser device” and the stream of droplet particles fell down through the furnace (400 - 800° C). Reaction inside the furnace occurred to produce the Single Wall Carbon Nanotubes (SWCNT) material. The preliminary results of the experiments in this *Phase* showed that it is possible to produce SWCNT.

This investigation also considered an economic analysis of reducing gas flaring. A Visual Basic (VB) programme was developed to make a cost comparison between the proposed options and current conventional plants. The consideration of the economic analysis demonstrated that the cost of natural gas flaring exceeds those for syngas and Single-Walled Carbon Nanotubes production.

Chapter -1

CHAPTER-1: INTRODUCTION

1.1 Overview of the Topic

Gas flaring is, as given by an all-inclusive definition, a high-temperature oxidation process of burning unwanted produced natural gas, which cannot be processed or sold during oil and gas production and processing operations, in an open flame, at well-site or facility. Until the past few decades, gas flaring was believed to be environmentally tolerable (Shewchuk, 2002). However, scientists have discovered its environmental impact and have started working on its diminution to achieve an *acceptable level of gas flaring* worldwide.

Natural gas is a mixture of gaseous hydrocarbons, with methane being the dominant component, and it has been used in different industries since its initial discovery. The huge expansion within the oil industry in recent decades has resulted in a growth in oil production. Wherever there is a large quantity of associated gas produced with crude oil, and wherever some obstacles to natural gas utilisation are present, gas flaring has increased. This increase has alerted the public to its dangerous impact on the environment. Instead of flaring, excess gas can be used on site to produce synthesis gas, i.e. a mixture of carbon monoxide and hydrogen, which is the first stage required for natural gas conversion into liquid chemical products using the Fischer-Tropsh synthesis (Aasberg-Petersen et al., 2003). Also, the natural gas can be used as the main raw material to produce carbon nanotubes and hydrogen.

The partial oxidation of methane (POM) is a promising route for syngas production. It is an exothermic reaction and its H₂/CO product ratio is 2, which is suitable for Fischer-Tropsch (GTL) technology (Wang et al., 2006).

The use of excess gas as an alternative to flaring is the base case of this research. The first proposed method for this research is a theoretical investigation of the production of syngas through the partial oxidation of methane (flare gas) using ceramic perovskite membranes.

The novelty of this approach is that the production of syngas using oxygen selective membranes can be achieved at the “Wellhead” with no requirement for the gas to be transported and a consequent reduction in transport costs. Furthermore in contrast to steam reforming, syngas can be produced at lower temperatures and with less maintenance using this approach. Although partial oxidation of methane using oxygen permeable membranes has been proposed frequently in the literature, the application to the gas produced at oil and gas wells "in situ" has not been considered hitherto.

The second proposed method is the use of spraying and atomisation techniques for the generation of Single-Walled Carbon Nanotubes (SWCNT). This is a novel method of producing fine spray droplets of $\leq 5\mu\text{m}$ using a designed atomiser device. The technique is to spray a solution of catalyst droplets into the methane gas stream. This method is divided into two phases: in *Phase-I*, a small laboratory scale apparatus was designed to produce fine droplets which had a number mean diameter of less than or equal to 5 μm . In *Phase-II*, a furnace was installed at the bottom of the *Phase I* experimental apparatus and the stream of droplet particles falls down through the furnace (400-800 °C). Reaction inside the furnace will occur to give carbon plus hydrogen. The carbon, after

diffusing through the catalyst metal particle, will reorganise to form SWCNT material, and the hydrogen may be stored for other use. Based on knowledge gained from these two options and for comparison, a Visual Basic economic programme has been created.

1.2 Aims

The aims of this research are:

- i. To develop alternatives systems to continuous gas flaring in the oil and gas industry.
- ii. To derive the required knowledge base for flare gas utilisation, via ceramic perovskite membranes for syngas production and via experimentation using sprays and atomisation techniques to produce Single-Walled Carbon Nanotubes
- iii. To consider and apply an economic comparison model for alternatives to gas flaring based on knowledge gained from (i) and (ii).

1.3 Objectives

To meet the above aims, the specific research objectives are:

- i. To categorise and rank possible methods of flare gas minimisation and/ or utilisation.
- ii. To consider the related environmental impacts for these processes.
- iii. To study theoretically the production of syngas through the partial oxidation of methane using ceramic membranes. (From a literature survey, one ceramic membrane material has been selected, LSCF (6428)).

- iv. To study experimentally the method for generation of fine droplets for the synthesis of carbon nanotubes by spraying catalyst solution droplets into a hydrocarbon gas stream (methane), using Mastersizer–X laser instrument.
- v. To build a Visual Basic programme to carry out the comparison and economic analysis of flare gas proposed utilisation methods.

1.4 Thesis Structure

The thesis consists of nine chapters including this introductory chapter. Chapter 2 follows and presents a general review of natural gas utilisation and flaring processes together with an overview of the work that has been previously performed in the area of gas flaring reduction. Chapter 3 presents a general background on membranes and their applications, focussing on perovskite membranes, which were used in the first proposed option in this research work. A theoretical investigation of the partial oxidation of methane (as flare gas) to produce syngas, using perovskite membranes is presented in Chapter 4. Chapter 5 outlines a general review of sprays and atomisation techniques and their applications. An experimental rig was designed and built during the course of the research. The experimental apparatus design and the set-up followed in this work are described in Chapter 6, in addition to the experimental procedure. The results, analysis and discussion for the two proposed methods are presented in Chapter 7. A Visual Basic programme, which was created for the comparison and economic analysis of the proposed options, is presented in Chapter 8, in addition to the analysis results. Finally, the conclusions drawn from this research and recommendations for future work are presented in Chapter 9.

Chapter -2

CHAPTER-2: GENERAL BACKGROUND

2.1 Introduction

This chapter presents a general background and an overview of some of the relevant literature on the subject of gas flaring diminution. Petroleum hydrocarbon deposits vary considerably in their physical and chemical properties and consist of a complex mix of a wide range of organic compounds (Khan and Islam, 2007). Natural gas plays an important role in the energy needs of the world. It is mainly composed of methane but it is typically mixed with varying amounts of heavier hydrocarbons such as ethane, propane, butane and pentane (Devold, 2009). In addition, raw natural gas contains water vapour, hydrogen sulphide, carbon dioxide, helium, nitrogen, and other compounds. Natural gas processing essentially depends on the reservoir's characteristics (Hughes, 1992 and Zaman, 1999).

Using natural gas, that otherwise would be flared, would help economies particularly those of developing countries. The challenge is to improve the quality of gas utilisation, to achieve market value and also to deal with environmental concerns. Therefore, concerted efforts are needed to reduce gas flaring worldwide. Improving the disposal methods of waste gases has become one of the main long-term environmental goals within the industry. The first serious step towards greenhouse warming reduction was the Kyoto Protocol, which was a document that was signed by the Protocol partnership countries in 1997 in Kyoto, Japan, for the reduction of greenhouse gases by 2008 - 2012 (Park, 2003 and Indriani, 2005).

The World Bank and the Government of Norway established the Global Gas Flaring Reduction Initiative (GGFR) in November 2001, in Marrakech. It is aimed at assisting national governments and the petroleum industry in their attempts to eliminate gas flaring (Djumena, 2004). This can be done by improving the political and regulatory framework for investments in flaring minimisation, getting better market access for natural gas, and propagating information on international best practices by publicising key activities. The Initiative's focus of attention is to classify and find ways to overcome barriers that currently hamper flaring reduction investments. The continuing rise in global gas prices has encouraged many companies and governments to develop gas infrastructure, eventually providing opportunities to market associated gas (Gerner et al., 2004). Only a small number of oil-producing countries have significantly reduced gas flaring volumes and, in most jurisdictions, flaring volumes continue to increase with increased oil production.

Many efforts are being made to eliminate gas flaring by gathering excess gas and using it commercially, or by re-injecting it into reservoirs. Moreover, gas flaring reduces the opportunities for using gas for energy purposes in a region with large and un-met energy needs (Christiansen and Haugland, 2001 and Christopher et al., 2007).

In spite of the many efforts that have been taken to reduce gas flaring, the levels of annual gas flaring have remained stable (140– 170 Bcm) for the last two decades (Christopher et al., 2007 and Elvidge et al., 2009). This is ascribed to the increase in oil production due to an upsurge in growth in the oil industries, which has led to an increase in the amount of associated gas produced with the crude oil. Also, the lack of regulatory and contractual structures, and the constraints placed on gas utilisation, its

infrastructure and market development are contributory factors (Djumena, 2004). According to the World Bank data, this amount of gas flaring creates about 400 million tonnes of CO₂ in annual emissions, and is, therefore, a significant contributor to the concentration increase of CO₂ in the atmosphere worldwide (Gerner et al., 2004, Djumena, 2004 and GGFR, 2010).

2.2 Problem Definition

In petroleum field production operations, typically, three product streams are produced: oil, gas and associated water, which are called reservoir fluids. Some fields produce only gas and they are classified as gas fields. Business competency is required to effectively manage these resources to ensure their full exploitation. During production operations, the reservoir fluids flow from well locations through pipelines to the manifold and then to the separation plant. The produced oil and condensate liquids are relatively easily stored and transported to refineries or to market. The associated produced water is re-injected, or treated and cleaned, before discharging into the environment.

A portion of natural gas, after treatment, is used as fuel in the plant facilities and the remainder is prepared for processing, reinjection or sale. In case it is not possible to process or sell it due to a lack of a gas infrastructure, a nearby gas market, or because of the impossibility of economic conservation, the natural gas produced in excess of operational needs is flared into the atmosphere (Devold, 2009). This flared gas is generally a low calorific waste by-product of natural gas (product). A typical flow diagram of oil and gas production and processing is shown in Figure 2.1.

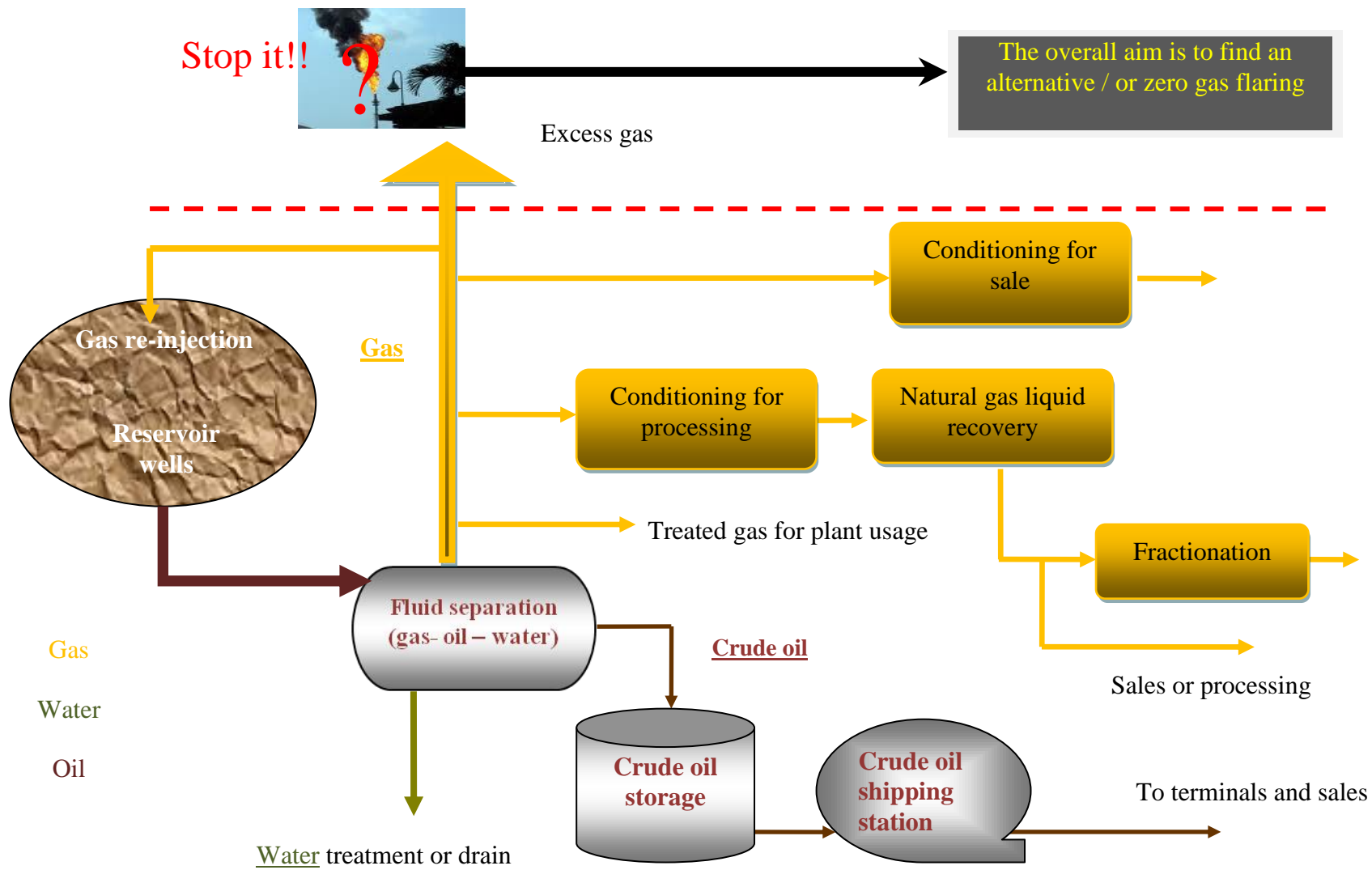


Figure 2.1: Typical processes flow diagram of oil and gas production

2.3 Gas Flaring Emission

The flared gas emanates into the atmosphere as carbon dioxide, which is a leading contributor to greenhouse gases (GHGs). In addition to carbon dioxide, other minor chemicals may also be formed, which include water vapour, unburned hydrocarbons, particulate matter (soot and ash), volatile organic compounds (benzene, toluene and xylene), polycyclic aromatic hydrocarbons, as well as other chemicals such as aldehydes and ketones. Studies indicate that most of the minor chemicals are bound up in the soot emitted from the flares (Kostiuk and Johnson, 2000).

Most developing oil countries flare large volumes of associated gas owing to a lack of infrastructure. Gas flaring is a main source of carbon dioxide contamination produced within the oil industry (Alemagi, 2007). It adds to greenhouse gas emissions and wastes a potentially valuable energy resource (Elvidge et al., 2009).

Due to the pollutant emissions arising from gas flaring, its reduction has become an important global issue. Several research findings have confirmed that gaseous emissions and thermal radiation arise from gas flaring activities during the separation of flow streams in upstream and downstream petroleum processing operations (Sonibare and Akeredolu, 2006 and Abdulkareem and Kovo, 2006). Oil companies are under pressure to reduce gas flaring due to its impact on the global ecosystem (Golombok and Teunissen, 2003). In developing countries, governments can help diminish gas flaring by increasing opportunities for its usage and by forming legal, regulatory, financial and environmental laws that assist operators to utilise gas (Gerner et al., 2004). There are some countries which are classified as leading gas flaring contributors (such as Russia, Nigeria and Iran etc). These countries are responsible for more than a third of global gas

flaring. Table 2.1 shows the estimated gas flaring volume obtained from satellite data (based on 2008 data) of the top twenty gas flarer countries, (Elvidge et al., 2009). In contrast, there are other countries which control their gas flaring and utilise their gases and, thus, demonstrate good practice.

No.	Country	Gas Flared (Bcm)
1.	Russia	40.2
2	Nigeria	14.9
3	Iran	10.3
4	Iraq	7.0
5	Algeria	5.5
6	Kazakhstan	5.2
7	Libya	3.7
8	Saudi Arabia	3.5
9	Angola	3.1
10	Qatar	3.0
11	Uzbekistan	2.7
12	Mexico	2.6
13	Venezuela	2.6
14	Indonesia	2.3
15	USA	2.3
16	China	2.3
17	Oman	1.9
18	Malaysia	1.9
19	Canada	1.8
20	Kuwait	1.8

Table 2.1: Worldwide top twenty gas flarer countries in 2008

Clean technology involves identifying the human benefit that is provided by an activity and then looking for methods to provide that benefit at a lower environmental impact when the lifecycle sum is considered. Because gas flaring is energy-wasting and results in the pollution of the atmosphere by creating acid rain and greenhouse gases, it is consequently a target for 'green' pressure and legislative curbs. Owing to the air pollution level resulting from gas flaring, and to the increasing pressure from environmentalists, governments and oil industry organisations worldwide have become committed to achieving *zero gas flaring*. The massive flames that are often seen in the world's oil and gas fields and on offshore platforms due to gas flaring processes could be a thing of the past in the near future. It is clear that gas flaring is a big contributor to CO₂ emissions by the burning of useful amounts of natural gas, and this adds to potential climate change problems.

2.4 Sources of Gas Flaring

The classification of flare sources (*routine or non-routine*) is important for flare reduction method determinations and its options priority. According to OGP (2000) and Elvidge et al. (2009), gas that is being flared may come from different sources such as:

- i. Excess gas which can be supplied commercially to customers;
- ii. Unburned process gas from the processing facilities;
- iii. Vapours collected from the tops of tanks as they are being filled;
- iv. Gas from process upsets, equipment changeover and maintenance.

A production shutdown may require the temporary flaring of all the gas stored on, or arriving at, a facility in order to release high pressure and avoid a catastrophic situation.

2.5 Typical Composition of Natural Gas

Natural gas composition can vary widely depending on the location of where it is produced. Its processing consists of separating all of the various hydrocarbons and fluids from the pure natural gas to produce what is known as “pipeline quality” dry natural gas (Devold, 2009). Table 2.2 below gives the typical composition of natural gas before it is refined. Hydrogen sulphide in sour gas is toxic and heavier than air; if it is not flared or treated, it could pose a risk to workers and neighbours. Flaring converts the hydrogen sulphide into less toxic sulphur dioxide.

<i>Component</i>	<i>Chem. formula</i>	<i>Range (Mole %)</i>
Methane	CH ₄	70-90%
Ethane	C ₂ H ₆	0-20%
Propane	C ₃ H ₈	
Butane	C ₄ H ₁₀	
Carbon Dioxide	CO ₂	0-8%
Oxygen	O ₂	0-0.2%
Nitrogen	N ₂	0-5%
Hydrogen sulphide	H ₂ S	0-5%
Rare gases	He, Ne, Xe	Trace

Table 2.1: General typical composition of natural gas

2.6 Flare Stack

A flare stack is an elevated vertical stack used for burning off the gas produced in excess of operational needs and the gas released by pressure relief valves during emergency cases and the over-pressuring of plant equipment (Shore, 2006). In the oil industry, the main application of the flare stack is to act as a safety means to protect vessels or pipes from over-pressuring due to unplanned upsets. The pressure relief valves on the oil and gas plant equipment automatically release gases, and sometimes liquids, whenever the pressure rises above a set point. These released fluids are routed through large pipes called flare headers to the flare stacks and they are burned in the flare stacks.

The flare systems in oil and gas fields are normally divided into low pressure (LP) and high pressure (HP) flare systems. The LP system is operated slightly above atmospheric pressure to prevent atmospheric gases such as oxygen from flowing back into the vent and flare system and creating a combustible mixture. For low gas flows, inert gas is injected at the flare nozzle to prevent air ingress.

2.7 Barriers to Gas Utilisation

The expansion of energy utilisation in the future will be affected by the following factors: population and urbanisation increase, increasing per capita consumption, better energy efficiency, lower energy subsidies, and industrialisation (Ardestani and Shafie-Pour, 2007). Nowadays, there are technical, political, economic and social issues that may impede the implementation of gas flaring reduction projects (Christiansen and Haugland, 2001 and Indriani, 2005). The questions are how the oil industry and

governments will attempt to overcome the existing barriers to gas utilisation and how to plan for future?

The major global obstacles are:

- i. A limited access to international gas markets as well as weak local markets;
- ii. A lack of financing to put the necessary infrastructure in place;
- iii. An undeveloped regulatory framework.

2.8 Natural Gas Utilisation Options

Several gas utilisation options have been developed. Selecting a suitable option depends on upstream conditions such as field characteristics and the gas-to-oil ratio, on downstream market opportunities for gas recovery and on lawful and fiscal frameworks which may contain a variety of incentives and penalties (GGFR, 2002).

There are several options for gas utilisation such as:

- i. Gas re-injection into a reservoir;
- ii. Gas transportation;
- iii. Liquefied natural gas (LNG);
- iv. Hydrogen production;
- v. Gas to liquid technology (GTL).

2.8.1 Re-injection of Natural Gas

Gas reinjection is one of the oldest methods used to improve oil recovery and its use has increased in recent years (Lyons and Plisga, 2005). Once the oil production rate by primary recovery methods becomes uneconomic (due to the diminution of sufficient reservoir energy) injecting either water or gas (secondary recovery method) into the reservoir to build up the pressure that had decreased during the primary recovery process, can increase the oil production. Re-injection of natural gas into a reservoir for enhanced oil recovery, pressure maintenance, storage (for later use when markets are further developed) and also the important goal of routine flaring reduction, is one of its utilisation options. Due to the high cost of the process and to low incremental oil reserves, re-injection of associated gas is not always economic. Because of its contribution to causing dangerous environmental impacts, re-injection of carbon dioxide sometimes takes place in order to reduce its emission into the atmosphere. In addition to emission reduction, there are some advantages to gas re-injection, which are related to its reservoir characteristics (Schmidt, 2007). The rise in the flow of crude oil due to the pressure increase within the reservoir and viscosity reduction is one of these characteristics. Carbon dioxide swells the oil and reduces its viscosity so that it is neither hazardous nor explosive. Nevertheless, in some fields, re-injected gas may blemish oil production by adversely affecting its flow (Gaudernack, 1997). Combustion of natural gas in a cleaned environment to provide CO₂ can be used for miscible CO₂ flooding in enhancing or improving oil recovery from depleted reservoirs and consequently extending their life. It can act as an immiscible and a miscible displacement agent, depending on the composition and condition of the oil reservoir (Poettman, 1983).

2.8.2 Gas Transportation

Due to its volume, natural gas needs to be transported after production and treatment to where the industry needs. There are many options for gas energy transportation from natural gas sources to market (Marongiu-Porcu et al., 2008). Natural gas can be transmitted via several methods and the method must be determined taking into account technical, commercial and marketing issues such as:

- i. The volume of gas to be transported is dependent on both the gas reserve in the field and the demand in the market;
- ii. The availability of infrastructure between the gas production facilities and the market, such as gas pipeline transportation and a distribution network;
- iii. The nature of the geographical terrain of the gas field (land or onshore, offshore, swamp, desert etc.);
- iv. The distance between the gas gathering system and the market;
- v. The political stability of the host country, the security around the location and the possibility of supply interruption.

Natural gas transportation options are briefly discussed below.

2.8.2.1 Gas to Pipelines

Gas can be transported by means of large diameter pipelines (depending on capacity) for further processing or to be treated to become pipeline sales gas, which can then be delivered to consumers (Hughes, 1992). An increase in the capacity for transportation to industrial and domestic markets allows more gas volume to be transported. These pipelines utilise a series of compressor stations, usually spaced at about 50 – 100 miles'

intervals along the pipeline, to transport the gas over long distances. The processing of natural gas can be quite intricate and typically embraces different processes to remove oil, water and gases such as H₂S, SO₂, helium, carbon dioxide and natural gas liquids (EIA, 2006). The gas must be purified before its pipe transportation to prevent formation of liquid condensate or hydrate. Natural gas suitable for pipeline transmission should contain less than the levels of contaminants shown in Table 2.3 (Mohitpour et al., 2005).

Expanding the natural gas pipeline network is one of the ways to increase the domestic utilisation of natural gas and reduce its flaring (Sonibare and Akeredolu, 2006). The transportation of natural gas through pipelines is the most cost-effective method, but it can provide only small quantities of natural gas for which large-scale transportation, since pipelines have geographical and economic limits (Adegoke, 2006).

Sulphur, S	115	mg/m ³
Hydrogen sulphide, H ₂ S	23	gm/m ³
Carbon dioxide, CO ₂	2	% volume
Oxygen, O ₂	0.4	% volume
Water, H ₂ O	65	mg/m ³

Table 2.2: Pipeline gas quality specifications

2.8.2.2 Power Generation

Natural gas is used as a fuel in gas turbines for electricity generation. Power generation is one of the major potential markets for natural gas. In addition to a demand for power, there is also a demand for heat. After the treatment of natural gas, it may be transported

to power plants and combusted in boilers and turbines to generate electricity. Utilisation of natural gas for power generation looks to be a good alternative for diminishing gas flaring (Sonibare and Akeredolu, 2006). As an alternative fuel in power generation facilities, the utilisation of gas can lead to economic, environmental and efficiency benefits (Indriani, 2005). Using gas to make the power supply cheaper for urban households can create a more sustainable practice (GGFR, 2004). It is possible to generate electricity at, or near, the gas source by a conversion of the combustion heat of natural gas into electrical energy and then transport it by cable to the required destinations (Mokhatab et al., 2006). Two options which are classified as small-scale projects are electrical power generation at an oil field for transmission to an existing grid, and power generation at an oil field for the electrification of non-electrified rural areas.

2.8.3 Liquefied Natural Gas

Liquefied natural gas (LNG) technology has been in use since the mid-1970s. It is an option for natural gas utilisation where natural gas can be used as a feedstock for the natural gas-based chemical manufacturing industry. When distances become too great for pipelines, the option of transportation of natural gas via tankers across the oceans is recommended. It needs to be converted into a condensed form to minimise the volume storage requirement. Economically, because of gas volume, the transport cost of natural gas is much more than that of liquids. Firstly, the gas is pre-treated to remove any pollutants and then the gas is cooled by refrigerant streams to separate the heavier hydrocarbons. Liquefaction of natural gas produces liquid natural gas (LNG) at temperature of about -162 °C at atmospheric pressure (Ayala, 2006). LNG has a volume

ratio of about 1/600 to gas at room temperature (Mokhatab et al., 2006). Huge double insulation tanks are used for storage of LNG before transportation to consumers, who re-gasify from the liquid to gas for industrial use. The whole supply sequence for LNG includes: gas liquefaction, shipping, storage and re-gasification.

2.8.4 Hydrogen Production

Globally, approximately 45-50 million tonnes of hydrogen are produced annually, the majority of which is produced using fossil fuel feedstocks and about a half of the world's hydrogen demand is supplied via the steam reforming of methane, due to an increase in natural gas production (Evers, 2008). As mentioned in previous sections, natural gas contains mainly methane (CH₄) which can be used to produce hydrogen and carbon monoxide (syngas) via thermal processes such as steam reforming, partial oxidation or autothermal reforming (which is a combination of the other two processes). Steam reforming of natural gas is created in a tubular reactor with catalyst-filled tubes to produce syngas. H₂ can be separated from syngas by membrane or by the pressure-swing adsorption method. Furthermore, companies, organisations and scientists are still looking for other methods to utilise flare gas.

2.8.5 Gas to Liquid Technology

Gas to liquid technology (GTL) is the chemical conversion of natural gas (*mainly methane*) into liquid fuels. It is an appropriate natural gas utilisation option. The reasons to convert natural gas into liquid products using GTL technology include:

- i. Most gas reserves are far away from consumers and difficult or costly to transport, due to the greater volume of gas as compared to the liquid phase;
- ii. The presence of large quantities of associated gas, which is difficult to utilise at site, produced with oil;
- iii. The need for high quality, cleaner transport fuels.

The GTL process is based on two primary steps:

- i. The conversion of natural gas into synthesis gas by reaction with oxygen in a process of catalytic partial oxidation to produce synthesis gas, consisting primarily of carbon monoxide and hydrogen;
- ii. The conversion of synthesis gas into synthetic crude, in a reaction based on Fischer-Tropsch (FT) process. The synthesis gas flows into a reactor containing a proprietary catalyst, converting it into viscous liquid hydrocarbons.

Global oil companies, governments and environmentalists are looking at the need for new sources of transportation fuel. GTL is being marketed as a clean, environmentally friendly fuel in several countries. It produces liquid fuels from natural gas by catalytic processing to give either diesel, methanol, gasoline or waxes. The Fischer-Tropsch process, which was discovered in 1923 by German scientists, has been used for a long time for gas to liquid technology (Almeida, 2003). Two main technologies are used for gas to liquid (GTL) technology to produce synthetic petroleum products: an indirect conversion via syngas and a direct conversion from gas using partial oxidation (Keshav and Basu, 2007).

The GTL process produces very high quality fuel such as diesel, methanol or gasoline. They are colourless and completely free of both sulphur and aromatics (Aasberg-Petersen et al., 2003). Economically, due to volume, gas transport costs are 3 to 10 times more expensive than oil transportation costs (Almeida, 2003). The increased cost of natural gas over increasing transportation distances is a major problem (Dong et al., 2001). Because of this, the *onsite conversion* of natural gas, that previously would have been flared, into a liquid product is the best option to take advantage of the energy that once would have been wasted. The main technologies for syngas production from natural gas are steam reforming and partial oxidation (Ruiz et al., 2008).

Conversion of natural gas into liquid chemical products requires the production of synthesis gas in the first stage, which is a mixture of hydrogen and carbon monoxide. In the second stage, the syngas produced is converted into liquid fuels using GTL technology via the Fischer-Tropsch process. Economically, gas transport costs are much higher than that of liquid transport costs due to volume and GTL plant products present important environmental advantages when compared to conventional products (Almeida, 2003). The products produced by this technology, present essential environmental advantages compared to conventional products.

There are three major thermo-chemical reforming techniques used for natural gas to liquid transformation. These are steam reforming, autothermal reforming and partial oxidation (Chan and Wang, 2000).

2.8.5.1 Methane Steam Reforming

The first known use of steam reforming application was in 1923, when the first synthetic methanol was produced by BASF in Leuna, Germany. Steam reforming of natural gas (also designated as methane-steam reforming (SMR)) is one of the main industrial methods for the production of synthesis gas. It has been used for several decades in the production of hydrogen. (Van Beurden, 2004). The traditional steam methane reforming process consists of the pre-treatment and preheating of feed gas, reforming, high and low temperature shift, CO₂ removal and methanation. Catalysts (nickel-alumina) are used in this process in order to accelerate it and to attain acceptable reaction rates, and the reaction between natural gas or other hydrocarbons and steam takes place to produce carbon monoxide and hydrogen. Natural gas steam reformation is a strongly endothermic reaction whereby a large amount of heat is supplied by fuel burning in the furnace chamber (Olivieri and Veglio, 2008).

(i) *Chemistry of SMR*

The steam reforming of methane follows the following sequential reactions: a two-step process whereby, natural gas is exposed to high-temperature steam in order to produce hydrogen, carbon monoxide and carbon dioxide. This is followed by a water gas shift reaction. Thus, the process consists of the following two steps:

- i. *Reformation of Natural Gas:* The first step involves methane reacting with steam at 750-800° C to produce a synthesis gas;
- ii. *Shift Reaction:* In the second step, known as a water gas shift (WGS) reaction, the carbon monoxide produced in the first reaction is reacted with steam over a

catalyst to form hydrogen and carbon dioxide (CO₂). This process occurs in two stages, consisting of a high temperature shift (HTS) at 350 °C and a low temperature shift (LTS) at 190-210 °C. The second stage is to convert the carbon monoxide with steam to produce additional hydrogen and carbon dioxide.

The reactions are:



Reactions 2.1 and 2.3 are endothermic reforming reactions and reaction 2.2 is an exothermic water-gas shift reaction. Carbon dioxide is not only produced via reaction 2.2 but also directly via the steam reforming reaction 2.3. CH₄ conversion is enhanced by increasing the amount of steam, which requires more energy for its production. The steam to carbon ratio ranges between 3 and 4, which will suppress carbon formation during the reaction (Rostrup-Nielsen et al., 2002).

(ii) Steam reforming kinetics

The kinetics of the steam reforming of methane has been the subject of several studies. In 1933, Fujimoto investigated the kinetics of methane steam reforming and methane decomposition (Hook, 1980).

Steam reformers are fed with a high temperature mixture of natural gas and steam. Because of the endothermicity of the reaction, an external heat source is required. For the complete conversion of methane high temperatures in the catalyst system are

essential. In fact, 80% conversion of methane at temperatures up to 850 °C is commonly achieved with H₂O/CH₄ feed ratios in the range 2 to 5.

A traditional steam-reformer is operated at about 15 – 30 atm and at 850 – 900 °C with a nickel-based catalyst. The catalyst is loaded into a number of tubes located in the furnace, (Abashar, 2004). At these high temperatures and in the presence of a catalyst, steam reacts with methane to give hydrogen and carbon monoxide. The produced carbon monoxide can be integrated with more steam to produce hydrogen through the water gas shift reaction. However, this process requires large amounts of energy and also suffers from the limitation of a high H₂/CO product ratio, which is unsuitable for methanol or for the Fischer–Tropsch synthesis.

(iii) Membrane steam reforming reactor

Recent developments that improve methane steam reforming are by the use of new materials and the technology of the reactor. In conventional technology, the SMR reaction is carried out using multitubular fixed-bed reactors. As reported in recent literature, by using membrane reactors (MRs) it is possible to reduce some of the operating constraints such as pressure and temperature (Oklany et al., 1998). Membrane reactors combine chemical conversion with a membrane separation step. Their application with methane steam reforming allows the equilibrium of the reaction to shift in a favourable direction. Thus, they can be operated at lower temperatures (Dixon, 2003).

Major potential applications for mixed-conducting ceramic membranes in the chemical and petroleum industries are as separators for air separation and as membrane reactors

for partial oxidative reactions. The ceramic membrane technology for air separation is economically attractive when integrated with a hot-turbine system (Kung et al., 1996).

2.8.5.2 Autothermal Reforming

Autothermal reforming of natural gas (ATR) is a combination of steam reforming with a partial oxidation reaction in which the endothermic and exothermic reactions are coupled (Moulijn et al., 2001). These systems can be very productive, fast starting and compact, since the exothermic partial oxidation reaction can supply heat to the steam reforming reaction directly. This solution does not require an external heat source and allows a more compact construction with respect to conventional SMR.

The ATR process consists of a natural gas preheat section, a reactor and heat recovery section and a gas separation unit. The steam reforming of natural gas takes place in the autothermal reformer. A mixture of natural gas steam and oxygen is fed to the reactor. Partial oxidation reactions occur in a combustion zone and the products then pass through a catalyst bed where reforming reactions occur. The ATR reactor consists of a refractory lined pressure vessel with a burner, a combustion chamber and a catalyst bed. It has a design similar to that of the methane partial oxidation (POM) reactor but contains a catalyst bed in the last part. The produced syngas temperature is about 1,025°C as compared to 1,375 °C for the POM reactor (Jager and Espinoza, 1995). This reduction in the syngas temperature is required by the presence of the catalyst which does not support higher temperature values.

2.8.5.3 Partial Oxidation of Methane

Partial oxidation of methane (POM) is the catalytic conversion oxidation process of methane to synthesis gas ($\text{CO} + \text{H}_2$), which is used as a feedstock for many important industrial processes such as methanol synthesis or for the Fischer–Tropsch (FT) process. Studies on the process of partial oxidation of methane to syngas have been conducted by a number of investigators (Ashcroft et al., 1990, Choudhary et al., 1992 and Li, 2007). The H_2/CO product ratio is 2, which is suitable for Fischer-Tropsch (GTL technology) or for methanol synthesis (Wang et al., 2006). The reaction is denoted by the following equation:



Pure oxygen is used instead of steam, at an elevated pressure and temperature as an oxidiser of the natural gas. One of the main problems with this process is the oxygen source which is conventionally produced by cryogenic distillation of air in an air separation plant. Oxygen must be separated from the air before being fed to the syngas reactor. Partial oxidation of methane using a dense ceramic membrane reactor is a very good option for synthesis gas production.

2.8.5.4 Comparison Between Steam Reforming and Partial Oxidation of Methane

In a comparison between the partial oxidation process and the steam reforming process, the partial oxidation process is more acceptable than the steam reforming process (Keshav and Basu, 2007 and Ruiz et al., 2008) due to:

- i. A simpler and less expensive reactor design;

- ii. The H_2/CO ratio is close to 2 with very small amounts of CO_2 in the product, while the product from SMR has a H_2/CO ratio of 3 or higher with a significant amount of CO_2 ;
- iii. The SMR process requires a large amount of gas to be used for heating because of the endothermic process.

The use of oxygen is a big disadvantage for the partial oxidation process, as compared to the SMR process, due to the additional capital required and the operating cost of an air separation plant. Therefore, in order to reduce the overall cost of synthesis gas production using the partial oxidation process by minimising the cost of oxygen generation, certain ceramic membrane tubes may be used for their ability to separate oxygen from air and thus avoid the need of a separation plant (Zeng et al., 2003).

The production of synthesis gas ($CO + H_2$) using ceramic membranes and the generation of single-walled carbon nanotubes using sprays and atomisation techniques are the two proposed options which were studied in this research for the utilisation of natural gas that was previously flared. The next sections present a brief overview of these processes.

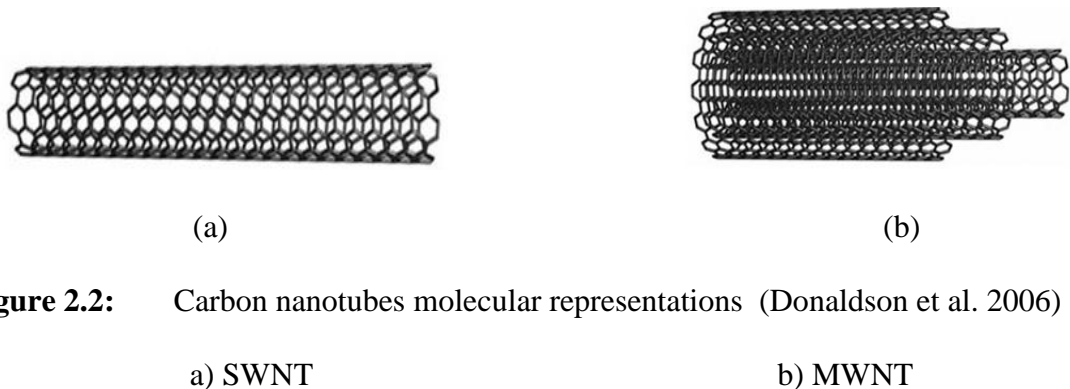
2.9 Synthesis Gas Production

Synthesis gas or syngas is described as a mixture of carbon monoxide and hydrogen. It is produced by the gasification of coal, oil residue, biomass and by the reforming of natural gas which provides the lowest cost route at present when compared to other carbon-based feed stocks (Wilhelm et al., 2001). The transformation of natural gas into other types of liquid chemical products requires, advantageously, the production of

synthesis gas in a first stage (Ikeguchi et al., 2005 and Eliseev, 2009). With an increasing demand for syngas in the global energy market, new methods for its production need to be discovered. One of the promising methods for syngas production is using ceramic membranes (metal oxides) as an oxygen supplier and oxygen distributor (Balachandran et al., 1997). In this research, the conversion of natural gas, that was previously flared, to syngas through partial oxidation (see Section 2.8.5.3) by using ceramic membrane reactors is investigated as one of the two proposed options in this study. This process is discussed in detail in Chapters 3 and 4.

2.10 Carbon Nanotubes

A carbon nanotube is a hexagonal lattice of carbon atoms rolled into a cylinder. Since their discovery in 1991 by Sumio Iijima (Iijima, 1991 and Reich et al., 2004) carbon nanotubes (CNTs), in the form of cylinders both long and thin, have been investigated by many researchers worldwide. CNTs can be classified into two kinds: Single-Walled Carbon Nanotubes (SWNTs) which are formed by only one single graphite layer and Multi-Walled Carbon Nanotubes (MWNTs) which consist of multiple concentric graphite layers (Donaldson et al., 2006 and Samal and Bal, 2008) as shown in Figure 2.2.



These graphite layers are wrapped around themselves to form a cylinder. CNTs can be either metallic or semi-conductive, depending on the number of the concentric walls and the ways that the graphite sheets are rolled into a cylinder (Dresselhaus et al., 1996). In their single-walled form SWNTs are typically around 0.7 - 3 nm in diameter (Jorio et al., 2001) and are of the order of 100 nm in length. MWNT normally range from 10 to 200 nm in diameter (Hou et al., 2003). They occur in three different structural forms with different diameters. Carbon nanotubes can have different individual structures and properties which are determined by the production method. The atomic structure variations of the tubes may result in some changes to their properties (Lieber, 2001).

Due to their low power, low weight and small size, CNTs have been used in many applications such as semiconductors, electronic memory, drive products, energy storage (H₂ storage and fuel cells), chemical and biological separations, molecular electronics, scanning probes, field emission devices for X-ray instruments and nano-electronic devices (Meyyappan, 2005).

In December 2010, the Sunday Times reported the investigation of carbon nanotubes that Leake and Flynn, from King's College London, discovered for creating the world first space elevator. Space elevators are extremely tall with theoretical structures that stretch beyond the earth's atmosphere to carry satellites and shuttles into outer space without the cost and environmental impact of rocket fuelled launches. The team claimed that advances in carbon nanotubes could make it theoretically possible, create a tie that would be strong enough to stretch more than 22,000 miles into space.

The purification of CNTs is typically achieved by washing with them dilute acid to remove impurities like “soot” and to free them of any remaining catalyst and any support materials.

2.10.1 Carbon Nanotubes Synthesis

The first observations that Sumio Iijima made in 1991 were of multi-walled nanotubes and, after a further two years, single wall nanotubes were observed. In 1996 Smalley synthesized bundles of single wall carbon nanotubes for the first time (Paradise and Goswami, 2007).

The common methods that are used to synthesise CNTs are (Thess et al., 1996, Bhusham, 2006 and Donaldson et al., 2006):

- i. Laser vaporisation of graphite;
- ii. Chemical vapour deposition (CVD);
- iii. Arc discharge.

These methods are described briefly in the following subsections.

2.10.1.1 Laser Vaporisation Method

In 1995 Smalley’s group at Rice University reported the generation of CNTs by laser vaporisation (Gue et al., 1995). In this method, the laser is used to vaporise the carbon that condenses as SWNT. Graphite is vaporised using a pulsed or continuous laser inside a furnace at 1200 °C, which is filled with helium or argon gas in order to keep the pressure at around 500 Torr. The vapour expands and cools quickly after the formation

of a very hot vapour plume. At the same time as the vaporised species cool, small carbon molecules rapidly condense to form larger clusters and then tubular molecules grow into SWNTs from these initial clusters.

2.10.1.2 Chemical Vapour Deposition

In the early stages of CNT research, it was believed that the Chemical Vapour Deposition (CVD) method was useful for synthesising MWCNT but not SWCNT. In 1996, Dai et al. concluded that SWNT could be produced by the CVD method. In this method, metal particles (Co, Ni, Fe etc.) are deposited on the support catalyst and then the catalyst on its support is placed in a quartz boat which is placed in the CVD furnace. A mixture of hydrocarbons and hydrogen is introduced into the reaction chamber. CNTs are then formed by the decomposition of hydrocarbon during the reaction at temperatures of 700 – 900 °C.

2.10.1.3 Arc Discharge

In this method, a vapour is created between two carbon electrodes (cathode and anode), with or without a catalyst, by an arc discharge which is generated by a high dc current in a helium or argon atmosphere and nanotubes self-assemble from the resulting carbon vapour (Bhusham, 2006). A high temperature discharge is provided between the two electrodes by a direct current of 50 to 100 amps at 20 volts. A tiny rod shape is formed from the anode rod vaporisation by the high temperature discharge and is deposited on the cathode rod. If both electrodes contain pure graphite, MWCNT can be synthesised.

For producing SWCNT the anode has to be doped with a metal catalyst such as Co, Ni and Fe.

2.10.2 CNTs Generation Using Sprays and Atomisation Techniques

The mechanism of generating single walled carbon nanotubes (SWCNTs) may depend on the production method used because there is a variation in the different methods. Due to the limitations and drawbacks in the methods currently being used, researchers are still looking for better processes. The Arc discharge method is reported to yield significantly less carbon nanotubes with a large amount of unwanted carbonaceous by-products. The high costs of operation and equipment, as well as a low production rate, limit the laser vaporisation method (Chai et al., 2004). An attractive alternative is the use of natural gas (instead of flaring the gas) to produce single-walled carbon nanotubes. The idea is to spray a solution of the transition metal catalysts such as Ni or Fe (to produce fine droplets of $D_{n0.50} < 5 \mu\text{m}$) into the methane gas stream which is used as a carbon feedstock. The stream of droplet particles falls down through the hot furnace (at about 800 °C). The reaction with CH_4 gives $\text{C} + 2\text{H}_2$ and the carbon, after dissolving in the metal particle, will reorganise to form the Single-Walled Carbon Nanotubes (SWCNT) material, while the hydrogen may be stored or used for another industry.

Chapter - 3

CHAPTER-3: MEMBRANES' OVERVIEW

3.1 Introduction

A general overview of membranes is presented in this chapter. The definition and classification of membranes are given and some perceptions of membrane reactors are considered. The fundamentals of the partial oxidation of methane to syngas using ceramic membranes are discussed. Membranes are used worldwide in many applications when one or more separation processes of one or more products are required. Their use for concentration, purification and separation of materials is important in industrial processes, as they provide higher efficiency and faster separations when compared with conventional operations. Currently, membrane technologies are becoming more frequently used for wide mixtures' separation in the oil industry and can compete with conventional methods.

3.2 What are Membranes?

The word membrane comes from the Latin word 'membrana' meaning thin skin or film and is regarded, commonly and macroscopically, as a selective barrier between two phases. Membranes can be described as thin physical barriers which separate two phases and control the transport of various chemical species in a rather specific manner (Hughes, 1996). This means that when a phase mixture is fed to the membrane, a part of it (permeate stream) will permeate through the membrane, while the remaining part (retentate stream) will not permeate (Geankoplis, 2003), as shown below in Figure 3.1.

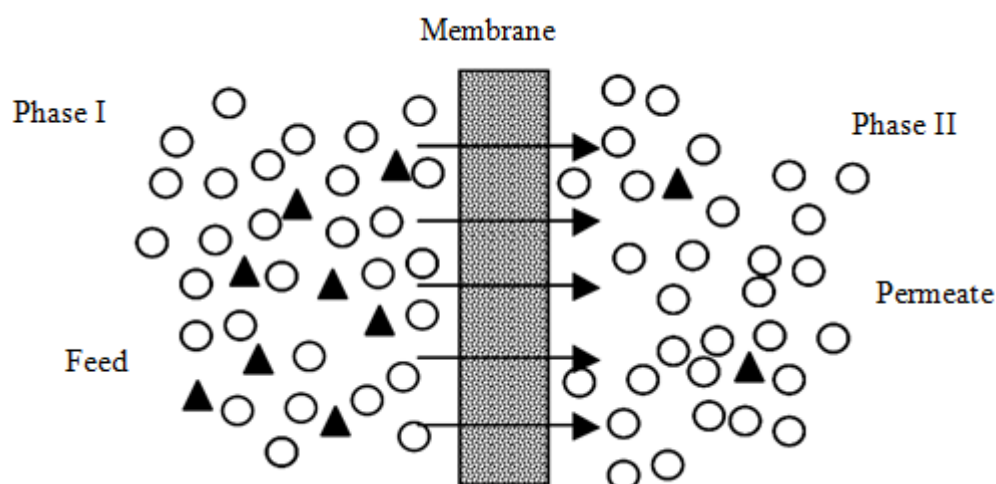


Figure 3.1: A membrane separation principle

Membranes are used as an active participant in a chemical transformation for increasing the reaction rate, selectivity and yield. They are used for different applications when separation processes for one or more products are required. Due to the wide range of components and chemicals in industrial processes, membrane usage for concentration, separation and purification is essential.

A membrane can be homogenous or heterogeneous, symmetric or asymmetric in structure, solid or liquid. It can also carry a positive or negative charge or can be neutral or bipolar. Membrane processes, in general terms, compete with conventional processes such as adsorption, absorption and cryogenics.

When compared with conventional processes which are complex and energy intensive (Asaeda and Yamasaki, 2001), the use of membranes generally presents faster separation and higher efficiency. The following advantages of membrane processes make them potentially attractive (Ravanchi, 2009):

- i. Ease of operation;

- ii. Low energy consumption;
- iii. Small space requirement;
- iv. Minimal utilities and maintenance;
- v. Fast start-up / shut-down;
- vi. Reduced capital and operation costs;
- vii. Long on-stream time;
- viii. Environmentally beneficial because only relatively simple and non-harmful materials are required.

Membranes can be divided into two classes based on synthesised materials, i.e. organic (mainly polymers) and inorganic membranes.

3.2.1 Organic Membranes

Organic (polymeric) membranes are used for a wide range of industrial applications such as gas separation, microfiltration, ultrafiltration and reverse osmosis. Polymeric membrane separation is an important process that is aimed at decreasing production costs, energy utilisation, waste generation and equipment size (Dautzenberg and Mukherjee, 2001). Some polymeric membrane materials suffer from the inherent drawback of a trade-off effect between permeability and selectivity, which means that membranes which are less permeable are more selective and vice versa (Hughes, 1996). However, there are some limitations in the use of conventional polymeric membranes which are:

- i- Their performance has achieved a maximum stage and it is difficult to gain further significant improvement;

- ii- They cannot operate in corrosive and high temperature environments.

To overcome these limitations many researchers have investigated inorganic membranes for wider processes' requirements.

3.2.2 Inorganic Membranes

Inorganic membranes have superior qualities when compared with polymeric membranes, including high thermal, mechanical and chemical stability. However, they are more expensive (Armor, 1992). Due to these factors their use in high temperature gas separation and catalytic reactors is attractive (Hwang, 2001). In contrast to organic membranes, inorganic membranes can operate in corrosive and high temperature environments, due to the wide range of materials that may be used in their fabrication. In addition, there are other advantages to these membranes, which are microbial resistance, high flux, easy cleaning and easy modification.

Inorganic membranes can be further classified into dense (nonporous) or porous membranes. The types that are commonly used in industrial applications are ceramic, glass, carbon and metal membranes (Hughes, 1996 and Jin et al., 2000b). The resistance to mass transfer is determined by the total membrane thickness, a decrease in which results in an increase in permeation rate.

3.2.2.1 Porous Membranes

Porous membranes present reasonably high permeability, but relatively low selectivity, while the opposite characteristics are observed in non-porous membranes (Uhlhorn and Burggraaf, 1991). Porous membranes consist of a porous wall or a porous top layer

(metal oxide) on a porous (metal-oxide) support. Based on the average pore width, porous membranes can be classified into macropores, mesopores and micropores as shown in Table 3.1. .

<i>Membrane type</i>	<i>Average pore width, nm</i>	<i>Selectivity</i>	<i>Permeability</i>
Macropores	50	Non selective	High
Mesopores	2-50	Low to moderate	Moderate to high
Micropores	>2	Can be very selective	Moderate

Table 3.1: Classification of porous membranes

The transport mechanisms of gases through porous membranes depend on the pore size distributions which cause local variations in diffusion rates within the void space. Diffusional transport can occur by either bulk diffusion or by Knudsen flow mechanisms. Bulk diffusion does not provide any separation, so efforts have generally been concentrated on the Knudsen regime.

- ***Knudsen flow mechanisms***

The occurrence of Knudsen flow is basically determined by the pore size. The proportions of flow are governed by the ratio of the pore radius (r_p) to the mean free path (λ) of the gas (Li, 2007).

The mean free path λ is defined as:

$$\lambda = \frac{RT}{\sqrt{2} \pi N d^2 P_a} \quad (3.1)$$

Where R is the gas constant, T , the temperature, K , d , the collision diameter of gas molecules, (m) , N , the Avogadro number, and P_a , the average pressure across the membrane (Pa).

The Knudsen molar flux can be expressed as:

$$J_k = -D_k \left(\frac{dc}{dz} \right) \quad (3.2)$$

Where D_k is the Knudsen diffusion coefficient and is dependent on the thermal mean velocity, v and pore radius r_p and is given by:

$$D_k = \frac{2}{3} v r_p \quad (3.3)$$

The thermal mean velocity of the gas molecules can be obtained from the kinetic theory of gases:

$$v = \sqrt{\frac{8RT}{\pi M}} \quad (3.4)$$

In the above equations, R is gas constant, J , the molar flux of gases, T , the temperature, P , the pressure, M , the molecular mass, and z , the distance coordinate. In a porous membrane, geometrical effects such as porosity (ϵ) and tortuosity (τ) play an important role. Taking these effects into account and substituting Equations 3.3 and 3.4 into Equation 3.2, the expression for Knudsen flow in a porous membrane is obtained by the equation:

$$J_k = - \frac{2 \epsilon r_p}{3 \tau} \left[\frac{8}{\pi R T M} \right]^{0.5} \frac{dp}{dz} \quad (3.5)$$

After the integration of Equation 3.5 over the membrane thickness b_m , the permeance F is found to be:

$$F_k = - \frac{J}{\Delta P} = \frac{2 \epsilon r_p}{3 b_m \tau} \left[\frac{8}{\pi R T M} \right]^{0.5} \quad (3.6)$$

The above equation shows that the permeation of gas in the Knudsen regime is proportional to the average pore radius r_p , is independent of the pressure and is proportional to the square root of its molecular mass, M .

3.2.2.2 Non-porous Membranes

Nonporous or dense membranes are mixed (electronic, ionic) conducting oxides for oxygen separation, or are made from a solid layer of metals (e.g. Pd alloys for hydrogen separation). Dense inorganic membranes are specific in their separation behaviour. Pd-metal based membranes are hydrogen specific and metal oxide membranes are oxygen specific (Khan and Islam, 2007).

Thin supported films and alloyed compositions have been recently developed in order to reduce membrane cost for Pd membranes. Dense ceramic membranes are also considered for gas separation and they have good permselectivity towards oxygen, which allows their use for the partial oxidation reactions (Iwahara et al., 2004 and Li, 2007). Dense oxygen ionic or proton conducting ceramic membranes are attracting increasing interest due to their technological advantages in high temperature (650-1000°C) gas separation (Jin et al., 2000b).

Solid oxide conductors are materials that present high ionic and low electronic conductivity and temperature plays an important role in these materials because, commonly, at high temperature these materials present high conductivity (Gao and Sammes, 1999). There is another class of these materials which has considerable importance for many applications requiring gas separations. This class is classified as mixed ionic-electronic conductors (MIEC), in which the electronic conductivity is as

important as ionic conductivity. The MIEC membrane is a dense material where the passage of molecules is not possible. It will permeate oxygen ions but not other gases in an air separation.

Ceramic materials such as dense perovskite type oxides have been proposed in the literature as useful oxygen permeating membranes (Balachandran et al., 1995, Tsai et al., 1997 and Li, 2000). Perovskite (calcium titanium oxide CaTiO_3) is the generic name for the structural family with the general formula ABO_3 . The A cations are generally alkaline earth or lanthanide ions, the B cations are usually transition metal ions and the O anions are either oxygen or halide ions. The parent mineral of this type was first described after samples were found in the Ural Mountains in 1839 by Gustav Rose, who named it after the famous Russian mineralogist Count Lev Aleksevich von Perovski (Michel, 2010). Recently, perovskite-type ABO_3 oxides have been comprehensively investigated by a number of researchers as materials for many applications such as oxygen separation, catalytic membrane reactors, or solid oxide fuel cell electrodes (Pena and Fierro, 2001).

Oxygen fluxes through these membranes may be improved if the thickness of the membrane tubes could be reduced as thin as they can be. Although it is not practical to produce single LSCF tubes of thicknesses as small as 0.002 cm, one possibility to achieve this is a deposition of a thin layer of LSCF powder onto porous substrate tubes such as alumina. Such thin layers' powder can be produced by sol-gel, solid-state and combustion spray pyrolysis methods which are briefly discussed in the following sections.

3.3 Synthesis of Ceramic Membrane Powders

Ceramic membranes are produced by mixing metal with non-metal, in the form of an oxide, nitride or carbide. They have been shown to permeate oxygen exclusively at high temperatures. Thus, the use of these materials in the form of membrane tubes, which can be used in a tubular reactor, enables oxygen to be separated from air (Richardson et al., 2004 and Thursfield and Metcalfe, 2007).

There are three major preparation techniques used to synthesis ceramic powders, which are sol-gel, solid-state and combustion spray pyrolysis. The following sections present the unique characteristics of each method.

3.3.1 Sol-gel Method

Sol-gel techniques use aqueous solutions in order to acquire homogenous fine powders. It involves the hydrolysis of metal alkoxides or nitrates in a presence of chelating ligands (Burggraaf, 1992). The major three chelating ligands frequently used are ethylene-diamine-tetraacetic acid (EDTA), citric acid and glycine. To enhance the polymerisation, heating and stirring for several hours are needed to obtain the solution of precursors with the chelating ligands and liquid. Aqueous ammonia is also often used to ease the dissolution of EDTA and control the pH in the range of 8 to 10. Then, a gel should be obtained without any visible precipitation which is then pyrolysed at 200-350°C to remove the organics. Afterwards, the resulting powder is then calcined at high temperatures (900-1200°C) to get the desired structure. The main drawbacks of the sol-gel method are the low production rate and the time consumption.

3.3.2 Solid-state Method

Because of its preparation simplicity, the solid-state method can be used for ceramic powder synthesis. It consists of mechanical mixing of the metal oxide or carbonate precursors of the membrane followed by calcining. To improve mixing, ethanol is normally added to the oxides. The solid-state method involves a mortar grinder used to mix and grind a stoichiometric ratio of the metal precursors for around a day in order to get the given membrane composition. According to Liu et al., 2002, some disadvantages are noticed such as contamination during the milling and mixing and large powder agglomerates.

3.3.3 Combustion Spray Pyrolysis Method

This method involves the preparation of a solution of the metal nitrates (oxidiser) of the required stoichiometry with a carbohydrate (fuel source). The solution is fed as a fine spray into a reaction chamber and dried by heating. An explosive exothermic reaction is initiated, when additional heat is supplied to the dry particles, to enhance the metal nitrates' conversion to their respective oxides and/or carbonates as nanometer sized particles (Kodas et al., 1998).

3.4 Membrane Reactors

A membrane reactor is a term describing a number of different types of reactor configurations that contain a membrane. Membrane reactors are defined as membranes that combine their separation characteristics with a chemical reaction to upgrade the reaction process (Hughes, 1996 and Thursfield and Metcalfe, 2007). Most membrane

reactors' applications use inorganic membranes, which can be dense or porous, inert or catalytically active. Because of the generally severe conditions of heterogeneous catalysis, this has led scientists to pay attention to this type of membrane because of the above mentioned properties. The importance of membrane reactors has been largely demonstrated at the laboratory scale, namely for hydrogenation, dehydrogenation, decomposition and oxidation reactions including partial oxidation and oxidative coupling of methane. In a membrane reactor, the separation properties of a membrane are utilised to improve the performance of a catalytic system. The key operating principle of a membrane reactor is to improve the reaction rate and shift any reaction equilibrium in a favourable direction by selectively removing reaction product(s) from the reaction chamber via permeation through a membrane (Uemiya, 2004).

The possibility of combining separation and reaction in one stage, which is the major advantage of using membrane reactors, could reduce the overall operation costs and overcome the equilibrium restrictions experienced in conventional reactor arrangements (Dixon, 2006). The factors that affect the performance of the membranes are partial pressure, temperature, the flow rate of gases, membrane thickness and membrane composition (Tan et al., 2003). The advantage of this type of membrane over the fixed bed reactor is the control of the reactant concentration. This can be done by adjusting the reactant feed pressure which will affect the product selectivity (Kao et al., 1997). To avoid the danger of explosion in oxidation reactions due to simultaneous feed of both hydrocarbon and air (or oxygen) into the reactor, both should be fed separately and flow rates can be controlled independently of each other (Santamaria et al., 1992).

According to the purpose of the membrane in the process, the combination of membranes and reactors is being explored in various arrangements, which can be categorised into the following three classes, as illustrated in Figure 3.2 (Julbe et al., 2001 and Miachon et al., 2003):

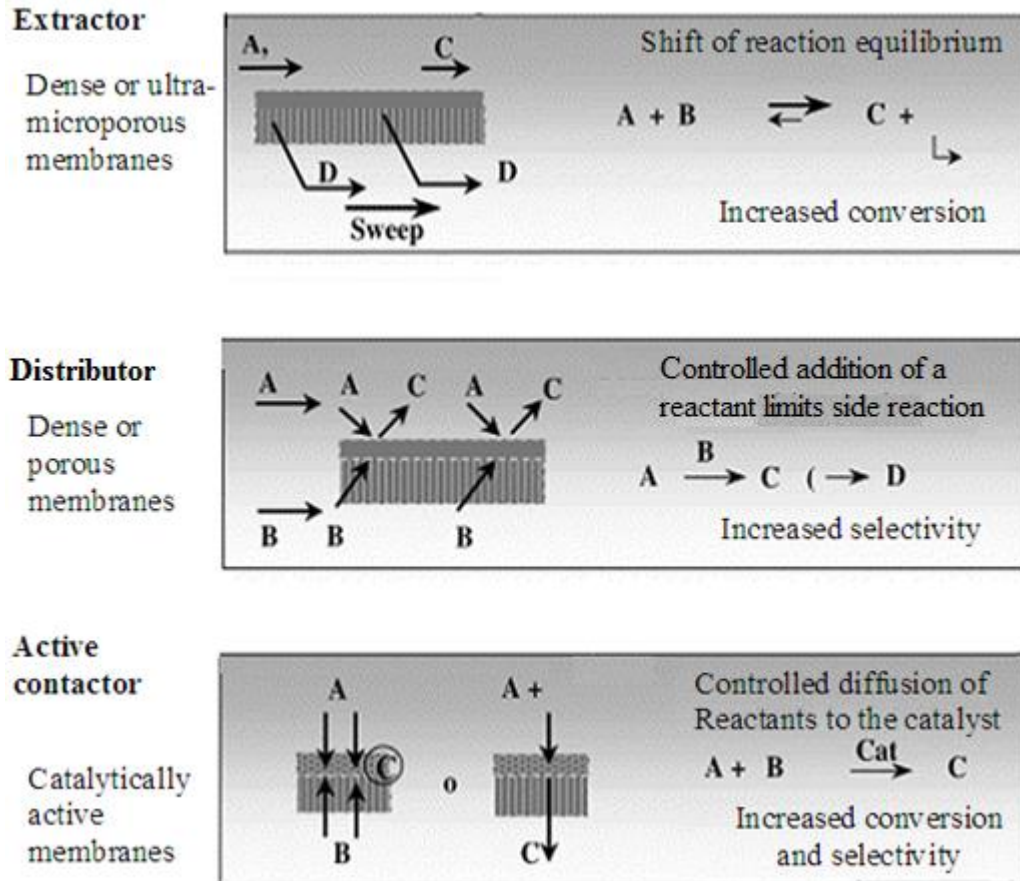


Figure 3.2: The main membrane functions in the membrane reactor

- i. An extractor;
- ii. A distributor;
- iii. An active contactor.

The extractor concept has been applied to increase the conversion of a number of equilibrium limited reactions such as alkane dehydrogenation, by selectively extracting the hydrogen produced.

The distributor concept is usually applied to consecutive parallel reaction systems such as partial oxidation of hydrocarbons or the oxidative coupling of methane. The membrane is normally used to control the oxygen supply in a fixed bed of catalyst in order to avoid the flammability area, to optimise the oxygen profile concentration along the reactor, and to maximise the selectivity in the required oxygenate product (Julbe et al., 2001). An example of the membrane distributor is the process for converting methane to syngas by partial oxidation. Using a membrane for the distributive feeding of oxygen along the axial coordinate to the catalyst bed allows high reactant conversions and high product selectivities to be combined (Deshmukh, 2004).

In the active contactor manner, the membrane acts as a diffusion hurdle and does not need to be permselective, but is catalytically active. The process can be used with a forced flow-mode or with an opposing reactant mode (Julbe et al., 2001).

According to Yang et al. (2005), there are many requirements that need to be met in order to have viable industrial membrane reactors such as:

- i. The membrane material must have a very high reactant flux during the reaction period;
- ii. It must show considerable long-term mechanical and thermal stability under a reaction reducing environment;
- iii. The membrane material and its preparation method must be reasonably priced.

3.5 Ceramic Membrane Reactors

3.5.1 Natural Gas Conversion into Syngas by Partial Oxidation

With an increasing demand for syngas in the global energy market, attention is being paid to new methods for its production. One of the promising methods, as shown in the literature, is using ceramic membranes as an oxygen supplier and oxygen distributor (Balachandran et al., 1997). In recent decades, mixed ionic and electronic conductive (MIEC) ceramic membranes have received considerable attention for many applications requiring gas separation. These materials have ionic conduction properties due to the presence of oxygen vacancies in the pattern structure (Li, 2007). These ceramic membranes are selective to oxygen and the oxygen produced from them is cheap and safe. Also, they eliminate the need for a high cost air separation plant, as they can be integrated into the syngas generator (Gopalan, 2002).

Partial oxidation of natural gas (see Section 2.8.5.3) is an alternative route for syngas production, due to the fact that the reaction produces a favourable H₂ and CO (2:1) ratio and is mildly exothermic (Hickman and Schmidt, 1993). A membrane reactor for partial oxidation of methane to syngas is simpler and consumes less energy than the methane steam reforming (MSR) process (see Section 2.8.5.4) due to its exothermic reaction. Also, it has a fast start-up compared with the MSR process. Zeng et al. (2003) have stated that if the rate of oxygen supplied to react with methane is high, the ratio of O₂/CH₄ near the membrane is high and combustion reactions are favoured. If it is low, the ratio of O₂/CH₄ could be closer to 0.5 than 2 and partial oxidation reactions are more likely.

Oxygen permselective dense membranes include metallic (Ag) or ceramic membranes (e.g. Yttrium-stabilized zirconia (YSZ), BiMeVO_x , $\text{La}_2\text{NiO}_{4+\delta}$ or $(\text{La-Sr})(\text{Fe-Co})\text{O}_{3-\delta}$ perovskites and related oxides).

A semi-permeable ion conducting ceramic membrane is a dense membrane that utilises oxygen (Li et al., 2000). Conventional methods for oxygen production employ cryogenic distillation or pressure swing adsorption, both of which are very costly methods as they cost more than a third of the process capital cost (Zeng et al., 2003 and Tan et al., 2005). In order to reduce the overall cost of the partial oxidation process, the minimisation of oxygen generation cost is the major goal (Kumar et al., 2009). An alternative is a reactor made of mixed ionic-conducting perovskite tubes through which oxygen ions can be transported under an oxygen partial pressure or an electric potential gradient across the membranes (Zeng et al., 2003). A good candidate material is $\text{La}_{0.6}\text{Sr}_{0.4}\text{Co}_{0.2}\text{Fe}_{0.8}\text{O}_{3-\delta}$, known as LSCF (6428), which has the ability to filter oxygen out of air (Thursfield and Metcalfe, 2007).

3.5.1.1 Oxygen Permeation in Perovskite Membranes

The high costs of pure oxygen generation have led to the exploration of the use of mixed ionic-electronic conducting ceramic membranes (MIECs) as an alternative oxygen source for syngas production reactors (Dong et al., 2001). The permeation of oxygen ions through ceramic membranes is affected by driving forces, which are the partial pressure on both sides of selected membrane and operating temperature (Tong et al., 2002 and Wang et al., 2003). Increase of operating temperature and partial pressure gradient of oxygen; increase the oxygen permeation through ceramic perovskite

membranes (Bhalla et al., 2000). The geometry of membrane systems, also, can affect the increase in oxygen permeation, as the oxygen ions can easily go through the ceramic membranes comprising a larger area. According to Thursfield et al. (2006), hollow-fibres are a promising membrane geometry as they can provide a much higher surface area per unit volume.

A number of researchers have been working in fabricating and characterising the structure and oxygen permeation performance of a number of perovskite hollow fibre membranes (Luyten et al., 2000; Tan and Li, 2002; Tablet et al., 2005 and Li et al., 2006).

Teraoka et al. (1985) were the first to study oxygen permeation through $\text{La}_{1-x}\text{Sr}_x\text{CO}_{1-y}\text{Fe}_y\text{O}_{3-\delta}$ perovskite-type oxide. It is common practice to abbreviate the chemical formula of complex perovskites by using the first letter of the chemical symbol of each of the constituent element, e.g., “L” for La, “S” for Sr, but often oxygen is omitted from the list of symbols. This string of letters is then followed by a string of digits each of which corresponds to the stoichiometry of the corresponding letter (Thursfield and Metcalfe, 2004). The $\text{La}_{0.6}\text{Sr}_{0.4}\text{Co}_{0.2}\text{Fe}_{0.8}\text{O}_{3-\delta}$ membrane (LSCF) has attracted many researchers due to its high degree of chemical and mechanical stability and its high ionic and electronic conductivities (Jin et al., 2000a). The oxygen transport through dense LSCF (6428) membranes has been investigated in the literature in both tubular and disc forms. Li et al. (1999) investigated the oxygen permeation properties of a tubular LSCF (6428) membrane. Air flowed in the shell side while helium flowed in the tube side. At 850°C, an oxygen permeation flux of 0.14 ml (SATP) / $\text{cm}^2\cdot\text{min}$ was observed. In another study by Jin et al. (2000b), partial oxidation of methane was investigated using

a tubular LSCF (6428) membrane packed with Ni/Al₂O₃. They found that the methane conversion was larger than 96% and CO selectivity was larger than 97%.

Li et al. (2000), in their study on the tubular La_{0.6}Sr_{0.4}Co_{0.2}Fe_{0.8}O_{3-δ} perovskite membrane, measured the oxygen permeation fluxes at various downstream oxygen partial pressures and temperatures. The oxygen permeation flux was around 0.21 cm³/cm².min (SATP) at 1173 K, when the partial pressure on the feed side was 0.21 atm and on the permeate side was 1x10⁻³ atm. It increased sharply around 1073K due to an order-disorder transition of the oxygen vacancies. They concluded that the oxygen flux decreases with increasing downstream oxygen partial pressure, but it increases as the helium flow rate increased due to corresponding decrease in the oxygen partial pressure in helium.

Use of a catalyst can promote the partial oxidation reaction and improve the oxygen transport. Tsai et al. (1997), in a study of syngas production using a membrane associated with a 5% Ni/Al₂O₃ catalyst, demonstrated that when the catalyst was placed directly on the membrane surface, in contrast to when there was no catalyst, the oxygen permeation flux was five times higher and the methane conversion was enhanced four times.

The next chapter presents an investigation of syngas production.

Chapter - 4

CHAPTER-4: SYNGAS PRODUCTION INVESTIGATION

4.1 Introduction

As mentioned previously, syngas is a mixture of hydrogen and carbon monoxide; which is produced by a number of conventional methods. One of these is a partial oxidation of natural gas in which methane is a predominant component. Ceramic oxygen membrane reactors make possible the partial oxidation of methane and the separation of the oxygen within one operational unit and consequently reduce the capital cost significantly. Considerable development has been made in the improvement of ceramic oxygen membrane reactors in the last decade. This chapter presents a theoretical investigation into syngas production through partial oxidation of flare gas (mainly methane). The results, analysis and discussion of this section investigating the utilisation of ceramic membranes to produce synthesis gas, are presented in Chapter 7, together with that of spraying and atomisation techniques to produce SWCNT.

4.2 Feasibility Study for POM using Perovskite Membranes

4.2.1 Introduction

The aim of this research is to investigate the utilisation of excess produced gas instead of it being flared. An attractive route for natural gas utilisation is its conversion to syngas, which is one of the proposed methods that were investigated in this research. The chemical reaction and the separation of the product stream, in the oil and gas industry, are the two most important and costly steps. The efficient use of natural gas could be improved by the combination of these two steps into a single unit. Using

membrane separation and catalytic reaction together in a multitubular reactor is a promising approach to accomplish this combination (Dixon, 2003).

Up until the last few years, the conventional leading process for syngas generation from natural gas is steam reforming (SMR), which is a strongly endothermic reaction process. On an industrial scale, the majority of syngas is produced by steam reforming of natural gas carried out in large multitubular fixed bed reactors (Gallucci et al., 2009). In small scale applications, two alternative reactions are usually considered in addition to SMR, which are partial oxidation reactions (POM) and autothermal reforming (ATR) in which the latter is a combination of steam reforming with a partial oxidation reaction (Liu, 2009).

SMR gives higher H_2/CO ratio than the optimum required for syngas conversion (Kharton et al., 2005), which is inappropriate for methanol or Fischer-Tropsch synthesis, while POM gives an appropriate ratio of 2. Another advantage is that POM technology avoids the need for large amounts of expensive superheated steam. However, an oxygen separation plant may be required (York et al., 2003). Thus, the partial oxidation of natural gas (mainly methane) to syngas has attracted a great deal of attention as it is a mildly exothermic reaction.

Conversion of methane, which is usually the main component of flare gas, through partial oxidation to syngas is proposed in this research. As mentioned previously in Chapter 3, in conventional chemical industrial processes a pure oxygen source is one of the major costs related to partial oxidation processes, which is achieved through cryogenic air distillation. On the economic side, the emphasis on cost reduction for any project is the main target. Therefore, in order to lessen the overall cost of a partial

oxidation process for flare gas (methane) conversion into syngas, it is important to reduce the oxygen generation cost. Pure oxygen or air as an oxygen source is required for the oxidation reaction. According to Kumar et al. (2009), nitrogen separation from syngas is expensive and it is not conducive to separate it from the air. Hence, pure oxygen must be fed to the reactor or oxygen must be separated from the air before being fed to the reactor. This leads to the importance of the oxygen separation unit for syngas production by POM.

Extensive studies have been carried out on the upgrading of membrane materials with high oxygen permeability and thermal/chemical stability (Teraoka et al., 1985, Kharton et al., 1999 and 2003, and Wang et al., 2005); on the mechanism of oxygen permeation (Ma and Balachandran, 1997, Chen et al., 1997 and Shaula et al., 2004); on the application of an oxygen permeating membrane reactor for coupling reaction such as natural gas partial oxidation to syngas (Lu et al., 2000; Spinicci et al., 2001 and Tan and Li, 2006) and on reactor design and fabrication (Wang et al., 2006). As revealed in the previous chapter, Section 3.5, the interest concerning these membranes is mainly motivated by the probable reduction in energy consumption and in the capital cost for oxygen production as compared to the traditional industrial scale of cryogenic distillation of air (Badwal and Ciacchi, 2001).

In the past decade, significant attention has been paid to mixed ionic and electronic conductors (MIEC), which are made from dense ceramic membranes, due to their potential applications in oxygen generation and partial oxidation of hydrocarbons to syngas ($H_2 + CO$), which then produces a series of important chemical products (Dyer, et al., 2000, Armstrong et al., 2005 and Yin et al., 2007). Dixon (1999) summarised the

early research in the area of partial oxidation of methane and focused on the use of perovskite membranes and related materials. Perovskite ceramic membranes such as LSCF (6248) can be used as selective separators of oxygen from air, reducing the costs relating to oxygen purification. Consequently, oxygen separation from air and reaction with methane can take place in one single reactor (Dixon, 2001 and Thursfield and Metcalfe, 2004).

4.2.2 Consideration of LSCF Membrane

Extensive attention has been paid to perovskite type ionic membranes (Tu et al., 1999), ABO_3 (see Section 3.2.2.2), since Teraoka et al. (1985) reported that $La_{1-x}Sr_xCo_{1-y}Fe_yO_{3-\delta}$ perovskite oxides have a higher oxygen ion and higher electronic conductivity than other perovskites. Using this perovskite membrane compound in a tubular form has attracted many researchers due to its high degree of chemical and mechanical stability and, as mentioned, its high ionic and electronic conductivities at high temperatures (Jin et al., 2000a, Armstrong et al., 2005 and Wang et al., 2009). This type of membrane is selectively permeable to oxygen at elevated temperatures in the range of 650-1000°C; thus only oxygen from air can be transported through the membrane to the reaction side (Thursfield and Metcalfe, 2007).

Pure oxygen can be transported through these membranes by the combination of mobile oxygen vacancies and electronic defects, while at the same time excluding the transport of other gas phase species. This process can, however, be obstructed by slow surface kinetics at the membrane surface and in case of large membrane thicknesses. The impact of these factors can be eliminated by using high surface area membranes and

small wall thickness. This can be done with perovskite membranes which provide a high surface area per unit volume compared with conventional tubular forms used. If membrane thickness can be reduced, this will increase the oxygen permeation rate and, at the same time, lower the process cost. If the thickness is very small (1–50 μm) the fabrication of the membrane tubes will be a problem. As mentioned previously in Section 3.2.2.2, oxygen fluxes through these membranes may be improved if a thin-layer deposition of the same material as the membrane is used on a porous substrate. Therefore, a supported modified layer of LSCF on top of a porous support (e.g. Al_2O_3) would be a way forward, for further reduction in the effective membrane thickness. The preparation techniques used for synthesis ceramic powders for a thin layer deposit on the top of membrane tubes are presented in the previous chapter, Section 3.3.

4.2.3 Thin Layer Membranes on a Porous Substrate

Decreasing dense membrane thickness is the most straightforward conceptual approach to increasing oxygen flux through perovskite membranes. However, surface treatments are a promising way for improvement if thickness decreases alone do not yield sufficient oxygen transport. If membrane stability were assigned its proper priority in the membrane reactor design, the need to enhance diffusion in other ways than decreasing dense layer thickness would become critical.

Increase of oxygen flux through membranes has been studied by a number of researchers. Teraoka et al. (1985) were the first researchers to report on very high oxygen fluxes through $\text{La}_{1-x}\text{Sr}_x\text{Co}_{1-y}\text{Fe}_y\text{O}_{3-\delta}$ membranes. Chen et al. (1999) envisaged that thin ion conducting films should have fundamentally higher ion transport efficiency

which would allow a similar performance to a thick membrane under less intense conditions. Using pulsed laser deposition, Van Der Haar (2001) formed supported thin-film membranes (as thin as 7.5 μm thick) giving a dense membrane supported on a porous substrate of the same material.

Tunney et al. (2002) illustrated that an increase in the electronic conductivity of MIEC film occurred as its thickness is decreased from 300 nm to 30 nm. Bouwmeester (2003) stated that an oxygen flux of 1-10 ml (STP)/cm.min has been deemed to be required for the commercial use of syngas production. Li et al. (1999) and Diethelm et al. (2004) reported on oxygen flux in the range of 0.04-0.14 ml (STP)/cm².min with LSCF (6428) thickness of 1.5 mm. This was performed using tubular membranes at a temperature of 1000 °C with membranes of different thicknesses ranging from 0.96-1.5 mm.

Tahiri et al. (2010) studied the oxygen permeation flux through perovskite membranes as a function of temperature (1,073–1,223 K) and oxygen partial pressure (0.1–1.0 bar). The oxygen permeation fluxes for the membranes LSCF (6482) and LSCF (8264) with a thickness of 0.85 mm were observed as 1.02×10^{-5} (mol/cm².min), and 0.6×10^{-5} (mol/cm².min), respectively, in these cases at 1,153 K. They concluded that the oxygen permeation process is mainly controlled by the oxygen bulk diffusion through these membranes. Lee et al. (2003) measured at 900 K an oxygen permeation flux of about 0.15 ml (STP)/cm².min for La_{0.6}Sr_{0.4}Co_{0.2}Fe_{0.8} with a 1.7 mm thickness. Teraoka et al. (2002) at the same temperature, measured an oxygen permeation flux of about 1.1 ml (STP)/cm².min for La_{0.2}Sr_{0.8}Co_{0.2}Fe_{0.8} with a 1 mm thickness.

Table 4.1 summarises some of experimental results for O₂ flux in LSCF membranes.

<i>Membrane material</i>	<i>Thickness, mm</i>	<i>Temperature, °C</i>	<i>Flux J_{O_2} ml/cm².min</i>	<i>Atmospheres used Low p_{O_2}"/high p_{O_2}'</i>	<i>Reference</i>
$La_{0.6}Sr_{0.4}Co_{0.2}Fe_{0.8}O_{3-\delta}$	0.2	700–900	0.1–0.8	Ar/air	Tan et al., 2005a
$La_{0.6}Sr_{0.4}Co_{0.2}Fe_{0.8}O_{3-\delta}$	0.3	800–900	0.1–1.2	Ar/air	Tan et al., 2005b
$La_{0.6}Sr_{0.4}Co_{0.2}Fe_{0.8}O_{3-\delta}$	0.2	858	0.26–0.8	0.022 atm CH ₄ /He/air	Thursfield and Metcalfe, 2006
$La_{0.6}Sr_{0.4}Co_{0.2}Fe_{0.8}O_{3-\delta}$	0.2	650–1000	0.02–1.0	He/laboratory air	Thursfield and Metcalfe, 2007
$La_{0.6}Sr_{0.4}Co_{0.2}Fe_{0.8}O_{3-\delta}$	1.5	900	0.21	0.001/0.21,	Li et al., 2000
$La_{0.6}Sr_{0.4}Co_{0.2}Fe_{0.8}O_{3-\delta}$	1.7	900	0.15	0.1/1	Lee et al., 2003

Table 4 1: Oxygen flux summary for some work on LSCF membrane

Chen et al. (2001) concluded in their investigation on dense $\text{La}_{0.6}\text{Sr}_{0.4}\text{Co}_{0.2}\text{Fe}_{0.8}\text{O}_{3-\delta}$ membranes that the membranes show good oxygen permeability at elevated temperatures. Also, they stated that the overall oxygen permeation process is entirely limited by the transport of oxide ions in the bulk of the membrane, when the membrane thickness is larger than 1.25 mm and it becomes controlled by the surface oxygen exchange and bulk transport as the membrane thickness is reduced to 0.62 mm.

One of the controlling factors that affect the reaction of the syngas production process is the catalyst type employed in the membrane reactor which has an important impact on the reaction rate and the hydrocarbons' conversions (Feng et al., 2004).

4.2.4 Assumptions and Calculation Procedures

As stated in the previous section, decreasing dense membrane thickness is the most straightforward conceptual approach to increasing oxygen flux through a perovskite membrane. However, surface treatments are a promising avenue for improvement if thickness decreases alone do not yield sufficient oxygen transport. If membrane stability were assigned its proper priority in the membrane reactor design, the need to enhance diffusion in other ways than decreasing dense layer thickness would become critical.

Air separation and partial oxidation of methane are integrated in a single unit, in order to eliminate the need for an extremely costly air separation unit. In the proposed mechanism of a tubular reactor, as seen in Figure 4.1, air is introduced into the shell side of the reactor through which oxygen is transported to the other side (membrane tubes) where it reacts with the natural gas (flare gas) feedstock, which is introduced into the tube side, to produce synthesis gas. This takes place at elevated temperatures, at

about 750°C or higher. Nickel-based catalysts facilitate the partial oxidation of methane, which indicate their appropriate use in a ceramic tubular membrane.

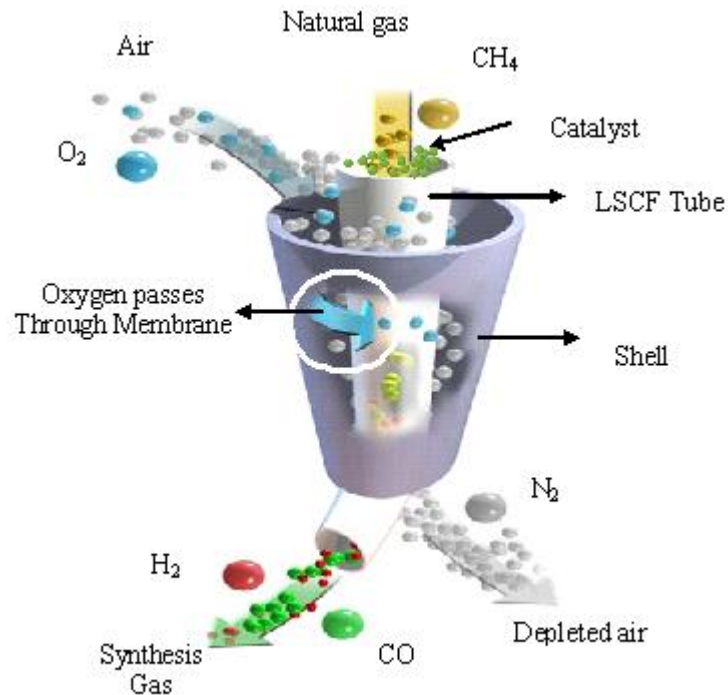


Figure 4.1: Dense membrane reactor mechanisms

The studies on oxygen permeable dense membranes in the literature (Tsai et al., 1997, Bouwmeester, 2003, Diethelm, 2003 and Li, 2007) indicate that the oxygen permeation flux is proportional to the membrane temperature and the logarithm of the ratio of oxygen partial pressures across the membranes and is inversely proportional to the membrane thickness.

Tubular membranes' reactors with thick walls were developed to lessen the engineering design difficulties. Practically, these membrane reactors are not favourable as they

reduce the oxygen flux due to their small surface area to volume ratio and thick walls (Wang et al., 2002). Membrane tubes with a thin wall can overcome these obstacles.

The assumptions made for this study are based on the use of thinner membranes to improve oxygen flux and to lower the costs found in conventional operations. These assumptions and the calculation procedures for a feasibility study of this process are given in the following sections, where a multitubular assembly of membrane tubes is enclosed in a shell through which air passes.

It was assumed that flare gas that was previously flared, i.e. methane, is fed to the reactor tube side packed with Ni catalyst and air is fed to the shell side of the reactor in co-current flow pattern. At the air inlet, the oxygen concentration was assumed at 21%. Some of oxygen permeates the membrane and reacts with methane, as air flows through the reactor. Therefore, oxygen concentration on the air side decreases and methane on the catalyst side is converted.

The $10 \text{ ml/m}^2 \cdot \text{min}$ maximum oxygen flux is assumed and it is used only at this stage to show that at this flux the process is feasible. A flare gas flow rate of $25,000 \text{ m}^3/\text{day}$ is assumed which is an average rate for a typical plant.

Assume O_2 permeation rate i.e. $10 \text{ ml/ (cm}^2 \cdot \text{min)}$.

Assume tube size diameter, $d_o = 0.015 \text{ m}$ and length, $L = 1.5 \text{ m}$.

4.2.4.1 Number of Tubes Required Calculation

The procedure is adapted from Chapter 8 of (Kakac and Liu, 2002).

Assume flare gas flow rate of a typical oil and gas production plant is $25,000 \text{ m}^3/\text{day}$.

Subtract 20% of the flare gas flow rate for emergency flaring.

$$25000 - 5000 = 20000 \text{ m}^3/\text{day}$$

The next step is to determine the approximate number of tubes needed.

All estimations are based on the following overall equation for one reactor:



Based on the above equation, as the stoichiometric oxygen flow rate is half that of methane, the flare gas flow rate (20,000 m³/day) requires 10,000 m³/day of oxygen and the oxygen level in the air is in the range of 21 %, so the air flow rate required is 47,920 m³/day.

First, oxygen permeation is assumed at 10 ml/ (cm².min) and then the calculations for other values (12, 15 and 20 ml/ (cm².min)) were performed using Excel spreadsheet.

$$10 \text{ ml/ (cm}^2\text{.min)} \times 1440 \text{ min/day} = 14400 \text{ cm}^3/\text{cm}^2\text{.day}$$

$$\text{O}_2 \text{ permeation} = 1.44 \times 10^{-2} \text{ m}^3/\text{day.cm}^2$$

The approximate surface area, for the reactor:

$$A_s = \text{O}_2 \text{ flow rate} / \text{O}_2 \text{ permeation rate} \quad (4.2)$$

$$A_s = (10000 \text{ m}^3/\text{day}) / (1.44 \times 10^{-2} \text{ m}^3/\text{day.cm}^2)$$

$$\text{Area} = 694,444 \text{ cm}^2 = 69.44 \text{ m}^2$$

Assume the tubes are made of LSCF (6428) powder due to its high oxygen permeation rate and oxygen stability (Li, 2007):

$$A_s = N_T \pi d_o L \quad (4.3)$$

Where N_T is the number of tubes, d_o is the outside diameter of a tube and L is its length.

For the above assumptions,

$$N_T = 69.44 / (\pi * 0.015 * 1.5) = 983 \text{ tubes}$$

4.2.4.2 Amount of LSCF (6428) and Cost

Assume thickness of tube = 0.002 m

Tube thickness $b_m = (d_o - d_i)/2$

From the above equation; $d_i = d_o - 2b_m = 0.011$ m

Net volume of LSCF powder needed per tube:

$$\text{Volume, } V = AL, = (\pi d^2/4) L = \pi * L /4 (d_o^2 - d_i^2) \quad (4.4)$$

For easy calculation, the units are converted to centimetres

$$= \pi * 150 /4 * (2.25 - 1.21) = 122 \text{ cm}^3$$

Volume of LSCF (6428) powder needed for one membrane tube = 122 cm^3

ρ (density) = Mass/Volume

Density of LSCF (6428) powder $\approx 2 \text{ gm} / \text{cm}^3$

Approximate weight of powder per tube \approx Density x volume

$$= 2 \text{ gm} / \text{cm}^3 \times 122 \text{ cm}^3 = 244 \text{ gm}$$

Price of powder \approx £600/kg \approx £0.6/gm

Price of powder per tube = £0.6/gm x 244 gm = £146.4

Total price of powder for the tubes = $982 \times 146.4 =$ £143,765

Flare gas flow rate assumed at $20,000 \text{ m}^3/\text{day}$ (mainly CH_4)

Half of the flow rate through the reactor (oxygen flow rate) = $10,000 \text{ m}^3/\text{day}$

$$= 10000 * 10^6 / (3600 * 24 * 982) = 118 \text{ cm}^3/\text{s}$$

Velocity = flow rate /tube cross area = $118/1.767 = 67 \text{ cm/s}$

Thus, it can be seen that with the above assumptions it is feasible to construct a reactor system of LSCF tubes which is capable of producing syngas ($\text{H}_2 + \text{CO}$) from the high flows inherent in a commercial flare operation. Although, the material cost may be high,

the costs quoted above are for laboratory quantities and would be lower in practice for the levels required in the present proposal.

A theoretical mechanism of the oxygen permeation through a pirovskite membrane suggested by Tsai et al., 1997 is followed in this work.

$$J_{O_2} = A e^{E_a/RT_m} \frac{T_m}{b_m} \ln \left(\frac{P_{O_2}^s}{P_{O_2}^t} \right) \quad (4.5)$$

Where J_{O_2} is the oxygen permeation rate, E_a is the activation energy and the pre-exponential factor A for the LSCF (6482) material are 62,700 J/mol and 7.34×10^{-7} mol/(ms K), respectively (Tsai et al., 1997), T_m is the membrane temperature, b_m is the membrane thickness and $\frac{P_{O_2}^s}{P_{O_2}^t}$ is the ratio of oxygen partial pressure at the air shell side (feed) and tube side (permeate).

4.3 Analysis

Based on Equations 4.2 - 4.5 and the above assumptions, Microsoft Excel spreadsheet was used to draw the subsequent Figures (see Appendix A), which show the relationships between different parameters for the multitubular reactor. Figure 4.2 shows that the number of tubes decreases as the oxygen permeating through the LSCF tubes increases, reducing from 983 tubes at a permeation rate of 10 ml/cm².min to 491 tubes at a permeation rate of 20 ml/cm².min. In practise, the length of the ceramic LSCF tubes is governed by structural strength and a length of 2 meters is probably the maximum that can be sustained.

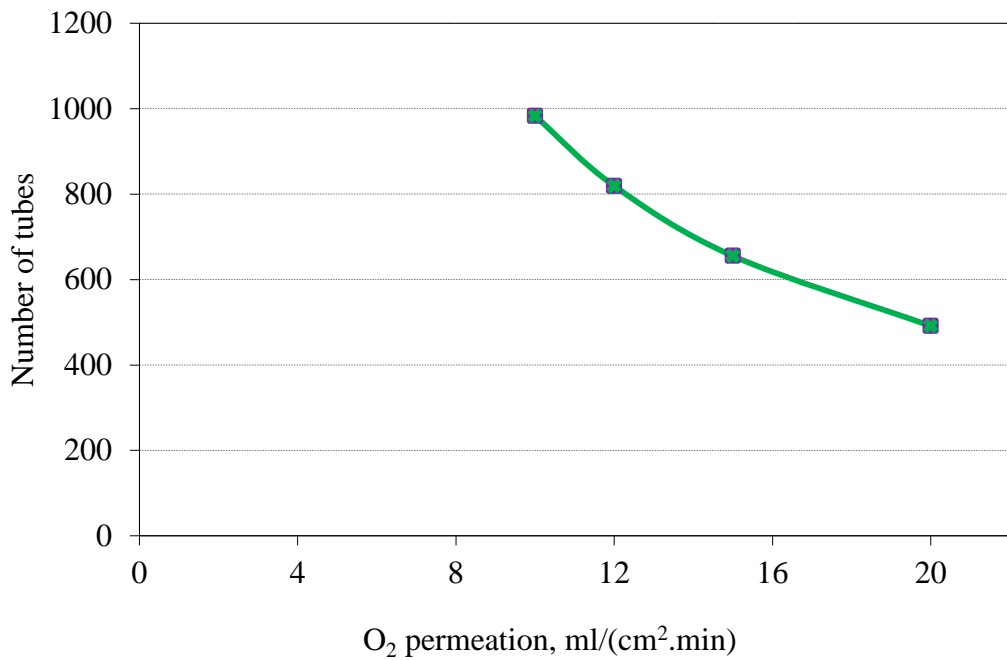


Figure 4.2: Effect of oxygen permeation on a number of tubes (O₂ flow rate = 10,000 m³/day, tube outer diameter, 0.015 m, tube thickness= 0.002 m and tube length = 1.50 m)

Figure 4.3 indicates that a significant decrease in the number of tubes required is obtained by increasing the relative tube length to diameter ratio from 50 to 100.

Flare gas flow rate also has an important effect on the number of tubes required, high gas flow rates requiring an increase in the number of tubes as shown in Figure 4.4.

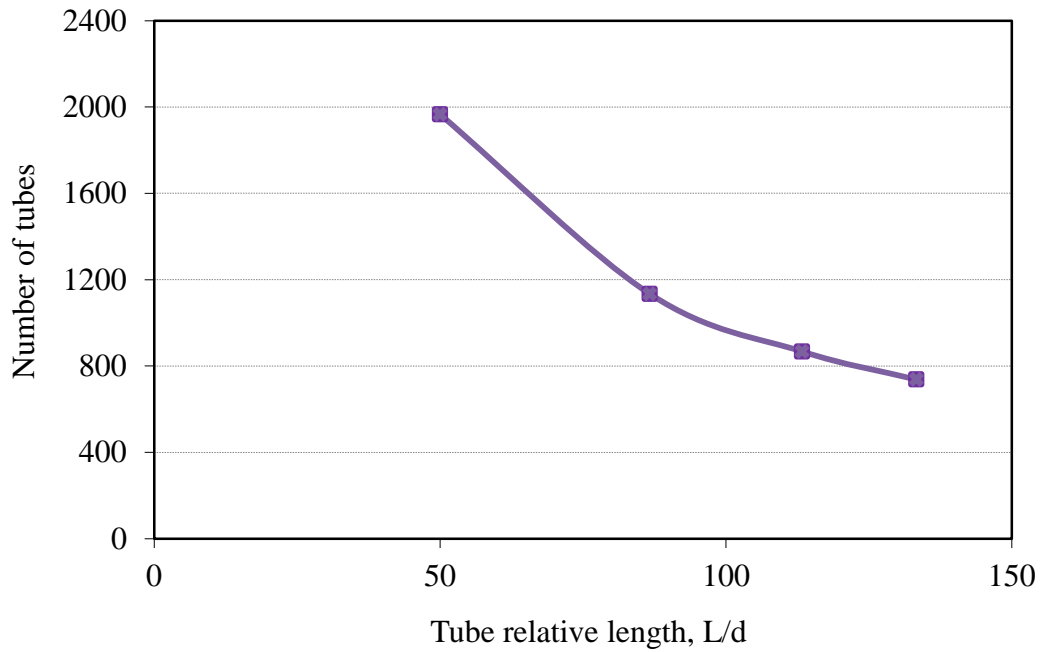


Figure 4.3: Effect of tube relative length on a number of tubes (O_2 flow rate = $10,000 \text{ m}^3/\text{day}$, tube outer diameter, 0.015 m and tube = 0.002 m thickness)

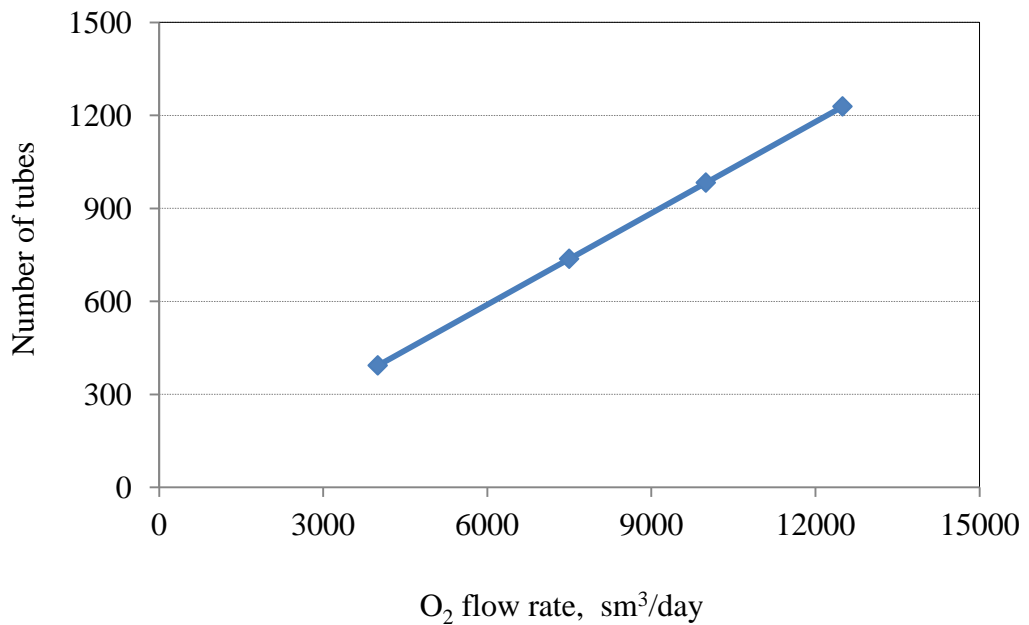


Figure 4.4: Effect of oxygen flow rate on a number of tubes (tube outer diameter = 0.015 m , tube thickness = 0.002 m , tube length = 1.50 m , O_2 flux = $10 \text{ ml}/(\text{cm}^2 \cdot \text{min})$)

The cost of the LSCF material is a major item of the overall expense of such a reactor. Figure 4.5 shows how important a price reduction is for the cost of a tube and how a reduction in tube thicknesses would provide significant cost savings.

Although, it is not practical to produce single LSCF tubes of thicknesses as small as 0.002 cm, one possibility to achieve this is a deposition of a thin layer of LSCF onto porous substrate tubes.

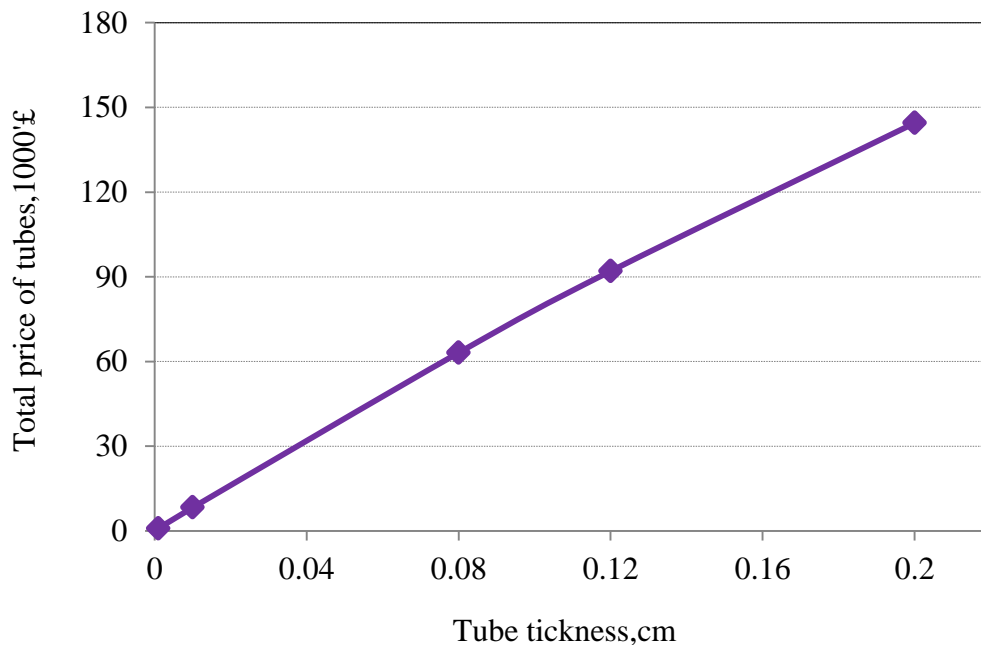


Figure 4.5: Effect of tube thickness on the price of tubes (tube outer diameter = 0.015 m, tube length = 1.50 m, O₂ flux = 10 ml/(cm².min))

Depending on the flow rate of flare gas, and based on the assumption of a 20,000 m³/day, it possible to use more than one reactor. In this case to reduce the load on one reactor, the flow rate is distributed into many reactors with equal flow rates.

The above calculations indicate that it is feasible to convert flare gas to syngas (CO+H₂) in a membrane reactor system using O₂ permeating perovskite membranes at flow rates of flare gas commensurate with general production facilities.

One way forward is the use of a thinner membrane and the results for this will be given in Chapter 7.

Chapter - 5

CHAPTER-5: THE BACKGROUND TO SPRAYS AND ATOMISATION

5.1 Introduction

The atomisation process of a liquid into smaller droplets in the form of a fine spray plays an important role in various industrial applications. Sprays and atomisation techniques have attracted the attention of many researchers and have been the subject of a wide range of theoretical and experimental studies during the past decade. Many studies concerning different aspects of sprays and atomisation have been performed and major advancements in spray analysis and spray characterisation have been made. This chapter presents a general background to sprays' and atomisation processes. Spray properties and different representative mean drop sizes' diameters are defined. In addition, details are given on the classification of atomisers and there is a focus on swirl atomisers, as they are used in this investigation.

5.2 Definition of an Atomisation

Atomisation is a process in which a bulk liquid is broken up into small drops or droplets by internal and/or external forces as a result of the interaction between the liquid and the surrounding medium. It begins by forcing a liquid through an atomiser via its orifice. In terms of the relative velocity between the atomised liquid and the surrounding atmosphere, the atomisation process can be considered as two subsequent mechanisms, which are primary atomisation followed by secondary atomisation (Liu, 2000 and Nasr et al., 2002).

Atomisation of liquids is widely used in several applications such as chemical processing, agriculture, evaporative cooling, combustion systems, crop spraying, air/gas conditioning, fire suppression, spray drying and many other applications (Nasr et al., 2002).

5.2.1 Basic Mechanisms of Atomisation

Jet break-up, sheet break-up and drop break-up are the main mechanisms of atomisation, as the growth of interruptions on the atomised jet face occur. The atomisation process is a very complicated process and involves primary and secondary break-up and droplet interaction, as shown in Figure 5.1.

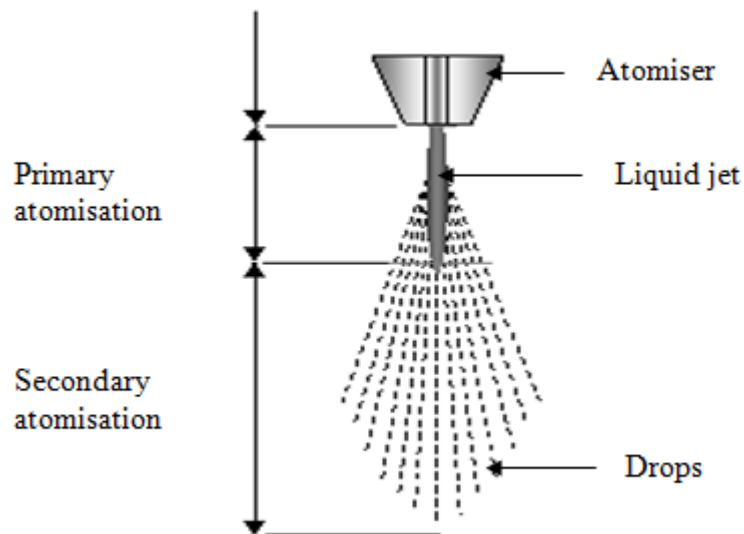


Figure 5.1: General atomisation mechanisms

It is well known that the break-up of liquid sheets or liquid jets is caused by the unstable growth of waves at the interface due to the aerodynamic forces between the liquid and surrounding atmosphere (Ibrahim, 2006). During the primary atomisation, liquid jets or

sheets are disintegrated into unstable ligaments which then break down into drops. While in the secondary atomisation, these drops deform and further break-up into small droplets due to aerodynamic interaction between the drops and the ambient air, in which a relatively slow-moving liquid is revealed to a high velocity air or gas stream (Liu, 2000 and Nasr et al., 2002). In both the above mentioned classes, the final droplet size distribution produced by the process of atomisation is determined by the flow characteristics and the fluid properties. The variation effect in fluid properties, atomiser geometry and operating parameters on drop size distribution is important for controlling the resulting spray distribution (Lefebvre, 1989).

Previous studies have shown that the properties of sprays are affected by many factors, including atomiser internal flow effects resulting from cavitation, the jet speed profile and turbulence in the atomiser exit and the physical and thermodynamic states of both liquid and gas (Wu et al., 1992).

5.2.1.1 Break-up of Liquid Jets

When a liquid jet flows from an atomiser, oscillations and perturbations form on the jet surface as a result of the competition of cohesive and disruptive forces (Liu, 2000). Yule and Dunkley (1994) studied the visual phenomena during jet break-up when the relative velocity between liquid jet and gaseous medium increased. As shown in Figure 5.2, at the lowest flow rate (a) there is a disfiguration of the round liquid jet dilatationally and individual droplets are formed and, at the same time, there is possibility of smaller drops forming in between those mentioned drops. As jet velocity increases (b) the curtailment point of the jet (break point) moves closer to the atomiser

and smaller drops are formed due to a shorter wavelength of disturbance effect. At higher flow rates of the liquid jet (c, d and e), the break-up is thought to result from the unstable growth of short wavelength waves (Reitz and Bracco, 1982).

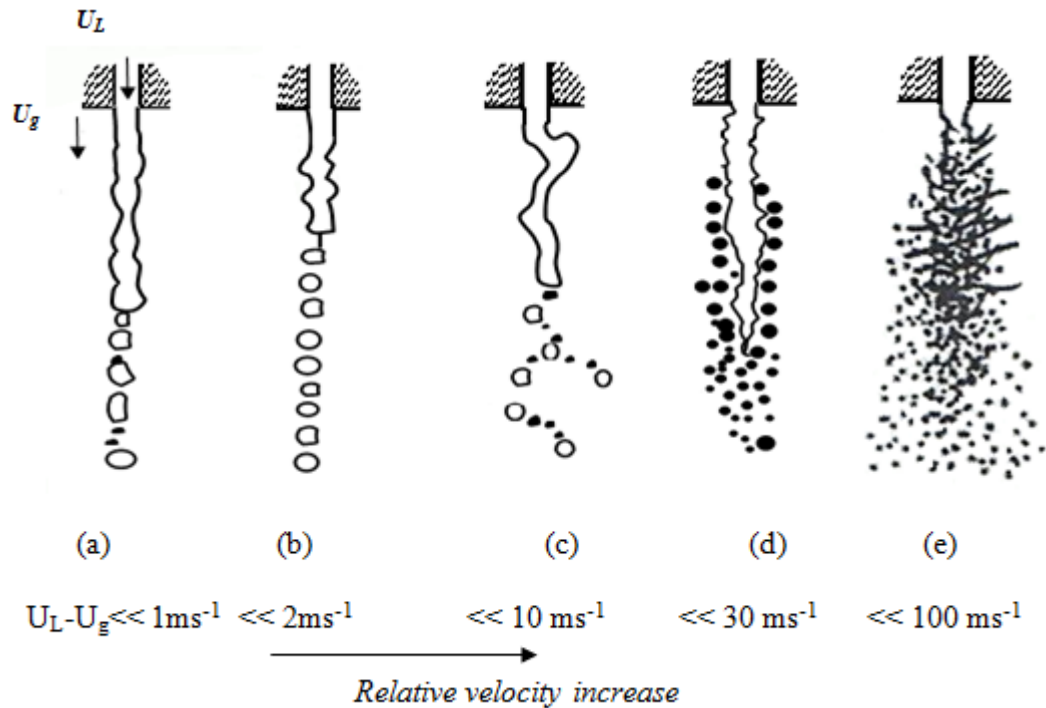


Figure 5.2: Liquid column break-up at different velocities (Nasr et al., 2002)

5.2.1.2 Break-up of Liquid Sheets

A liquid sheet is a thin layer of liquid, similar to a flag in the wind. As a three dimensional flow generally occurs in the sheet break-up it is more complicated than that of a liquid jet break up (Azzopardi, 1998 and Nasr et al., 2002). The unsteadiness of the liquid sheet leading to the growth of waves, can be analysed by considering that the sheet is destabilised by aerodynamic forces and stabilised by surface tension and that ligaments are formed by detaching from the crests of the waves. Gas jets and sheets intermingle and local thinning of the sheet is caused by wave growth, then perforations

occur (Yule and Vamvakoglou, 1999). As can be seen in Figure 5.3, the process stages are such that the liquid emerges as small ligaments due to the potential energy of the liquid along with the geometry of the atomiser; these ligaments then break up further into very small drops.

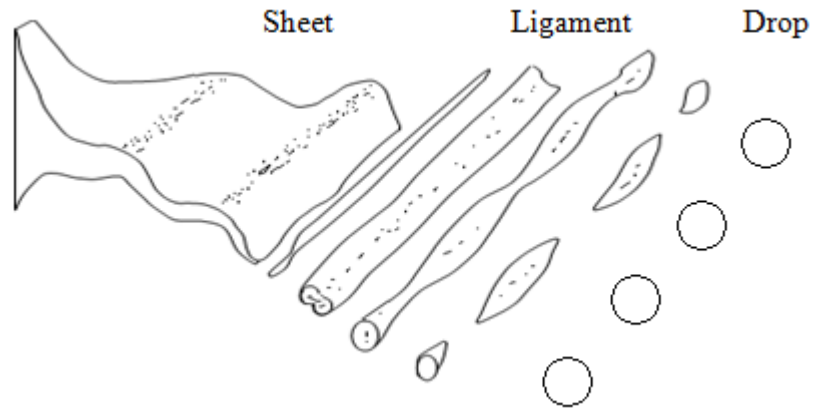


Figure 5.3: Break-up mechanism of a liquid sheet into ligaments and droplets

5.2.1.3 Break-up of Droplets

Droplet break-up is very important in producing fine sprays. If the drops are too large, they can break up under the influence of aerodynamic forces or shock waves. Figure 5.4 illustrates the best known break-up mechanisms. In both cases at low and high Weber number, which is the ratio of aerodynamic and surface tension forces, Equation (5.1), shows that the originally spherical drop is flattened due to the pressure difference between the trailing and leading sides (Liu, 2000).

$$We = \frac{\rho U^2 D}{2\sigma} \quad (5.1)$$

Where $1/2\rho U^2$ is the proportional to the aerodynamic forces, σ is the surface tension, U is the relative velocity between the drop and flowing air or gas, D is the drop size diameter.

At low Weber numbers, the squeezing process is continuous and the material is flattened and then blown into a bag. Before breaking up, the stretched bag might be become 4 to 6 times longer than its diameter. The thin sheet skin breaks into small ligaments and then into fine drops. The remaining material forms a rim of coarse ligaments and large drops. At high Weber numbers, edges of the jet column are dragged forward into a sheet and atomisation occurs from there.

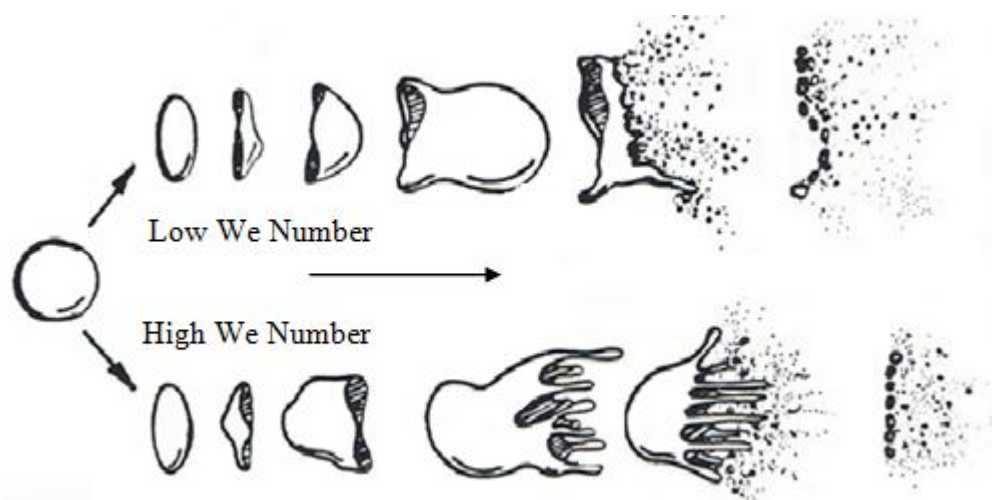


Figure 5.4: Drop break-up mechanism in low and high Weber numbers (Liu, 2000)

5.3 Characterisation of Sprays

A *spray* is “a dispersion of droplets in a gaseous medium with sufficient momentum energy to penetrate it” (Nasr et al., 2002). In other words, a spray is an assortment of moving droplets that are usually the result of atomisation as they are moving in a

controlled manner. The main spray properties such as penetration, spray cone angle, dispersion, relative span factor and patternation are described by Lefebvre (1989) and Nasr et al. (2002). Some means of describing and obtaining quantitative information is important in order to analyse and compare sprays.

The *penetration* of a spray is the maximum distance covered by a spray for a given time after injection started. It is basically affected by the kinetic energy of the jet at the nozzle orifice and the aerodynamic resistance of the surrounding air or gas. Sprays of wide cone angle encounter more air resistance and have low penetration compared with narrow sprays which have high penetration.

The *spray cone angle* (Figure 5.5) is defined as the angle between two straight lines drawn from the discharge orifice to cut the spray contours at a specific distance downstream.

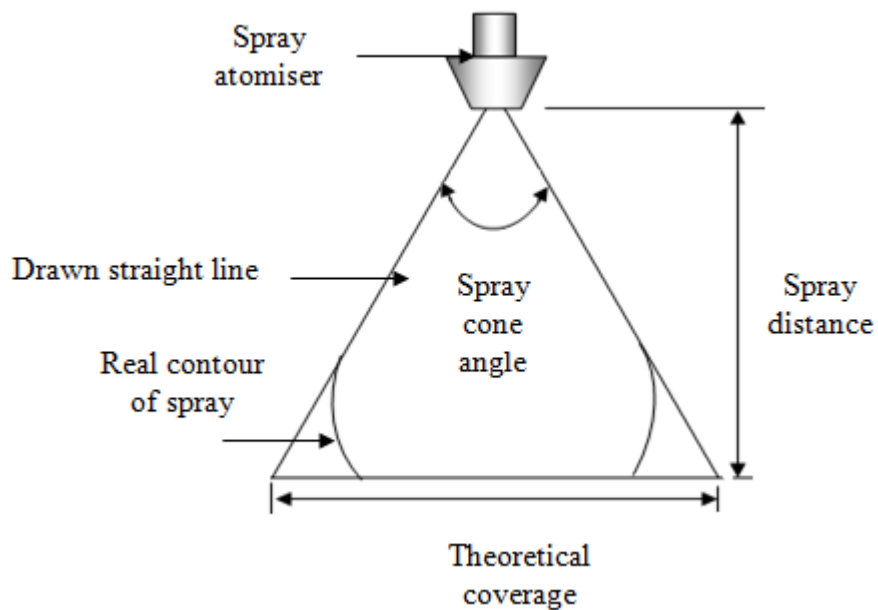


Figure 5.5: Spray cone angle definition

In some cases it may be difficult to accurately determine the cone angle as sprays have no straight boundaries. These angles may vary depending on atomiser dimensions, liquid properties and the density of the media into which the liquid is sprayed.

The degree of the *dispersion* of a spray is the ratio of the spray volume to the liquid volume contained within it. This term is sometimes used as an alternative to distribution to express the range of drop sizes in a spray. Good dispersion indicates fast mixing of the sprayed liquid with the surrounding gas.

The *Relative Span Factor (RSF)* is a dimensionless parameter providing a direct indication of the range of drop sizes relative to the Mass Mean Diameter (MMD). It is defined as:

$$RSF = \frac{D_{0.9} - D_{0.1}}{D_{0.5}} \quad (5.2)$$

The definitions of $D_{0.9}$, $D_{0.1}$ and $D_{0.5}$ are presented in Section 5.3.2.

“The *patterning* refers to both the shape of the spray boundary and the distribution of droplets within the boundary” (Nasr et al., 2002). The symmetry of spray pattern is an important parameter in most practical applications of sprays and atomisation. Different spray patterns are produced from different types of spray atomisers. There are three major types of spray patterns that are commonly used in industry, hollow cone spray, full cone spray and flat spray, as illustrated in Figure 5.6.

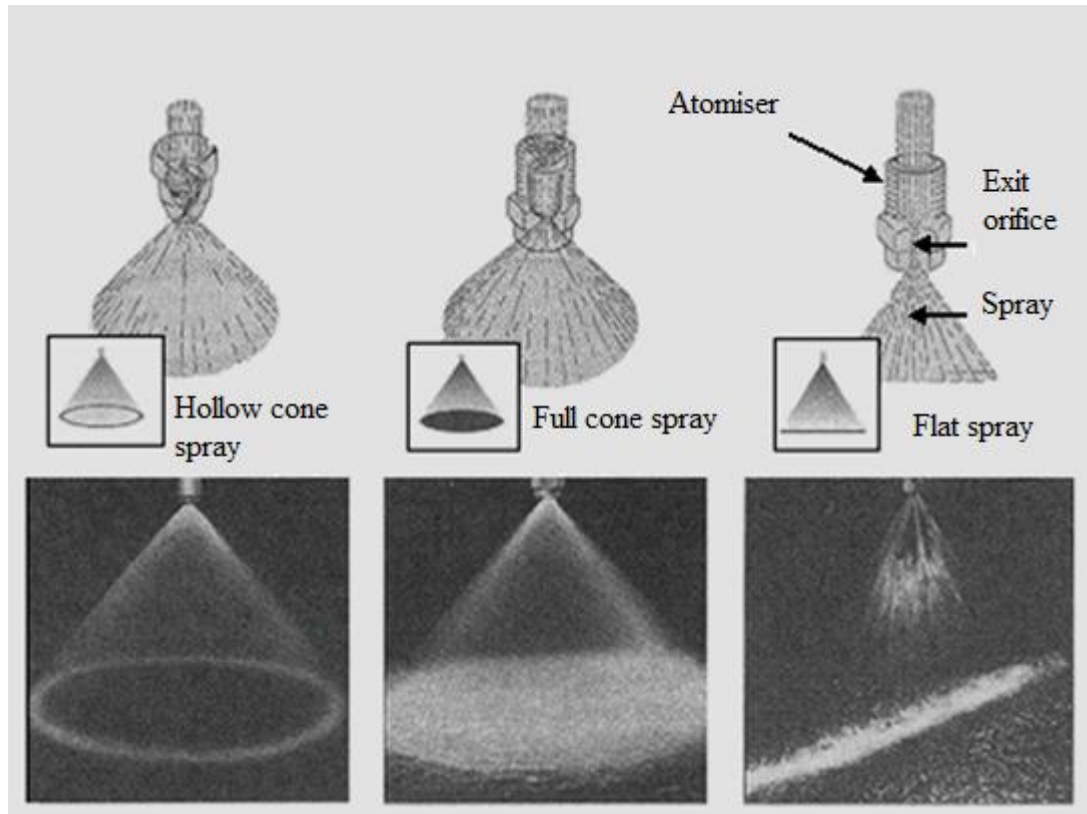


Figure 5.6: Various spray patternations

5.3.1 Factors Affecting a Spray

A range of factors affect droplet size and how easily a stream of liquid atomises after emerging from an orifice. Among these factors are fluid properties, pressure, temperature and flow rate.

5.3.1.1 Fluid Properties

The fluid properties that have a major effect on spray and drop sizes are:

i. Surface tension

Surface tension is the property of a liquid that causes droplets to pull together in a spherical form and resist spreading out. This property causes the thin ligaments of liquid to be unstable, that is, they break up into droplets. Fluids with higher surface tensions tend to have a larger average droplet size during atomisation.

ii. Density

Density causes a resistance to fluid acceleration and higher density tends to result in a larger average droplet size.

iii. Viscosity

The viscosity of a fluid causes it to resist agitation, tending to stop its breakup and leading to a larger average droplet size.

5.3.1.2 Pressure

Pressure has an opposite effect on droplet size as its increase will reduce the droplet size, and vice versa.

5.3.1.3 Temperature

Temperature is a significant factor in spray performance as it affects viscosity, surface tension and density which can affect the spray performance.

5.3.1.4 Flow Rate

The flow rate is an important parameter that affects spray and atomisation. At low flow rates dripping occurs as there is not enough energy to atomise the fluid, while as the

flow rate increases, a cylindrical jet will be formed by individual drops. At higher flow rates a sinuous distorting jet occurs.

5.3.2 Drop Size Distribution

A key element in choosing an atomiser for a specific application is drop size. Drop size distribution is an important parameter of the atomisation process in addition to droplet mean diameter. Certain shapes may be better for certain operations (for example, narrow, wide, a few large drops or a few small drops). It is known that, to improve the quality of atomisation, it is important to reduce droplet size. According to Lefebvre (1989), drop size distribution may be obtained by plotting a histogram of drop size, each ordinate representing the number of drops whose diameter ranges between $(D-\Delta D)/2$ and $(D+\Delta D)/2$, as shown in Figure 5.7, in which $\Delta D = 5\mu\text{m}$.

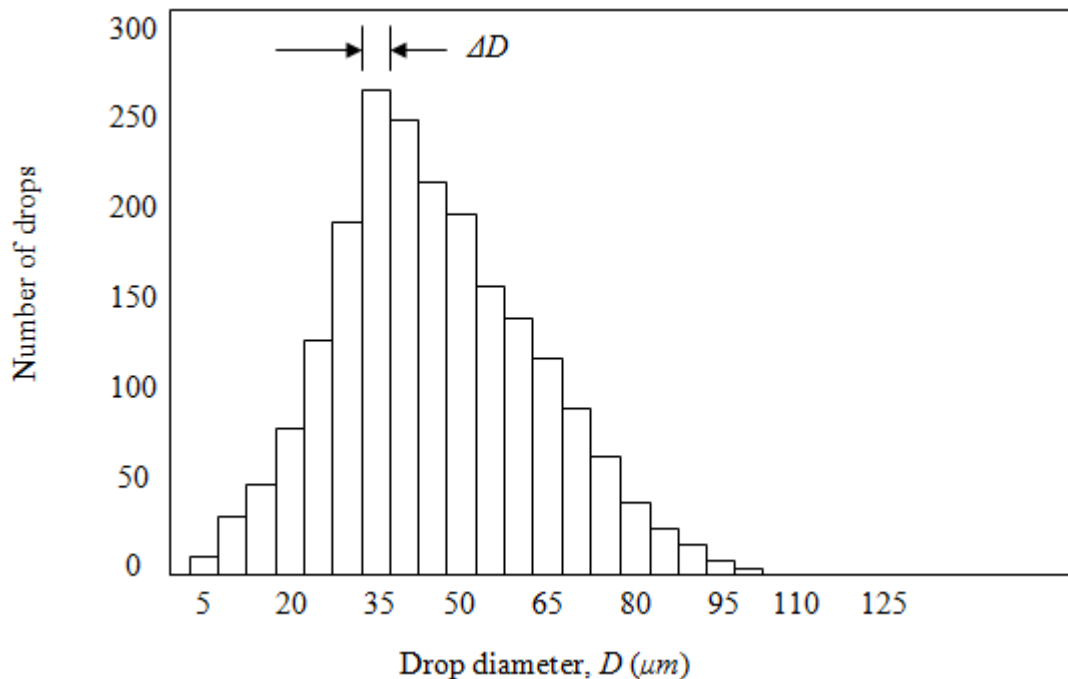


Figure 5.7: Typical drop size distribution

If the spray volume corresponding to a range of drop size between $(D-\Delta D)/2$ and $(D+\Delta D)/2$, is plotted as a function of drop size, as shown in Figure 5.8, the resulting distribution is skewed to the right due to the larger drops' weighing effect.

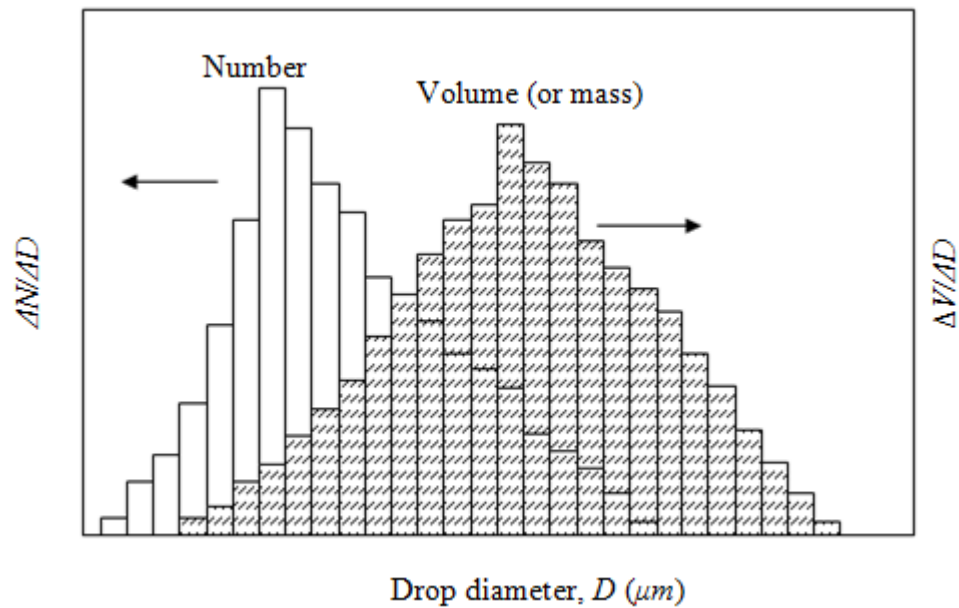


Figure 5.8: Drop size histograms based on number and volume (Lefebvre, 1989)

By making ΔD very small and using sufficiently large samples of droplets, a continuous size distribution (number and volume) curve, usually referred to as a frequency distribution curve, can be obtained, as shown in Figure 5.9.

In the literature, (Lefebvre, 1989 and Nasr et al., 2002) the ordinate values in size distribution curves are expressed in several different ways such as the number of drops with given diameter and the number or volume fraction of the total number or volume as a percentage.

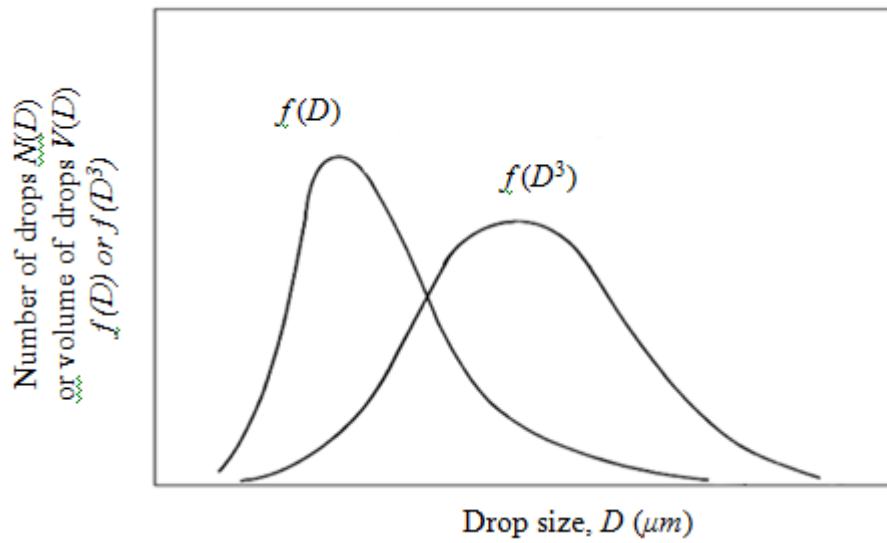


Figure 5.9: Typical drop size frequency distribution curves (*number and volume*)

It may also be useful to use a cumulative representation which is a plot of the integral of the size distribution curve. This may stand for the percentage of the total number, surface area or volume of a spray contained in drops at a given size, as shown in Figure 5.10.

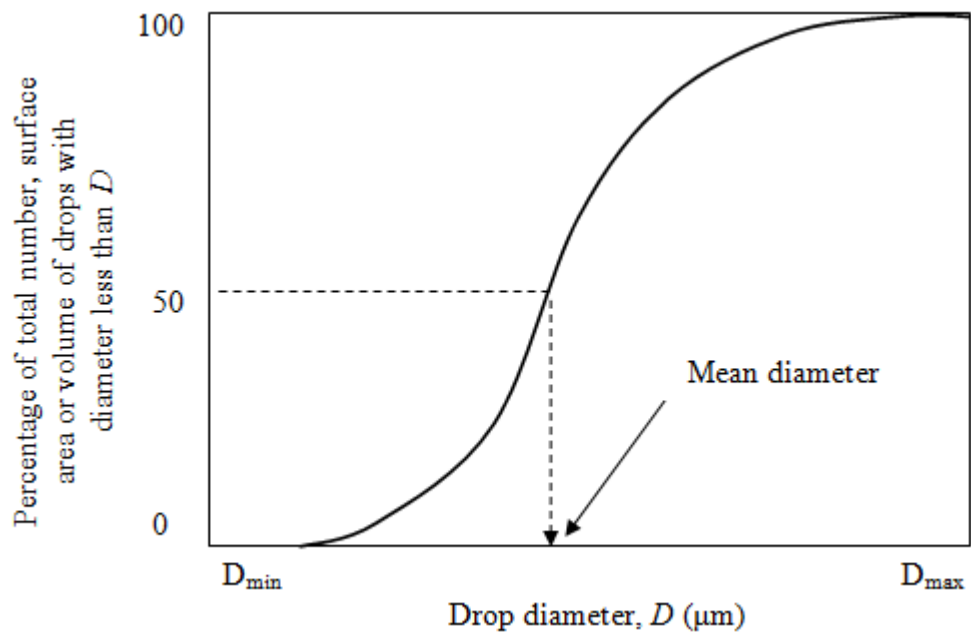


Figure 5.10: Typical shape of cumulative drop size

Any spray produces a set of drops, which can be subdivided into classes and each class comprises drops, whose diameters (D) are in the range of $(D-\Delta D, D+\Delta D)$.

Considering the size distribution of N droplets, which pass through an area of ΔA in a time t , the number distribution of the droplets is expressed as (Nasr et al., 2002):

$$n(D) = \lim_{\substack{\Delta D \rightarrow 0 \\ N \rightarrow \infty}} \left(\frac{\text{Number of droplets between } (D-\Delta D)/2 \text{ and } (D+\Delta D)/2}{\Delta DN} \right) \quad (5.3)$$

$$\int_{D_0}^{D_n} n(D) dD = 1 \quad (5.4)$$

To determine the volume size distribution, the following equation is derived:

$$V(D) = \lim_{\substack{\Delta D \rightarrow 0 \\ V \rightarrow \infty}} \left(\frac{\text{Number of droplets between } (D-\Delta D)/2 \text{ and } (D+\Delta D)/2}{\Delta DV} \right) \quad (5.5)$$

The key diameter in the experimental case of this research is the Number Mean Diameter (NMD), $D_{n0.50}$, which is a value where 50% of the total number of droplets is made up of drops with diameters larger than the mean value and 50% are smaller.

There are other various representative diameters that can be used, such as Volume Mean Diameter (VMD), $D_{v0.50}$, which is a value where 50% of the total volume (or mass) of liquid sprayed is made up of drops with diameters larger than the mean value and 50% are smaller. The general mean diameter is calculated by the Equation (5.6), where a and b are selected for a particular mean diameter, i denotes the size range, N_i is the number of drops in the size range i and D_i is a middle diameter of size range i (Lefebvre, 1989).

$$D_{ab} = \left[\frac{\sum N_i D_i^a}{\sum N_i D_i^b} \right]^{1/(a-b)} \quad (5.6)$$

Hence, the Sauter Mean Diameter (SMD) D_{32} is calculated as follows:

$$D_{32} = \frac{\sum N_i D_i^3}{\sum N_i D_i^2} \quad (5.7)$$

Thus, for example, D_{30} (Volume Mean Diameter) is the diameter of a drop whose volume, if multiplied by the number of drops, equals the total volume of sample.

$D_{0.9}$ is a volume diameter such that 90% of the total liquid volume is in drops of smaller diameter. Table 5.1 shows how mean diameters are defined from the measured droplets, where N_i is the number of drops in size range i , and D_i is the middle diameter of size class i according to equation (5.6) (Lefebvre, 1989). It is necessary to compare the concept of a representative diameter and a diameter that provides an indication of the quality of atomisation. Several empirical relationships have been proposed to characterise the drop size distribution in a spray.

The most common drop size distribution and the most widely used function in industry is the Rosin-Rammler distribution function, which gives a good fit to most of the particle size distribution, and which was originally developed for powders (Lefebvre, 1989) which may be expressed in the form:

$$1-Q = \exp - \left(\frac{D}{X} \right)^q \quad (5.8)$$

Where Q is the fraction of the total volume contained in drops of diameter less than D , X and q are constants. The exponent q provides a measure of the spread of drop sizes.

Another parameter which is widely used in the design process of atomiser devices is the *fall velocity* or *settling velocity* of a particle, which is briefly presented in the next section.

<i>a</i>	<i>b</i>	<i>Symbol</i>	<i>Name of mean diameter</i>	<i>Expression</i>	<i>Application</i>
1	0	D_{10}	Arithmetic Mean Diameter	$\frac{\sum N_i D_i}{\sum N_i}$	Comparisons
2	0	D_{20}	Surface Mean Diameter	$\left(\frac{\sum N_i D_i^2}{\sum N_i}\right)^{1/2}$	Surface area controlling
3	0	D_{30}	Volume Mean Diameter	$\left(\frac{\sum N_i D_i^3}{\sum N_i}\right)^{1/3}$	Volume controlling
2	1	D_{21}	Relative Surface Area Mean Diameter	$\frac{\sum N_i D_i^2}{\sum N_i D_i}$	Absorption
3	1	D_{31}	Relative Volume Mean Diameter	$\left(\frac{\sum N_i D_i^3}{\sum N_i}\right)^{1/2}$	Evaporation, molecular diffusion
3	2	D_{32}	Sauter Mean Diameter (SMD)	$\frac{\sum N_i D_i^3}{\sum N_i D_i^2}$	Mass transfer, reaction
4	3	D_{43}	Mass, De Brouckere or Hardan	$\frac{\sum N_i D_i^4}{\sum N_i D_i^3}$	Combustion equilibrium

Table 5.1: Mean diameters and their applications

5.3.2.1 Settling Velocity

The settling velocity (U_{ps}) of a particle is defined as the velocity achieved when the particle is settling in an extended fluid under the action of gravity (see Figure 5.11). According Jimenez and Madsen (2003) and NASA (2008), a free-falling particle attains its settling velocity when the upward force of drag (F_d) equals the downward force of gravity (F_g), which results an acceleration of zero.

The settling velocity is given by:

$$U_{ps} = \sqrt{\frac{2mg}{\rho A C_d}} \quad (5.9)$$

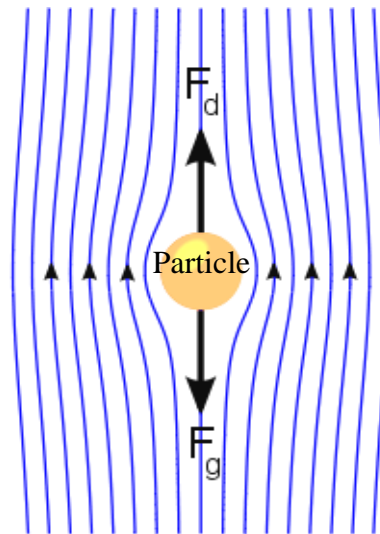


Figure 5.11: Creeping flow past a spherical particle

Where:

U_{ps} = Settling velocity (m/s)

m = Mass of the falling particle (kg)

g = Acceleration due to gravity (m/s^2)

C_d = Drag coefficient

ρ = Density of the fluid through which the particle is falling (kg/m^3)

A = Projected area of the particle (m^2)

According to the drag equation, the net force acting on an object falling near the surface of earth is:

$$F_{net} = mg - \frac{1}{2}\rho U_{ps}^2 AC_d \quad (5.10)$$

At equilibrium, the net force is zero ($F_{net} = 0$);

$$mg - \frac{1}{2}\rho U_{ps}^2 AC_d = 0 \quad (5.11)$$

Solving for U_{ps} yields;

$$U_{ps} = \sqrt{\frac{2mg}{\rho AC_d}} \quad (5.12)$$

When the buoyancy effects are taken into account, a particle falling through a fluid under its weight can reach a settling velocity if the net force acting on the particle becomes zero. When the settling velocity is achieved, the weight of the particle is exactly balanced by the upward buoyancy force and drag force.

$$W = F_b + F_d \quad (5.13)$$

Where:

W = Particle weight, (kg)

F_b = Buoyancy force acting on the particle, (kg.m/s^2)

F_d = Drag force acting on the particle, (kg.m/s^2)

If the falling object is spherical in shape, the expressions for the three forces are given below:

$$W = \frac{\pi}{6} D^3 \rho_s g \quad (5.14)$$

$$F_b = \frac{\pi}{6} D^3 \rho g \quad (5.15)$$

$$F_d = C_d \frac{1}{2} \rho U_{ps} A \quad (5.16)$$

Where:

D = Diameter of the droplet (mm),

g = gravitational acceleration (m/s^2)

ρ = Density of the fluid, (kg/m^3)

ρ_s = Density of the particle, (kg/m^3)

$A = \pi d^2 / 4$ = projected area of the sphere (m^2)

C_d = Drag coefficient

U_{ps} = Settling velocity (m/s)

The substitution of equations (5.14 - 5.16) in equation (5.13) for settling velocity, U_{ps} to give the following expression:

$$U_{ps} = \sqrt{\frac{4gD}{3C_d} \left(\frac{\rho_s - \rho}{\rho} \right)} \quad (5.17)$$

In the cases of very slow motion of the fluid, the fluid inertia forces are negligible in comparison to other forces. Such flows are called creeping flows and the condition to be satisfied for a flow to be a creeping flow is the Reynolds number, $Re \leq 1$.

The analytical solution for the creeping flow around a sphere was first given by Stokes in 1851. From Stokes' solution, the drag force acting on the sphere can be obtained as:

$$F_d = 3\pi\mu D U_{ps} \quad (5.18)$$

Or

$$C_d = \frac{24}{Re} \quad (5.19)$$

Where the Reynolds's number,

$$Re = \frac{\rho D U_{ps}}{\pi} \quad (5.20)$$

The expression for the drag force given by equations (5.18 and 5.19) is called Stokes' law.

When the value of C_d is substituted in the equation (5.17), the expression for the settling velocity of a spherical object moving under creeping flow conditions is obtained as:

$$U_{ps} = \frac{gD^2}{18\mu} (\rho_s - \rho) \quad (5.21)$$

The following section highlights the general description of instrumentation that is used in this investigation in characterising the spray.

5.3.3 Drop Size Measurements

The problem of measuring the sizes of very small particles has been encountered in many applications in engineering science and many different methods have been used with varying success degrees (Lefebvre, 1989). A number of techniques using laser instrumentation has been developed over the last few years to determine droplet characteristics, such as the Phase Doppler Anemometry (PDA) and Laser Diffraction (Malvern laser), the optical area probe technique. Nevertheless, different studies have shown a wide variation in mean droplet sizes for the same atomiser specifications when using different techniques, as noted by Powell et al. (2002). The PDA measurement system concurrently measures the size and velocity of spherical particles in liquid and gaseous flows and it allows data processing to predict concentration or droplet mass

flux. This measurement permits correlation between both the velocity and size to be derived. The measurement of droplet size is based on comparing the signals from multiple detectors located at different scattering angles. The signals from the multiple detectors have a phase difference which is linearly dependent on the particle diameter under definite conditions. The PDA measurement method provides a wide dynamic range combined with high accuracy.

Drop size analysers collect and record data, which is arranged into a mathematical representation referred to as a drop size distribution. This mathematical representation is most often dependent on the measuring equipment used. Recently, some manufacturers have allowed the user to select from a list of distribution functions rather than a default drop size distribution function. As the Malvern Mastersizer-X was used in this research for measuring the droplet sizes, the following section describes it in detail.

5.3.3.1 The Malvern Mastersizer-X

Laser diffraction is one of the few available techniques that are commonly used for the measurement of droplet size distributions. The Malvern laser drop-sizing measurement system is a non-intrusive system since sizing is done without forming particle image and it instantly samples a large number of droplets occupying a given volume. It is a piece of laboratory equipment, which was developed by Malvern Instruments, UK, based on the work conducted by Swithenbank et al. (1976).

The Malvern Mastersizer-X, utilised in this investigation, is a particle size analyser that can measure particles and liquid droplets; it is the most common laser diffraction instrument in use. It is one of the most effective, simple and reliable methods

commercially available for the rapid measurement and characterisation of sprays. Its measuring principle is laser diffraction (Fraunhofer diffraction) which is based on measuring the density of scattered light caused by the drops as they pass through the analyser sampling area. The density of scattered light is measured using a series of photo diodes built in the receiver unit (Musculus and Pickett, 2005). The Malvern Mastersizer-X consists of an optical bench, one end of which is called the transmitter end and other is the receiver end. The transmitter end houses a low power laser producing unit (He-Ne: 2mW) and a spatial filter, that together produce a coherent and monochromatic beam typically of 18 mm diameter, which is referred to as the “analyser beam”. The receiver end consists of a range lens, a detector array and an obscuration monitor along with associated hardware and a computer interface (Malvern Instruments, 2008). Figure 5.12 shows the schematic optical arrangement employed in a Mastersizer-X instrument.

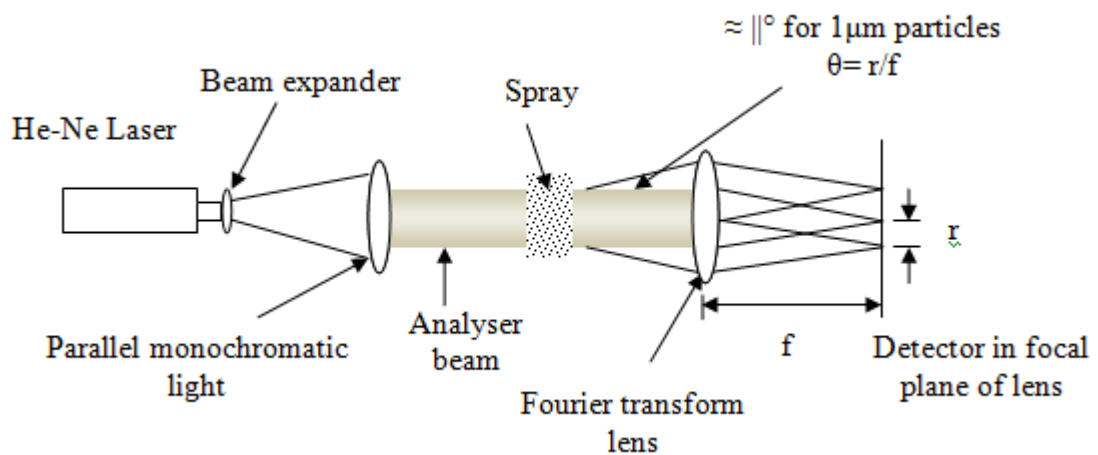


Figure 5.12: Optical arrangement employed in Malvern Mastersizer-X

Drop size analysers accumulate and record data that is normally in the form of number count per class size. Each spray provides a range of drop sizes and the data is arranged into a mathematical illustration referred to as a drop size distribution (Lefebvre, 1989 and Nasr et al., 2002). The cumulative volume distribution and the percentage count for each size class are included. The graphical data form includes all the information included in a tabular form and the cumulative volume percentage with volume frequency percentage versus drop size is represented by a graph. Knowledge of the scattering theory and particle properties is used to transform the scattered light data into a distribution of particle size information. The main advantages of this instrument are speed and cost efficiency and also that it measures particle size in real time. Also, it can be used on-line and in-situ for many different purposes.

5.3.3.2 Operating Procedure of Malvern Mastersizer-X

During the operation of the Malvern Mastersizer-X the droplets' or particles' stream is introduced to the analyser beam by spraying it directly on the measuring area and it is passed through a focused laser beam. This stream scatters light at an angle that is inversely proportional to the droplets' sizes. When a droplet is in the analyser beam, its diffraction pattern is stationary and centred on the optical axis of the range lens. The angular intensity of the scattered light is then measured by a series of photosensitive detectors. The number and positioning of these detectors in the Mastersizer-X has been optimised to achieve maximum resolution across a broad range of sizes.

The map of scattering intensity versus angle is the primary source of information used to calculate the droplet size. The scattering of droplets is accurately predicted by the Mie scattering model. This model is rigorously applied within the Mastersizer-X.

5.3.3.3 Limitations of Mastersizer-X and Measurement Errors

The Mastersizer-X is capable of measuring drop size only in a certain range. The selection of receiver lens size depends upon the size range of particles to be measured. The source of errors within this type of instrument is multiple light scattering in which there is a possibility that the scattered light from one drop might be scattered again by other drops further down the beam axis, depending on the density of the spraying fluid. The Malvern Mastersizer-X is equipped with an “obscuration level” indicator which can be used to determine if the spray is too dense or not; such a determination is often difficult. To circumvent this in the lab, the operator typically moves the atomiser (see Section 5.4) farther away or uses special shielding to permit only a portion of the spray to enter the sample area.

5.4 Atomiser Types

The atomiser’s function is not only to break the liquid down into tiny drops, but also to discharge these drops into the surrounding gaseous medium in the form of a symmetrical spray. Some atomisers achieve this by discharging liquid at high velocity into a relatively slow moving stream of air or gas (Lefebvre, 1989). To exemplify, different pressure atomisers and also rotary atomisers are in the above category. However, atomisers used to expose relatively slow-moving liquid to a high-velocity air

stream are known as twin-fluid, air assist or air blast atomisers. Atomisers can be classified into several different categories depending on their operation method such as twin-fluid and single-fluid atomisers. The classification of all types of atomisers is presented in detail by Nasr et al. (2002). It is better to know which atomiser type is best suited for any given application and how the performance of any given atomiser is affected by the liquid properties and the operating conditions.

Twin-fluid atomisers include (i) the internal-mix and (ii) the external-mix versions, where these terms describe the location where the atomising fluid first contacts the fluid to be sprayed. The single-fluid atomisers are (i) the rotary atomisers, (ii) the ultrasonic atomisers, (iii) the electrostatic atomisers and (iv) the pressure atomisers. In the following section, a brief description of each of these atomisers is provided with a particular reference to the pressure swirl atomiser which was used in this study.

5.4.1 Twin Fluid Atomisers

There is a variety of existing twin fluid atomiser designs to produce optimum conditions for liquid-air contact for atomisation. Twin-fluid atomisers utilise the kinetic energy carried with high velocity gas streams to break up the relatively low velocity liquid sheet or jet into droplets. For the most commonly used designs, the contact between the liquid and the gas phase takes place at the nozzle exit. The atomisation principle of these types of atomisers is that the liquid jet or sheet interacts with the high speed gas flow and the shear forces at the interface cause disturbances on the liquid surface. These disturbances can cause the extending and formation of ligaments and finally the break-up into droplets.

External mixing atomisers introduce the liquid and high velocity gas to each other at the outside of the atomiser. Whereas *internal mixing* atomisers introduce a high gas pressure and velocity supply to the liquid inside the atomiser before forcing the mixture out through one or more orifices. The design principles of the internal and external two-fluid atomisers may be seen in Figure 5.13.

The twin-fluid atomiser utilises the kinetic energy of high velocity gas streams to break-up the liquid sheet or jet into droplets (Lefebvre, 1989). A two-fluid atomiser is incompatible with the requirements of this research work as it cannot provide the required spray pattern. Also, it is not always convenient to use and is relatively costly.

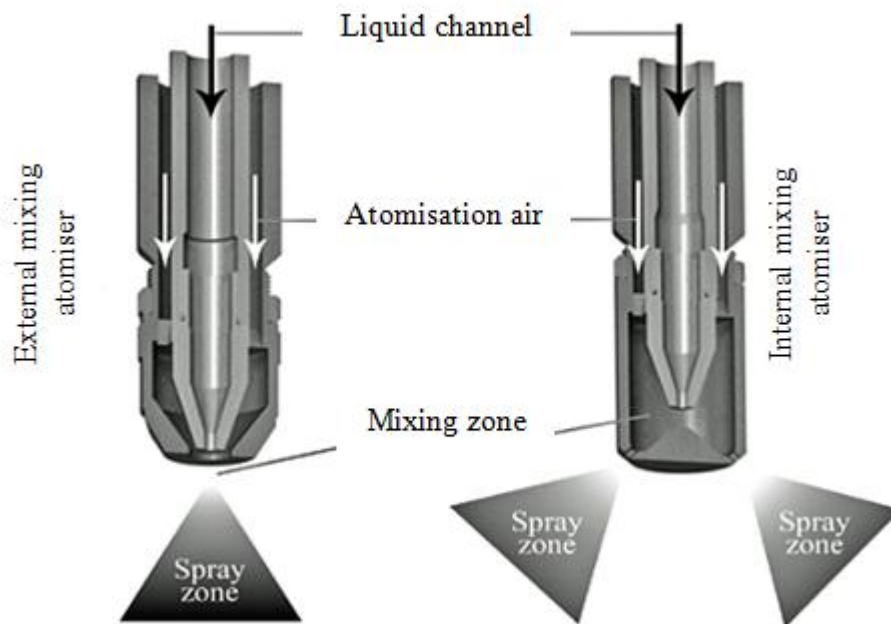


Figure 5.13: Two-fluid atomiser design (Salman et al., 2007)

5.4.2 Single Fluid Atomisers

5.4.2.1 Rotary Atomiser

Rotary atomisers use the centrifugal energy created by a spinning disc to create a spray, rather than by using liquid pressure. In this type of atomiser (Figure 5.14), liquid is fed onto a rotating surface, where it spreads out fairly uniformly under the action of centrifugal force (Lefebvre, 1989 and Nasr et al., 2002). Droplets are formed directly from the edge or from ligaments, as the fluid is launched from the rotating device edge, depending upon the rotational speed and the liquid flow rate.

This technique has two major potential advantages. The first is the possibility of producing very narrow droplet size distributions, and the second is the additional flexibility of the use of mechanical forces to pre-film the liquid rather than relying on small orifices.

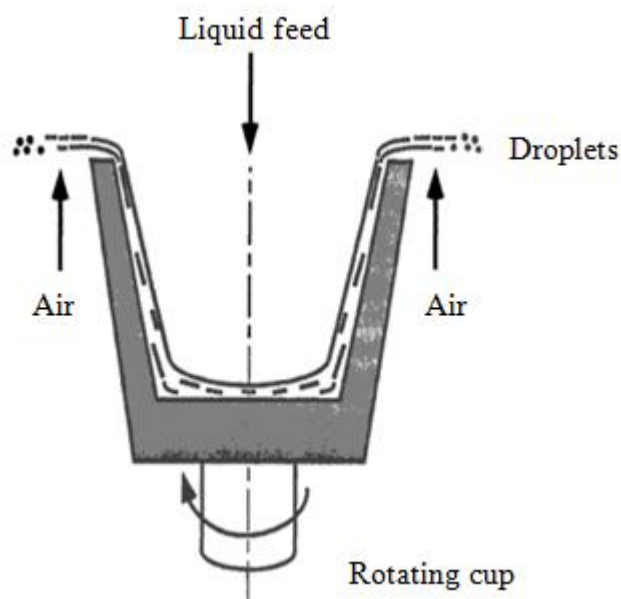


Figure 5.14: Schematic diagram of rotary atomiser

5.4.2.2 Ultrasonic Atomiser

Ultrasonic atomisers are used relatively little when compared with other techniques but they are particularly suited for producing low flow rates ($< 0.2 \text{ l/min}$) with very low kinetic energy and narrow size distributions. There are assorted configurations on the face of the ultrasonic atomiser and also different ways of introducing the liquid to that face. Generally, one or more piezoelectric crystals are used to vibrate the surface and a “stepped horn” acts as a velocity transformer. Larger ultrasonic vibration devices have been developed and are used for producing relatively narrow size distributions of low melting point metals, for the manufacture of metal powders. Figure 5.15 shows a diagram of an ultrasonic atomiser.

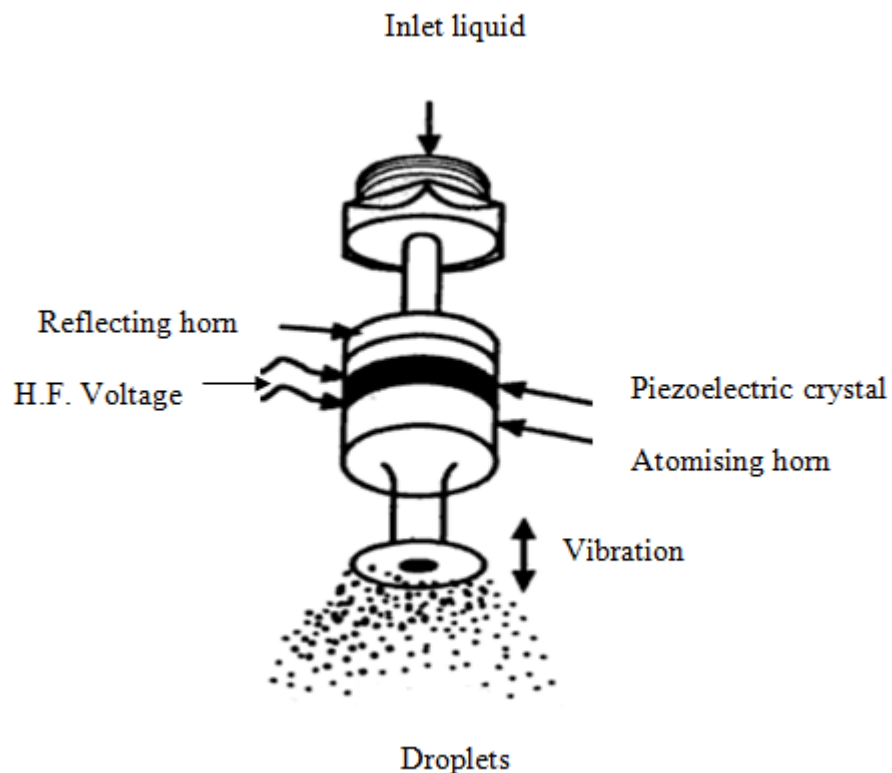


Figure 5.15: Schematic diagram of ultrasonic atomiser

5.4.2.3 Electrostatic Atomiser

An electrostatic atomiser (Figure 5.16) uses electrostatic energy for atomisation. It injects a charge from a high voltage (H.V) source into the liquid so that the charge at the surface of a jet or sheet of liquid acts against surface tension and causes a break-up (Lefebvre, 1989).

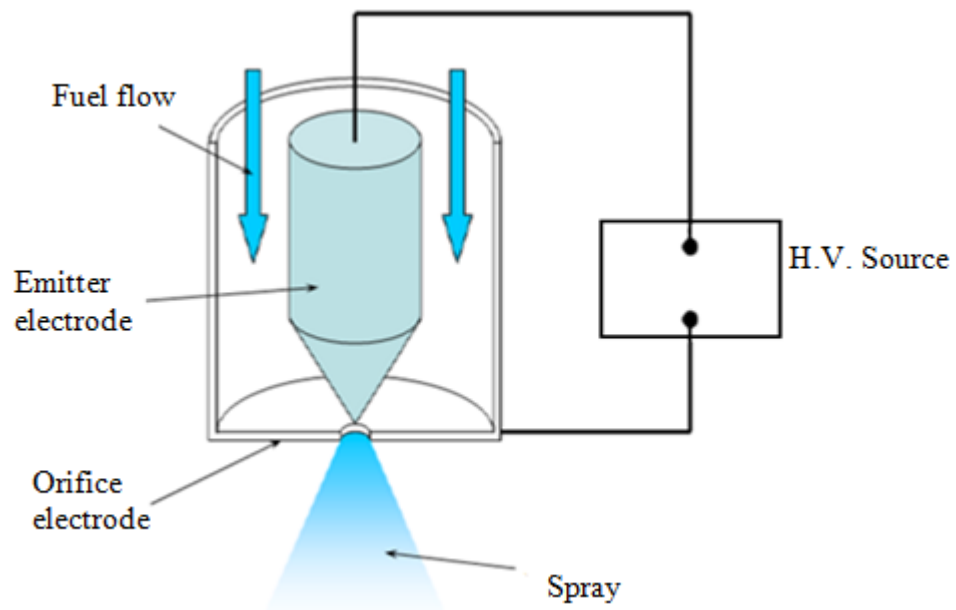


Figure 5.16: Schematic diagram of electrostatic atomiser

Electrostatic atomisers are not often used in practical devices but their use is actively being employed in several areas including liquid atomisation. This is usually achieved by the application of mechanical or aerodynamic forces being applied to the fluid. However, with electrostatic atomisation this disruption is achieved by the repulsive forces acting between like charges on the surface of the liquid. As the process is completely internal to the fluid, and no external mechanical or aerodynamic forces are required, liquid break-up can be achieved with very small amounts of power. The potential advantages include the production of relatively narrow drop size distributions,

the flexibility of controlling drop size by varying the charge injection and the possibility of manipulating the charged drops.

5.4.2.4 Pressure Atomisers

Pressure atomisers are used in a wide range of applications. In this type of atomiser, pressure energy is converted into kinetic energy in order to speed up the liquid to a high velocity relative to surrounding atmosphere (Liu, 2000). A high relative velocity enhances the liquid jet disintegration into a well-atomised spray. Depending on its design and geometry, the corresponding sprays could have different patternations (see Section 5.3 and Figure 5.6). There are several types of pressure atomisers which are briefly discussed below:

5.4.2.4.1 Plain orifice atomiser

The plain-orifice atomiser (see Figure 5.17) is the simplest type of pressure atomiser and is widely used for injecting liquids into a flow stream of air or gas. A circular orifice is used to inject a round jet of liquid into the surrounding air at high velocity under the action of high pressure. The best known of this type of application is possibly diesel injectors. They are widely used for spraying liquids into a flow stream of air or gas. In this type of atomiser, a small orifice size (usually $< 0.3\text{mm}$) and high pressure ($>100\text{MPa}$) are needed to produce a fine spray (Nasr et al., 2002).

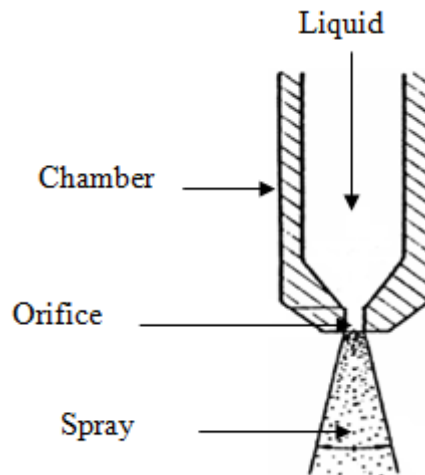


Figure 5.17: Typical plain orifice pressure atomiser

5.4.2.4.2 Fan jets atomiser

Fan jets or flat sprays atomisers use the simple orifice variation, in which the flow of liquid convergence shape of the orifice and the elliptically shaped exit hole combine to diverge the liquid streamlines as they leave the exit orifice (Nasr et al., 2002). Fan jets atomisers generally produce a triangular liquid sheet, the angle (0° - 110°) of which is determined by the orifice shape and the upstream convergence of the orifice. Figure 5.18 shows a typical Vee Jet atomiser.



Figure 5.18: Fan (Vee) Jet atomiser

5.4.2.4.3 Features and performance of pressure swirl atomiser

The useful features of the pressure swirl atomiser include simplicity of construction, ease of manufacture, reliability, good atomisation quality, low congestion propensities, and low pumping power needs. These benefits have resulted in the widespread use of pressure swirl atomisers (Ibrahim and Jog, 2006). Figure 5.19 shows the various designs of the pressure swirl atomiser.

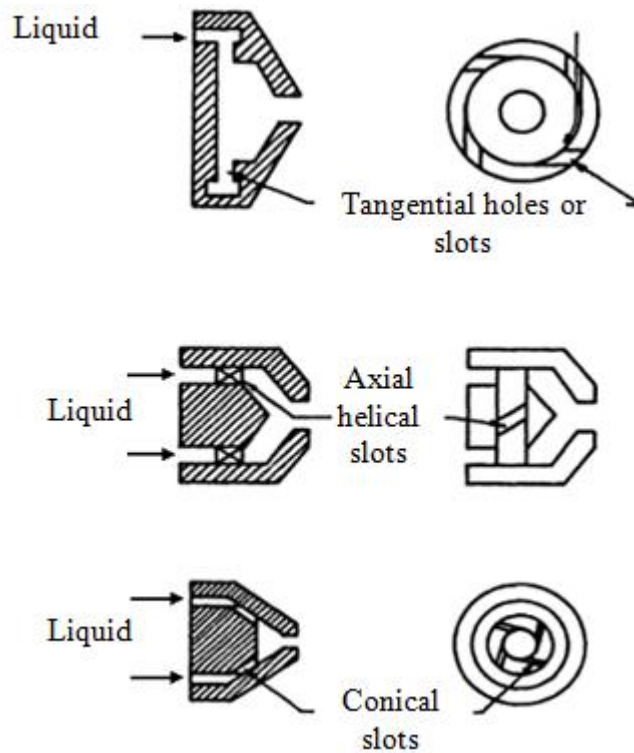


Figure 5.19: Various designs of pressure swirl atomiser

This type of atomiser is classified as the most competent atomiser in producing a fine spray using pressurised liquid. A minimum supply pressure is necessary to provide a particular drop size (Nasr et al., 2002). In this type of atomiser, swirling motion is imparted to the liquid inside the atomiser. It spreads out as a conical sheet once it leaves

the orifice under the action of centrifugal force. The atomiser consists of a cylindrical swirl chamber with arrangements of inlet and exit orifices.

Swirl atomisers differ from other atomisers in the quality of atomisation, and in the simplicity of construction and the reliability of operation (Khavkin, 2004). There are two major types of the swirl atomiser: the *hollow-cone spray* atomiser and the *full-cone spray* atomiser.

In the hollow-cone atomiser, most of the drops are concentrated at the outer edge of the conical spray pattern, while in the full-cone spray atomiser the drops are distributed across the spray.

In comparison, the hollow-cone atomisers provide better atomisation than solid-cone as solid-cone atomisers provide relatively coarse atomisation. Moreover, hollow-cone atomisers are preferred for many industrial applications due to their radial liquid distribution.

Horvay and Leuckel (1984) and Bayvel and Orzechowski (1993) accredit the swirl atomiser invention to Korting in 1902. Its applications include: aerosol products, oil fired combustors, agriculture, fire suppression, spray drying, fuel injection systems and many chemical processes.

Typically, solid- or full-cone atomisers have a larger drop size compared with hollow-cone atomisers. The aim of the experimental work in this study was to produce fine droplets ($\leq 5 \mu\text{m}$) by using a spraying and atomisation techniques; therefore, a hollow-cone atomiser has been selected in this research because it produces smaller drop sizes compared with the full cone atomiser (Nasr et al., 2002 and Lefebvre, 1989).

The characteristics of the spray produced by hollow-cone spray atomisers have been studied by a number of investigators. Rizk and Lefebvre (1984) reported that the mean drop sizes are relatively large close to the atomiser but decrease with the increase in downstream distance. Tokuoka et al. (1991) studied the radial distribution of the drop size, velocity and volume flux of the spray and they reported that the spray produced from hollow-cone atomisers contain, in general, large drops at the fringe and smaller drops entrained towards the central region. The important performance characteristic of this atomiser reinforced the selection that was made at the design stage of the present study, because the hollow-cone atomiser is capable of producing fine drops.

The effects of injection pressure and atomiser characteristics on hollow-cone sprays have also been studied by Zhang et al. (1991). They reported that the boundary between the sheath region and the central part of spray became clearer and the thickness of the sheath region decreased with increasing injection pressure.

The operating pressure is the major factor that affects the flow rate through an atomiser, which may be calculated by using the following relationship:

$$P_1 = P_2 (Q_1 / Q_2)^2 \quad (5.22)$$

Where P_1 is the calculated pressure for the desired spray discharge flow rate, Q_1 , P_2 and Q_2 are the known pressure and the spraying flow rate. This relationship is acceptable for most industrial applications and was used in the design of the atomiser in this research.

The relative velocity between the fluid and the air affects the droplet sizes. The fluid's velocity is created by pressure in the atomiser. Velocity increases as the fluid pressure

increases, and the average droplet size decreases. Figure 5.20 illustrates the development stages of the spray as the liquid injection pressure is increased.

The next chapter presents the design, construction and set-up of the experimental apparatus used in this research, in addition to the experimental procedure.

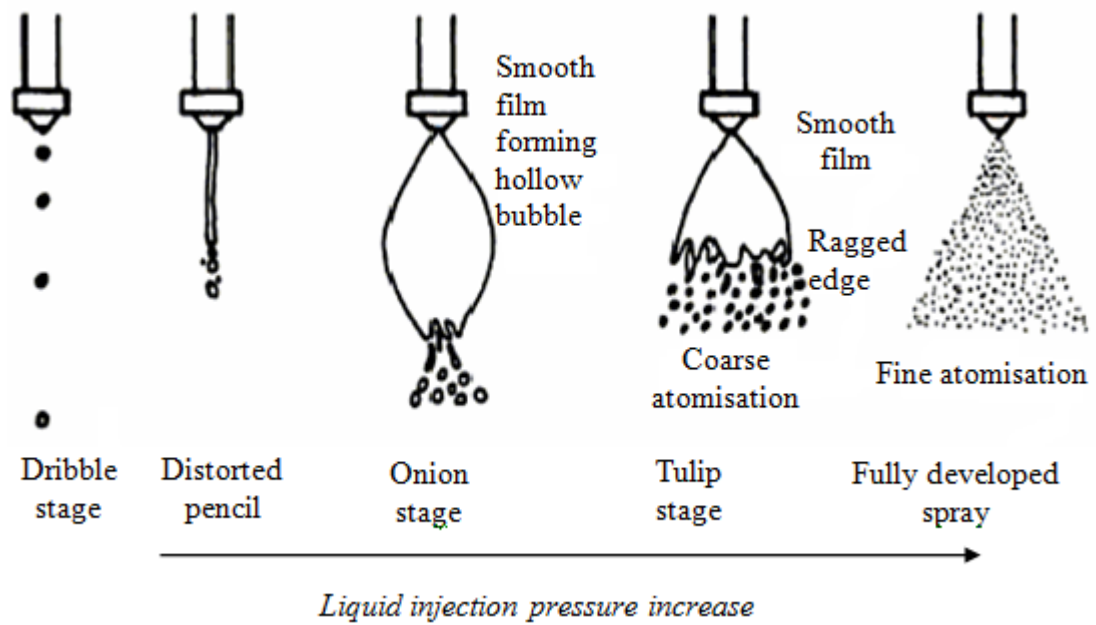


Figure 5.20: Spray development stages with fluid pressure increase (Lefebvre, 1989)

Chapter - 6

CHAPTER - 6: DESIGN OF A FINE SPRAY ATOMISER DEVICE, EXPERIMENTAL SET-UP AND PROCEDURE

6.1 Introduction

This chapter presents the design, construction and set-up of the experimental apparatus of the second method used in this research, in addition to the experimental procedure. The first method of this work (previously mentioned in Chapter Four) was a theoretical investigation of partial oxidation of natural gas (*mainly* methane) to produce syngas. The second method is the generation of Single-Walled Carbon Nanotubes (SWCNT) from the excess natural gas that was previously flared in oil industry activity.

The second method is divided into two phases: *Phase-I* was implemented at the University of Salford, Spray Research Group Laboratory, to develop sprays and atomisation techniques to produce fine droplets that have a number mean diameter ($D_{n0.50}$) of less than or equal 5 μm . *Phase-II* was implemented at the University of Oxford, in which a furnace was installed at the bottom of the *Phase-I* rig and the droplet particles' stream of methane and a catalyst solution was passed through the furnace (400 – 800°C). These reacted within the furnace to form $\text{C} + 2\text{H}_2$. The carbon, after dissolving in the iron (Fe) metal, will reorganise to form the Single-Walled Carbon Nanotubes material and the hydrogen may be stored for other use. The following sections describe in detail the design of the spray device, in addition to the construction and set-up of the experimental apparatus and the experimental procedure.

6.2 Design Philosophy and Procedure

The usual sequence of steps involved in developing a typical project is given in Figure 6.1. This is basically a series of steps which are to be followed in designing a project and it is known as a “Design Decision Tree” (Pugh, 1991).

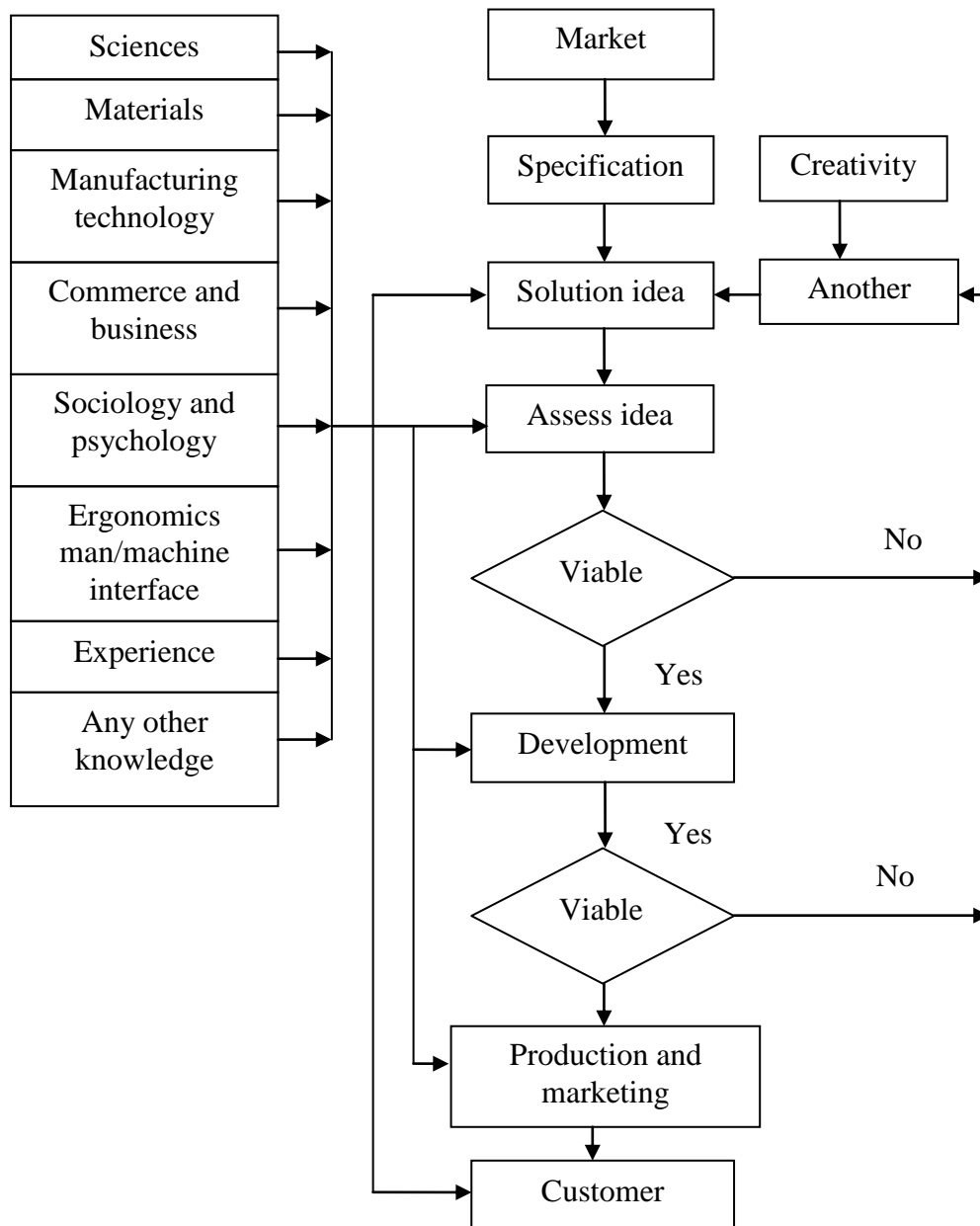


Figure 6.1: General design decision tree process (Pugh, 1991)

The basic contents of the design decision tree are investigation and gathering of information, generation and evaluation of ideas, evaluation, synthesis and development of design specification and production and marketing of the product.

This is the general procedure involved in developing or designing a new project. Each project comes with its peculiar features, which may require more or less steps being involved in having a successful design. Because of these possible peculiarities, it is also important to note that each project may come with different requirements. Figure 6.2 shows the sequence of steps involved in the atomiser device design process which are briefly presented in the following sections.

6.2.1 Atomiser Device Design Specification: B1*

The first step in the design procedure (Figure 6.2, B1) is to compile the design specifications of the atomiser device, which are:

- i. Droplet size produced as small as possible ($< 5 \mu\text{m}$);
- ii. Viscosity of aqueous phase about the same as water;
- iii. Temperature up to $80 \text{ }^\circ\text{C}$;
- iv. Rate of addition of aqueous phase $0.001\text{-}0.005 \text{ l/min}$;
- v. Rate of flow of methane $0.3 - 0.4 \text{ l/min}$;
- vi. All methane or only a portion can be used for the atomiser and the rest can be added separately;
- vii. Pressure of gas: the lower the better. Up to 1 bar , (0.1 MPa);
- viii. Pressure of liquid up to 120 bar (12 MPa).

**This refers to the flowchart "Box's" shown in Figure 6.2*

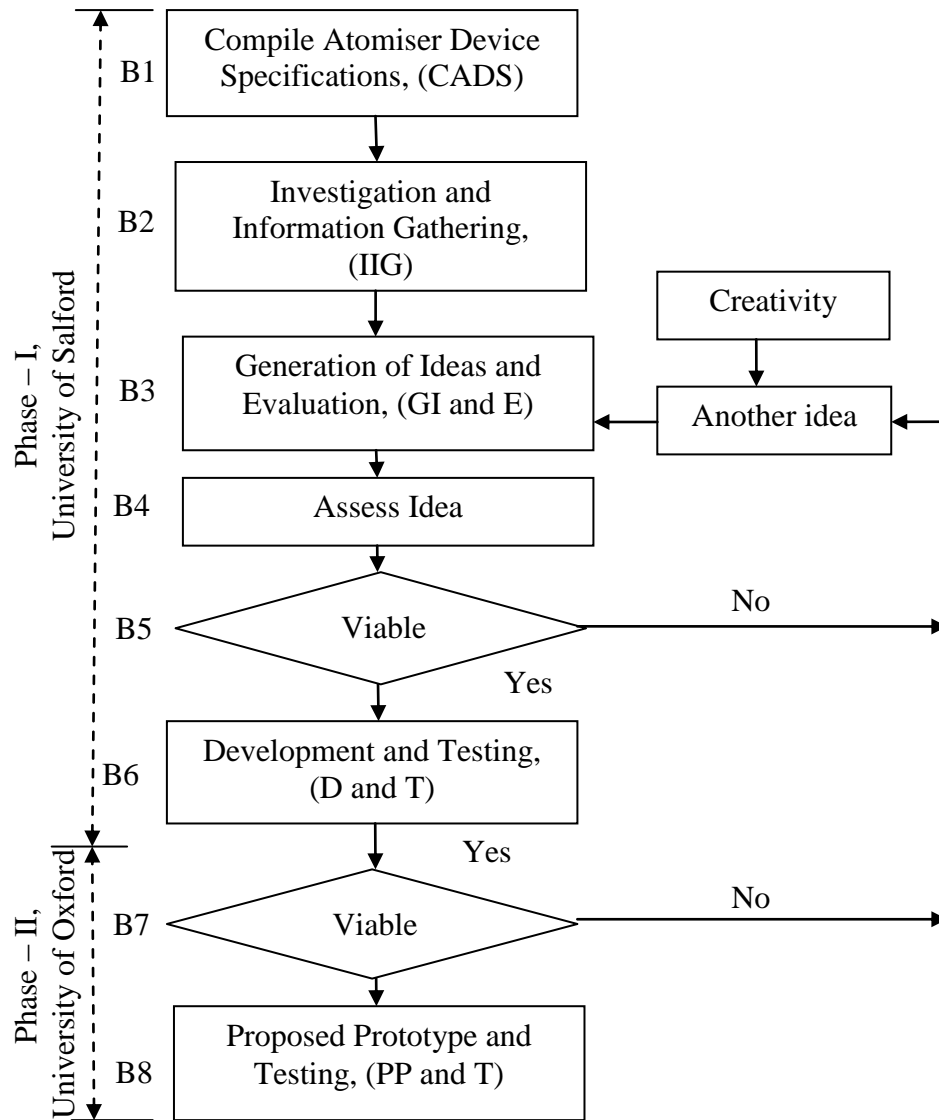


Figure 6.2: The design process for the atomiser device for carbon nanotubes production

6.2.2 Design of Fine Spray Atomiser Device

6.2.2.1 The Investigation and Gathering of Information (IGI): B2

In Figure 6.2, B2 is the second step of the design process. The design of the atomiser device is based on the specifications that are stated in a previous section, Section 6.2.1.

The design of the fine spray atomiser device for carbon nanotubes' production is partly based on the concept of "cascade impactors" method. Cascade impactors are widely used to classify particle sizes at different flow rates for industrial purposes (Yuji et al., 2005 and Dahlin et al., 2008). The impactor devices are also utilised for the sampling and the size-selective collection of aerosol particles such as dry powder inhalers and metered dose inhalers, product development and for the quality control of finished products. They consist of a number of impaction stages connected in series with increasingly smaller cut-off diameters as shown schematically in Figure 6.3 (Marple and Oslon, 2009). In the operation, an aerosol stream passes through an atomiser and impinges upon a collection plate.

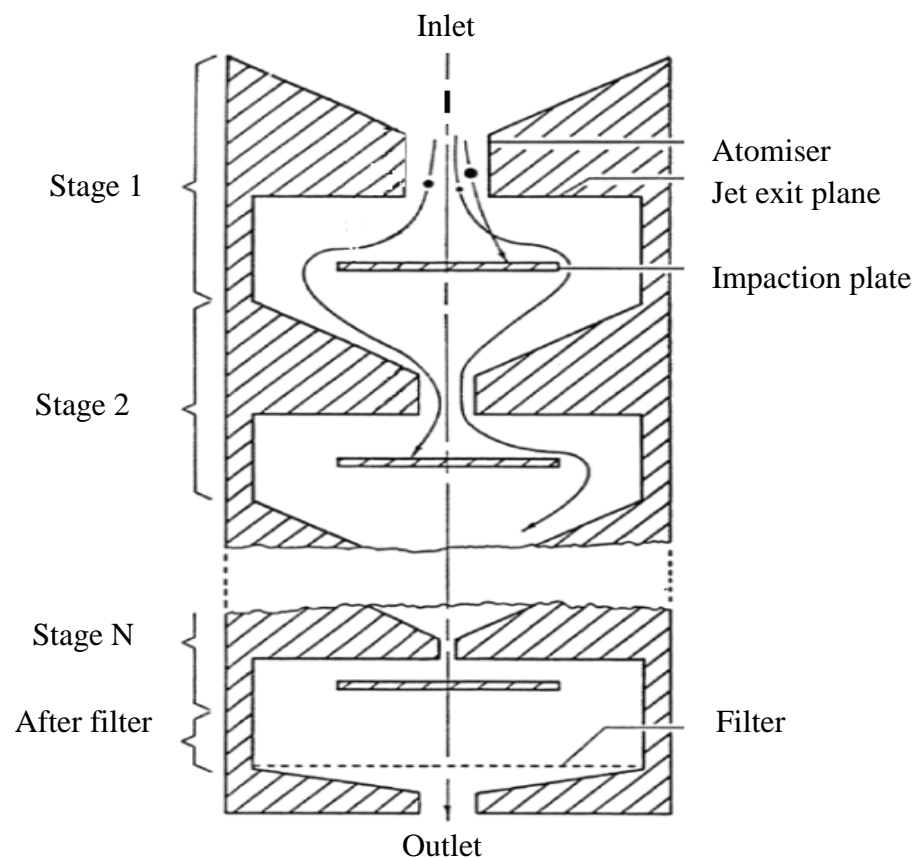


Figure 6.3: Schematic diagram of typical cascade impactor

Particles in the aerosol stream having large enough inertia will impact upon the collection plate, while the other particles will follow the air flow out of the impaction region. However, it was not possible to use one of these off-the-shelf devices during this investigation for the generation of carbon nanotubes, utilising simultaneously a catalyst and methane gas. During the initial stage, it was clear that the commercial pressure swirl atomisers that are currently available are not able to produce drop size of $\leq 5 \mu\text{m}$. Therefore, it was necessary to design a system which could subsequently break-up the droplets to the required sizes. The alternative atomiser design that could have been utilised was to design an atomiser device in which the supply liquid had to be atomised by a required velocity in air or gas.

The closest commercially available pressure swirl atomiser to meet the requirements was a type 121, stainless steel hollow-cone atomiser, as shown in Figure 6.4, manufactured by Schlick Ltd. (Schlick Atomising Technologies, Germany). A hollow cone atomiser was selected because it has the finest drop sizes compared with full and flat cone atomisers. The atomiser has a nominal spray angle of 60° and exit orifice of 0.1 mm diameter. Table 6.1 and Figure 6.5, which were used in the design of the atomiser device, show the performance specification and the variations of mean volume droplet size (μm) with orifice diameter (mm) for different liquid supply pressures respectively. Nevertheless, to incorporate the pressure swirl atomiser in conjunction with the cascade impactor conceptual idea imposed a design challenge. The unified design approach of atomisers in different fields requires interrelation between the different spray characteristics of the atomisers with the pertinent input parameters such as: liquid fuel properties, injection conditions and atomiser geometries.

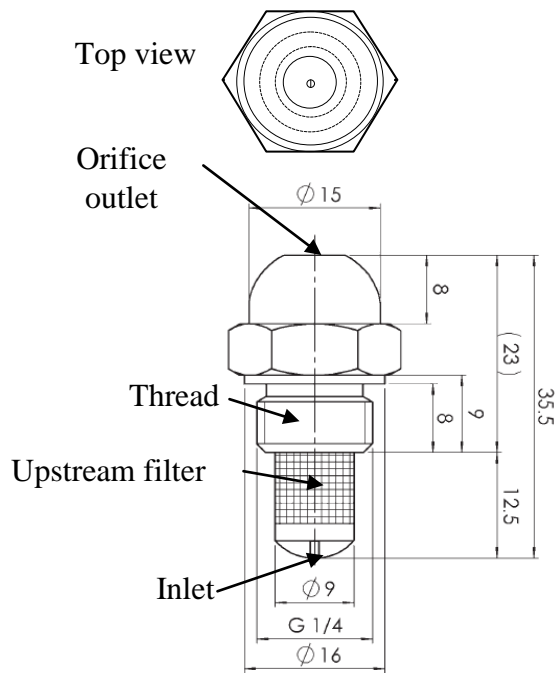


Figure 6.4: Schlick hollow-cone atomiser, type 121 (dimensions are in mm)

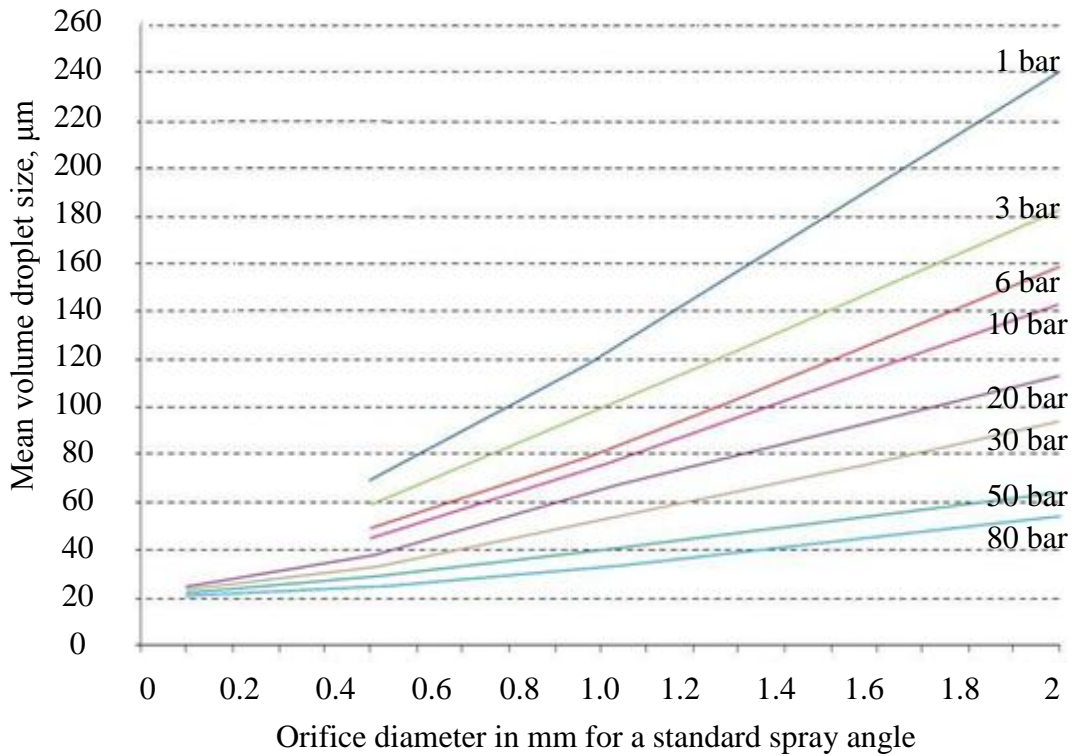


Figure 6.5: The variations of mean volume droplet size with orifice diameter for different liquid supply pressure **

Orifice diameter, mm	Flow rate in l/min									
	1bar	2 bar	3 bar	4 bar	6 bar	8 bar	10 bar	15 bar	20 bar	30 bar
0.10 *					0.01	0.016	0.018	0.022	0.025	0.031
0.15					0.02	0.024	0.027	0.033	0.038	0.047
0.20					0.03	0.034	0.038	0.047	0.055	0.067
0.25					0.04	0.048	0.054	0.066	0.076	0.094
0.30					0.05	0.057	0.064	0.076	0.090	0.111
0.35			0.047	0.055	0.06	0.078	0.087	0.106	0.123	0.151
0.4			0.062	0.072	0.08	0.102	0.114	0.139	0.161	0.197
0.45			0.079	0.091	0.11	0.129	0.144	0.176	0.203	0.249
0.50			0.097	0.112	0.13	0.159	0.178	0.218	0.252	0.308
0.55		0.09	0.118	0.136	0.16	0.192	0.215	0.263	0.304	0.373
0.60		0.11	0.141	0.163	0.19	0.230	0.257	0.315	0.364	0.445
0.70		0.15	0.191	0.220	0.27	0.312	0.348	0.427	0.493	0.603
0.80		0.20	0.250	0.288	0.35	0.408	0.456	0.559	0.645	0.790
0.90		0.25	0.316	0.365	0.44	0.516	0.577	0.706	0.815	0.999
1.00	0.2	0.31	0.391	0.451	0.55	0.638	0.713	0.874	1.009	1.236
1.10	0.2	0.38	0.473	0.546	0.66	0.772	0.863	1.057	1.221	1.495
1.20	0.3	0.46	0.563	0.650	0.79	0.919	1.029	1.258	1.453	1.780
1.30	0.3	0.53	0.660	0.762	0.93	1.077	1.205	1.475	1.704	2.087
1.40	0.4	0.65	0.766	0.884	1.08	1.251	1.398	1.712	1.977	2.422
1.50	0.5	0.71	0.879	1.015	1.24	1.435	1.604	1.965	2.269	2.779
1.60	0.5	0.816	1.000	1.154	1.41	1.633	1.825	2.236	2.581	3.162
1.70	0.6	0.92	1.129	1.303	1.59	1.843	2.061	2.524	2.915	3.570
1.80	0.7	1.03	1.266	1.462	1.79	2.067	2.312	2.830	3.268	4.003
1.90	0.8	1.15	1.410	1.628	1.99	2.302	2.574	3.152	3.640	4.458
2.00	0.9	1.27	1.563	1.805	2.21	2.552	2.853	3.494	4.035	4.942
2.10	0.9	1.40	1.723	1.989	2.43	2.831	3.145	3.852	4.448	5.448
2.20	1.0	1.54	1.890	2.182	2.67	3.086	3.450	4.226	4.879	5.976
2.30	1.1	1.68	2.067	2.387	2.92	3.375	3.773	4.621	5.336	6.536
2.40	1.2	1.83	2.250	2.598	3.18	3.674	4.107	5.031	5.809	7.115
2.50	1.4	1.99	2.441	2.818	3.45	3.986	4.456	5.458	6.302	7.719

Table 6.1: Performance specification, 121 hollow-cone spray atomisers **

*Chosen atomiser

**Adapted from: <http://www.duesen-schlick.com>

Thus design estimations (see Section 6.2.2.4) were carried out which demonstrated that on the basis of 5 μm size of drops, or less, the liquid droplet settling velocity (see Section 5.3.2.1) required is approximately 0.068 cm/sec. This value compared with the gas velocity of 3 cm/sec is acceptable since it shows that the gas velocity is faster than the aerosol droplet velocity. Also, the estimation provided the corresponding information on the required dimensions of the confinement tube which was made from Perspex.

6.2.2.2 Generation of Ideas and Evaluation (GIE): B3 - B5

During the design procedure and preliminary trials (Figure 6.2, B3 – B5), several options were examined based on the design calculations such as the positions of both the baffle plate and the aerosol tube and the arrangement (*inverted, horizontal or vertical*) of the atomiser device relative to the Malvern Mastersizer-X instrument. These are discussed in detail in the next chapter, in Section 7.6.2, which deals with the results, analysis and discussion. Figure 6.6 shows the proposed diagram of an atomiser manifold and Figures 6.7, 6.8 and 6.9 show the proposed diagrams of inverted, horizontal and vertical atomiser device positions.

6.2.2.3 Atomiser Device Development and Testing (D and T): B6

After these steps, the following stage is the development and testing of the atomiser device, Figure 6.2, B6. This Section and Section 6.2.2.4 present this stage in detail, including the estimation of the Settling Velocity of droplets.

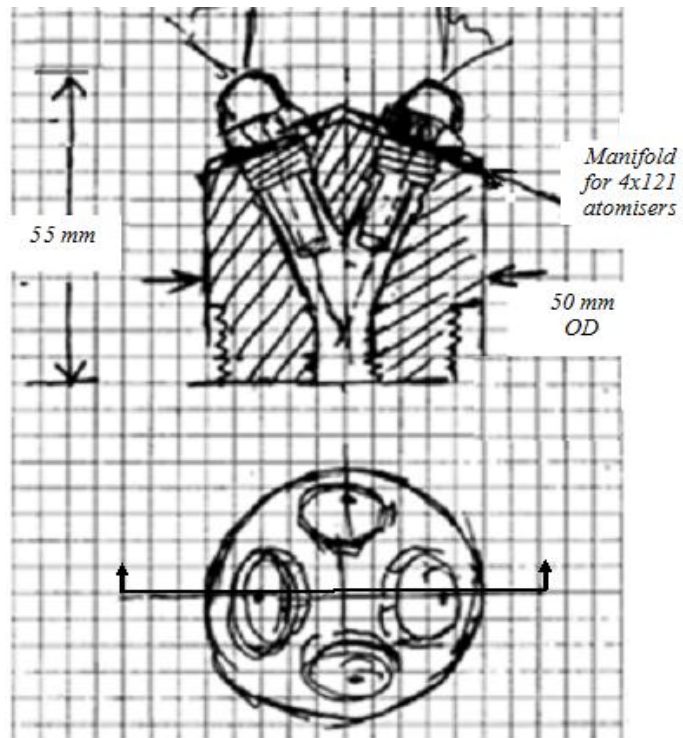


Figure 6.6: Proposed diagram of atomiser manifold

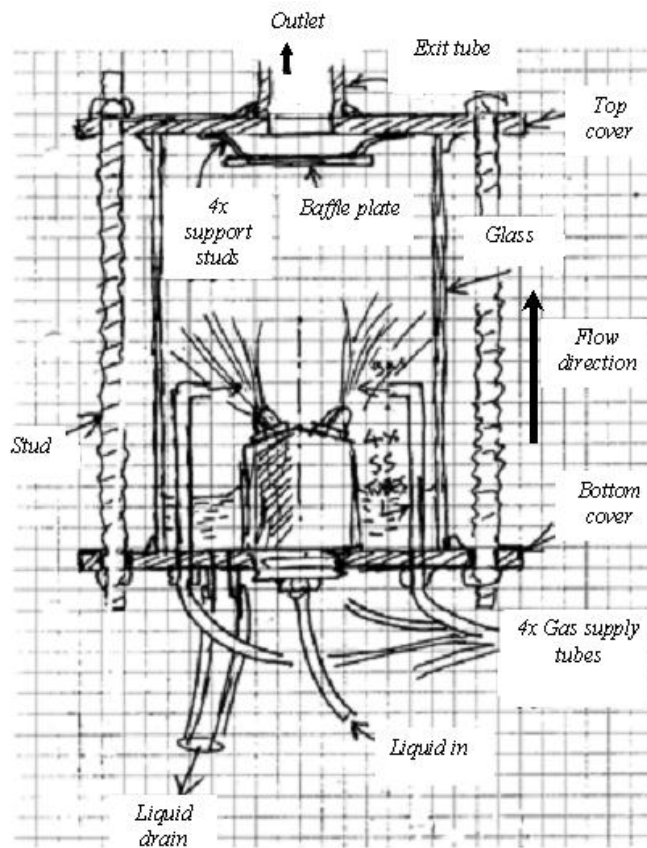


Figure 6.7: Proposed diagram of atomiser device (inverted)

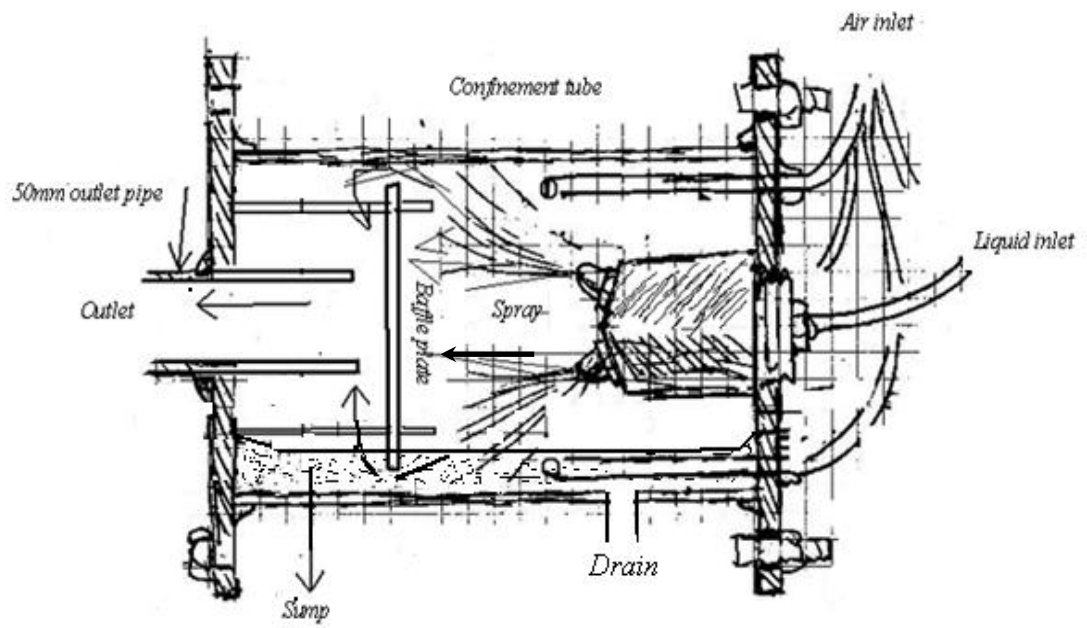


Figure 6.8: Proposed diagram of atomiser device (horizontal)

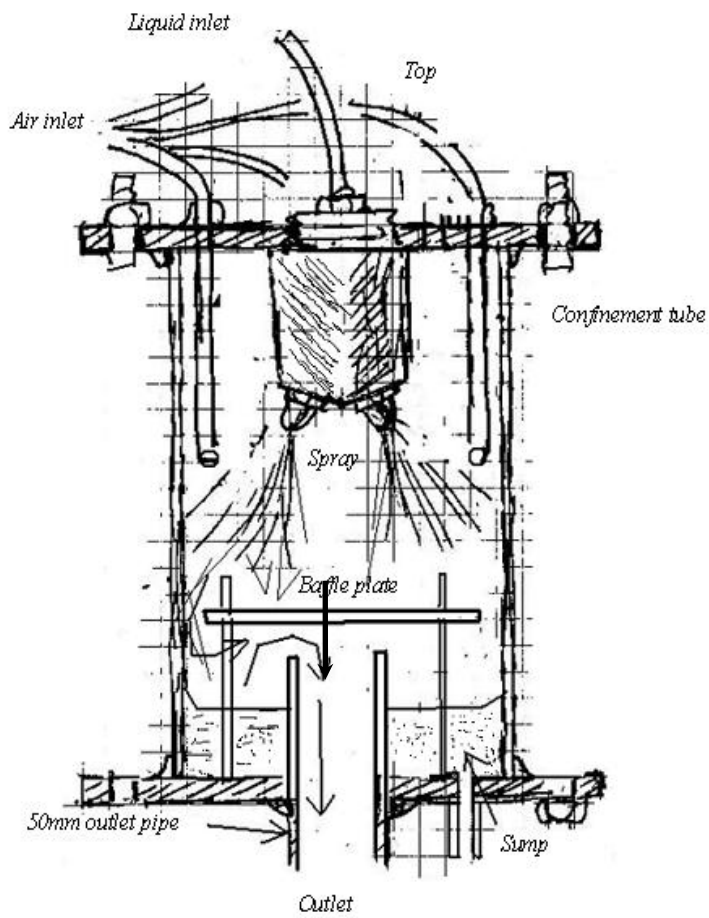


Figure 6.9: Proposed final diagram of atomiser device (vertical)

The atomiser device was designed to operate at low pressure and consisted of a confinement tube with a cover for each open end, into which they were screwed onto the tube; an atomiser holding block and a manifold of hollow cone commercial swirl atomiser that interacted with a baffle plate (or *impactor*) in order to separate the larger droplets and produce a fine aerosol in the outlet of the device (exit tube), as shown in Figures 6.10 and 6.11. The confinement tube was constructed from perspex with dimensions: 250 mm length, 180 mm inside diameter and 3 mm wall thickness according to the design estimation as highlighted in Section 6.2.2.4.

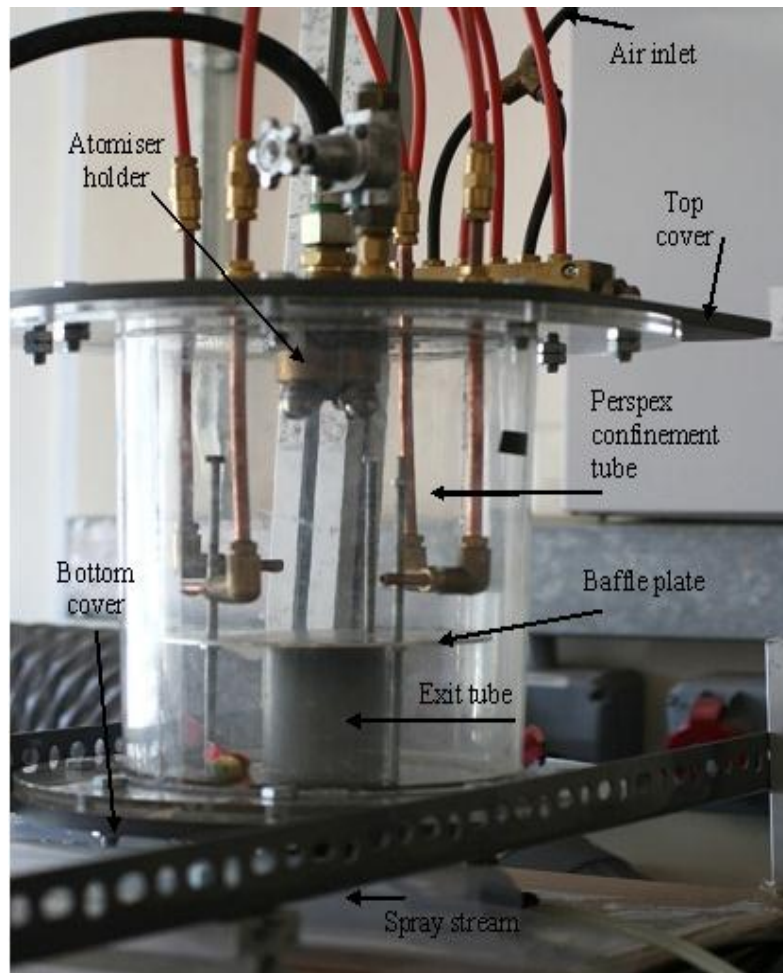


Figure 6.10: Illustration of atomiser device set-up

On the centre of the top cover, an atomiser holding block of 80 mm diameter was fixed, for mounting the manifold of the four atomisers as shown in Figure 6.11. The atomiser holding block and manifold were reconstructed allowing for the mounting of more than four atomisers (up to eight) in order to increase the spray flow rate if required in the *Phase II* trials, as shown in Figures 6.12 (a and b).

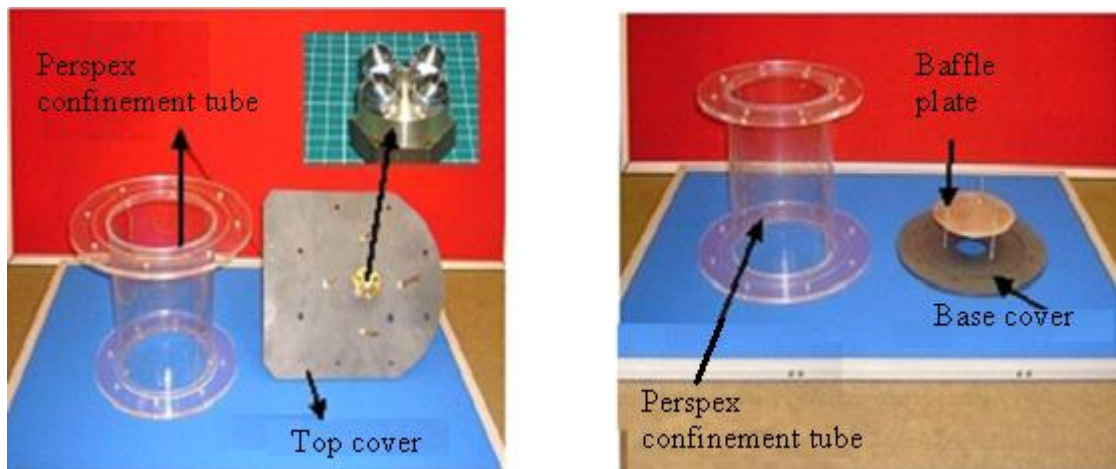
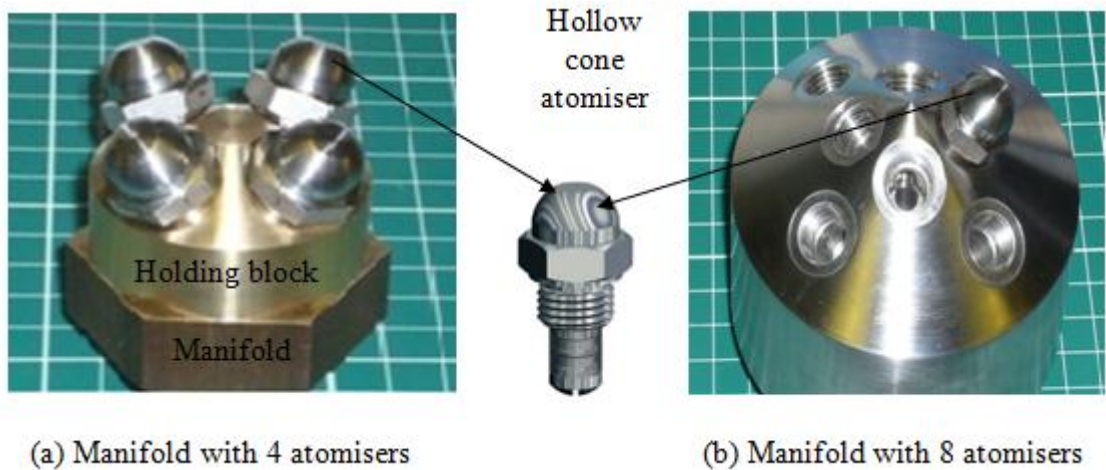


Figure 6.11: Confinement tube with top cover and base cover



(a) Manifold with 4 atomisers

(b) Manifold with 8 atomisers

Figure 6.12: Liquid spraying atomisers and holding block

In this research, the *Phase I* trials were performed using four atomisers. The atomisers were used to spray the liquid into the gas/or air stream which was fed through four inlet 3 mm gas tubes fixed on the top cover around the atomisers' holding block position.

The concentration and drop size of the aerosol at the outlet exit for given liquid properties are determined by the following factors:

- i. Supply pressure and flow ratio of liquid supplied to the swirl atomisers;
- ii. Flow rate of air/or gas supplied to the device;
- iii. Vertical gap between the baffle plate and the top of the outlet of the aerosol.

A movable aluminium baffle plate, which could be moved up and down, with a 148 mm diameter and 2 mm thickness, was fixed with 3 studs on the bottom cover of the tube (see Figure 6.11). This baffle plate was used to separate the larger droplets and to produce a fine spray in the aerosol tube of the device. This is a novel method of producing fine spray droplets of $\leq 5\mu\text{m}$ using standard pressure atomisers. A movable tube (exit tube) of 50 mm diameter was also inserted in the centre of the bottom cover. The outlet side of this tube was reduced to 15 mm to narrow the spray stream slot (see Section 7.2.2.2). Both baffle plate and the tube were movable and their positions were changing during the trials in order to find the optimum set-up of the rig.

The dimensions of the tube in terms of diameter and height must be precise in order to ensure that the required settling velocity could be achieved. This is the velocity which is equivalent to the velocity of aerosol drops that tend to fall back down the tube if greater than $5\mu\text{m}$ and thus accumulate to drain away with smaller ones carried away to the exit.

6.2.2.4 Estimation of Settling Velocity (D and T): B6

The design of the atomiser device is based on the following calculation:

The selected atomiser type was hollow cone, type121, for low flow rates and fine atomising.

From Table 6.1:

At 0.1 mm orifice diameter, the liquid flow rate $Q_1 = 0.031$ l/min at liquid pressure $P_1 = 30$ bar.

From equation (5.22):

$$P_1 = P_2 (Q_1/Q_2)^2$$

At 100 bar,

$$\text{Atomiser liquid flow rate } Q_2 = Q_1 * (P_2/P_1)^{1/2}$$

$$Q_2 = 0.031(100/30)^{1/2} = 0.057 \text{ l/min,}$$

Flow rate of 4 atomisers:

$$Q_3 = 0.057 * 4 = 0.23 \text{ l/min}$$

From Figure 6.4:

$$D_{v0.5} = 20 \mu\text{m at } 80 \text{ bar}$$

$$D_{v0.5} \approx 19 \mu\text{m at } 100 \text{ bar}$$

From Rosin-Rammler graph (Appendix B1):

$$7\% \text{ by volume } \leq 5 \mu\text{m}$$

$$Q_{\text{req}} = 0.07 * 0.23 \text{ l/min} = 0.016 \text{ l/min at } 100 \text{ bar}$$

Settling velocity:

From equation 5.21:

$$U_{ps} = (\rho_L - \rho_{CH_4}) \frac{g D_p^2}{18 \mu_{CH_4}}$$

Where; $\rho_L = 1000 \text{ kg/m}^3$; $\rho_{\text{CH}_4} = 0.781 \text{ kg/m}^3$; $d_p = 5 * 10^{-6} \text{ m}$; $g = 9.81$;

$\mu_{\text{air}} = 1.85 * 10^{-5} \text{ kg/ms}$; $\mu_{\text{CH}_4} = 2 * 10^{-5} \text{ kg/ms}$

U_{p_s} = velocity of drops falling back based down

$$U_{p_s} = (1000 - 0.781) \frac{9.81 * (5 * 10^{-6})^2}{18 * 2 * 10^{-5}}$$

$$= 0.000681 \text{ m/s} = 0.0681 \text{ cm/s}$$

Velocity in cylinder:

Diameter = D, $Q_{\text{CH}_4} = 0.3 \text{ to } 0.4 \text{ l/min}$

$$(0.4/60) * 10^3 = \frac{U_{p_s} \pi D^2}{4}$$

If $u_{p_s} = 0.0681 \text{ cm/s}$,

$$D = 12 \text{ cm} = 120 \text{ mm}$$

However, internal diameter of the confinement tube of 120 mm found to be restricting the placement of the corresponding manifold, which has a diameter of 50 mm (OD), as shown previously in Figure 6.6. Thus, it was necessary to increase the diameter of the confinement tube to 180 mm (OD) without affecting the drop sizes, whilst the settling velocity reduced to approximately third of its original estimation.

The set-up of experimental apparatus is presented in the next section.

6.3 Experimental Apparatus Set-up

6.3.1 Overview

The experimental apparatus set-up used to conduct this research is presented in this section. This work was carried out in collaboration with the Inorganic Chemistry Group (ICG), at the University of Oxford, and was divided into two phases as mentioned in Section 6.1.

Phase-I experiments were carried out at room temperature with a target of achieving the optimum set-up for the apparatus to attain the desired fine droplets, at an air flow rate of 0.3 - 0.4 l/min and pressure of 1 bar (0.1 MPa), while the liquid flow rate ranges between 0.001 to 0.005 l/min and flowing pressure in the ranges of 60 to 110 bar (6 to 11 MPa).

6.3.2 Apparatus Set-up

The major components of the apparatus used in the experimental set-up of the *Phase-I* experiments are shown schematically in Figure 6.13. The system consisted of the following interrelated parts:

- i. Reservoir tank and water pump;
- ii. Air supply and flow metering;
- iii. Atomiser holding and positioning assembly;
- iv. Atomiser device (*described in detail in Section 6.2.2.3*);
- v. Spray measurement unit (Malvern Mastersizer-X);
- vi. Still camera.

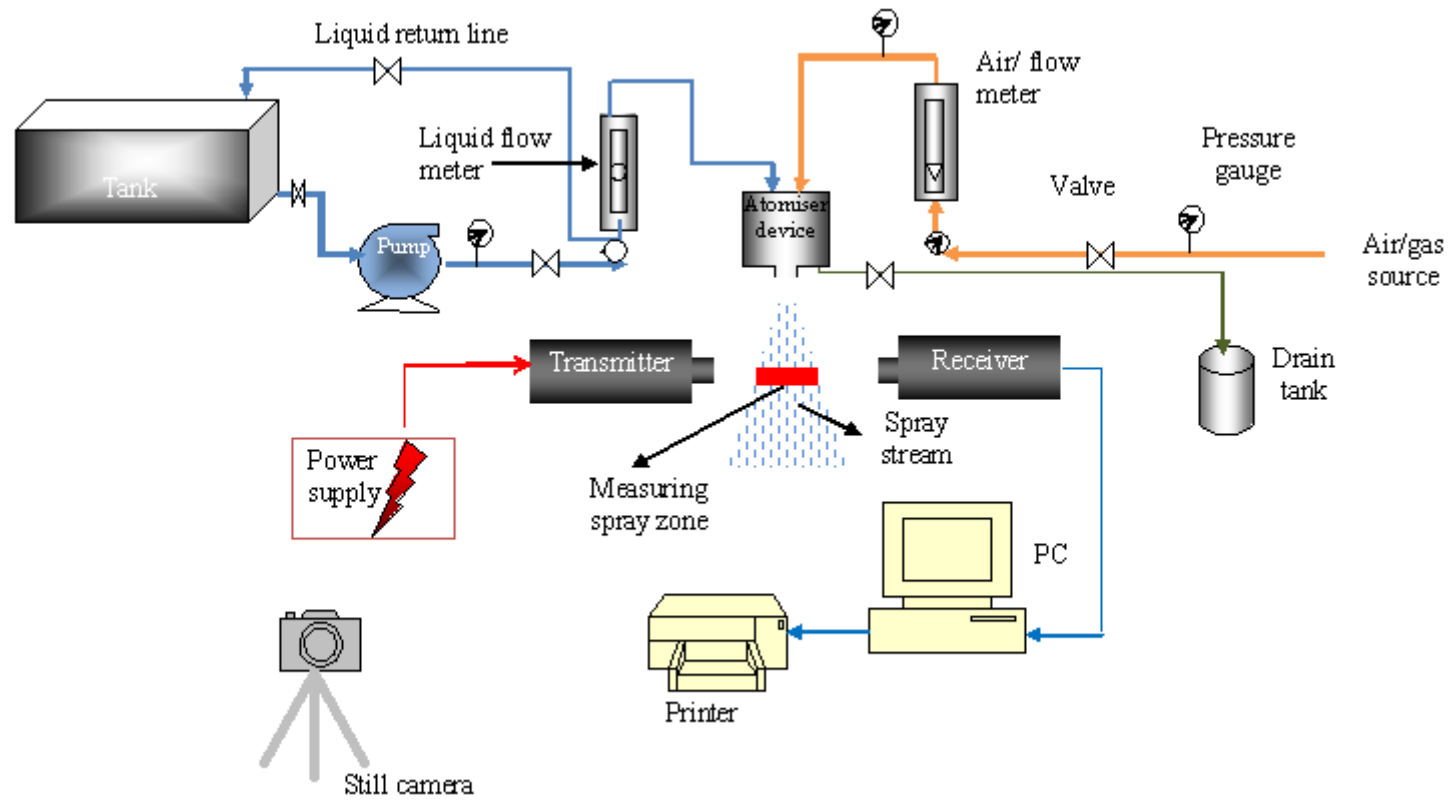


Figure 6.13: Schematic flow diagram of experimental set up (phase-I)

6.3.2.1 Reservoir Tank and Water Pump

Water was used in the *Phase-I* trials to simulate the metal catalyst (used at the University of Oxford). As shown in Figure 6.13, a 25 gallon plastic tank fed a Speck Kolben pump (see Figure 6.14) to deliver high pressure water to the spray head. The water pressure and flow rate to the spray head were regulated by the metering system to provide optimum conditions for minimum droplet size. The pump had the following specifications:

- i. Manufacturer: Speck Kolben
- ii. Type NO25/50-120
- iii. Maximum flow: 48.7 l/min
- iv. Power: 11.50 kW
- v. Maximum operating pressure: 12MPa
- vi. Maximum temperature: 70°C

A liquid return line (see Figure 6.13) is used to return excess liquid to the reservoir. A valve is also used for pressure adjustment and to by-pass the atomiser. To prevent the blocking of the atomisers and to maintain liquid-free unwanted particles, a stainless steel wire screen was fitted to the outlet (inside) of the reservoir tank. A hydraulic pipe was used to manage the pump discharge towards the spray head and had the following dimensions:

- i. Nominal Diameter: 2.175 cm
- ii. Maximum Working Pressure: 450 bar (45MPa)

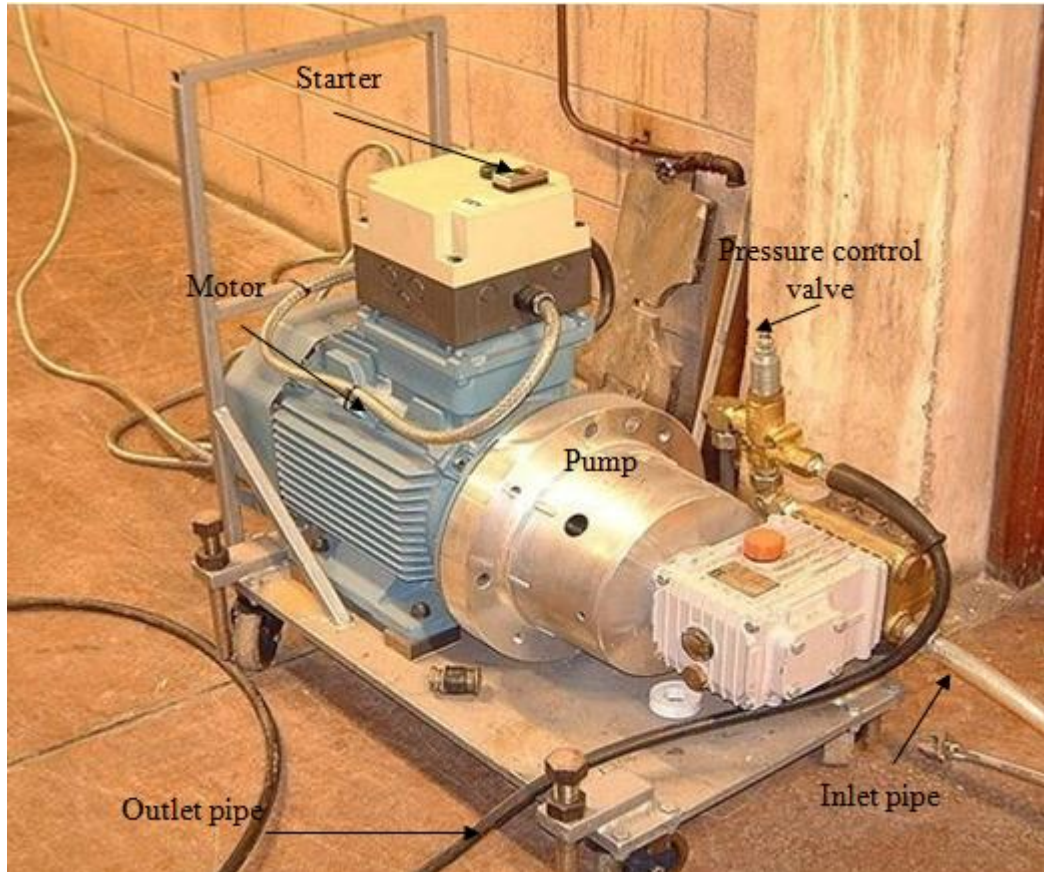


Figure 6.14: Speck Kolben water pump

6.3.2.2 Air Supply and Flow Metering

The inlet air was fed through 3mm O.D. nylon tubing connected with “Enots” solderless brass fittings from the laboratory high-pressure airline and was regulated using a pressure regulator. The air flowed through the system at 1 bar (0.1 MPa) and was controlled by means of mass flow controllers and measured with rotameter flow meters, which provide calibration data and a direct reading scale for the air, as shown in Figure 6.13. Before the start of each experiment, the calibration of the air/or gas flow rate was set by the use of standard calibration charts as shown in Figure 6.15. Also, Figure 6.16 partly shows the air flow meters A1, A2, A3 and A4. The rotameters could be calibrated to an accuracy of within ± 0.50 percent of full scale.

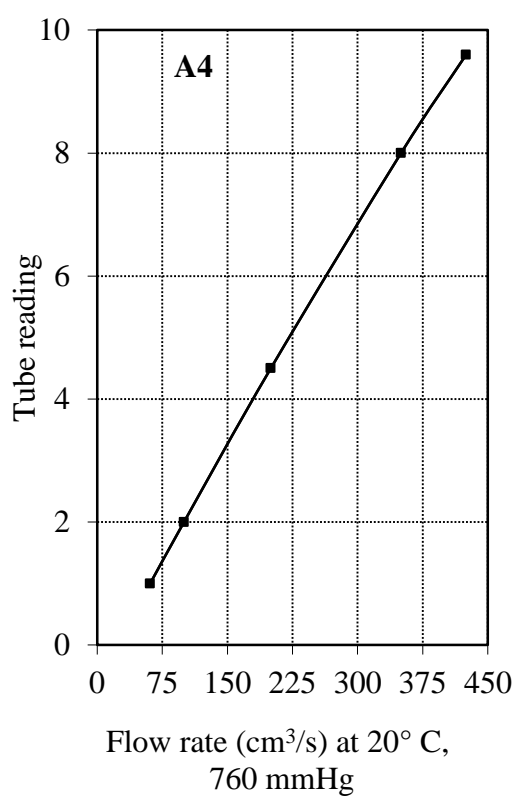
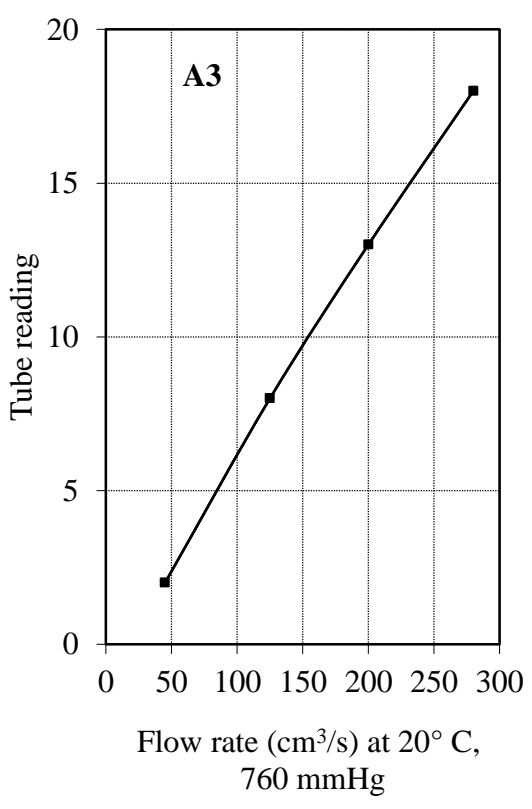
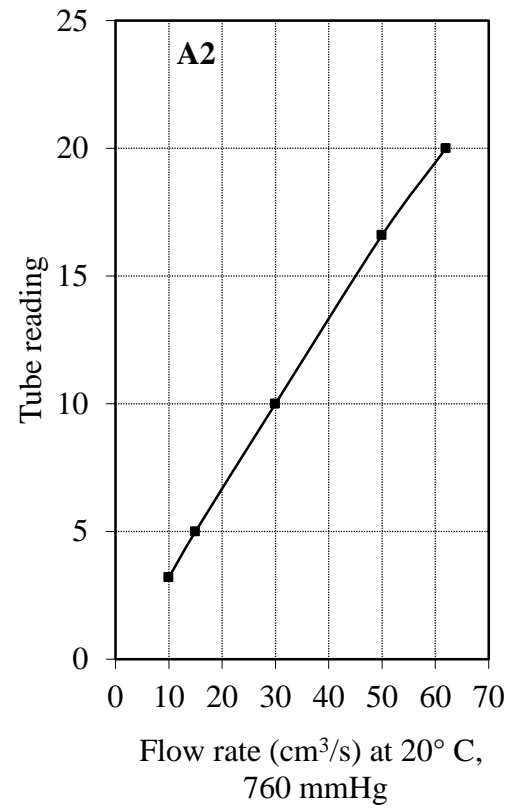
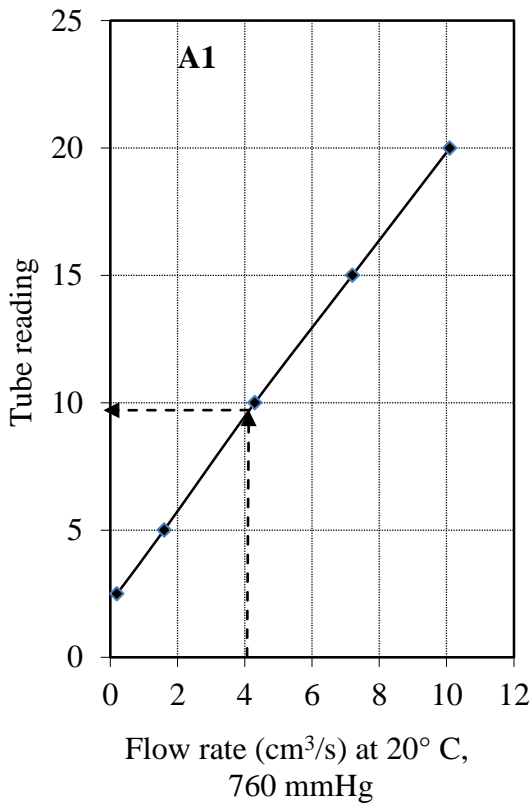


Figure 6.15: Air flow rate standard calibration charts

6.3.2.3 Atomiser Holding and Positioning Assembly

The atomiser holding and positioning assembly is made of iron and aluminium bars, as shown in Figure 6.16. It was designed and constructed to have free movement in relation to the Malvern Mastersizer-X (Malvern Instruments Ltd., Malvern, U.K.) in order to enable testing of the atomiser at various positions as required, and also to avoid movement caused by tension in the flexible high pressure liquid supply pipeline.

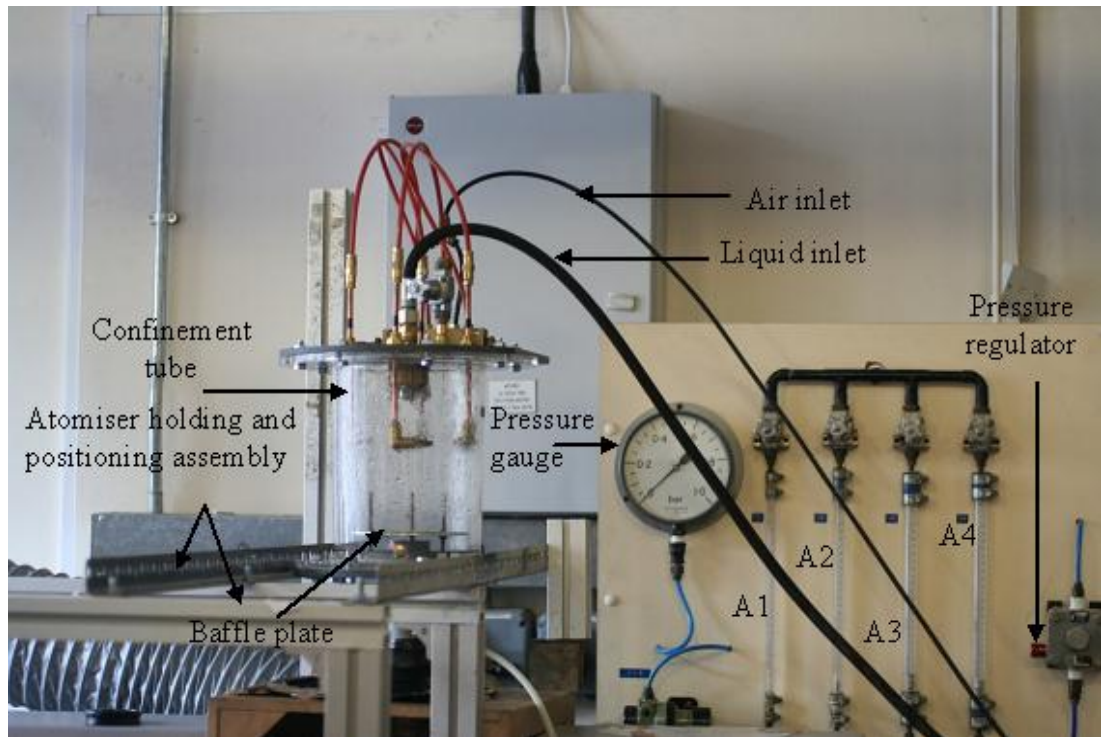


Figure 6.16: Atomiser device connected to air flow meters

6.3.2.4 Malvern Mastersizer-X Set-up

To specifically characterise droplet sizes' distribution from the designed atomiser device, a measurement device is needed. As described in the previous chapter, Sections 5.3.3.1 and 5.3.3.2, the Malvern Mastersizer-X, as illustrated in Figure 6.17, is the

measuring device used. As shown schematically in Figure 6.18, with a spray device set-up, the instrument consisted of a single lens laser diffraction system, used to analyse the droplets' sizes of the liquid/gas mixture stream. The lens had a focal length of 300 mm and a 2.40 mm active beam length, which was able to analyse particles in the range of 0.1-900 μm .



Figure 6.17: Malvern Mastersizer-X

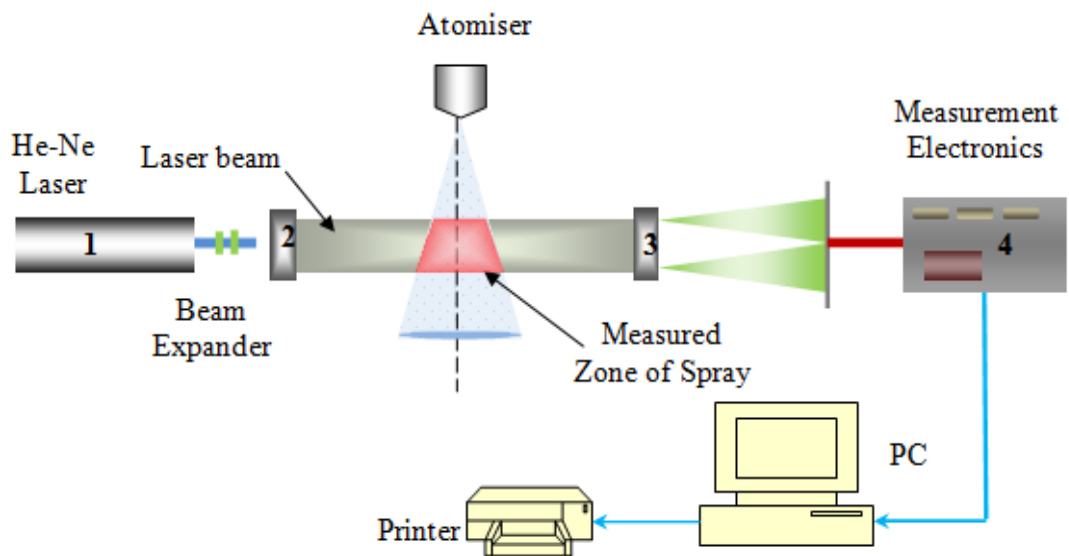


Figure 6.18: Malvern Mastersizer-X schematic diagram and the spray device set-up

The receiving optics have to be set-up and the instrument must be aligned. Before each measurement, the background reading was taken to ensure that the instrument is ready for the new measurement. It was pertinent to obtain the correct positioning of the spray device outlet relative to the laser beam and corresponding lens. Failure to do so could provide incorrect drop size diameters. The atomiser device was placed above the laser beam in a vertical position as the final optimum position, after testing the inverted and horizontal positions, as described in detail in the next chapter, Section 7.3.

The results from the Malvern Mastersizer-X particle analyser were printed and the drop size distributions were shown in a tabular or graphical representation for specific operating conditions and post processing.

6.3.2.5 Still Camera

Images of the equipment and the spray produced by the atomiser were captured with the use of an EOS 350D Canon digital camera with 1 Gigabyte of memory. The camera was mounted to view the desired area of the spray. It was switched on and the lighting source turned on to highlight the area upon which the camera was focused. A sharp image along the centreline of the atomiser was obtained by focusing in on a plumblin suspended from the centre of the atomiser, using the focal length adjustment on the lens of the camera, and the image was displayed on the LCD of the camera. The spray was turned on and an image was taken by the camera. A sequence of images was obtained and the spray was turned off. The sequence of images was transferred as a file to a PC for further qualitative visualisation.

6.3.3 Experimental Procedure

6.3.3.1 Phase I: Spraying and Atomisation Experimental Procedure

As mentioned in Section 6.3.1, spraying and atomisation experiments were conducted at room temperature and at an air flow rate of 0.3 - 0.4 l/min and pressure of 1 bar (0.1 MPa), while the liquid flow rate ranges were between 0.001 to 0.005 l/min and the flowing pressure was in the ranges of 60 to 110 bar (6 to 11 MPa), using small laboratory scale apparatus.

Before the start of the experiments, all the components of the rig were checked to make sure they were operating satisfactory. The Mastersizer-X was switched on, aligned and the background reading was taken before each trial. The atomiser device was mounted on the holding and positioning assembly and positioned at the required distance to spray through the laser beam of the Malvern Mastersizer-X. The laboratory lights were switched off during the spray measuring trials, since the detector is sensitive to external lighting and the lights could have influenced the measurement and thus the drop size distribution. Measurements were taken at the intersection of the spray with the laser beam at least 3 times for each spray test for confirmation. The pressure regulator on the air supply line was adjusted to the operating working pressure of 1 bar (0.1 MPa) and the recommended flow rate of air was adjusted using the calibration charts (see Section 6.3.2.2 and Figure 6.15). The water pump was then started at the recommended pressure to deliver liquid to the spray head. The pressure was determined by the pressure gauge installed downstream of the pump outlet. The drop sizes were then measured and the results were subsequently recorded and post processed.

It was also pertinent to maintain consistency in the drop number density and the volume concentration of the droplets. Thus accurate control of the liquid and gas flow rates was necessary throughout the trials.

6.3.3.2 Phase II: Proposed Prototype and Testing (PP and T): B8

This section briefly highlights the experimental apparatus and procedure of *Phase II*, for the generation of single-walled carbon nanotubes, which was implemented at the University of Oxford. The fabricated containment tube of the atomiser was reconstructed from non-shattering glass instead of Perspex with the same dimensions as the *Phase I* rig and a furnace (Carbolite type, STF 16/450 model) was installed at the atomiser's underside to allow the spray stream to fall down through the furnace.

The experimental apparatus set-up is given here and typical results will be discussed in the next chapter. The researcher was also involved in the set-up of the experimental apparatus in this phase of the investigation. Figure 6.19 illustrates the apparatus used to produce single walled carbon nanotubes (SWCNTs) by using methane as a carbon source. A Quadro 1000 TST liquid pump was used to provide high pressure liquid to the spray head with the following specifications:

- i. Maximum operating pressure: 220 bar (22 MPa)
- ii. Connection load: 7.5 kW
- iii. Maximum inlet water temperature: 60 °C
- iv. Pump output: 15.5 l/min
- v. Automatic timed Stop/Start operation
- vi. Motor output: 5.5 kW

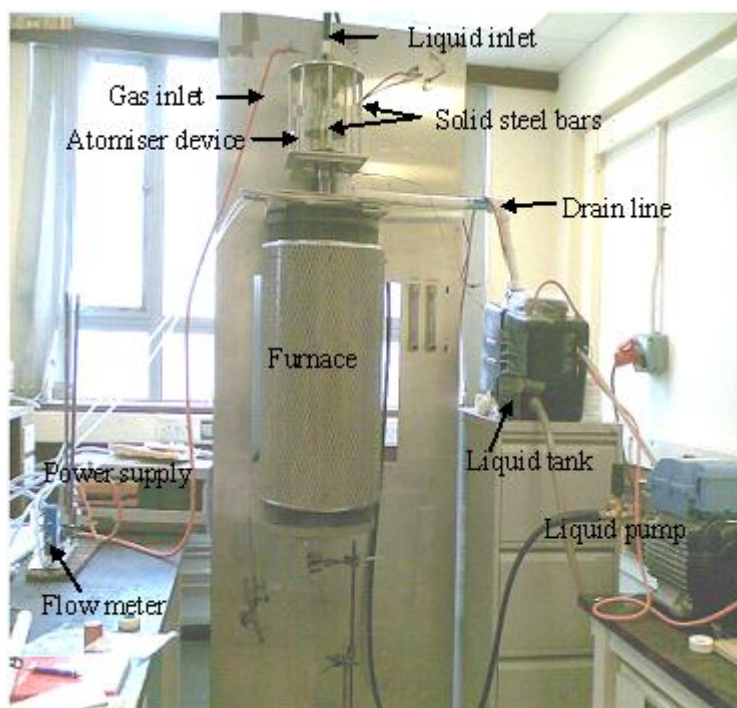


Figure 6.19: Experimental apparatus of single-walled carbon nanotubes generation

The produced stream of droplets from spraying a simulated catalyst material into a hydrocarbon gas flows down through the furnace which was installed at the bottom of the atomiser device and heated up to 800°C. The products were collected and analysed using a Transmission Electron Microscopy (TEM) technique. This is one of the most useful methods to clarify the structure in carbon materials.

The spray has the potential to cause damage to the equipment including the glass confinement tube. Thus to protect the tube from shattering, a number of reinforced high strength solid steel bars (5 mm diameter) were placed outside the glass tube. The spray device was also thermally insulated from the furnace. Static charge was also noted to build up on the tube wall when spraying; thus the device was earthed electrically to the same earth used by liquid supply pump.

Chapter - 7

CHAPTER-7: RESULTS, ANALYSIS AND DISCUSSION

7.1 Introduction

This chapter deals with the results, analysis and discussions for both proposed methods in this research and it is divided into two sections. The first section presents the investigation results, the analysis and a discussion on the partial oxidation of methane (*flare gas*) to synthesis gas through membrane reactors.

The second section deals with the results, analysis and discussion of the experiential work on the spraying and atomisation techniques, which were carried out to investigate the feasibility of Single-Walled Carbon Nanotubes' generation.

7.2 Results and Discussion: Feasibility Study of the Partial Oxidation of Methane to Syngas

Partial oxidation of natural gas (mainly methane) has been studied by a number of researchers to investigate the feasibility of this process and how it can be applied on an industrial scale. The utilisation of natural gas in a good manner instead of flaring is the main idea in this research. This section presents the results of the feasibility study which was performed in this research (see Appendix A). The assumptions and calculation procedures were highlighted in Chapter 4.

The objective of this investigation was to study the performance of the partial oxidation of methane (flare gas) to syngas in a tubular perovskite type membrane reactor packed with Ni/ γ -Al₂O₃ catalyst.

The tubes for the tubular membrane are assumed to be made of perovskite-type oxide La_{0.6}Sr_{0.4}Co_{0.2}Fe_{0.8}O_{3- δ} , known as LSCF (6428). This membrane has a good chemical stability and high oxygen permeability as reported by Tai et al. (1995), Xu and Thomson (1998) and Li (2007). The assumptions made were for the catalyst to be packed in the tube side only, into which methane flows, while air flows through the shell side. Co-current flow is adopted which is a better operating flow pattern than the counter-current flow pattern as reported by Tan and Li (2002). In the proposed investigation, air is introduced into the shell side of the reactor through which oxygen is transported to the other side (*membrane tubes*) where it reacts with the methane (*flare gas*) feedstock to produce synthesis gas. This takes place at elevated temperatures, at about 750°C or higher. Nickel based catalysts facilitate the partial oxidation of methane, which indicate their appropriate use in a ceramic tubular membrane.

7.2.1 Oxygen Permeation through Membrane Tubes

High oxygen permeation rate is required to improve the performance of the mixed conducting membrane reactor. As mentioned in Chapter 4, this can be realised by reducing the membrane thickness. Based on the assumptions those were made in Chapter 4 and Equation 4.5; dense LSCF 6428 membranes were theoretically investigated with different thicknesses varying from 0.05 to 0.2 cm and different operating temperatures ranging between 873 – 1173 K, while keeping the oxygen partial

pressure of the shell side 0.21 atm and that of tube (permeate) side 0.001 atm. In Figure 7.1, the predicted O₂ permeation fluxes are given as a function of the temperature and thickness, and it shows that oxygen permeation fluxes are clearly dependent on the membrane thickness and operating temperature. From this figure it is clear that increasing the membrane temperature leads to an increase in oxygen permeation rate. This is reasonable compared to the experimental data of Tsai et al., 1997 and Li et al., 2000 and the modelling data of Hoang and Chan, 2006. Also, Figure 7.1 shows that the membrane thickness has a major effect on the oxygen permeation as it increases with thickness decrease.

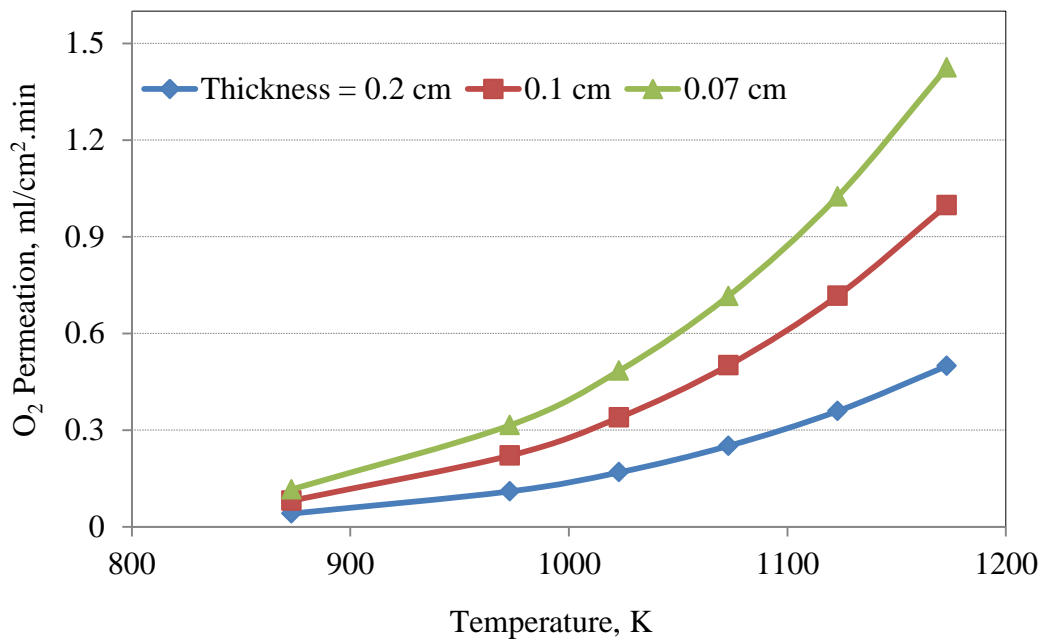


Figure 7.1: Effect of temperature on O₂ permeation in LSCF 6482 membranes reactor, for different membrane thicknesses (O₂ partial pressure 0.21/1x10⁻³ atm)

Figure 7.2 shows the relationship between the membrane thickness and O₂ permeation flux for different temperatures. The trends show that the O₂ permeation fluxes increase with decreasing membrane thickness and increasing operating temperature.

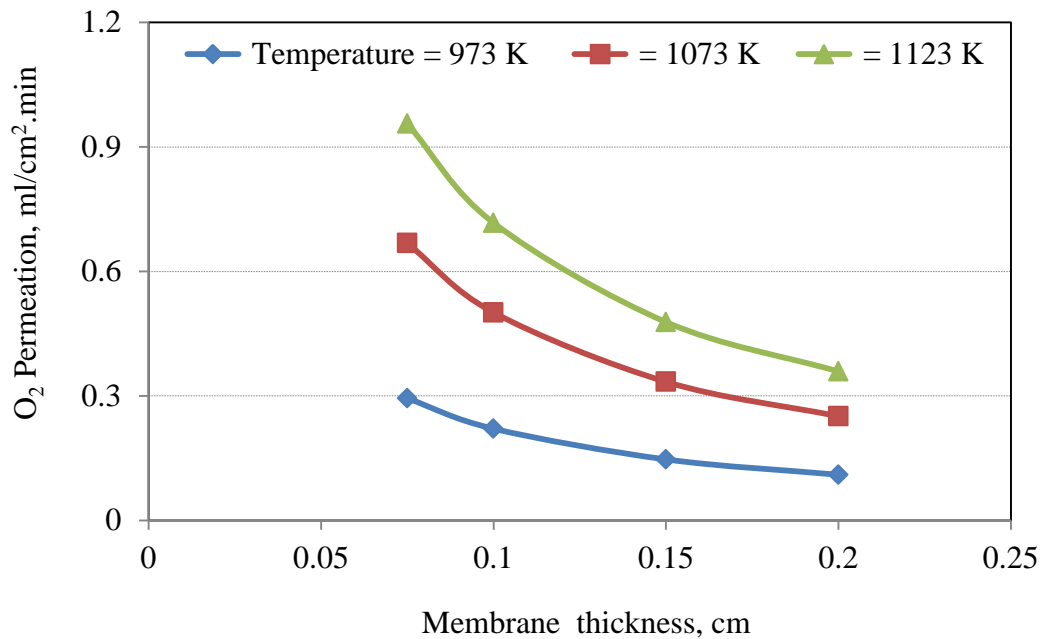


Figure 7.2: Variation of O₂ permeation for different membrane wall thicknesses and different temperatures (O₂ partial pressure 0.21/1x10⁻³ atm)

7.2.2 Effect of Oxygen Partial Pressure on Oxygen Permeation

Based on the previous assumptions, Figure 7.3 is a plot of oxygen permeation flux against various permeation side (tube side or downstream) oxygen partial pressures which were assumed in the range 0.1 -0.005 atm, and at different temperatures ranging between 923-1173 K, while the oxygen partial pressure in the shell side was maintained constant at 0.21 atm. From this figure, as expected, it is noted that oxygen permeation flux increased as the oxygen partial pressure in the permeation side is decreased because

the driving force for oxygen permeation becomes greater. Figure 7.3 also indicates that the oxygen permeation flux increases with increasing operating temperature under the same oxygen partial pressure driving force. This is rational compared to experimental data of Tan et al., 2005b, who demonstrated that, if the downstream oxygen partial pressure is very low, the value of oxygen flux is dependent on the operating temperature. Also, they stated that the increase in the oxygen permeation flux visibly results from the improved membrane design.

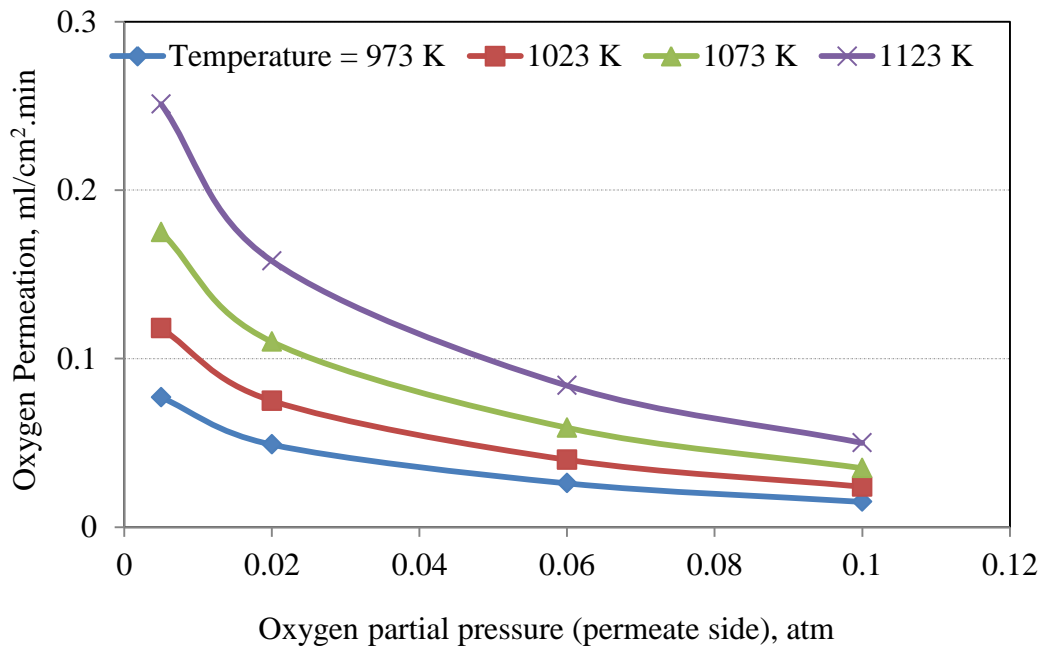


Figure 7.3: O₂ permeation flux at various permeate side partial pressures and at different temperatures (O₂ feed side partial pressure = 0.21 atm, tube thickness = 0.20 cm)

The effect of upstream oxygen partial pressure (feed side) on oxygen permeation flux is also investigated. This is shown in Figure 7.4, which demonstrates that although the oxygen permeation flux increases with increase of oxygen partial pressure in the feed

side of the membrane reactor, the effect is not large, but increases in importance as the temperature is increased. This can be explained by the fact that the driving force for oxygen permeation through the membrane becomes larger with increasing pressure difference. Figure 7.4 also, as stated in previous figures, shows that the oxygen permeation flux increases with increasing operating temperature under the same oxygen partial pressure.

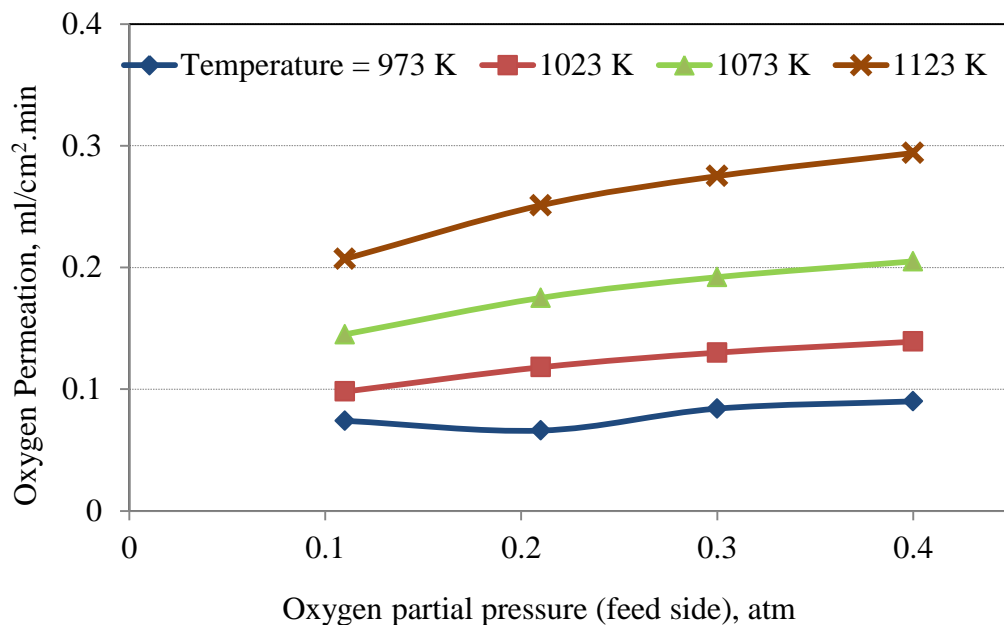


Figure 7.4: O₂ permeation flux at various feed side partial pressures and at different temperatures (O₂ permeate side partial pressure = 0.005 atm, tube thickness = 0.20 cm)

7.2.3 Modelling of Partial Oxidation of Natural Gas

Modelling of POM in oxygen permeable membrane reactors has been of great interests in recent years (Jin et al., 2000b). The objective of the POM modelling is to study the

performance of the partial oxidation of methane to syngas in a tubular perovskite type membrane reactor packed with Ni/ γ -Al₂O₃ catalyst.

This section presents the modelling procedures. The tubes for the tubular membrane are assumed to be made of perovskites-type oxide La_{0.6}Sr_{0.4}Co_{0.2}Fe_{0.8}O_{3- δ} , known as LSCF (6428). This membrane has a good chemical stability and high oxygen permeability as reported by Tai et al. (1995), Xu and Thomson (1998) and Li et al. (2000). The model assumes isothermal conditions and the catalyst is packed in the tube side only. Mass balances were carried out for both tube and shell side, in which methane and air are flowing respectively, for co-current flow, which is a better operating flow pattern than counter-current flow pattern as reported by Tan and Li (2002). Figure 7.5 shows the diagram of the permeate stages.

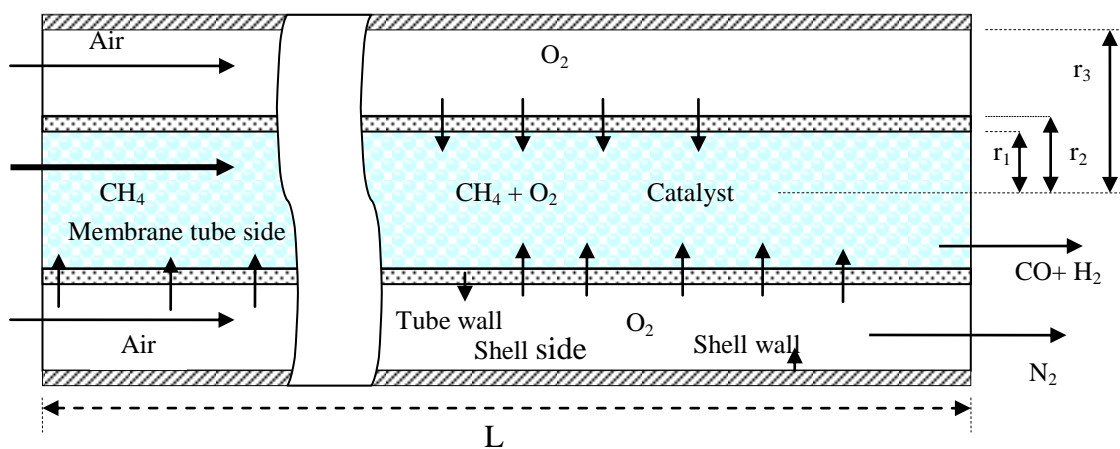


Figure 7.5: Schematic diagram of dense membrane reactor

Many researchers on oxygen permeable dense membrane in the literature demonstrated that the oxygen permeation flux is proportional to the membrane temperature and the logarithmic ratio of oxygen partial pressures across the membrane and inversely proportional to the membrane thickness.

Assuming that a steady state operation has been reached and therefore, the reaction rate is constant within any point of the reactor, the material balance can be performed:

$$\text{Accumulation} = \text{input} - \text{output} - \text{loss through reaction} \quad (7.1)$$

Due to the steady state operation, there is no accumulation on the reactor. Also, the loss through the reaction can be described by the reaction rate multiplied by the volume of the reactor element (dv). The input and output are simply the inlet and outlet methane flow rates, respectively. Therefore, Equation 7.1 can be re-written as follows:

$$0 = F_{CH_4}^{in} - F_{CH_4}^{out} - r_{CH_4} * dv \quad (7.2)$$

From the definition of conversion:

$$r_{CH_4} = \frac{F_{CH_4}^{in} - F_{CH_4}^{out}}{F_{CH_4}^{in}} \quad (7.3)$$

Substituting Equation 7.3 into Equation 7.2:

$$r_{CH_4} = \frac{X_{CH_4} * F_{CH_4}^{in}}{dv} \quad (7.4)$$

Equation 7.4 used to determine the reaction rate for the methane oxidation reaction. A mechanism for the partial oxidation of methane to syngas has been proposed in which methane combustion is followed by steam and carbon dioxide reforming (Ashcroft et al., 1990). An alternative process assumes catalytic pyrolysis followed by H₂ desorption and carbon oxidation (Hichman and Schmidt, 1993).

The mechanism incorporating the methane combustion is assumed; also, a Ni/Al₂O₃ catalyst is assumed to be present in the reaction tube.

The three reactions to be considered are (De Groote and Froment, 1996):

Methane combustion:



With reaction rate

$$R_1 = A_1 P_{\text{CH}_4} P_{\text{O}_2} \exp\left(-\frac{E_1}{RT}\right) \quad (7.6)$$

Steam reforming:



With reaction rate

$$R_2 = A_2 P_{\text{CH}_4} P_{\text{H}_2\text{O}} \exp\left(-\frac{E_2}{RT}\right) \left(1 - \frac{P_{\text{CO}} P_{\text{H}_2}^3}{K_2 P_{\text{CH}_4} P_{\text{H}_2\text{O}}}\right) \quad (7.8)$$

Water gas shift reaction:



With reaction rate

$$R_3 = A_3 P_{\text{CO}} P_{\text{H}_2\text{O}} \exp\left(-\frac{E_3}{RT}\right) \left(1 - \frac{P_{\text{H}_2} P_{\text{CO}_2}}{K_3 P_{\text{CO}} P_{\text{H}_2\text{O}}}\right) \quad (7.10)$$

In the tube side (catalytic layer) $0 < r < r_1$

$$\frac{dF_j}{dl} + 2\pi r_1 J_j|_{r=r_1} - \pi r_1^2 \rho_B \sum_{i=1}^n v_{ji} R_i = 0 \quad (7.11)$$

Where the subscript j represent the reaction gas species, CH_4 , O_2 , CO , CO_2 , H_2 and H_2O .

In the dense membrane $r_1 < r < r_2$

$$J_{\text{O}_2} = \frac{r_1}{r} J_{\text{O}_2}|_{r=r_1} \quad (7.12)$$

$$J_m = 0,$$

Where the gas species m includes CH_4 , O_2 , CO , CO_2 , H_2 , H_2O and N_2 :

In the shell side $r_2 < r < r_3$

$$\frac{dQ_k}{dl} - 2\pi r_2 J_k|_{r=r_2} = 0 \quad (7.13)$$

In which the subscript k denotes O_2 or N_2 , respectively.

The initial condition at $L = 0$,

$$F_{CH_4} = F_{CH_4}^0$$

$$F_{j,j \neq CH_4} = 0$$

$$Q_{O_2} = Q_{O_2}^0$$

$$Q_{N_2} = Q_{N_2}^0$$

At the catalytic layer/dense membrane layer interface:

$$r = r_1$$

$$J_{O_2} = J_{O_2}|_{r=r_1}$$

For the gas species m

$$J_m = 0$$

$$P_j = \frac{F_j}{\sum_{i=1}^M F_i} P_t \quad (7.14)$$

Where $M = 6$, (CH_4 , O_2 , CO , CO_2 , H_2 and H_2O).

At the dense membrane layer/shell side interface:

$$r = r_2$$

$$J_{O_2} = \frac{r_1}{r_2} J_{O_2}|_{r=r_1} \quad (7.15)$$

$$J_{N_2} = 0$$

$$P_k = \frac{Q_k}{\sum_{i=1}^M Q_i} P_s \quad (7.16)$$

$M = 2$, (O_2 and N_2).

Where:

A_i	Pre-exponential factor
E_i	Activation energy of the reaction i , J/mol
F_j	Molar flow rate of species j in tube side, mol/s
J_j	Permeation flux of component j , mol/m ² .s
l	Dense membrane reactor axial distance, m
L	Dense membrane reactor total length, m
K_2, K_3	Equilibrium constants for reactions 2 and 3
P_j	Component j partial pressure, atm
P_s	Total pressure of in the shell side, Pa
P_t	Total pressure of in the tube side, Pa
Q_k	Molar flow rate of species k in shell side, mol/s
R	Universal gas constant, 8.314 J/mol K
r_0	Inner radius of dense membrane tube, cm
r_1	External radius of dense membrane tube, cm
r_2	Inner radius of reactor shell, cm
R_j	Rate of reaction j , mol/s
T	Temperature, K
ν_{ji}	Stoichiometric coefficient of component j for reaction i
ρ_B	Bulk density of catalytic bed, kg/m ³

Examples of the results obtained for the fixed bed (MATLAB model) are shown in Figures 7.6 and 7.7, for two different temperatures and same operating parameters,

where the gas profiles are shown as a function of reactor length. Similar profiles should be obtainable for the membrane system. From these figures, it can be shown that the molar flow rates of methane and oxygen decreased rapidly along the reactor length as the species are being consumed and as a result, significant amounts of carbon monoxide and hydrogen are observed along the reactor length, some amount of water is also produced from the water-gas shift reaction.

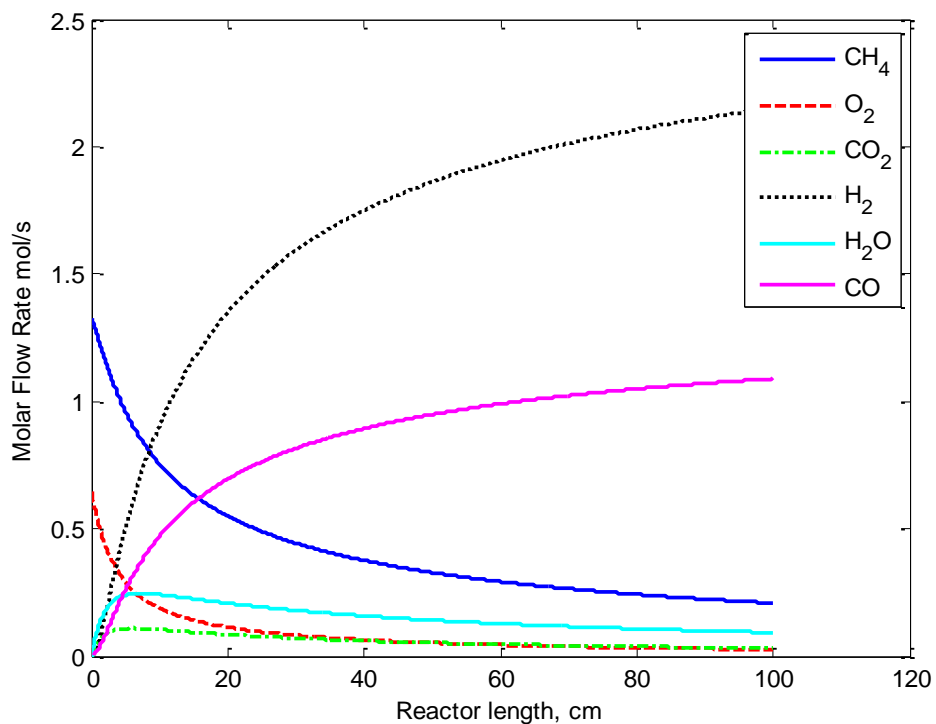


Figure 7.6: Predicted molar flow rate profiles for each species as a function of reactor length, (Fixed bed reactor), O₂ inlet 0.65 mol/s, CH₄ inlet =1.33, T = 873 K

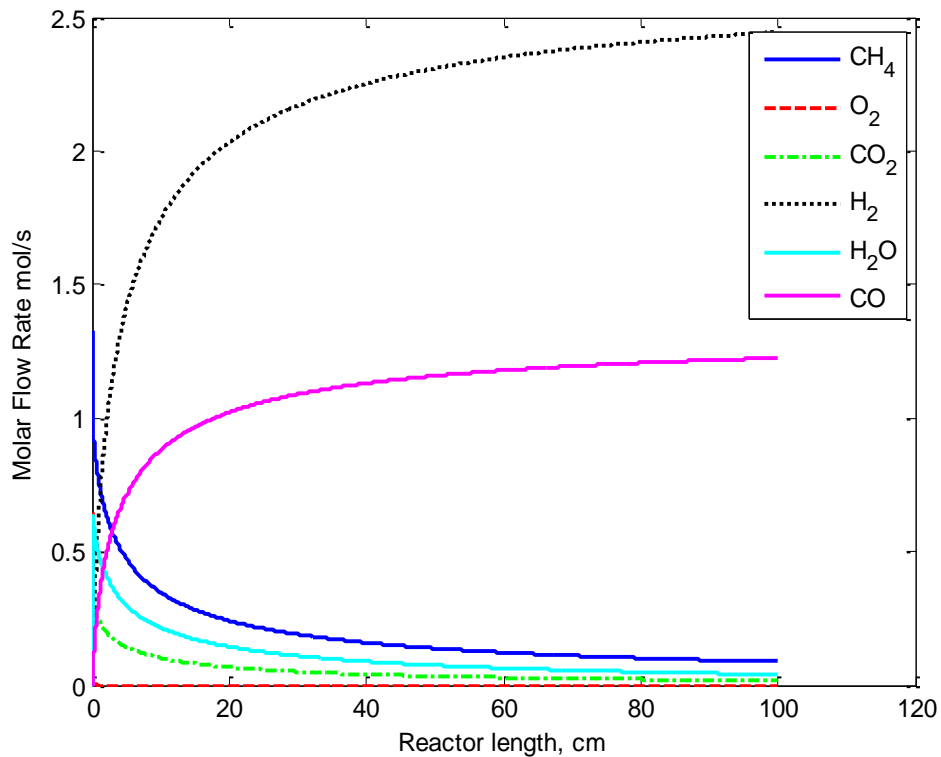


Figure 7.7: Predicted molar flow rate profiles for each species as a function of reactor length, (Fixed bed reactor), O₂ inlet 0.65 mol/s, CH₄ inlet =1.33 mol/s, T = 1073 K

If compared with Figure 7.6, Figure 7.7 shows that methane and oxygen consumption rates are higher as the operating temperature was higher (1073 K). The molar flow rate of the different species is approaching equilibrium value at the end of the reactor.

In practice the individual single tube results would have to be incorporated into a multitubular reactor design which would have to allow for different flow patterns and heat transfer within the whole reactor.

The next section presents the results, analysis and discussions for the SWCNT generation using sprays and atomisation techniques.

7.3 Results and Discussion: Single-Walled Carbon Nanotubes

(SWCNT) Production

7.3.1 Overview

The results, analysis and discussion of the experimental work are divided into two phases as mentioned previously in Chapter 6, Section 6.1. This section describes *firstly* the droplet sizing measurement results of the fine sprays produced from the designed atomiser device which were undertaken during the *Phase I* experiments. The atomiser device was designed to generate a fine aerosol stream with droplet sizes of less than or equal to 5 μm , based on Number Mean Diameter (NMD) and compared with the Sauter Mean Diameter (SMD). Note that in the production of SWCNT, it is more important to consider the NMD of drops than the SMD, which is more related to mass surface and reaction processes. Moreover, using NMD ($D_{n0.50}$) range of drop sizes includes smaller drops than SMD (D_{32}). A Malvern Mastersizer-X was used for this measurement and it was described in Chapter 6. *Secondly*, this section highlights the results and a discussion of the *Phase II* experimental work.

Phase I experiments were carried out to find the optimum set-up of the equipment used in this investigation for fine droplet generation. *Phase II* trials were performed after the *Phase I* experimental work was successfully completed, in order to continue with the same designed atomiser device of the *Phase I* experiments, after it was reconstructed and installed on the top of a Carbolite type, STF 16/450 mode furnace, at the University of Oxford. This was in order to investigate the generation of Single-Walled Carbon Nanotubes (see Section 6.3.2.2). All of the results were obtained by following the

experimental procedure that was outlined in the previous chapter. The experimental results are presented for discussion in the following sections.

7.3.2 Phase I: Spray Characterisation

During the design procedure and preliminary trials, as mentioned in Section 6.2.2.2, several options were examined based on the design calculation, such as the position of both baffle plate and the aerosol tube and the arrangement of the atomiser device (see Chapter 6, Figures 6.7 - 6.9) relative to the Malvern Mastersizer-X instrument. The atomiser positions that were examined were:

- i- *Inverted (Section 7.3.2.1);*
- ii- *Horizontal (Section 7.3.2.2);*
- iii- *Vertical (Section 7.3.2.3).*

Table 7.7 summarises the operating parameters that were used for all of the *Phase I* experiments during this study.

<i>Parameter</i>	
Air pressure, <i>MPa</i>	0.1
Air flow rate, <i>l/min</i>	0.3 - 0.4
Liquid pressure, <i>MPa</i>	6 - 11
Liquid flow rate, <i>l/min</i>	0.001 – 0.005
Temperature, (room temperature) °C	20 - 25
Baffle plate position relative to base cover, <i>mm</i>	80 - 150
Baffle plate position relative to aerosol tube, <i>mm</i>	3 - 10
Atomiser device position relative to laser beam centreline, <i>mm</i>	40 - 100

Table 7.7: Operating parameters

7.3.2.1 Inverted Atomiser Device Position

The corresponding trials with the inverted atomiser device position (see Figure 6.7 in the previous chapter) were firstly tested by some repetitive runs without measurement, to observe the production of the aerosol stream at the atomiser outlet. These runs were conducted by placing the baffle plate and the aerosol tube at different positions and where the liquid supply pressure was 10 MPa, while that of air was 0.1 MPa. The liquid (*water*) and air flow rates were in the range of 0.001-0.005 l/min and 0.3-0.4 l/min, respectively.

These repetitive trials with the inverted position of the atomiser device did not generate any fine sprays. The spray droplets effectively could not travel through the aerosol tube bouncing back onto the base of the device due to the gravitational effect.

7.3.2.2 Horizontal Atomiser Device Position

After the inverted atomiser position trials, it was decided to place the atomiser device horizontally as shown in the previous chapter, Figure 6.8. The atomiser device was assembled in the holding and positioning assembly, which was needed to determine the best relative distance between its outlet and the centreline of the laser beam. It must be emphasised that the tests were numbered as “SA-1, SA-2etc.” in which SA referred to sprays and atomisation. The preliminary experiments using the horizontal position of the atomiser device were performed and the droplet sizes’ measurement conducted. The analysis is based on the measured droplet sizes obtained for different runs at different parameters. This was accomplished by measuring the effect of different parameters on the droplet size distribution such as the baffle plate and the aerosol tube positions, water

and air pressures and flow rates and the position of the atomiser device outlet relative to the laser beam centreline.

This set of experiments was performed at different downstream distances ranging from 50-70 mm (see Figure 7.8), i.e. the position of the atomiser outlet with respect to analysing the beam centreline. The aerosol tube outlet diameter was reduced to 15 mm instead of 50 mm to narrow the spray stream slot.

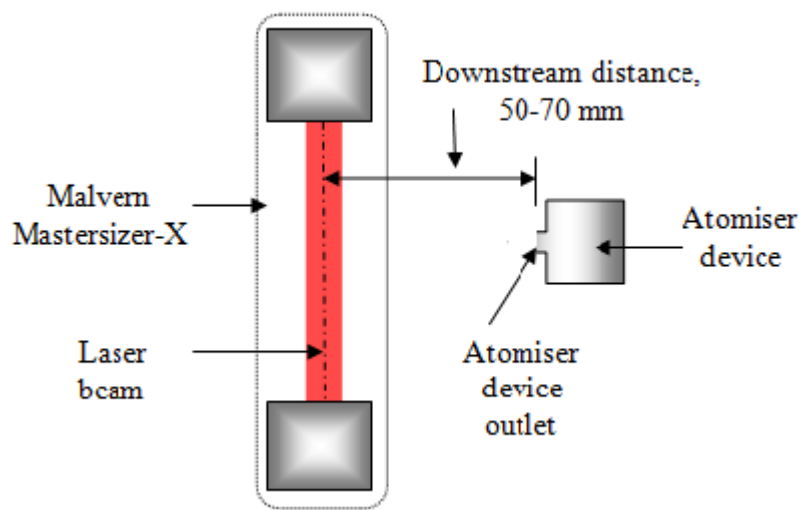


Figure 7.8: Sketch diagram of horizontal position of the atomiser device

Table 7.1 summarises the typical results for these experiments. It is a copy of the template data sheet which was used to record the results during the running experiments. Appendix B2 presents the estimation of the collected aerosol rate during the experiment measurement, whilst Appendix B3 provides all the results that were obtained during all trials in the same Table type. From close inspection of the results, and based on these preliminary tests, it was clear that the horizontal position of the atomiser device also did not generate any aerosol and thus was not suitable for SWCNT generation.



Malvern Mastersizer-X results data sheet

Date: May/2008,

Atomiser device position: *Horizontal*

Temperature: 22-24 °C

Test No.	Baffle position from base cover, mm	Air flow rate, Q_a , l/m	Air pressure, P_a , MPa	Water flow rate, Q_w , l/m	Water supply pressure, P_w , MPa	Aerosol collected, ml/min	D_{32} , μm	$D_{n0.5}$, μm	Comments
AS-1	150	0.4	0.1	0.005	10	0	↑	↑	<i>Note:</i> (i)The obscuration and volume concentration are zero with no aerosol. (ii)As a number of above, no aerosol collected
AS-2	150	0.4	0.1	0.005	10	0	↑	↑	
AS-3	110	0.4	0.1	0.005	10	0	↑	↑	
AS-4	110	0.4	0.1	0.003	10	0	See comments		
AS-5	80	0.4	0.1	0.003	11	0	See comments		
AS-6	80	0.4	0.1	0.001	11	0	↓	↓	
AS-7	80	0.4	0.1	0.001	8	0	↓	↓	
AS-8	80	0.4	0.1	0.001	8	0	↓	↓	

Table 7.1: Summary of horizontal position results of the atomiser device

This was mainly due to the condensation behaviour and to the attachment of the flow stream of the droplets to the inside wall of the confinement tube of the atomiser device. Although individual aerosol drops appeared to be captured in the laser beam, the total volume of collected aerosol, however, was considered to be insufficient for respective utilisation. It was, therefore, decided to situate the atomiser device vertically, on the top of the measuring instrument, while an aerosol stream crossed the laser beam orthogonally during the trial.

The next section presents the spray characterisation and the experimental results drawn from this position of the atomiser device.

7.3.2.3 Vertical Atomiser Device Position

All the trials in this set were conducted by measuring the droplet sizes at different positions of both the baffle plate and the aerosol tube relative to the base cover and the atomiser device outlet relative to the laser beam centreline, in order to find the optimum arrangement of the rig apparatus. The Malvern Mastersizer-X (see Section 6.3.2.4) results, which include the measurements of the spray characteristics together with MS Excel plots and DPlot contours, are presented in a series of figures and comparisons between some parameters and are discussed in detail. These parameters are listed below:

- i. The baffle plate and the aerosol tube positions inside the confinement tube;
- ii. Water flow rate and pressure;
- iii. Air flow rate and pressure;
- iv. Atomiser device position with respect to the laser beam.

7.3.2.3.1 Baffle Plate and Aerosol Tube Positions

This set of trials was carried out to find out the optimum position of both the baffle plate and the aerosol tube relative to the base cover of the atomiser device. When running the tests, the measurement was undertaken by placing the atomiser device perpendicular to the laser beam centreline initially at 100 mm.

The baffle plate was tested at 150, 110 and 80 mm as measured from the base cover of the atomiser device, while the aerosol tube was kept below the baffle plate at 10 mm in the first two positions and 3 mm in the last one, as shown in Figures 7.10 and 7.13. Note that the aerosol tube was also moveable with respect to the baffle plate, the base cover and the laser beam. Also, as mentioned in Section 7.3.2.2, the aerosol tube outlet diameter was reduced to 15 mm instead of 50 mm to narrow the spray stream slot. The air pressure was kept constant at 0.1 MPa for all runs. In this set, the water supply pressure was set at 8 MPa and the flow rates of both water and air were maintained constant at 0.003 l/min and 0.3 l/min respectively.

At the positions of 150 mm for the baffle plate and 140 mm for the aerosol tube, the atomiser device did not generate any aerosol stream, for the tests AS-9, AS-10 and AS-11, as illustrated in Figure 7.9 for test run AS-9. This was due to the long distance over which the aerosol stream had to flow.

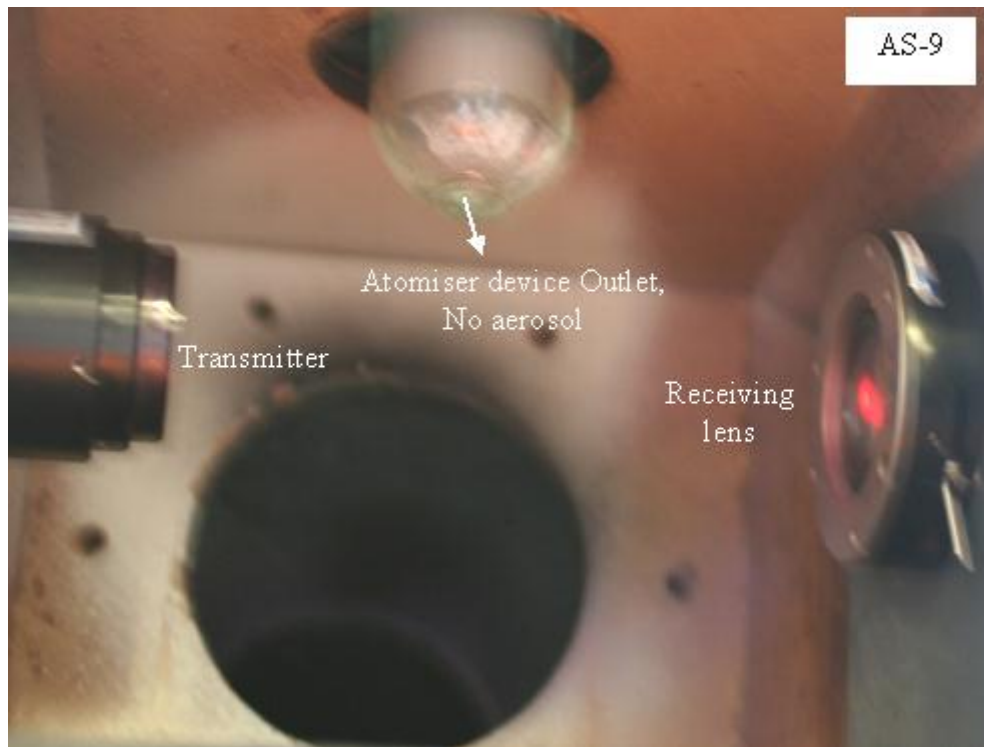


Figure 7.9: No aerosol stream crossing the laser beam during the measurement

Based on these results, it was decided to reduce the baffle plate and the aerosol tube positions to 110 and 100 mm respectively, as shown in Figure 7.10. In this trials' set, at the mentioned positions, the initial tests showed that little fine sprays were generated and measured while crossing the laser beam (see Figure 7.11, for test run AS-12).

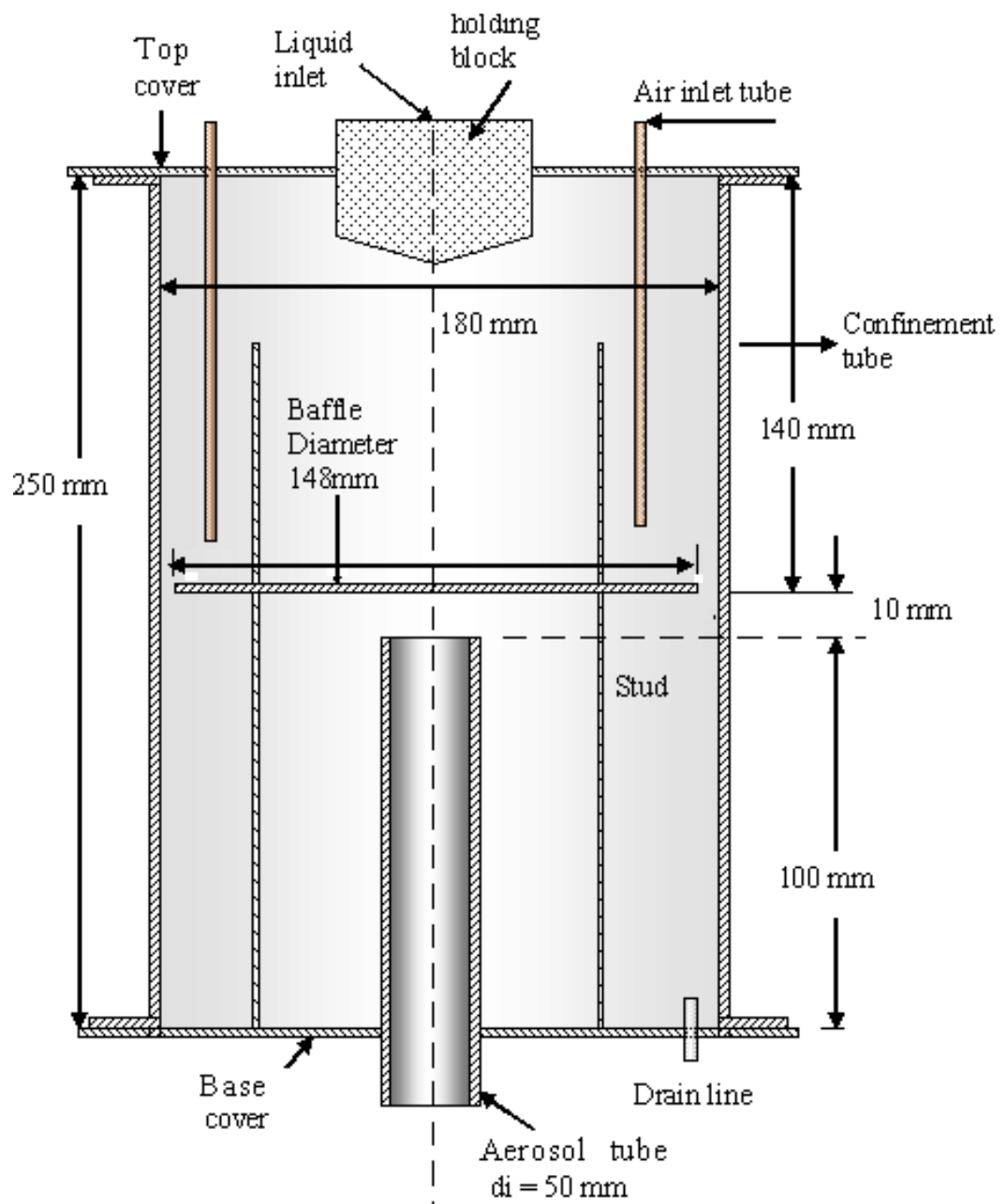


Figure 7.10: Positions of baffle plate (at 110 mm) and aerosol tube (at 100 mm)

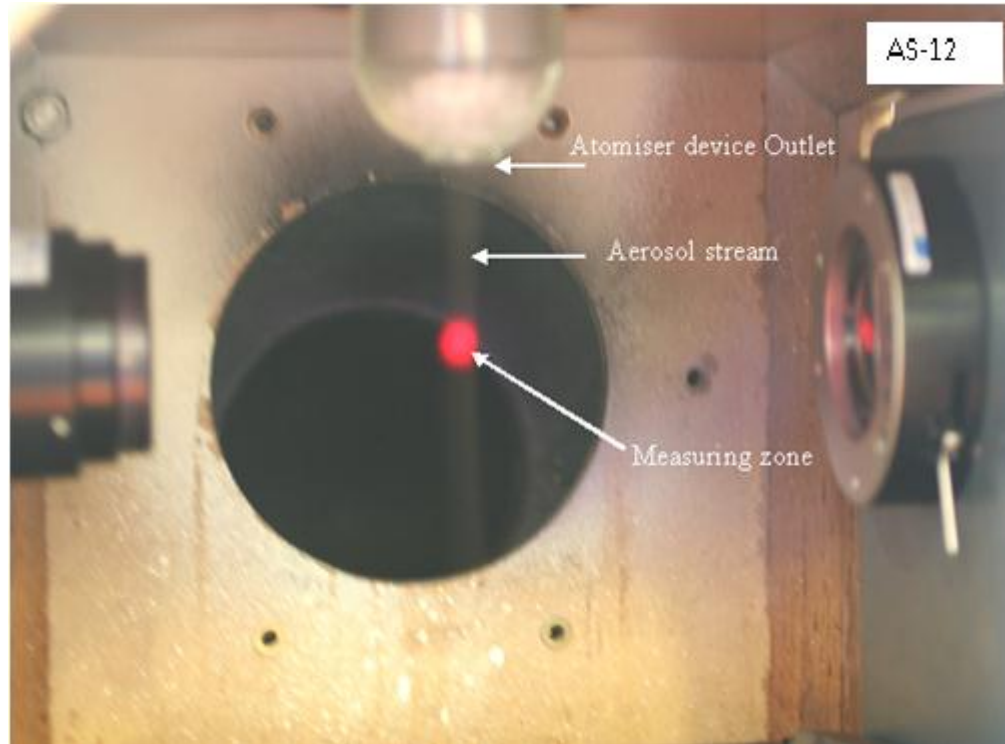
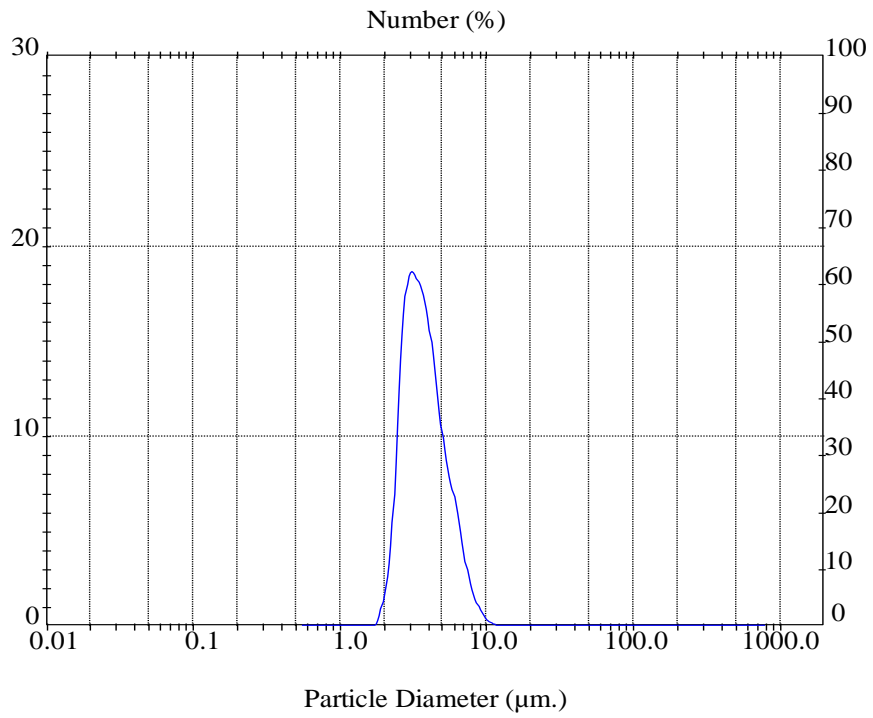
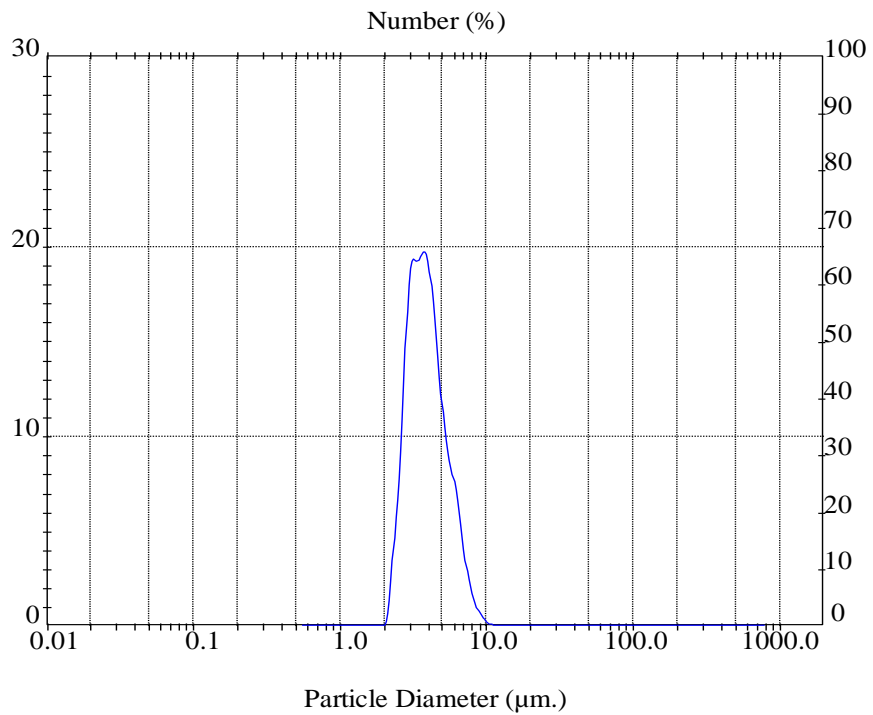


Figure 7.11: Fine spray stream crossing the laser beam during measurement, (Test AS-12: Baffle plate position = 110 mm, aerosol tube position = 100 mm based on the base cover)

Figures 7.12 and 7.13 show the distributions of particle diameters for the first two typical runs in this set, AS-12 (a) and AS-13 (b), based on NMD and SMD, respectively, obtained from Malvern Mastersizer-X for the baffle plate and aerosol tube positions of 110 and 100 mm respectively. The remaining data is presented in Appendix B4. The measuring tests were repeated a total of 3 times for accuracy. The droplet sizes were in the average of 5.08 μm based on SMD or 3.66 μm based on $D_{n0.50}$, which was less than 5 μm . Table 7.2 summarises the operating parameters and the droplet sizes for this set of experiments.

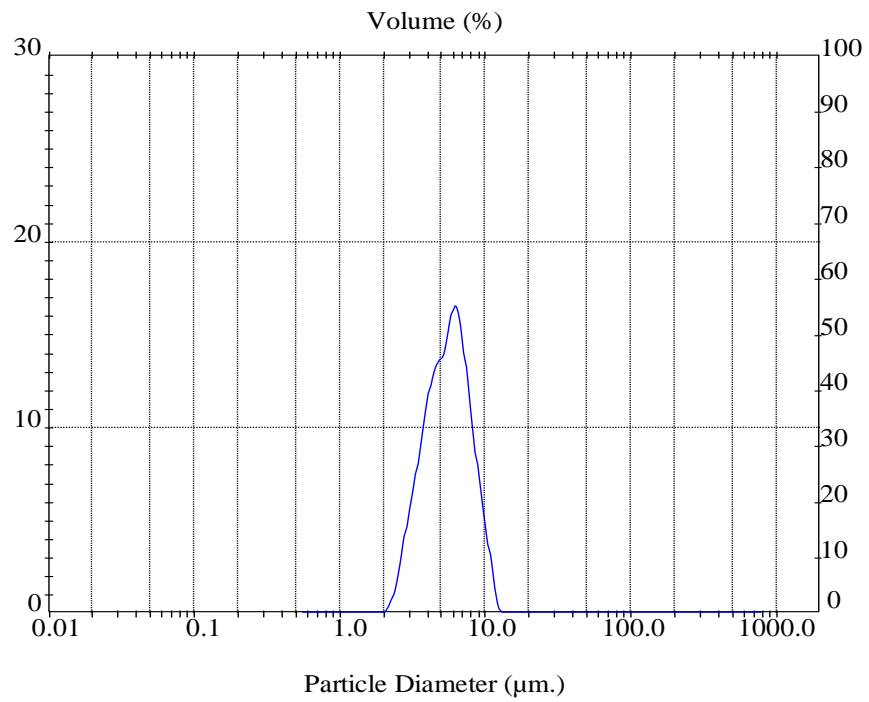


(a) Test: AS-12, $D_{n0.50} = 3.60 \mu\text{m}$

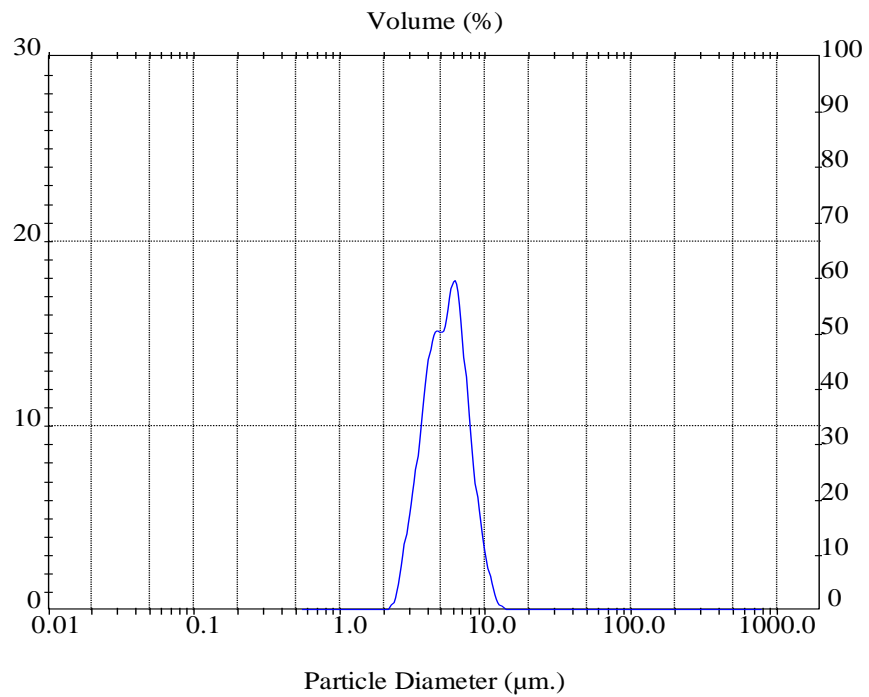


(b) Test: AS-13, $D_{n0.50} = 3.79 \mu\text{m}$

Figure 7.12: Typical particle diameter (μm) distributions for tests AS-12 (a) and AS-13 (b), based on $D_{n0.50}$



(a) Test: AS-12, $D_{32} = 5.08 \mu\text{m}$



(b) Test: AS-13, $D_{32} = 5.03 \mu\text{m}$

Figure 7.13: Typical particle diameter (μm) distributions for tests AS-12 (a) and AS-13 (b), based on D_{32}

<i>Test No.</i>	<i>Water supply pressure, MPa</i>	<i>Water flow rate, l/min</i>	<i>Air pressure, MPa</i>	<i>Air flow rate, l/min</i>	<i>Aerosol collected, ml/min</i>	<i>D₃₂, μm</i>	<i>D_{n0.50}, μm</i>
SA-12	8	0.003	0.1	0.3	0.0207	5.08	3.60
SA-13	8	0.003	0.1	0.3	0.0225	5.03	3.79
SA-14	8	0.003	0.1	0.3	0.0219	5.21	3.63

Table 7.2: Initial experimental results of atomiser device vertical position at baffle plate position of 110 mm and aerosol tube position of 100 mm from the base cover

Based on the sizes of these droplets (see Table 7.2), it was decided to further reduce the positions of both the baffle plate and the aerosol tube to 80 and 77 mm (3 mm space between them) respectively, relative to the base cover, in order to examine and capture sufficient volume with a smaller diameter of droplet sizes (i.e. $\leq 5 \mu\text{m}$). Other operating parametric conditions were kept the same as those tests that were conducted during previous trials. The 10 mm space was reduced to 3 mm to narrow the slot stream exit path as shown schematically in Figure 7.14.

At these positions, 80 and 77 mm, of the baffle plate and the aerosol tube relative to the atomiser base cover, the initial tests showed that fine sprays were successfully generated as illustrated in Figure 7.15, this being the image taken by the still camera during the drop size distribution measurement by Malvern Mastersizer-X instrument.

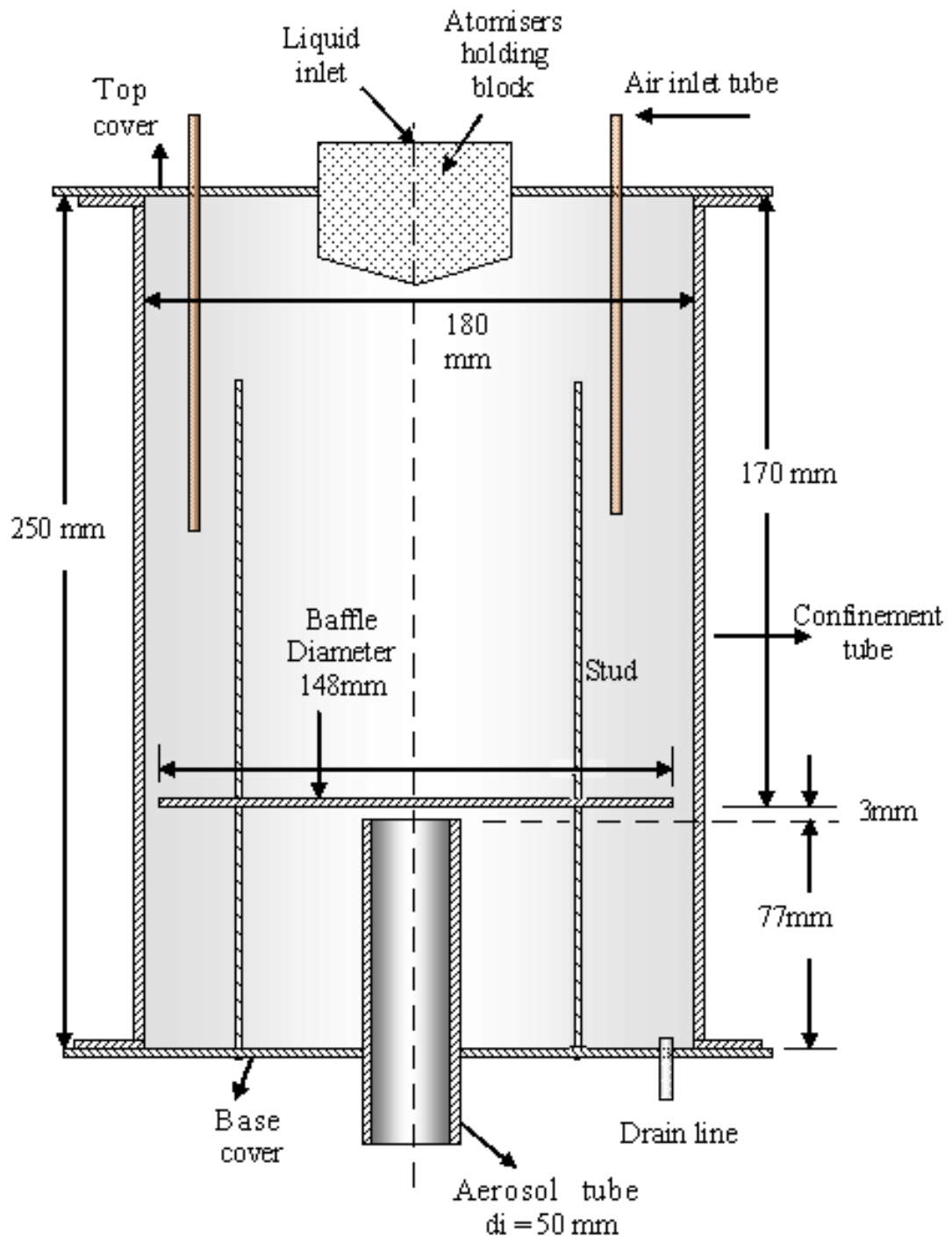


Figure 7.14: Optimum baffle plate (80 mm) and aerosol tube (77 mm) positions

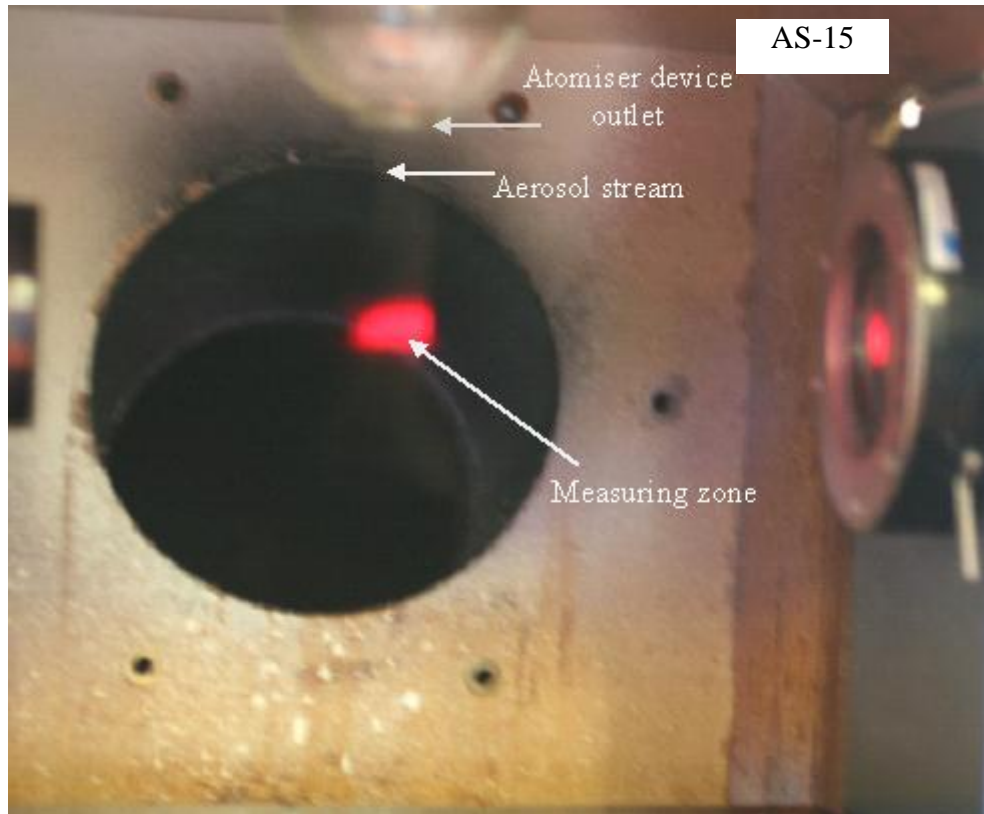
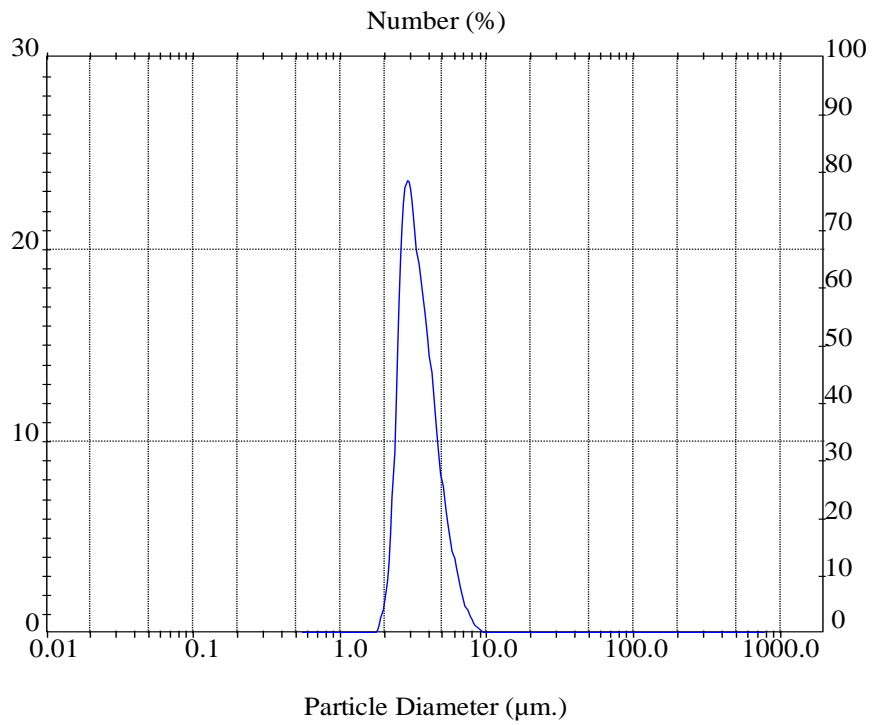


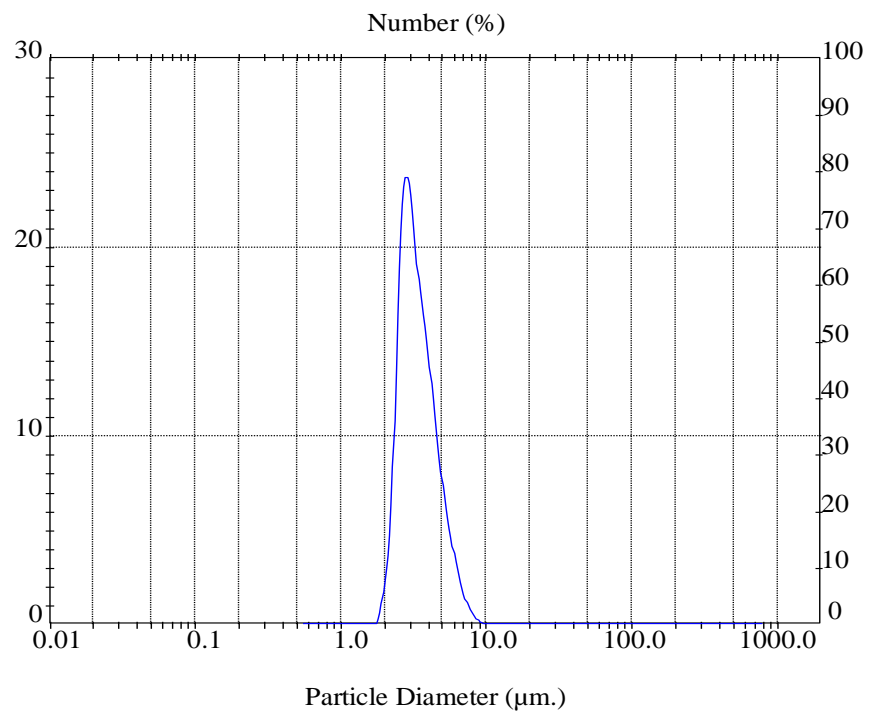
Figure 7.15: Fine spray stream crossing the laser beam during measurement (Test AS-15)

The droplet sizes were of an average of $4.33\mu\text{m}$ based on D_{32} or $3.26\mu\text{m}$ based on $D_{n0.50}$, which were less than those generated in the previous set (SA-12 to SA-14). Figures 7.16 and 7.17 show the distributions of particle diameters for tests AS-15 (a) and AS-16 (b), based on NMD and SMD, respectively, obtained from the Malvern Mastersizer-X for the baffle plate and aerosol tube positions of 80 mm and 77 mm.

Table 7.3 presents the droplet sizes' results for this set of experiments. From these results it is clear that the position of the baffle plate affects the droplet sizes, as they decrease with decreasing distance from the atomiser exit.

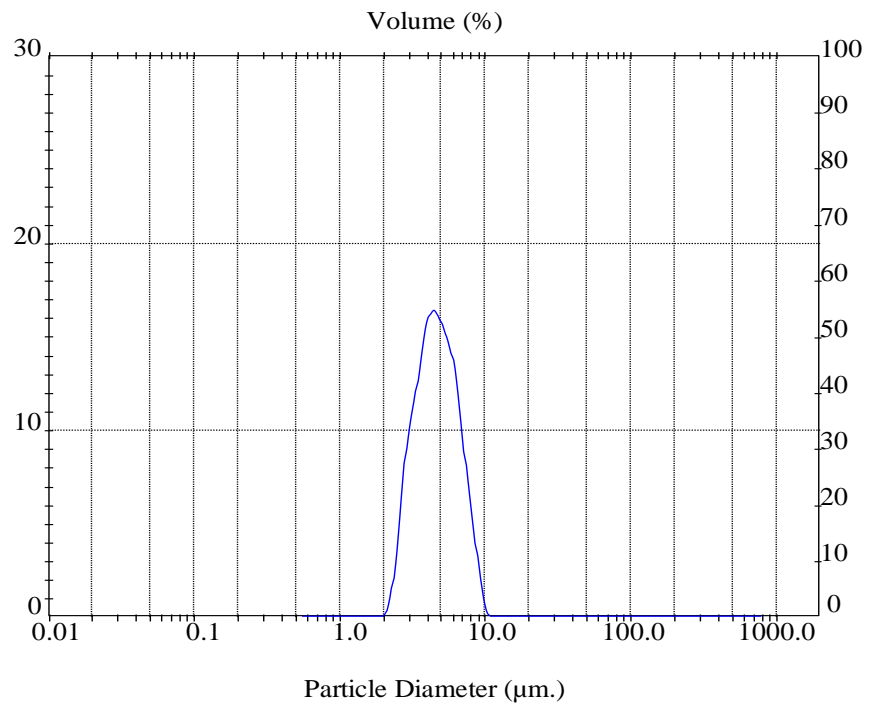


(a) Test: AS-15, $D_{n0.50} = 3.29\mu\text{m}$

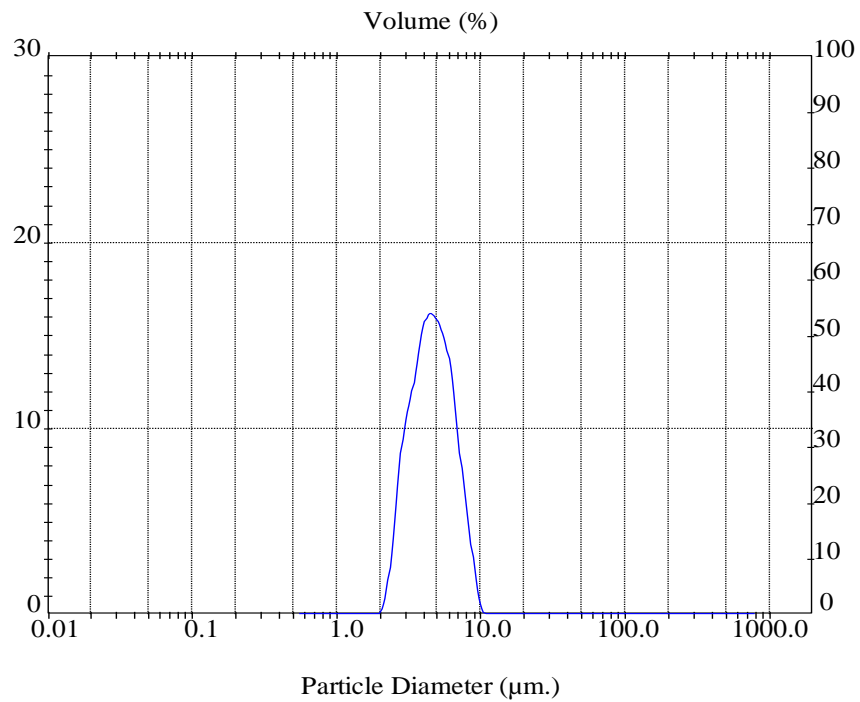


(b) Test: AS-16, $D_{n0.50} = 3.23\mu\text{m}$

Figure 7.16: Typical particle diameter (μm) distributions for tests AS-15 (a) and AS-16 (b), based on $D_{n0.50}$



(a) Test: AS-15, $D_{32} = 4.35\mu\text{m}$



(b) Test: AS-16, $D_{32} = 4.31\mu\text{m}$

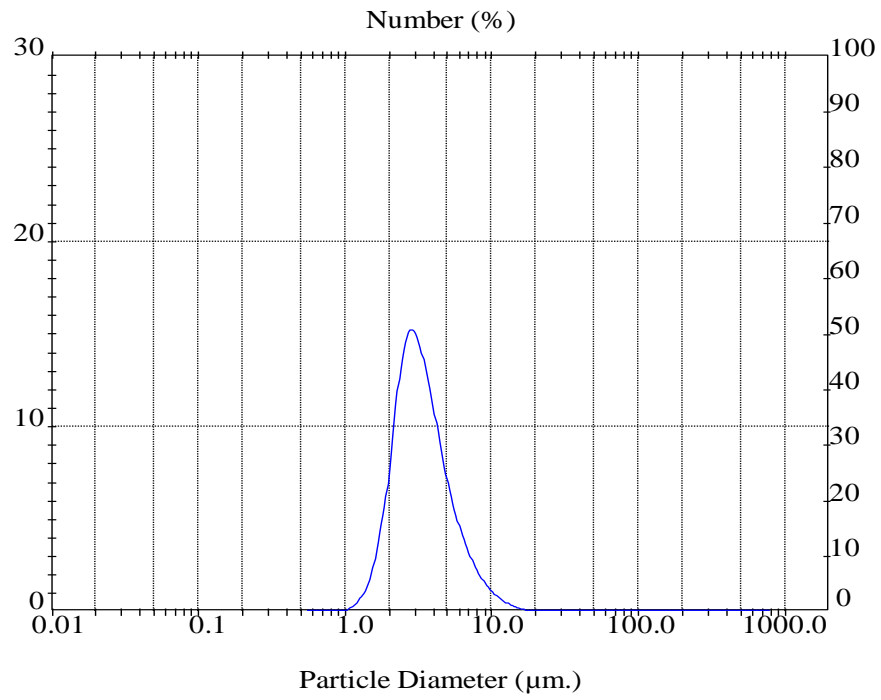
Figure 7.17: Typical particle diameter (μm) distributions for tests AS-15 (a) and AS-16 (b), based on D_{32}

<i>Test No.</i>	<i>Water pressure, MPa</i>	<i>Water flow rate, l/min</i>	<i>Air pressure, MPa</i>	<i>Air flow rate, l/min</i>	<i>Aerosol collected, ml</i>	<i>D₃₂, μm</i>	<i>D_{n0.50}, μm</i>
SA-15	8	0.003	0.1	0.3	0.0180	4.35	3.29
SA-16	8	0.003	0.1	0.3	0.0198	4.31	3.23
SA-17	8	0.003	0.1	0.3	0.0204	4.32	3.22

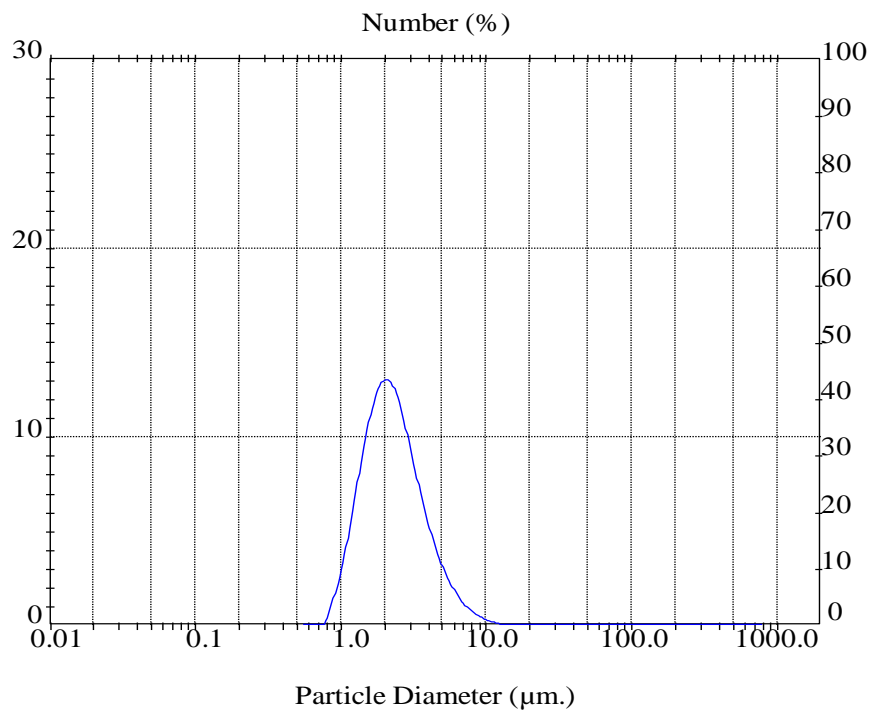
Table 7.3: Typical experimental data obtained for the optimum baffle plate and aerosol tube positions

7.3.2.3.2 Water Flow Rate and Pressure

Following the results gained during the previous experiments for the vertical atomiser device position, in which the produced fine spray had droplet sizes, for example, ($D_{n0.5}$) less than $5 \mu\text{m}$ gained as expected, both the baffle plate and the aerosol tube were fixed at these positions and work continued with the remaining trials to investigate the effects of other parameters such as water flow rate, water supply pressure, air flow rate and downstream distance on the spray characterisation. In this set, a series of experiments were performed at water (simulating the aqueous liquid catalyst for production of SWCNT) supply pressure varying from 6 to 11 MPa and its flow rate, varying from 0.001-0.005 l/min. The air pressure and flow rate were kept constant at 0.1 MPa and 0.3 l/min, respectively. Also the position of the atomiser device outlet was reduced to 75 mm from 100 mm with respect to the laser beam centreline, to improve the efficiency of collected aerosols. Due to the large number of tests, Figures 7.18 and 7.19 typify the particle diameters obtained using the Malvern Mastersizer-X, for tests AS-20 (a) and AS-27 (b) based on NMD and SMD, respectively and the remaining data is presented in Appendix B4.

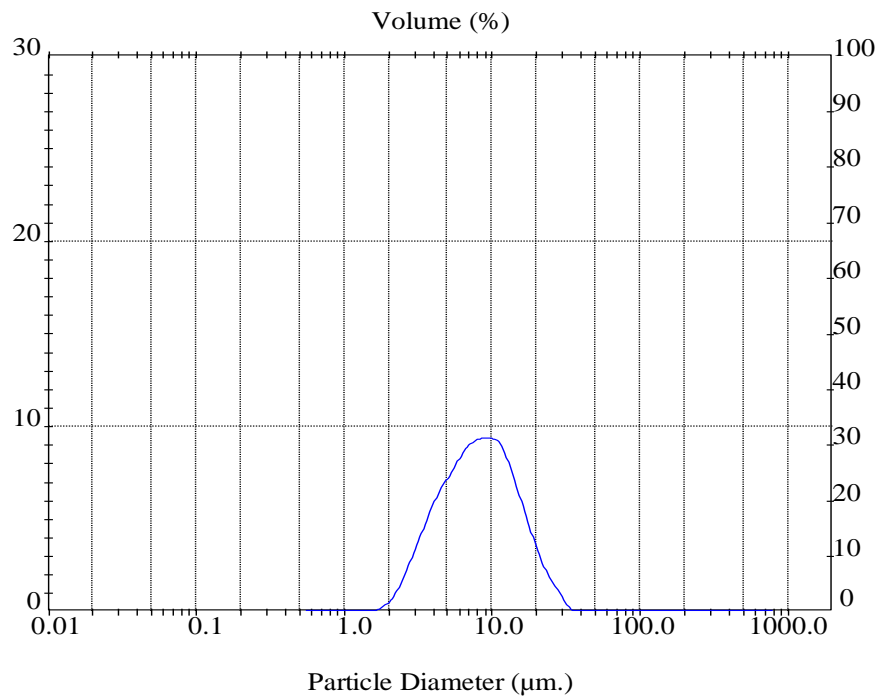


(a) Test: AS-20, $D_{n0.50} = 3.17\mu\text{m}$

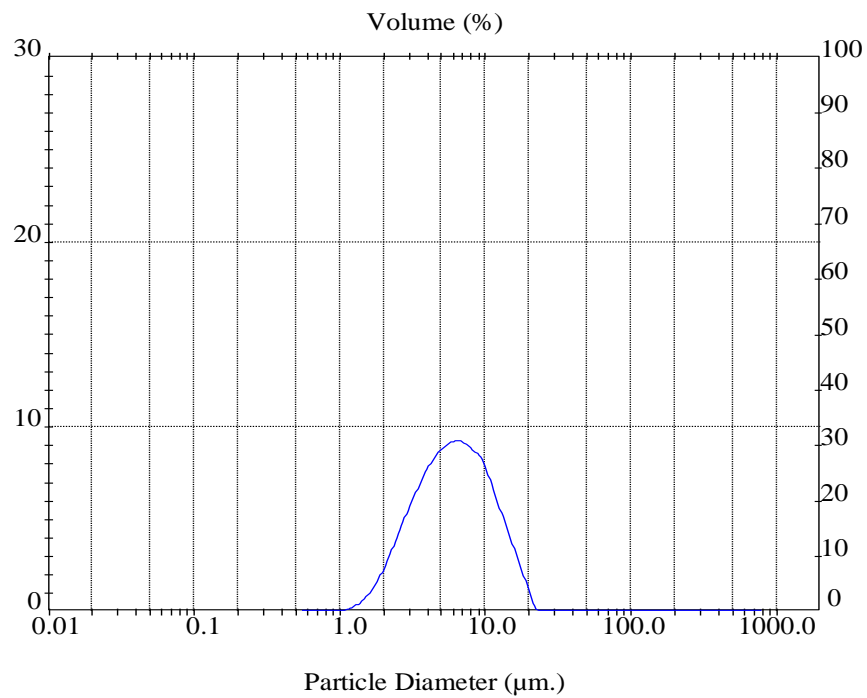


(b) Test: AS-27, $D_{n0.50} = 2.19\mu\text{m}$

Figure 7.18: Typical particle diameter (μm) distributions for tests AS-20 (a) and AS-27 (b), based on $D_{n0.50}$



(a) Test: AS-20, $D_{32} = 6.70\mu\text{m}$



(b) Test: AS-27, $D_{32} = 4.94\mu\text{m}$

Figure 7.19: Typical particle diameter (μm) distributions for tests AS-20 (a) and AS-27 (b), based on D_{32}

Table 7.4 summarises the results of these experiments in tabulated form.

<i>Test No.</i>	<i>Water supply pressure, MPa</i>	<i>Water flow rate, l/min</i>	<i>D₃₂, μm</i>	<i>D_{n0.50}, μm</i>
SA-18	6	0.001	6.83	2.86
SA-19		0.003	6.13	3.06
SA-20		0.005	6.70	3.17
SA-21	8	0.001	5.21	2.66
SA-22		0.003	6.77	2.76
SA-23		0.005	6.20	2.99
SA-24	10	0.001	4.18	2.38
SA-25		0.003	5.39	2.45
SA-26		0.005	5.54	2.84
SA-27	11	0.001	4.94	2.19
SA-28		0.003	4.94	2.56
SA-29		0.005	4.98	2.75

Table 7.4: Results of various tests showing the effect of water supply pressure and water flow rate on droplet sizes

Figure 7.20 shows the variation of the droplet sizes based on $D_{n0.50}$ with water supply pressures for different water flow rates. As can be seen from this figure, it is clear from these results that water flow rate has a direct effect on droplet size. An increase in water flow rate at constant water supply pressure will increase the droplet size. By contrast, as expected according to atomisation physics, the water supply pressure has an inverse effect, in which its increase reduces the droplet sizes, while its decrease increases the droplet sizes.

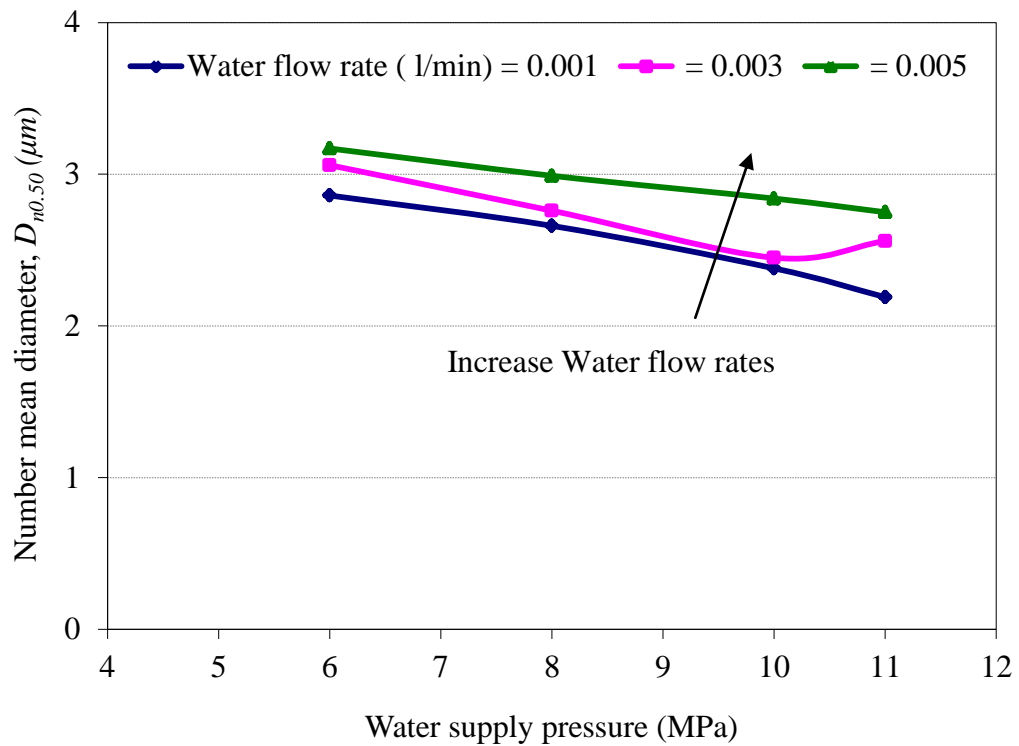


Figure 7.20: Variation of drop size ($D_{n0.50}$) with water supply pressure for different water flow rates

For example, at a pressure of 6 MPa and a flow rate of 0.001 l/min the number mean diameter $D_{n0.50}$ was 2.86 μm and it decreases to 2.66, 2.38 and 2.19 μm as water supply pressure increases to 8, 10 and 11 MPa, respectively. And vice versa, at water flow rates varying 0.001 - 0.005 l/min and at a constant pressure, the $D_{n0.50}$ tends to increase as the water flow rate increases at constant pressure.

To gain a better understanding of the water supply pressure and the flow rate an “iso-contours” 3-dimensional surface DPlot software package was used in further analysis. Figure 7.21 shows a typical $D_{n0.50}$ (μm) “iso-contours” for different water flow rates and water supply pressures up to 11 MPa, for tests (AS-18 to AS-29). As can be seen in

Figure 7.21, increasing the water supply pressure decreases the droplet sizes, while increasing the water flow rate at constant pressure increases the droplet sizes.

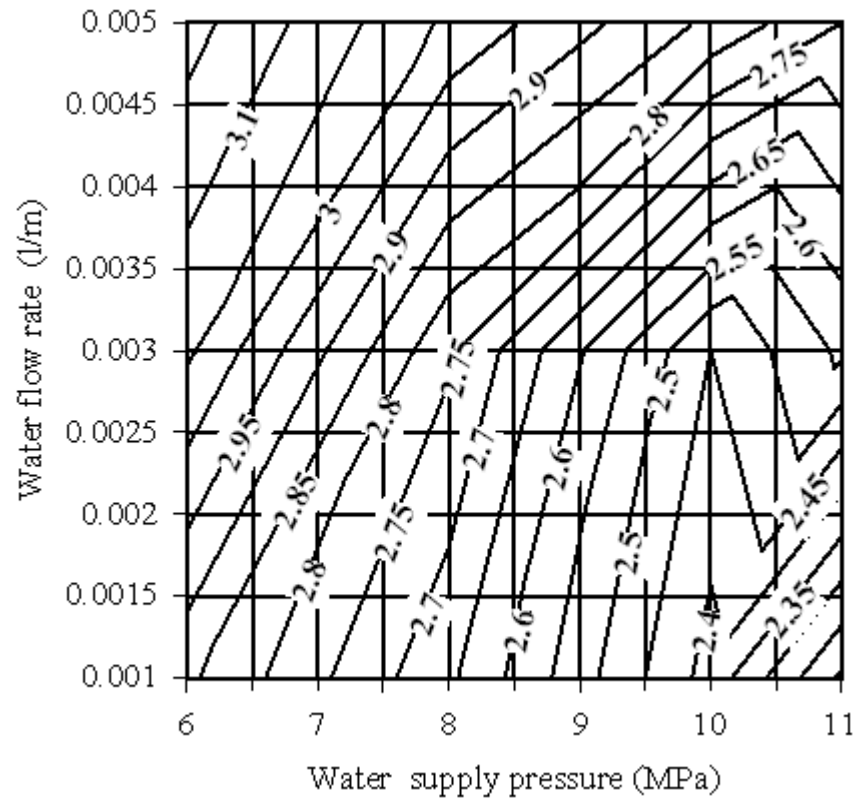


Figure 7.21: $D_{n0.50}$ (μm) “iso-contours” plots for different water flow rates (0.01-0.05) l/min and different water supply pressures (6 -11) MPa, for tests (AS-18 to AS-29)

7.3.2.3.3 Air Flow Rate

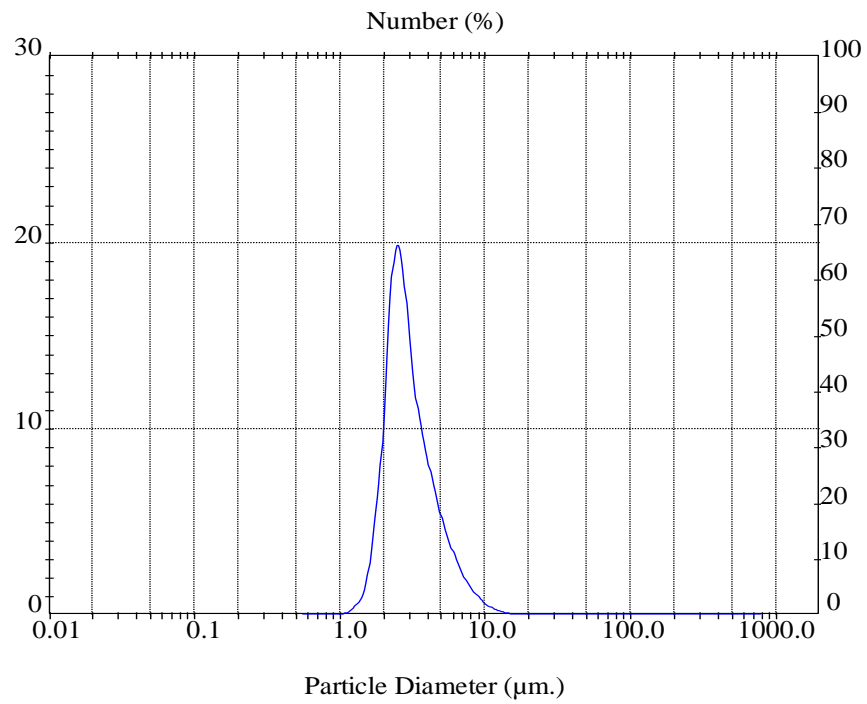
Air was used during the *Phase I* experimental work, simulating the methane which was used in the *Phase II* trials. The effect of air flow rate on the droplet size distribution was investigated in this set, which varied from 0.3-0.4 l/min (see Chapter 6, Section 6.3.2.2). The water supply pressure was varied from 6 to 11 MPa and its flow rate was

maintained at 0.001l/min as the smallest droplet sizes were gained at this rate (see previous section). The position of the atomiser device outlet was kept the same as that of the previous set (Section 7.3.2.3.2), at 75 mm with respect to the laser beam centreline. Figures 7.22 and 7.23 typify the particle diameters obtained using the Malvern Mastersizer-X, based on $D_{n0.50}$ for tests AS-30 and AS-41, and the remaining data is presented in Appendix B4.

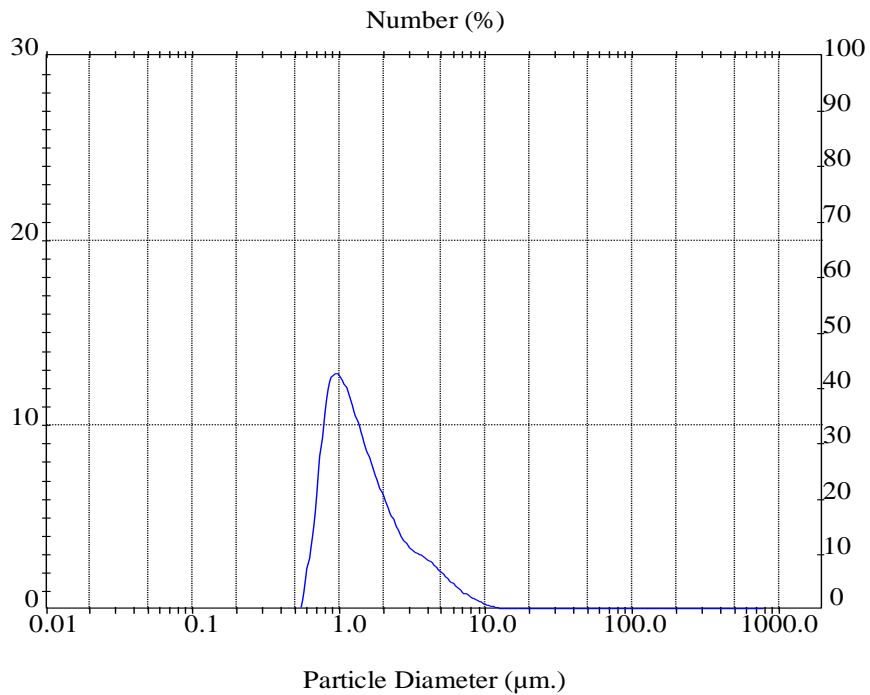
Table 7.5 presents the results of these experiments based on *SMD* (D_{32}) or *NMD* ($D_{n0.50}$).

<i>Test No.</i>	<i>Water supply pressure, MPa</i>	<i>Air flow rate, l/min</i>	<i>D₃₂, μm</i>	<i>D_{n0.50}, μm</i>
SA-30	6	0.3	5.79	2.80
SA-31		0.35	5.76	2.50
SA-32		0.4	5.56	2.39
SA-33	8	0.3	5.55	2.64
SA-34		0.35	5.13	2.22
SA-35		0.4	4.73	1.91
SA-36	10	0.3	5.98	2.17
SA-37		0.35	4.97	1.83
SA-38		0.4	5.72	1.58
SA-39	11	0.3	5.81	2.10
SA-40		0.35	5.53	1.66
SA-41		0.4	5.33	1.32

Table 7.5: Typical results of air flow rates and water supply pressures on droplet sizes

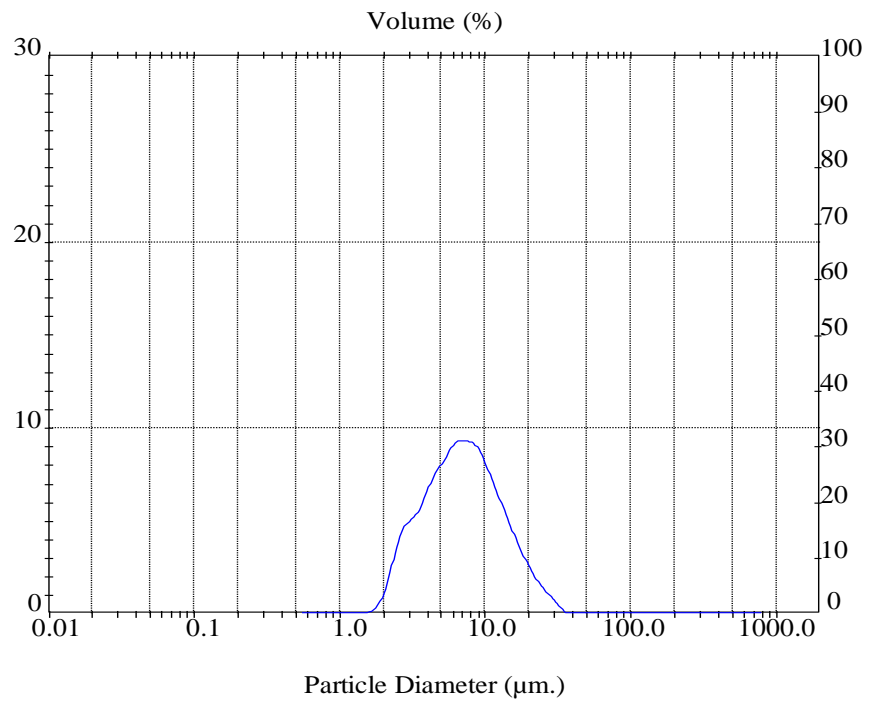


(a) Test: AS-30, $D_{n0.50} = 2.80\mu\text{m}$

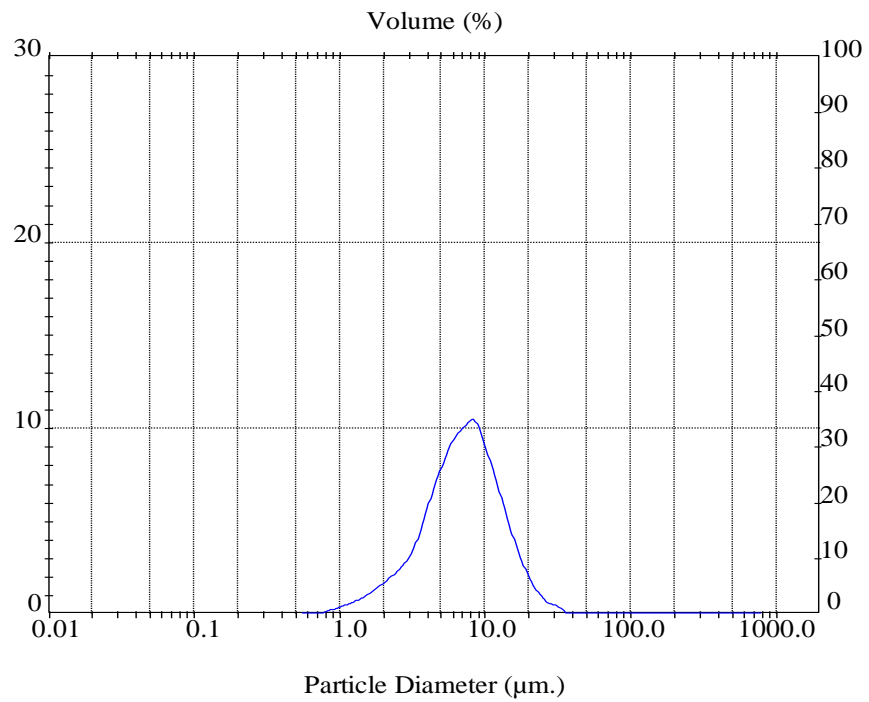


(b) Test: AS-41, $D_{n0.50} = 1.32\mu\text{m}$

Figure 7.22: Typical particle diameter (μm) distributions for tests AS-30 (a) and AS-41 (b), based on $D_{n0.5}$



(a) Test: AS-41, $D_{32} = 5.79\mu\text{m}$



(b) Test: AS-41, $D_{n0.50} = 5.33\mu\text{m}$

Figure 7.23: Typical particle diameter (μm) distributions for tests AS-30 (a) and AS-41 (b), based on D_{32}

As can be seen from Figure 7.24, a decrease in the droplet size occurs as the air flow rate increases. A similar trend has been observed for the water supply pressure and number mean diameter compared in Figure 7.20, but the air flow rate has an inverse effect on the drop size diameter compared with water flow rate (see previous section), which has a direct effect on droplet size diameter. This increase in air flow rate results in imparting a higher velocity to the water stream, which results in a break-up of the stream into finer fragments and thus reducing the droplet size.

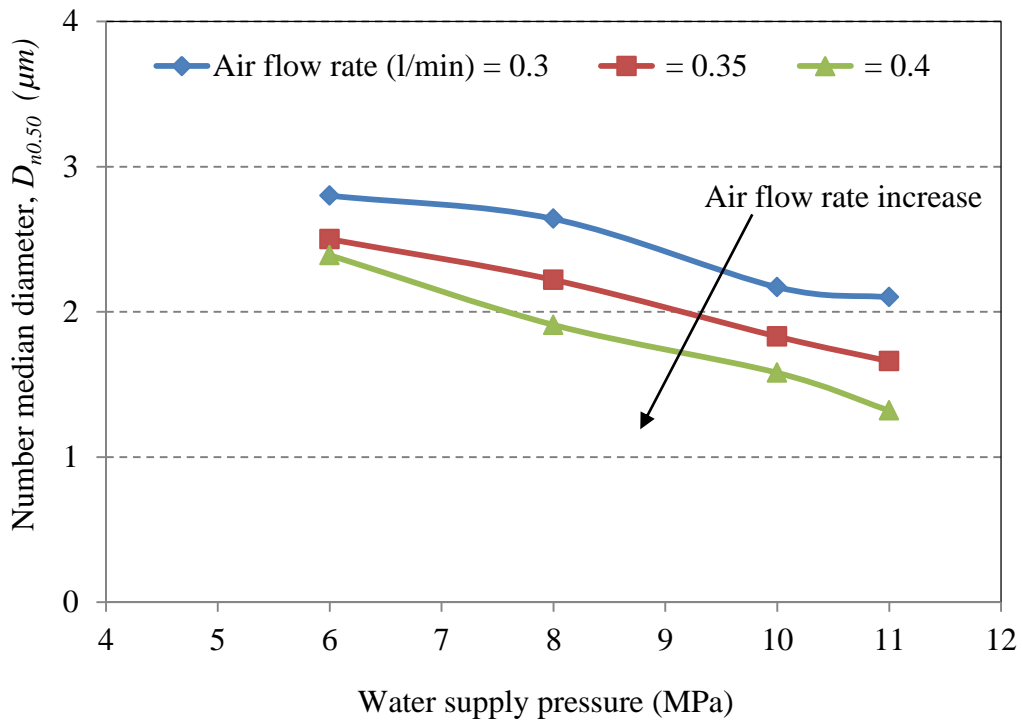


Figure 7.24: Variation of drop size ($D_{n0.50}$) with water supply pressure for different air flow rates

Figure 7.25 also shows $D_{n0.50}$ (μm) “iso-contours” 3-dimensional surface DPlot charts for different air flow rates and different water supply pressures up to 11 MPa, for tests

AS-30 to AS-41. This figure shows that increase in water supply pressure and air flow rate decreases the droplet sizes.

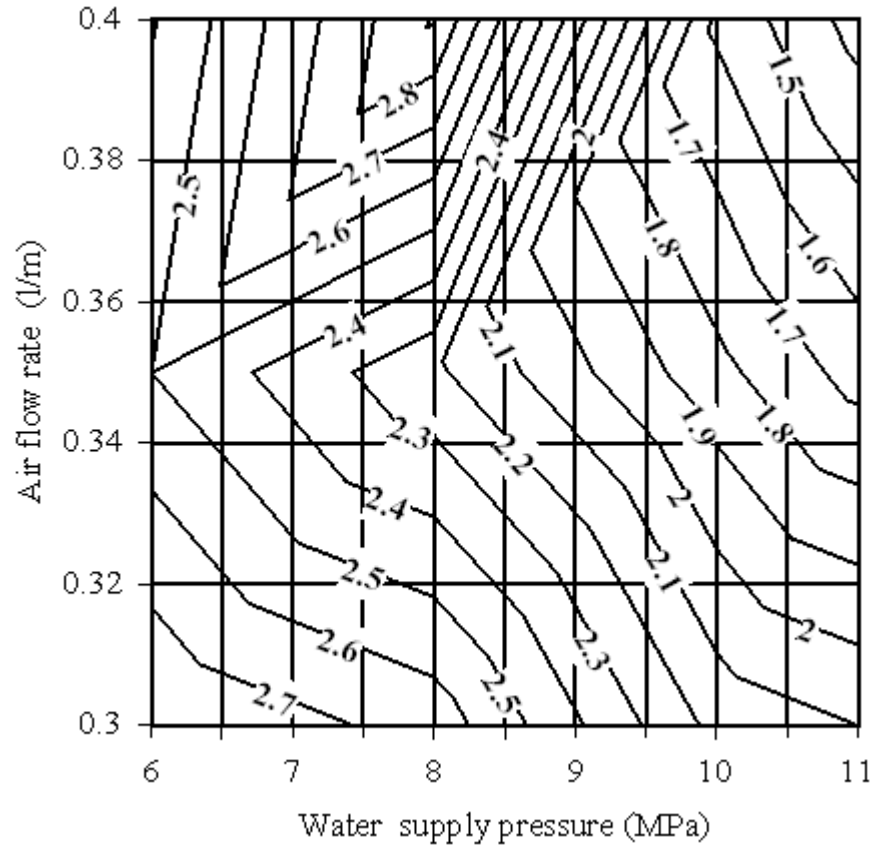


Figure 7.25: $D_{n0.50}$ (μm) “iso-contours” plots for different air flow rates (0.3 - 0.4) l/min and different water supply pressures (6 to 11) MPa, (Tests AS-30 to AS-41)

7.3.2.3.4 Atomiser Device Position with Respect to the Laser Beam

This set of experiments was performed to investigate the effect of the atomiser position with respect to the measuring instrument. The runs were made with the atomiser device exit located at downstream distances of 40, 50, 75 and 100 mm with respect to the centreline of the analysing beam (see Figure 7.26).

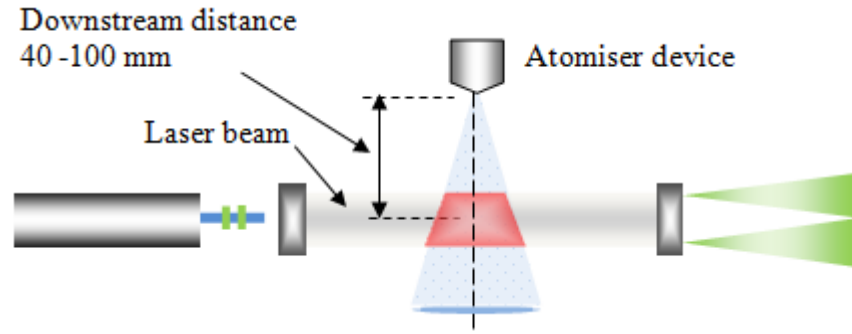


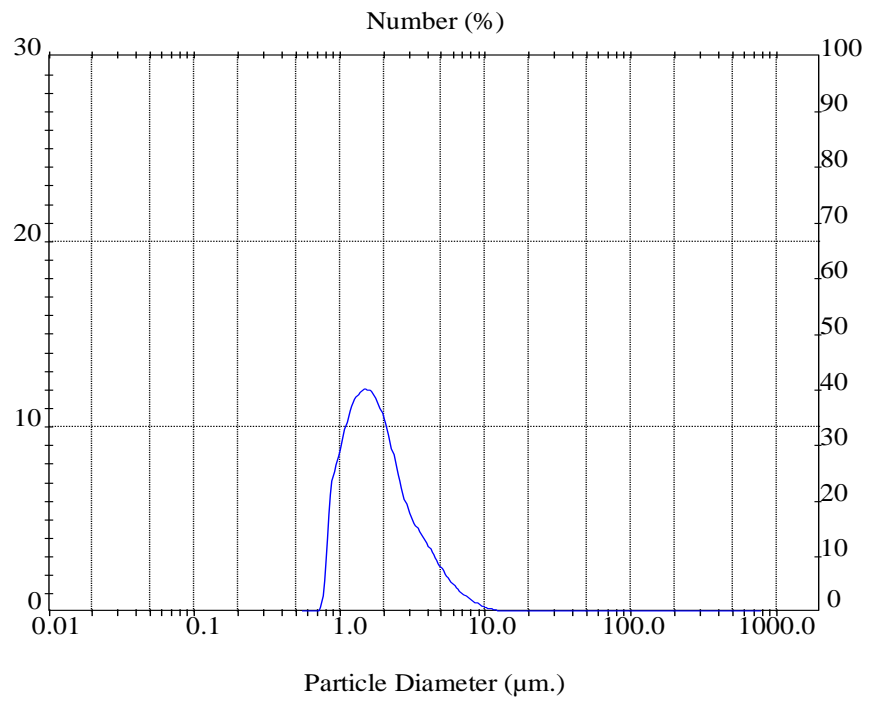
Figure 7.26: Spray device positions with respect to the laser beam

The particle diameters obtained using Malvern Mastersizer-X, for tests AS-44 and AS-47 are typified in Figure 7.27 based on NMD and Figure 7.28 based on SMD and the remaining data is presented in Appendix B4.

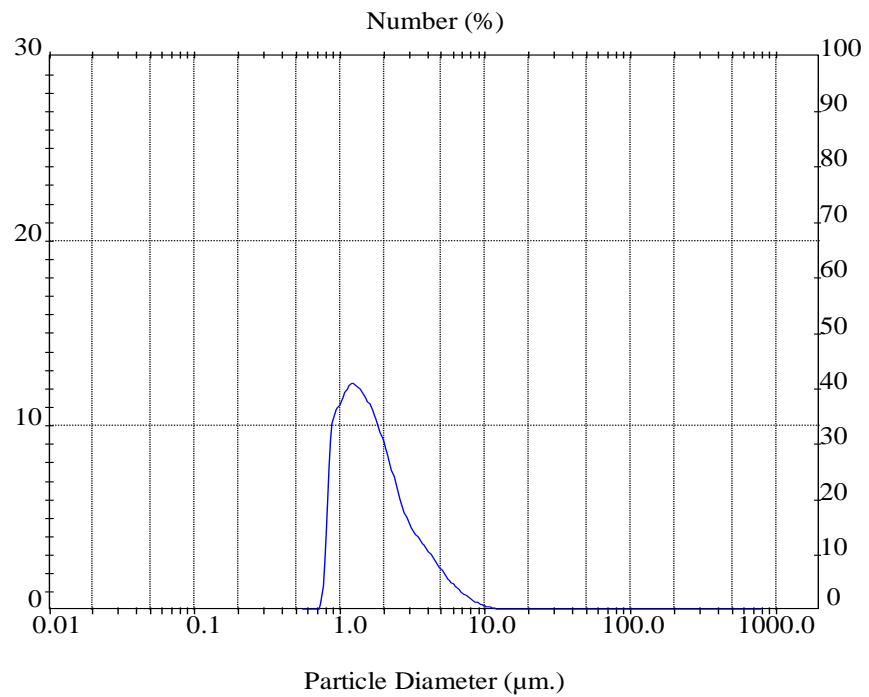
For each of these positions the pressure was kept constant at 10 MPa, the water flow rate was 0.001l/min and the air flow rates were 0.30 and 0.40 l/min. Table 7.6 summarises these results.

<i>Test No.</i>	<i>Air flow rate, l/min</i>	<i>Atomiser downstream distance to laser beam, mm</i>	<i>D₃₂, μm</i>	<i>D_{n0.50}, μm</i>
SA-42	0.3	100	6.41	3.27
SA-43		75	5.19	2.42
SA-44		50	5.15	1.72
SA-45		40	5.56	2.39
SA-46	0.4	100	5.89	3.07
SA-47		75	4.90	1.58
SA-48		50	4.96	1.39
SA-49		40	5.97	1.70

Table 7.6: Typical results showing the effect of downstream distance of atomiser exit on droplet sizes



(a) Test: AS-44, $D_{n0.50} = 1.72 \mu\text{m}$



(b) Test: AS-47, $D_{n0.50} = 1.58 \mu\text{m}$

Figure 7.27: Typical particle diameter (μm) distributions for tests AS-44 (a) and AS-47 (b), based on $D_{n0.5}$

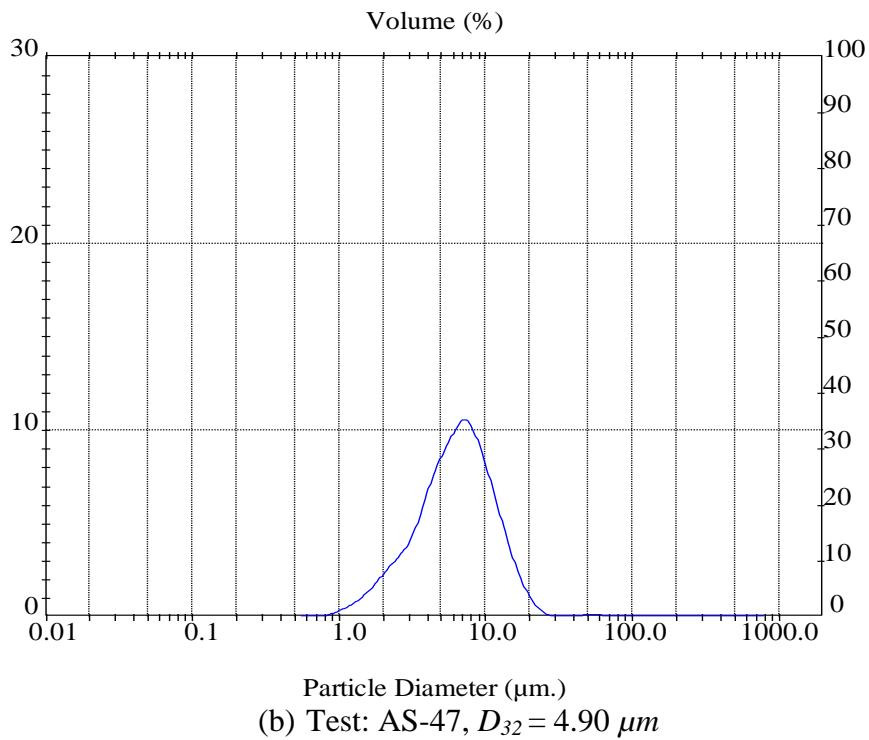
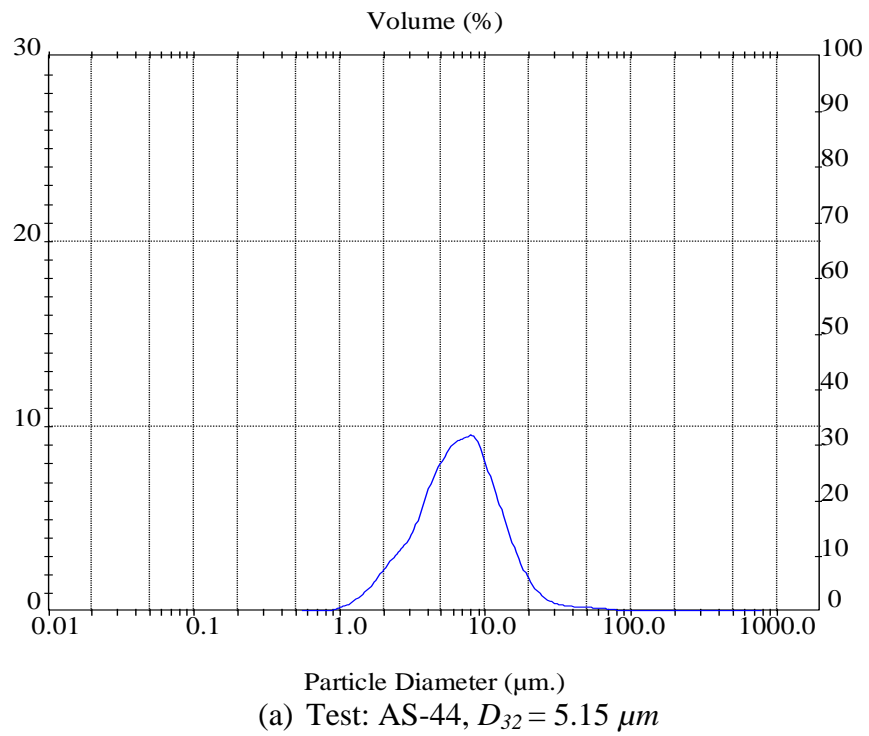


Figure 7.28: Typical particle diameter (μm) distributions for tests AS-44 (a) and AS-47 (b), based on D_{32}

Figure 7.29 shows the variation in droplet sizes as a function of downstream distance, for air flow rates of 0.30 and 0.40 l/min. It is clear that by decreasing the downstream distance at different water supply pressure, a decrease in droplet size occurs and vice versa. This is may be due to:

- i. Coalescence
- ii. Evaporation of smaller droplets

Also, it is clear that the increase in air flow rate decreases the droplet sizes, which confirms the obtained results in Section 7.3.2.3.3. The upper curve gives the results of 0.3 l/min and the lower one gives those of 0.4 l/min, as the latter gave lesser droplet sizes.

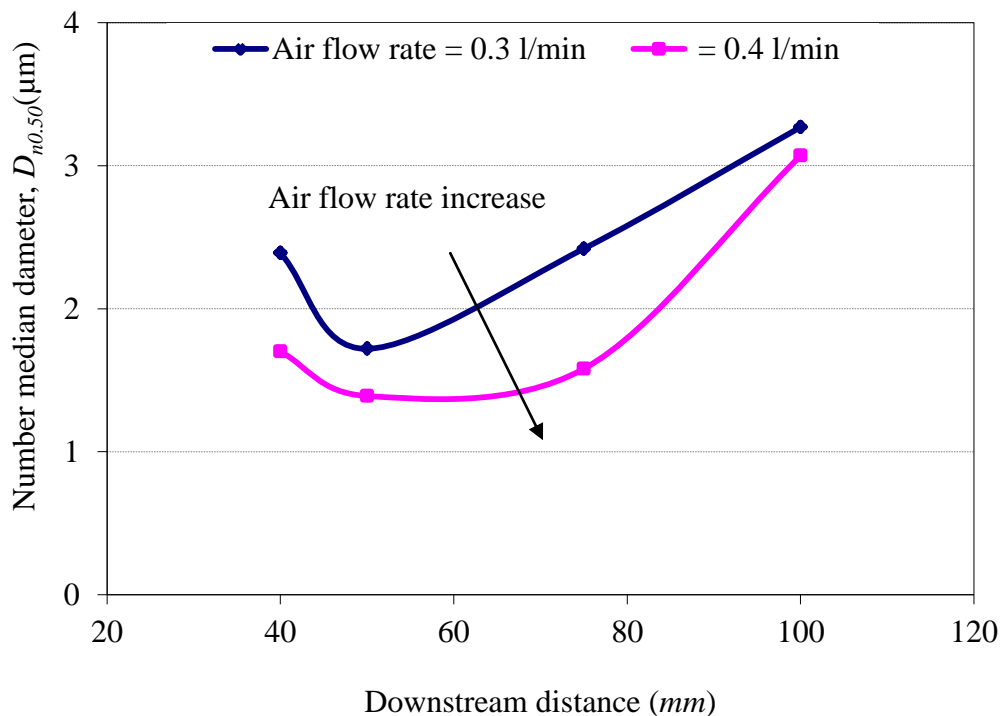


Figure 7.29: Droplet size ($D_{n0.50}$) as a function of downstream distance for 0.3 and 0.4 l/min air flow rates

Based on Table 7.6 and Figure 7.29, Figure 7.30 shows $D_{n0.50}$ (μm) “iso-contours” 3-dimensional surface plot charts for different downstream distances and air flow rates of 0.30 and 0.40 l/min, for tests AS-30 to AS-41. From close inspection of Figure 7.30, it is clear that the droplet sizes decrease as the air flow rate increases and they decrease with decreasing the downstream distance up to 50mm. After this distance i.e. at 40mm, a sudden increase occurred.

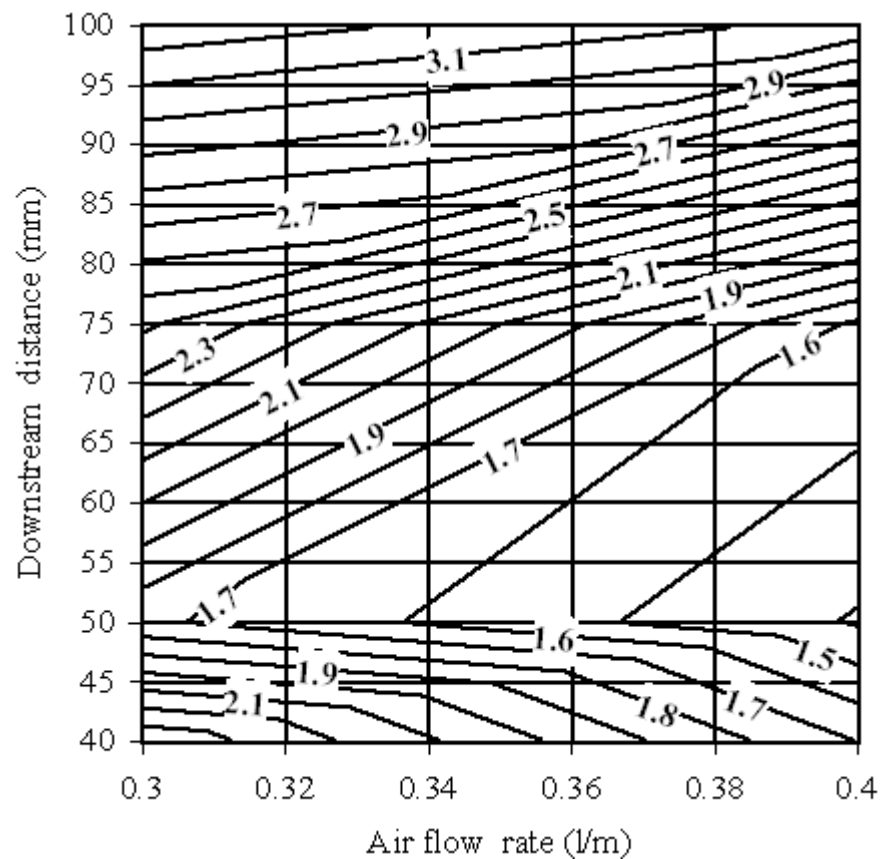


Figure 7.30: $D_{n0.50}$ (μm) “iso-contours” plots for different air flow rates (0.3-0.4) l/min and different downstream distance (40-100 mm) (Tests AS-41 to AS-49)

From this investigation, the result is true for distances of 50mm and over, but at 40mm a sudden drop size increase was noticed, which might be attributed to the very short distance to the measurement position. For shorter distances, the obscurescence level is so high for the laser beam travelling closer to the atomiser, that no light signal can be detected by the photodiodes.

7.3.2.4 Summary

The experimental work investigated in the previous sections has examined the generation of fine aerosol sprays which have droplet sizes of less than or equal 5 μm , produced from a designed atomiser device. This device was designed for the purpose of SWCNT production in collaboration with the University of Oxford. Up to this point, the *Phase I* experimental work was successfully completed and the produced aerosol stream had droplet sizes of less than 5 μm as expected. The results have shown that the vertical position of the atomiser device with respect to the measuring droplet sizes' unit is the most suitable configuration compared with the inverted and horizontal positions as they did not generate any aerosol stream. The effect of water supply pressure and flow rate and the gas flow rate together with the downstream distance of the atomiser device on the droplet size distribution were investigated and characterised.

The next section highlights the results and presents a discussion of the *Phase II* experimental work.

7.3.3 Phase II: Single-Walled Carbon Nanotubes Generation: Highlight of the Results and Discussion

After the successful completion of the *Phase I* experimental work and when the aerosol stream droplet sizes of less than 5 μ m were gained, the rig was sent to the University of Oxford, after reconstructing some of its parts, to complete the remaining experimental work for SWCNT generation.

An overview of the experimental apparatus was shown in Figure 6.19, in the previous chapter, whilst Figure 7.31 shows the assembly of the atomiser device and the furnace. To prevent the overheating of the high pressure pump, a solution in the reservoir tank ran through a radiator which was put in a bucket with running water as shown in Figure 7.32.

The experimental conditions of the first tests were as following:

- i. Solution of iron acetate 0.043M (30 gm in 4 l of distilled water) was stored in the reservoir tank;
- ii. The pump was run at pressure of 150 bar (15 MPa) to spray aqueous catalyst solution;
- iii. Oxygen gas was introduced, instead of methane, at the top of the atomiser with a flow rate of 4 ml/min;
- iv. The experiment was carried under 400 $^{\circ}$ C for 4 hours.

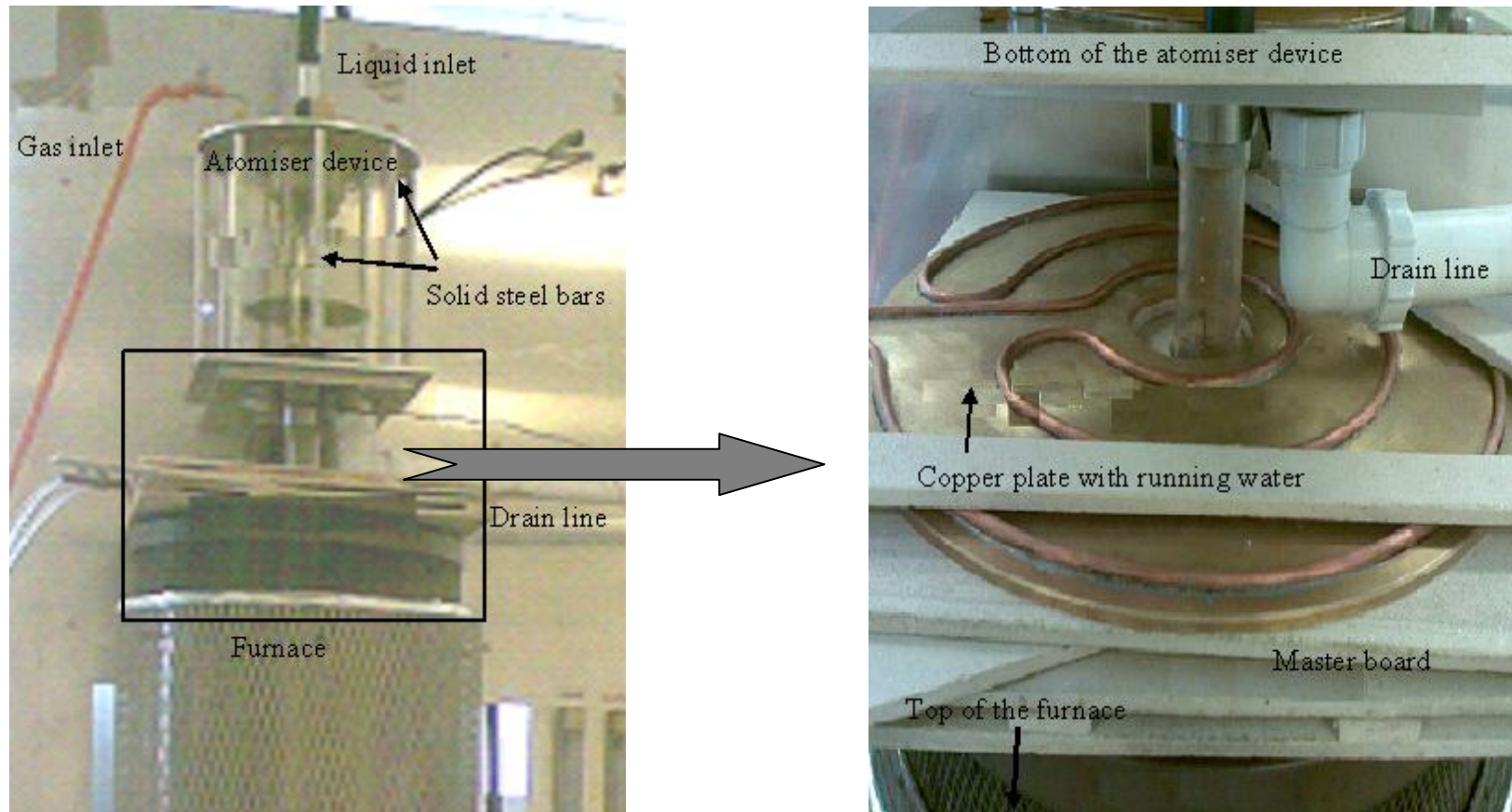


Figure 7.31: The atomiser device and the furnace connection overview

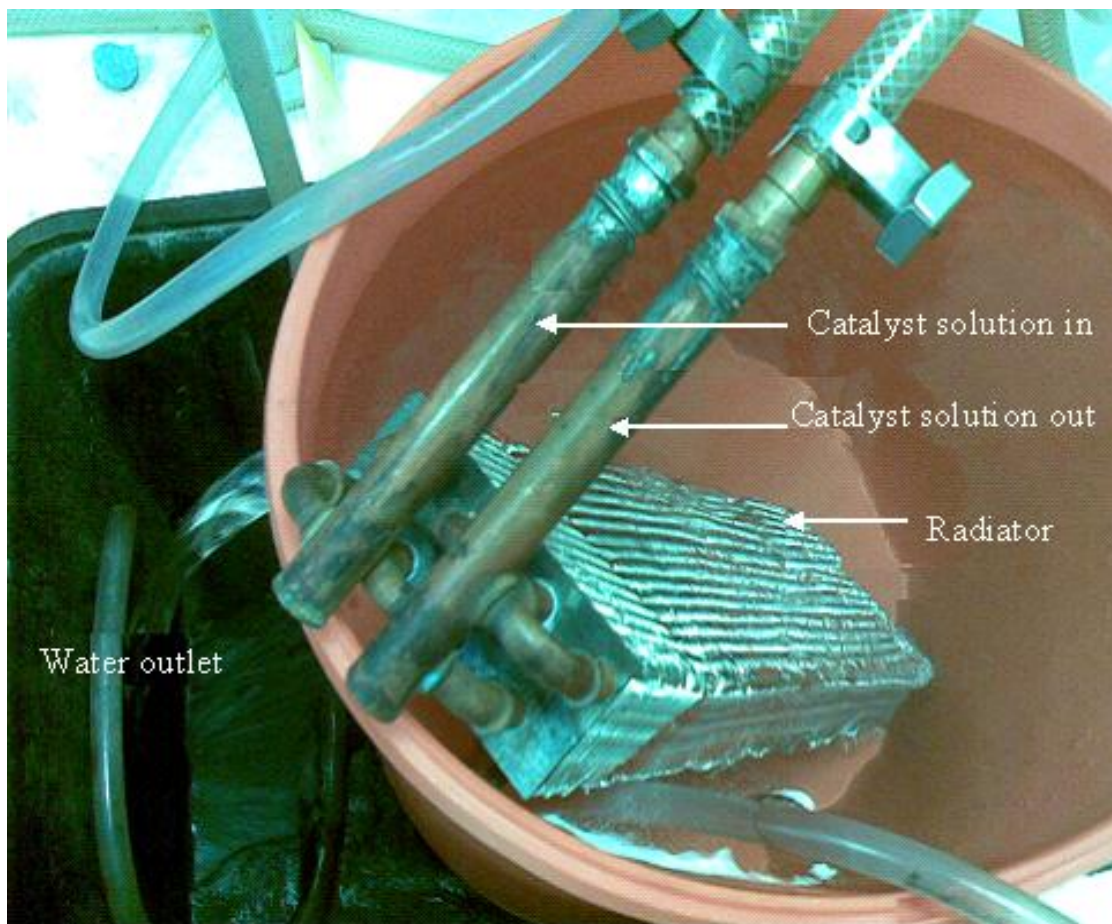


Figure 7.32: Radiator in a bucket with running water

At 400° C, the steel plate upon which the atomiser stands gets quite hot. This problem was solved by adding sheets of high temperature resistant master board and copper plate with cooling water running through (see Figure 7.31). “Smoke” could be seen at the bottom of the furnace. The higher the pressure, the more smoke produced. The laser pointer shows a red coloured path reflecting the existence of small particles as shown in Figure 7.33.

SWCNT particles were deposited as products and were studied using Transmission Electronic Microscopy (TEM). Figures 7.34 and 7.35 show the typical TEM images obtained during this prototype test run at the University of Oxford. These limited results provide further assurance that flare gas can be utilised to produce SWCNT using the novel design for the atomiser device. However, this currently an ongoing work and more comprehensive results will be jointly reported in the future with the University of Salford and by Miss V. Chang (PhD student) at University of Oxford (independently).

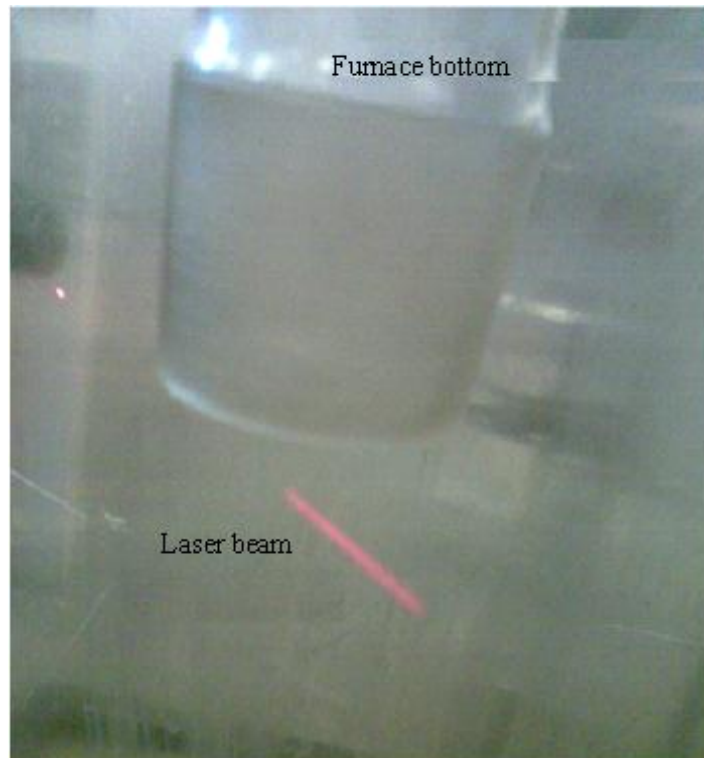


Figure7.33: Illustration of laser beam on the product particles



Figure 7.34: TEM image of the products of *Phase II* experiments (oxygen and Fe liquid catalyst)

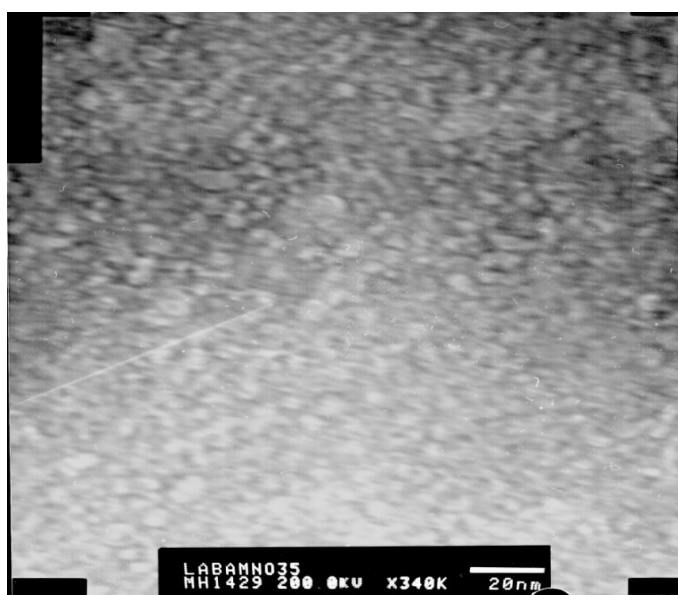


Figure 7.35: TEM image of the products of *Phase II* experiments (methane and Fe liquid catalyst)

Chapter - 8

CHAPTER-8: CONSIDRATION OF ECONOMIC ANALYSIS

8.1 Introduction

The economic analysis of any project involves an assessment of the costs and benefits of operating a project under various proposed modes and conditions. The base case for this research is the potential for the reduction of gas flaring for the reasons which were previously described in Chapter 2.

Flare gas has found its route into the atmosphere as an industrial waste. The result is that this practice has generated several severe consequences for humanity and nature. This chapter gives an economic analysis and comparison between the two options that were investigated in this research, in addition to the gas flaring option. These two options, which were presented in detail in the previous chapters, are the utilisation of the flare gas (mainly methane) for syngas production through partial oxidation and the generation of Single-Walled Carbon Nanotubes using sprays and atomisation techniques. The comparison was implemented using a Visual Basic (VB) programme and an Excel spreadsheet for data plotting. A typical oil and gas production plant was considered and the cost data is based on the Hakim field of Zueitina Oil Company, Libya.

Suitable planning was set out and structured based on the programme's objectives. The planning includes: system analysis and database design principles, HCI (Human Computer Interface), heuristics, diagrams and testing. Finding solutions to the practice of gas flaring will balance the benefits gained against the cost incurred. Therefore, the purpose of this chapter is to design a programme that can run a comparison between at

least two costs resulting from the economic analysis outcome. The objective is to achieve an overall expectation that will:

- i. Analyse the requirement;
- ii. Locate exactly where the software has to be used;
- iii. Assess the tools;
- iv. Deliver the minimum of work for completion to overall satisfaction.

8.2 Concept of a Visual Basic Programme

Visual Basic (VB) is a development tool that can be used to build software applications that perform useful work and look very attractive within a variety of settings (Halvorson, 2008). It is also defined as a programming environment in which a programmer uses a Graphical User Interface (GUI) to choose and modify preselected sections of code written in the basic programming language.

VB can help create applications for the Windows operating system, the Web, hand-held devices and a host of other environments and settings. The most important advantage of Visual Basic is that it has been designed to increase productivity in daily development work, especially if one needs to use information in databases or create solutions for the Internet (Halvorson, 2008).

8.2.1 Programming Fundamentals and Overview of the Economic Analysis

The rules of construction that must be used when one builds a programming statement are called *statement syntax*. Visual Basic shares many of its syntax rules with earlier versions of the BASIC programming language and with other language compilers.

Visual Basic undertakes a lot of the hardest work, so that the time spent in writing a programme code is relatively short and results can be reused in future programmes. Visual Studio IDE also points out potential syntax errors and suggests corrections, much like the AutoCorrect feature of Microsoft Office Word.

Variables are used to store information. They are used to create the code and can contain words, numbers, dates, properties, or other values. Using variables can assign a short and easy-to-remember name to each piece of data for the user plan to work with. Variables can hold information entered by the user at run time, the result of a specific calculation, or a piece of data that needs to be displayed upon a designed form. In short, variables are handy containers that the user can use to store and track almost any type of information. Using variables in a Visual Basic programme requires some planning. Before the user can use a variable, he/she must set aside memory in the computer for the variables' use.

Basically, a Visual Basic programme consists of the following steps:

- i. One or more forms;
- ii. Controls on the forms;
- iii. Code written in the Visual Basic programming language.

Applications are created by dragging controls onto forms and setting properties. To make these applications useful, codes are added to tie the controls together and perform calculations and data manipulation. The programme code is a set of instructions that tells Visual Basic how to manipulate data, perform input and output and respond to the user. Figure 8.1 shows the project request diagram.

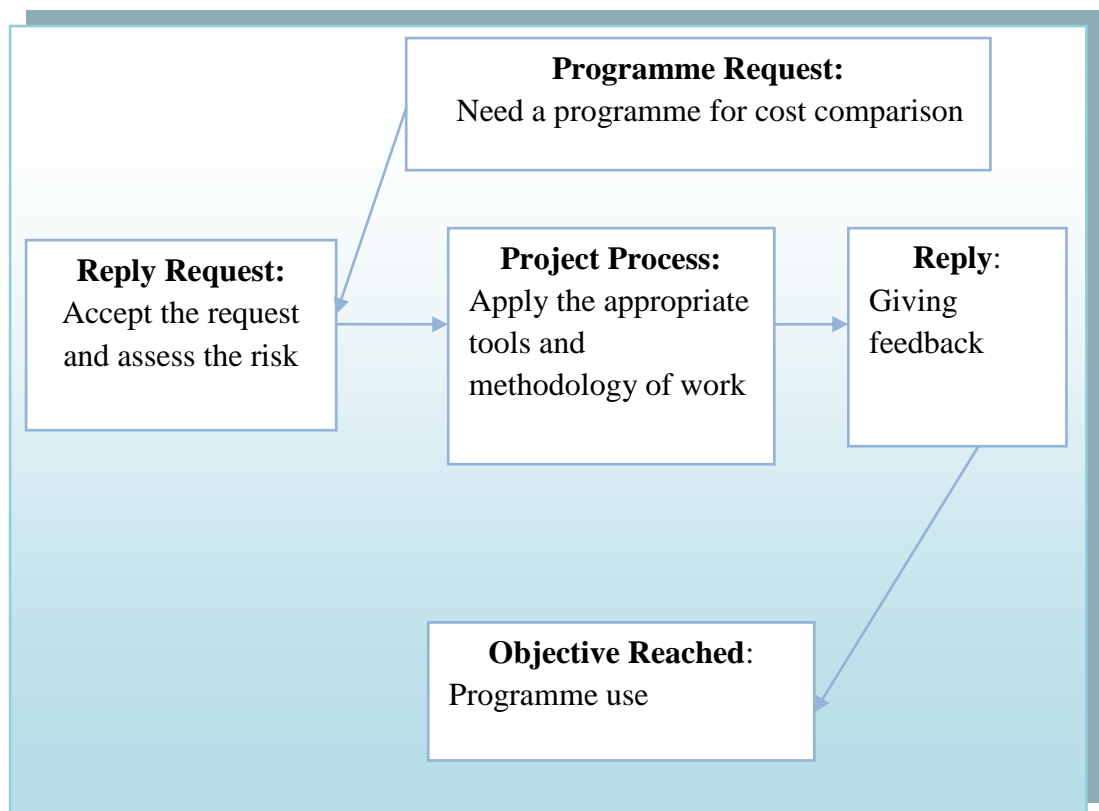


Figure 8.1: Diagram of cost comparison request

8.2.2 Feasibility Study

Once the needs of the programme have been defined, a detailed feasibility study has to be formed to comprehend the risks in advance, and to set a framework to impose boundaries for the project within a satisfactory time scale. Usually the feasibility study is partitioned into three parts: technical, economical and organisational feasibility. So,

the first task is to assess the technical practicability of the programme. To assess the feasibility of the programme, the following points have been highlighted:

- i- *Familiarity with the application:* This is a source of technical risk. As part of the selected software and programming languages, the one used for this programme is a part of them. Visual Basic programming language and an access database management system have been selected to accomplish this task.
- ii- *The domain of knowledge:* This factor allows considerable support in achieving the goal, and the risk of misunderstanding the requirements could be lower than any other aspect. The use of the same syntax helps to increase the level of familiarity with the application.

8.2.2.1 Software Identification

Visual Basic (VB) has been selected as the programming language to design the front end because it fits in with the requirement. As a component of this analysis, it has been decided that a database needs to be linked to the front end, for future records. The database management system selected was Access from Microsoft Office.

8.2.2.2 Analysis Stage

This stage guides the developer with a combination of many documents to assist in making the final decisions for the implementation. The documents presented in this section will be mainly related to the database and the front end design. Before starting to make a programme it is good practice to find out “for which purpose the programme

is needed". This is considered one of the critical parts of the project as it characterises one of the success factors.

The request requirement is an application for a plant final costs' comparison. Thus, the application needs to display the costs in some sort of form and compare them by displaying a message answering a single question: *Which plant is the most economic?*

The aim of this project is to demonstrate that, as the costs are, it is always preferable to recycle than to flare the gas. This theme has been inspirational in organising the project and understanding its priorities.

Figure 8.2 helps to understand the requirement previously stated.

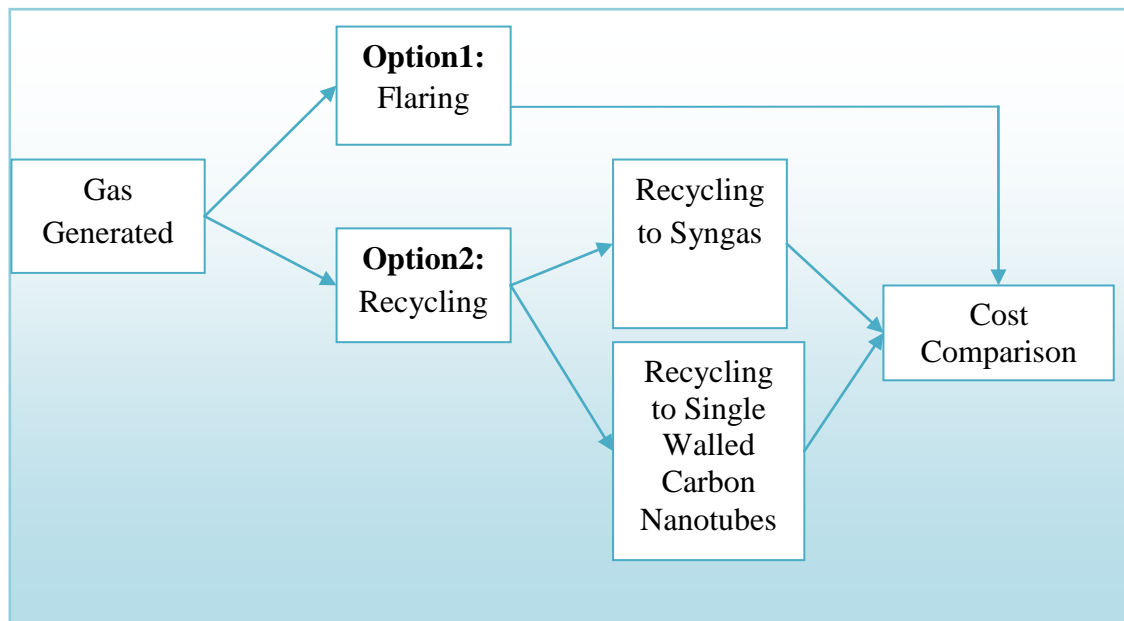


Figure 8.2: Process flow diagram

8.2.2.3 Functional and Non-functional Requirements

The application requirements are in two parts: functional and non-functional.

Functional requirement:

The functional system requirements cover the inputs and outputs and their behaviour within the application. The database created in this project is the main source of the data extraction, and the VB application applies calculations using these data.

Formulas have been scripted in VB to calculate the final costs of each option. Also suppositions have been made to apply the comparison and display the ultimate message. Each form represents an option: flaring, recycling 1 and recycling 2. The forms apply the same method of calculation, using appropriate data to give different results for each option.

The user has to select a number, in a 'Combo Box', representing the row where the requested data are stored in the database. He/she has to press 'total' and the results are instantly displayed. The same process has to be repeated for each option, by using the three related forms. He/she then finally goes to the comparison form and presses 'compare'. At this step, the comparison is done and the final message is displayed.

Many labels have been used to identify the costs and textboxes have been used to display these costs. The reason for using the textboxes, and not labels, will be explained later in the design section. The programme has been designed with a maximum of simplicity, to make its use as uncomplicated as possible. The implementation of the functional requirements is detailed in the design and implementation section.

Non functional requirement:

This part basically covers the testability of the application, the security factor and its capacity. This application will be used by students and tutors in University laboratories and for this reason it has to be secured. Therefore, it is necessary to set up a password to protect the application. The records can be backed-up monthly at the same time as the scheduled manipulation. The application is testable simply with limited resources. The data will be manipulated weekly or monthly and the data will be summarised in the last part of the year for statistical purposes.

The speed of the data movement was set to medium level. The calculations used were specifically limited and created in general arrangement for the purpose of being used anywhere. There is no demand for high-intensity performance. The last point of this section will be the space reserved for the data and its manipulation. As the application is a front-end linked to a database, most of the records will be stored where their original (database). So the space is essentially devoted to data declarations and to the remainder of the functionalities.

8.2.2.4 Entities and Attributes

The entities and attributes of the database have been identified and Table 8.1 lists them with their entire relevant attributes.

<p><u>Plant</u></p> <ul style="list-style-type: none"> • Plant type • Plant location • Plant capacity • Equipment type <p><u>Production</u></p> <ul style="list-style-type: none"> • Final product type • Process type • Spray liquid catalyst volume • Carbon quantity • Syngas volume • Hydrogen volume • Carbon cash flow • Syngas cash flow • Hydrogen cash flow <p><u>Record</u></p> <ul style="list-style-type: none"> • Date of record • Year of assessment • Flaring final cost • Syngas final cost • Carbon final cost 	<p><u>Price</u></p> <ul style="list-style-type: none"> • Multitubular membrane price • Stack price • Spraying equipment price • Spray liquid catalyst price • Furnace price • Carbon price • Hydrogen price • Syngas price <p><u>Cost</u></p> <ul style="list-style-type: none"> • Implementation of the database • Multitubular membrane installation cost • Furnace installation cost • Stack installation cost • Spray equipment installation cost • Multitubular membrane maintenance cost • Furnace maintenance cost • Spray equipment maintenance cost • Stack maintenance cost • Environmental cost • Stack utility cost • Syngas utility cost • Carbon nanotubes utility cost • Flaring auxiliary cost • Syngas auxiliary cost • Nanotubes auxiliary cost
--	---

Table 8.1: List of entities and relevant attributes

8.2.2.5 Entities Relationship Diagram

Figure 8.3 shows how the entities are related in the database.

8.2.2.5.1 Cardinalities

Plant to cost: one - to - one

This relationship should be one to many, but in this particular instance the researcher considers that the cost (as entity) is the final cost. A plant will only have one final cost; this costing concerning only the one plant.

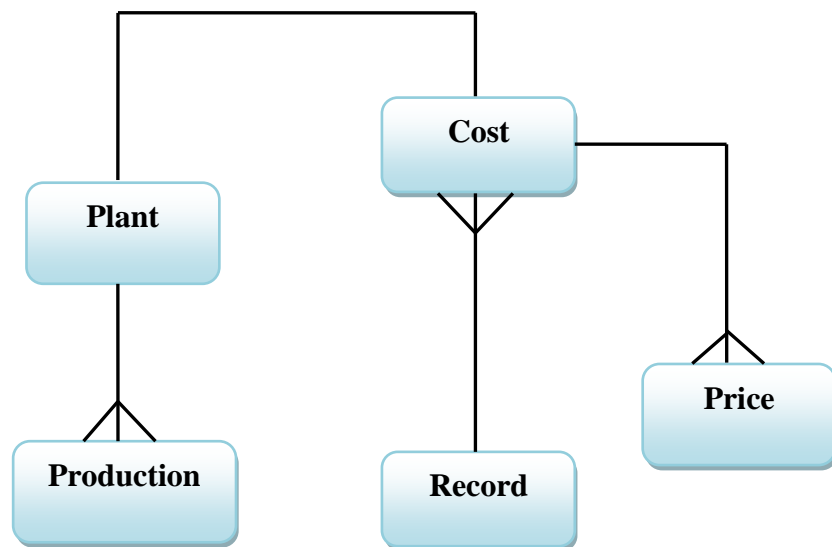


Figure 8.3: Entities relationship diagram

Cost to price: one - to - many

A cost could include many prices as presented in the market, but one price could be related to only one type of cost.

Plant to production: one - to - many

A plant could produce more than one product but a product could only be produced in one selected type of plant.

Record to cost: one - to - many

A record could include many costs, but a cost could be recorded only one time.

In conclusion, these cardinalities have resulted from the data assumptions.

8.2.2.5.2 Data Dictionaries

The data dictionaries are the description of each attribute and its role, in order to define the entity. In the case of this project, the data dictionaries are presented as a description of the database.

8.2.2.5.3 Normalisation

Normalisation is a systematic way of ensuring that a database structure is suitable for the purpose. This is a critical step in database design. See Appendix C for the normalisation table.

8.2.2.6 Context Diagram and Level 1 Data flow Diagram

In this section, diagrams will be presented to show the flow of information within the process.

Context diagram: This diagram represented by Figure 8.4, summarises the application boundaries and the elements involved.

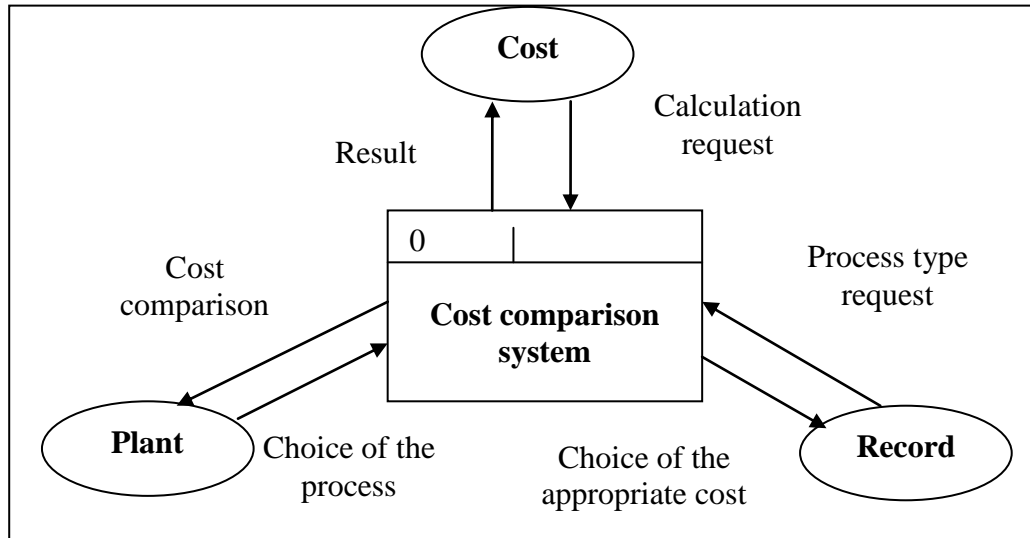


Figure 8.4: Context diagram

Level 1 dataflow diagram: This diagram represented by Figure 8.5, assists in understanding how the programme will work to achieve the requirement stated at the beginning.

8.2.3 Design Stage

8.2.3.1 Interface Structure

The interface has been designed so that it is enjoyable to view and easy to use. The condition imposed is the heuristics principle.

The interface plan:

The application developed is composed of 6 forms:

- i. The first form is the index of the application: the Main Menu form. It gives access to the rest of the forms.

- ii. Each option for gas destination is represented by one form, which gives 3 forms with a similar interface, but with different outputs and titles.
- iii. The fifth form is the comparison form. This form will display the 3 results of the 3 previous forms: the final comparison message.
- iv. The last form will enable the user to manage the database.

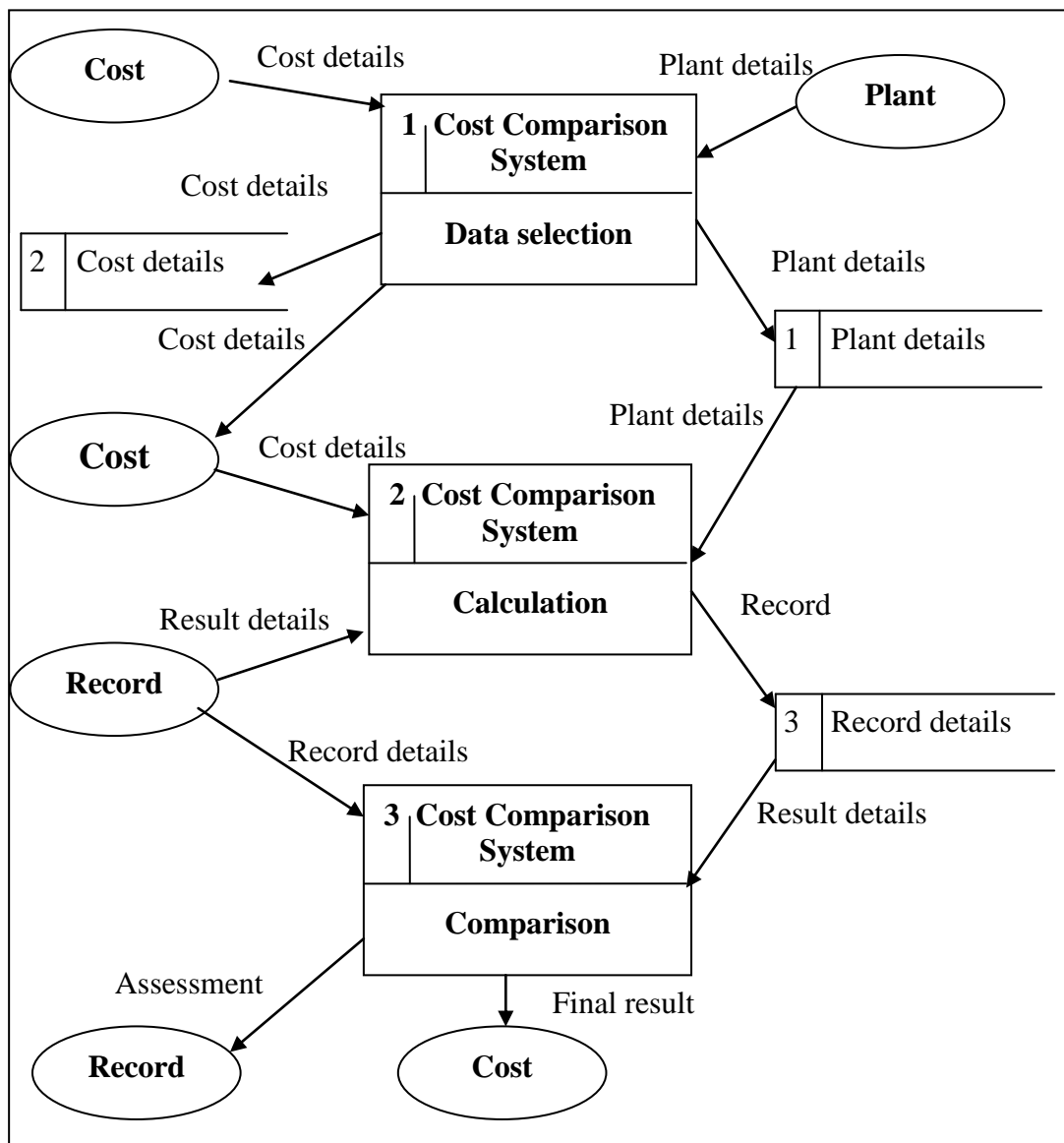


Figure 8.5: Level 1 data flow diagram

Heuristic principles:

Heuristics are rules that distil out the principles of effective user interfaces. In the context of this project the application is related to industry; the guidelines selected will be visibility and exploration of the interface.

Visibility:

The interface has not been laden with confusing objects, but has been kept simple for navigation. Also it contains the exact and essential information needed to guide the user with no hidden objects. The user is directed by a small label to indicate to him/her what he/she has to do.

Interface exploration:

The forms are named so it is easy to recognise the task that the form will execute. The interface is elementary to explore with no complicated links to follow. The syntax used in the application is fully fitting to its need. Metaphors have not been used to avoid user confusion.

8.2.3.2 Database Structure

The nomination of the attributes has been undertaken using syntax. The database is in plain design; the user does not use the database to produce daily reports or frequent queries. A report will be produced monthly with selective records from two tables: the production table and the record table. This report will include 4 weekly records. A query has been created for the cost table as it is the main table. The database has been created to facilitate the recording of data.

8.2.3.3 Links Between VB Interface and the Database

The data design tools have been used in Visual Studio and the database was created in Microsoft Office Access. The connection between themes was set up by creating a connection for the whole application using ADO.NET objects.

8.2.4 Implementation Stage

8.2.4.1 VB scripts

The calculation applies formulas which have been set up and the VB scripts are presented in Appendix D. The followings are the formulas which were used:

Flaring:

Stack Fixed Cost = Stack Price + Stack Installation Cost

Stack Variable Cost = Stack Maintenance Cost + Stack Utility Cost

Total cost1 = Stack Fixed Cost + Stack Variable Cost + Environmental Cost + Flaring

Auxiliary Cost - cashflow

Syngas:

Syngas Fixed Cost = Multitubular Membrane Price + Multitubular Membrane

Installation Cost

Syngas Variable Cost = Multitubular Membrane Maintenance Cost + Syngas Utility

Cost

Total Cost2 = Syngas Fixed Cost + Syngas Variable Cost + Syngas Auxiliary Cost

– Syngas Cash Flow

Syngas Cash Flow = SyngasVolume x SyngasPrice

Carbon Nanotubes :

Carbon nanotubes Fixed Cost = Furnace Price + Furnace Installation Cost + Spraying
Equipment Price + Spray Equipment Installation Cost

Carbon nanotubes Variable Cost = Furnace Maintenance Cost + Spray Equipment
Maintenance Cost + (Spray Liquid Catalyst Price x
Spray Liquid Catalyst Volume) + Carbon Nanotubes
Utility Cost.

Total Cost₃ = Carbon nanotubes Fixed Cost + Carbon nanotubes Variable Cost +
Carbon nanotube Auxiliary Cost – Carbon Cash Flow – Hydrogen Cash
Flow.

Carbon Cash Flow = Carbon Quantity x Carbon Price.

Hydrogen Cashflow = Hydrogen Volume x Hydrogen Price.

After the suppositions have been worked out they are implemented in the comparison
form.

8.2.4.2 Testing

After the implementation the programme was tested successfully (see Appendix E for
the test results).

8.2.4.3 User Guide

See Appendix F.

8.3 Economic Analysis and Comparison

The economic analysis (Microsoft Excel was used to plot the parameters' relationships of this analysis) was based on the VB programme, in order to investigate the feasibility of the options that were proposed in this study for flare gas utilisation (see Appendix G).

- Limits and considerations in the choice considered for the cost comparison

The following points describe some of the major simplifying limitations and assumptions involved in performing the cost estimation in this study:

- i. Plants' construction fees were excluded because of wide variability depending on the construction site.
- ii. Only the excess of gas is considered in the cost comparison.
- iii. The process flow diagrams were considered to be the same for areas where the excess of gas is flared or recovered.
- iv. Heat and mass balances were also excluded due to wide their variability depending on plant type.

8.3.1 Assumption

8.3.1.1 Scenario 1: Gas is Flared

Environmental performance: As previously stated, flared gas has several negative impacts on the environment. Thus the environmental performance of this option is considered to be zero (Shewchuk, 2002).

Assume flare gas flow rate is 25000 m³/day, (for scenario 2 also).

Note: Flare stack (see Chapter 2, Section 2.6) includes all the equipment for a gas flare system such as pipes, pumps, knockout drums, valves, controllers etc.

Total cost 1 = Stack fixed cost + Stack variable cost + Environmental cost (this is a percentage that a company will pay each time gas is flared, for example, for 1000 m³, the charge is £ 100).

Flare stack price = price of all the utilities such as pipe works, pumps and knock-out drums, etc. related to the flare system

Note that: Stack fixed cost = Stack price + Installation cost

Stack variable cost = Maintenance cost + Utility cost (energy required to run the stack)

8.3.1.2 Scenario 2: Gas is Recycled

Environmental performance: Since the excess of associated gas is not flared, this option is considered to have 100% environmental performance (Shewchuk, 2002).

Two options were examined for flare gas utilisation:

Option 1: Conversion to syngas (ceramic membrane tubular reactor)

Total cost 2 = Membrane tubes' fixed cost + Membrane tubes' variable cost - cash flow generated by 25000 m³/day (25000 m³ x gas price in market)

Note that: Membrane tubes' fixed cost = Membrane tubes' price + Installation cost

Membrane tubes' variable cost = Maintenance cost + Utility cost (Energy required to run the membrane tubes).

Option 2: Single-walled carbon nanotubes' production

Total cost 3 = Nanotubes' fixed cost + Nanotubes' variable cost — cash flow generated
by 25000 m³/day (25000 m³ x gas price on market)

Note that: Nanotubes' fixed cost = Nanotubes' price + Installation cost

Nanotubes' variable cost = Maintenance cost + Utility cost (Energy
required to run the nanotubes)

Objective: Total cost 3 or Total cost 2 < Total cost 1

The following assumptions were made in this analysis:

Carbon price- £0.22-0.25 per m³

Hydrogen price- £0.76-0.84 per m³

Syngas price- £0.036-0.045 per m³

Stack environmental costs include flaring fines and safety costs.

Auxiliary costs- 1.85x(Fixed Costs + Variable Costs)

Table 8.2 and Figure 8.6 summarise the analysis results. It can be seen that the costs for flare stack usage far exceed those for syngas and CNTs. Syngas costs also exceed that for CNTs. Considering the fact that syngas is only an intermediate product for GTL production, the associated costs in the long run will far outweigh those of CNTs which is a final product with many applications.

Over a 5 year period, as was considered in the analysis, the total costs for flare stack usage will amount to about £M17.071,000 while the costs for syngas and CNTs amount to about £M1.266,000 and £M1.074,000 respectively.

The costs for syngas and CNTs drop significantly after the first year due to the fact that associated costs no longer include fixed costs (mainly acquisition and installation costs)

after that time. This also is the case for flare stack costs but due to the resultant environmental costs (flaring fines etc), the costs of flare stack usage are fairly stable over the period considered.

<i>Year</i>	<i>Flare Stack Cost (£M/year)</i>	<i>Syngas Cost(£M/year)</i>	<i>CNT Cost (£M/year)</i>
1	3.516,800	0.877,500	0.850,600
2	3.001,300	0.085,500	0.056,500
3	3.405,900	0.103,600	0.056,500
4	3.405,900	0.098,500	0.059,400
5	3.741,500	0.101,300	0.052,000

Table 8.2: Economic analysis results

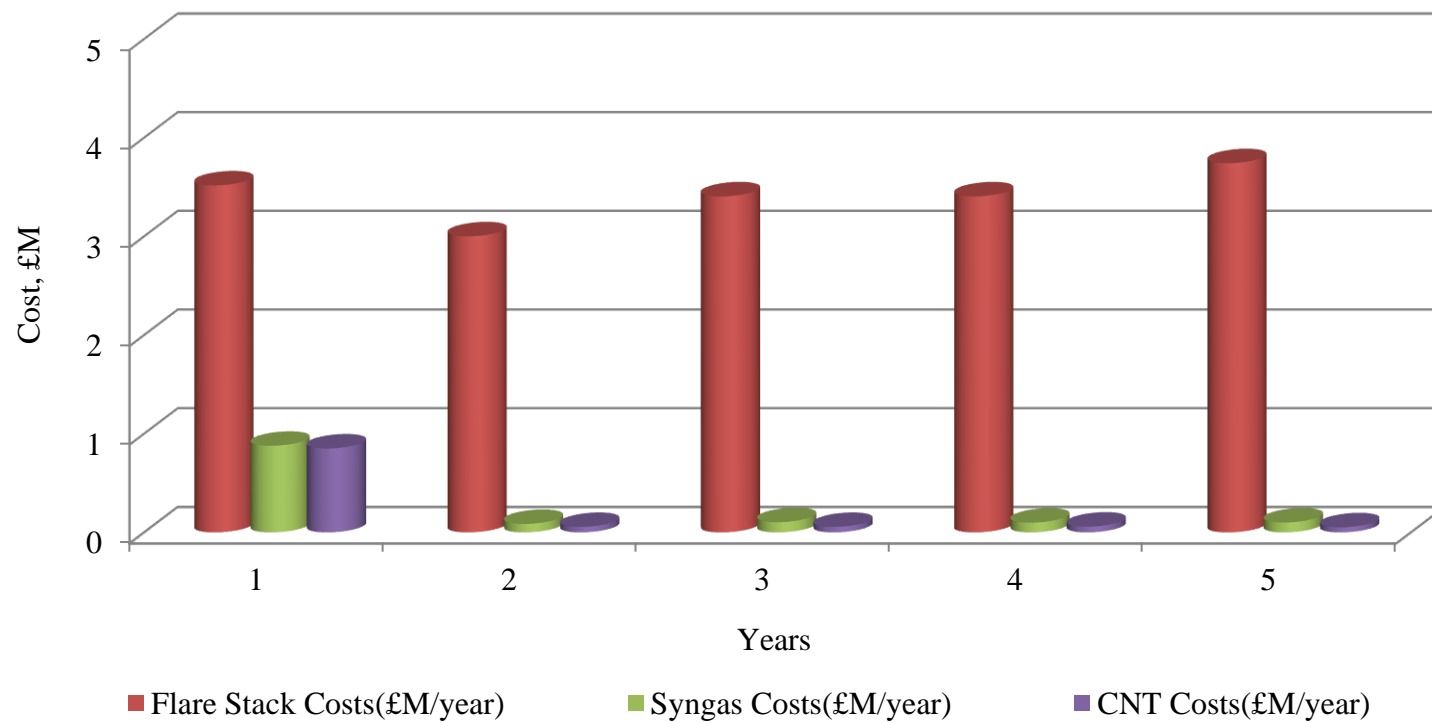


Figure 8.6: Typical cost analysis when comparing syngas and SWCNT generation with flare gas system

Chapter - 9

CHAPTER-9: CONCLUSIONS AND RECOMMENDATIONS

9.1 Conclusions

In this chapter the main conclusions obtained from this research study are presented. As mentioned previously, the aim of this investigation was to develop an alternative approach to continuous gas flaring in the oil and gas industry. Improving the disposal methods of waste gases in the oil and gas production activities has become one of the main environmental goals within these industries. Therefore, concerted efforts are needed to reduce gas flaring worldwide.

In this research, in order to study the benefits of gas flaring reduction, the first step was to give an overview on the base case of this research - “gas flaring reduction” - with focus (in addition to looking at gas flaring) on the concepts of ceramic membranes and sprays and atomisation techniques, as they were used in the two investigated options:

- The first option was a *theoretical investigation of synthesis gas production* through the partial oxidation of methane (flare gas) using ceramic perovskite membranes in a tubular reactor. After reviewing membranes background, one ceramic membrane material was selected, LSCF (6428), due to its high ionic and electronic properties in addition to its chemical and mechanical stabilities.
- It was found that this option is ideal for converting natural gas (flare gas) into synthesis gas ($\text{CO} + \text{H}_2$). This reduces capital and running costs, as

oxygen can be separated from the air stream with no need for an oxygen separation plant. The use of membrane technology to convert natural gas to useful liquids gives a gradual improvement in costs, in addition to environmental benefits. A membrane reactor for syngas production through the partial oxidation of natural gas is a feasible option at typical flare gas flow rates and is comparable in cost to steam reforming of natural gas.

- *Sprays and atomisation techniques* were experimentally employed as a *second* option, for the production of Single-Walled Carbon Nanotubes (SWCNT). This work was divided into two phases. In *Phase-I* a series of experiments were performed successfully with a designed atomiser device, to produce a fine aerosol with number mean diameters ($D_{n0.50}$) of less than or equal to 5 μm . The experimental work conducted (in *Phase I*) demonstrated that different factors can have an effect on the droplet diameter distribution, such as air flow rate, liquid pressure and flow rate, and downstream distance with respect to the measurement place.
- A study of fine spray behaviour from a certain type of atomiser device was conducted which was then employed in SWCNT generation (at the University of Oxford in *Phase II*) and the preliminary results of this *Phase's* experiments showed that it is possible to produce SWCNT by primarily utilising the designed "atomiser device".
- A Visual Basic economic comparison programme was created which enabled the design and development of technologies to curtail gas flaring.

The consideration of economic analysis demonstrated that SWCNT production cost was the lowest when compared with the other options.

9.2 Recommendations for Future Work

The following are recommendations for future research:

- An experimental study of the partial oxidation of natural gas is recommended as it will provide further insight knowledge and validation of the present results and a complete analysis of the produced gases would be a very effective parameter to acquire more knowledge of the processes occurring.
- Mathematical modelling of sprays and atomisation techniques in SWCNT generation will also provide further information on the fine aerosol structures.
- A mathematical model should be developed for a full scale ceramic membrane reactor for syngas production which incorporates appropriate flow patterns and non-isothermal conditions.
- Further study should be made to investigate the combination of sprays and atomisation techniques with membranes technology, which could improve the results using thin layer of same membrane material on supported substrate.

Appendices

APPENDICES

Appendix A: Tabulated Results of Chapter 4 and Chapter 7 (Section7.2) Analysis

Appendix B: Experimental Design and Experimental Results

Appendix C: Normalisation Table

Appendix D: Visual Basic Scripts

Appendix E: Visual Basic Programme Testing Results

Appendix F: User Guide for CCS System

Appendix G: Comparison and Economic Analysis Results

Appendix A: Tabulated Results of Chapter 4 and Chapter 7 (Section 7.2) Analysis

<i>Flare gas flow rate, m³/day</i>	<i>O₂ flow rate, m³/day</i>	<i>O₂ permeation, ml/(cm².min)</i>	<i>O₂ permeation, m³/(cm².day)</i>	<i>A_s, cm²</i>	<i>π</i>	<i>Tube diameter, d_o, cm</i>	<i>Tube length, L, cm</i>	<i>Number of tubes</i>
20000	10000	10	0.0144	694444	3.14	1.5	150	983
20000	10000	12	0.01728	578704	3.14	1.5	150	819
20000	10000	15	0.0216	462963	3.14	1.5	150	655
20000	10000	20	0.0288	347222	3.14	1.5	150	491

Table A.1: Effect of oxygen permeation on a number of tubes (Figure 4.2)

<i>Flare gas flow rate, m³/day</i>	<i>O₂ flow rate, m³/day</i>	<i>O₂ permeation, ml/(cm².min)</i>	<i>O₂ permeation, m³/(cm².day)</i>	<i>A_s, cm²</i>	<i>π</i>	<i>Tube diameter, d_o, cm</i>	<i>Tube length, L, cm</i>	<i>Tube L/d, cm</i>	<i>Number of tubes</i>
20000	10000	10	0.0144	694444	3.14	1.5	75	50	1966
20000	10000	10	0.0144	694444	3.14	1.5	130	87	1134
20000	10000	10	0.0144	694444	3.14	1.5	170	113	867
20000	10000	10	0.0144	694444	3.14	1.5	200	133	737

Table A.2: Effect of tube relative length on a number of tubes (Figure 4.3)

<i>Flare gas flow rate, m³/day</i>	<i>O₂ flow rate, m³/day</i>	<i>O₂ permeation, ml/(cm².min)</i>	<i>O₂ permeation, m³/(cm².day)</i>	<i>A_s, cm²</i>	<i>π</i>	<i>Tube d_o, cm</i>	<i>Tube length, L, cm</i>	<i>Number of tubes</i>
25000	12500	10	0.0144	868056	3.14	1.5	150	1229
20000	10000	10	0.0144	694444	3.14	1.5	150	983
15000	7500	10	0.0144	520833	3.14	1.5	150	737
8000	4000	10	0.0144	277778	3.14	1.5	150	393

Table A.3: Effect of oxygen flow rate on a number of tubes (Figure, 4.4)

<i>O₂ flow rate, m³/day</i>	<i>A_s, cm²</i>	<i>Outer tube diameter, d_o, cm</i>	<i>Inner tube diameter, d_i, cm</i>	<i>Tube length, L, cm</i>	<i>Number of tubes</i>	<i>LSCF tube thickness, b_m cm</i>	<i>LSCF powder volume, cc</i>	<i>Powder weight, gm</i>	<i>Powder price/tube, £</i>	<i>Tubes price 1000' £</i>
10000	694444	1.5	1.1	150	983	0.2	122.46	244.9	146.95	144.44
10000	694444	1.5	1.26	150	983	0.12	78.00	156.0	93.60	92.00
10000	694444	1.5	1.34	150	983	0.08	53.51	107.0	64.21	63.11
10000	694444	1.5	1.48	150	983	0.01	7.02	14.0	8.42	8.28
10000	694444	1.5	1.498	150	983	0.001	0.71	1.4	0.85	0.83

Table A4: Effect of tube thickness on the price of tubes (Figure, 4.5)

<i>Membrane thickness, b_m, cm</i>	<i>Operating temperature, T, K</i>	<i>O₂ partial pressure, P_{O_2s}, atm</i>	<i>O₂ partial pressure, P_{O_2t}, atm</i>	<i>$\ln(P_{O_2s}/P_{O_2t})$</i>	<i>O₂ permeation, ml/cm².min</i>
0.07	873	0.21	1.00E-03	5.347	0.116
0.07	973	0.21	1.00E-03	5.347	0.315
0.07	1023	0.21	1.00E-03	5.347	0.484
0.07	1073	0.21	1.00E-03	5.347	0.716
0.07	1123	0.21	1.00E-03	5.347	1.025
0.07	1173	0.21	1.00E-03	5.347	1.425
0.1	873	0.21	1.00E-03	5.347	0.081
0.1	973	0.21	1.00E-03	5.347	0.221
0.1	1023	0.21	1.00E-03	5.347	0.339
0.1	1073	0.21	1.00E-03	5.347	0.501
0.1	1123	0.21	1.00E-03	5.347	0.717
0.1	1173	0.21	1.00E-03	5.347	0.998
0.2	873	0.21	1.00E-03	5.347	0.041
0.2	973	0.21	1.00E-03	5.347	0.110
0.2	1023	0.21	1.00E-03	5.347	0.169
0.2	1073	0.21	1.00E-03	5.347	0.251
0.2	1123	0.21	1.00E-03	5.347	0.359
0.2	1173	0.21	1.00E-03	5.347	0.499

Table A5: Effect of tube thickness on the oxygen permeation flux at different temperatures (Figure, 7.1)

<i>Membrane thickness, b_m, cm</i>	<i>Gas constant, R, $J/(mol.K)$</i>	<i>Operating temperature, T, K</i>	<i>O₂ partial pressure, P_{O_2s}, atm</i>	<i>O₂ partial pressure, P_{O_2t}, atm</i>	<i>$\ln(P_{O_2s}/P_{O_2t})$</i>	<i>O₂ permeation, $ml/cm^2.min$</i>
0.2	8.314	973	0.21	1.00E-03	5.34711	0.110
0.15	8.314	973	0.21	1.00E-03	5.34711	0.147
0.1	8.314	973	0.21	1.00E-03	5.34711	0.221
0.075	8.314	973	0.21	1.00E-03	5.34711	0.294
0.2	8.314	1073	0.21	1.00E-03	5.34711	0.251
0.15	8.314	1073	0.21	1.00E-03	5.34711	0.334
0.1	8.314	1073	0.21	1.00E-03	5.34711	0.501
0.075	8.314	1073	0.21	1.00E-03	5.34711	0.668
0.2	8.314	1123	0.21	1.00E-03	5.34711	0.359
0.15	8.314	1123	0.21	1.00E-03	5.34711	0.478
0.1	8.314	1123	0.21	1.00E-03	5.34711	0.717
0.075	8.314	1123	0.21	1.00E-03	5.34711	0.956

Table A6: Variation of O₂ permeation for different membrane thicknesses and different temperatures (Figure, 7.2)

<i>Membrane thickness, b_m, cm</i>	<i>Gas constant, R, $j/(mol.K)$</i>	<i>Operating temperature, T, K</i>	<i>O₂ partial pressure, P_{O_2s}, atm</i>	<i>O₂ partial pressure, P_{O_2t}, atm</i>	<i>$\ln(P_{O_2s}/P_{O_2t})$</i>	<i>O₂ permeation, $ml/cm^2.min$</i>
0.2	8.314	973	0.21	1.00E-01	0.742	0.015
0.2	8.314	973	0.21	6.00E-02	1.253	0.026
0.2	8.314	973	0.21	2.00E-02	2.351	0.049
0.2	8.314	973	0.21	5.00E-03	3.738	0.077
0.2	8.314	1023	0.21	1.00E-01	0.742	0.024
0.2	8.314	1023	0.21	6.00E-02	1.253	0.040
0.2	8.314	1023	0.21	2.00E-02	2.351	0.075
0.2	8.314	1023	0.21	5.00E-03	3.738	0.118
0.2	8.314	1073	0.21	1.00E-01	0.742	0.035
0.2	8.314	1073	0.21	6.00E-02	1.253	0.059
0.2	8.314	1073	0.21	2.00E-02	2.351	0.110
0.2	8.314	1073	0.21	5.00E-03	3.738	0.175
0.2	8.314	1123	0.21	1.00E-01	0.742	0.050
0.2	8.314	1123	0.21	6.00E-02	1.253	0.084
0.2	8.314	1123	0.21	2.00E-02	2.351	0.158
0.2	8.314	1123	0.21	5.00E-03	3.738	0.251

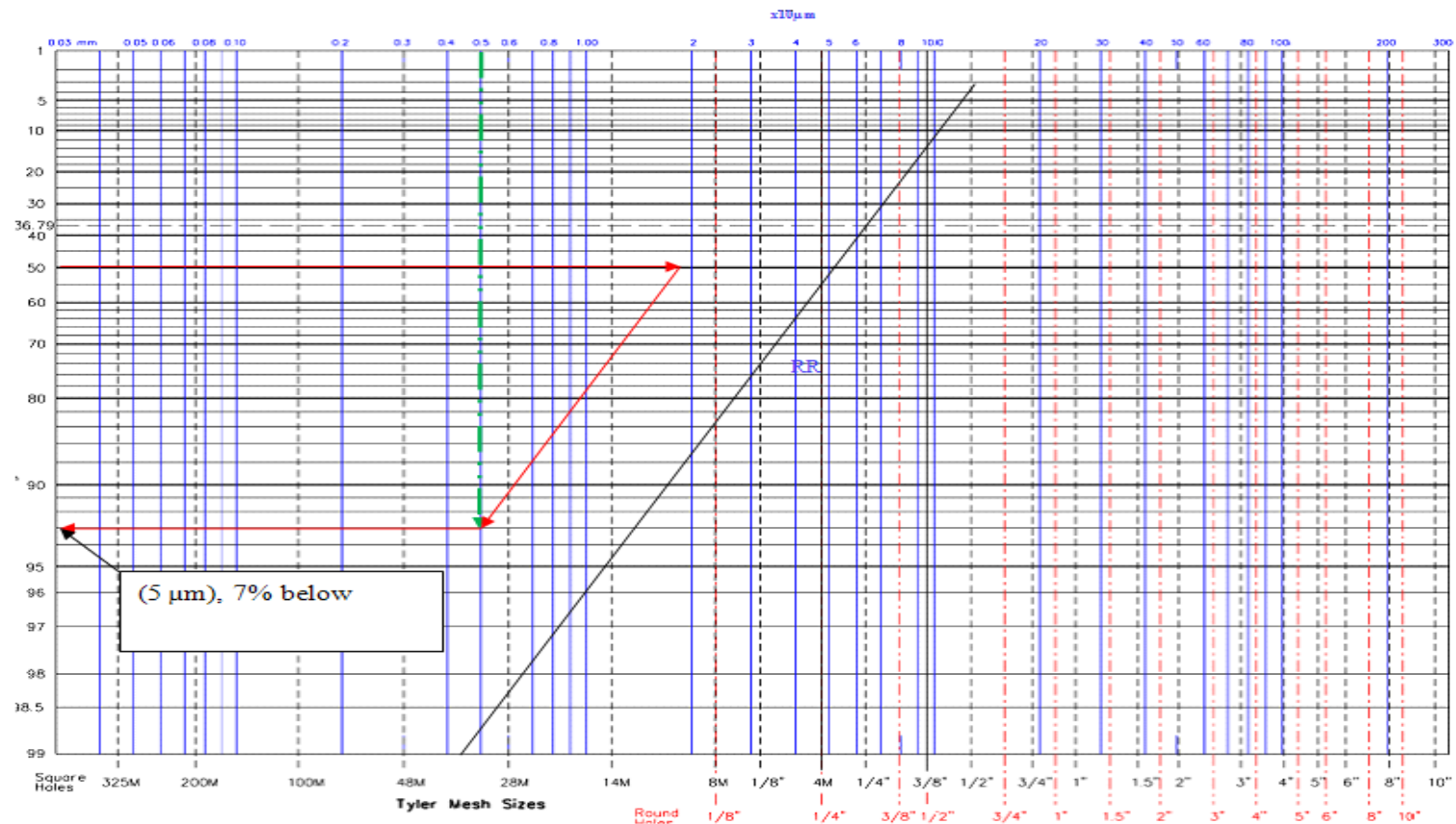
Table A7: O₂ permeation flux at various permeate side partial pressures and at different temperatures (Figure, 7.3)

<i>Membrane thickness, b_m, cm</i>	<i>Gas constant, R, $J/(mol.K)$</i>	<i>Operating temperature, T, K</i>	<i>O₂ partial pressure, P_{O_2s}, atm</i>	<i>O₂ partial pressure, P_{O_2t}, atm</i>	<i>$\ln(P_{O_2s}/P_{O_2t})$</i>	<i>O₂ permeation, $ml/cm^2 \cdot min$</i>
0.2	8.314	973	0.11	5.00E-03	3.091	0.064
0.2	8.314	973	0.21	5.00E-03	3.738	0.077
0.2	8.314	973	0.3	5.00E-03	4.094	0.084
0.2	8.314	973	0.4	5.00E-03	4.382	0.090
0.2	8.314	1023	0.11	5.00E-03	3.091	0.098
0.2	8.314	1023	0.21	5.00E-03	3.738	0.118
0.2	8.314	1023	0.3	5.00E-03	4.094	0.130
0.2	8.314	1023	0.4	5.00E-03	4.382	0.139
0.2	8.314	1073	0.11	5.00E-03	3.091	0.145
0.2	8.314	1073	0.21	5.00E-03	3.738	0.175
0.2	8.314	1073	0.3	5.00E-03	4.094	0.192
0.2	8.314	1073	0.4	5.00E-03	4.382	0.205
0.2	8.314	1123	0.11	5.00E-03	3.091	0.207
0.2	8.314	1123	0.21	5.00E-03	3.738	0.251
0.2	8.314	1123	0.3	5.00E-03	4.094	0.275
0.2	8.314	1123	0.4	5.00E-03	4.382	0.294

Table A8: O₂ permeation flux at various permeate side partial pressures and at different temperatures (Figure, 7.4)

Appendix B: Experimental Design and Experimental Results

B1: Rosin and Rammler Graph



B2: Estimation of Aerosol Flow Rate during the Experiments

The collected aerosol was estimated theoretically as following, using Excel spreadsheet:

$$A_{fr} = (\text{Concentration } \%) * Q_a (\text{l/min}) * 1000 (\text{ml/l}) \quad (\text{B2-7.1})$$

Where:

- i. A_{fr} : Aerosol flow rate (*ml/min*);
- ii. Conc. % : Concentration % by Volume taken from the analysis table for every test;
- iii. Q_a : Air flow rate during the experiment, *l/min*.

B3: Results Data Sheet



University of Salford
A Greater Manchester University



Malvern Mastersizer-X results data sheet

Date: May -June/2008,

Atomiser device position: *Vertical*

Temperature: 21-25 °C

<i>Test No.</i>	<i>Baffle position from base cover, mm</i>	<i>Air flow rate, Q_w, l/m</i>	<i>Air pressure, P_w, MPa</i>	<i>Liquid flow rate, Q_l, l/m</i>	<i>Liquid pressure, P_l, MPa</i>	<i>Aerosol collected, ml/min</i>	<i>D_{32}, μm</i>	<i>$D_{n0.5}$, μm</i>	<i>Comments</i>
AS-9	150	0.4	0.1	0.001	10	0	See comments		<i>Note:</i> <i>(i)The obscuration and volume concentration are zero with no aerosol.</i> <i>(ii)As a number of above, no aerosol</i>
AS-10	150	0.4	0.1	0.003	10	0			
AS-11	150	0.4	0.1	0.005	10	0			
AS-12	110	0.3	0.1	0.003	8	0.0207	5.08	3.60	
AS-13	110	0.3	0.1	0.003	8	0.0225	5.03	3.79	
AS-14	110	0.3	0.1	0.003	8	0.0219	5.21	3.63	
AS-15	80	0.3	0.1	0.003	8	0.0180	4.35	3.29	



Malvern Mastersizer-X results data sheet

Date: May-June /2008,

Atomiser device position: *Vertical*

Temperature: 21-25 °C

<i>Test No.</i>	<i>Baffle position from base cover, mm</i>	<i>Air flow rate, Q_w, l/m</i>	<i>Air pressure, P_w, MPa</i>	<i>Liquid flow rate, Q_l, l/m</i>	<i>Liquid pressure, P_l, MPa</i>	<i>Aerosol collected, ml/min</i>	<i>D_{32}, μm</i>	<i>$D_{n0.5}$, μm</i>	<i>Comments</i>
AS-16	80	0.3	0.1	0.003	8	0.0198	4.31	3.23	
AS-17	80	0.3	0.1	0.003	8	0.0204	4.32	3.22	
AS-18	80	0.3	0.1	0.001	6	0.0036	6.83	2.86	
AS-19	80	0.3	0.1	0.003	6	0.0021	6.13	3.06	
AS-20	80	0.3	0.1	0.005	6	0.0036	6.70	3.17	
AS-21	80	0.3	0.1	0.001	8	0.0156	5.21	2.66	
AS-22	80	0.3	0.1	0.003	8	0.0024	6.77	2.76	



Malvern Mastersizer-X results data sheet

Date: May-June /2008,

Atomiser device position: *Vertical*

Temperature: 21-25 °C

<i>Test No.</i>	<i>Baffle position from base cover, mm</i>	<i>Air flow rate, Q_a, l/m</i>	<i>Air pressure, P_a, MPa</i>	<i>Water flow rate, Q_w, l/m</i>	<i>Water pressure, P_w, MPa</i>	<i>Aerosol collected, ml/min</i>	<i>D_{32}, μm</i>	<i>$D_{n0.5}$, μm</i>	<i>Comments</i>
AS-23	80	0.30	0.10	0.005	8	0.069	6.20	2.99	
AS-24	80	0.30	0.10	0.001	10	0.0141	4.18	2.38	
AS-25	80	0.30	0.10	0.003	10	0.0387	5.39	2.45	
AS-26	80	0.30	0.10	0.005	10	0.0102	5.54	2.84	
AS-27	80	0.30	0.10	0.001	11	0.0036	4.94	2.19	
AS-28	80	0.30	0.10	0.003	11	0.0042	4.94	2.56	
AS-29	80	0.30	0.10	0.005	11	0.0072	4.98	2.75	
AS-30	80	0.30	0.10	0.001	6	0.0144	5.79	2.80	
AS-31	80	0.35	0.10	0.001	6	0.0249	5.76	2.50	
AS-32	80	0.40	0.10	0.001	6	0.0204	5.56	2.39	



Malvern Mastersizer-X results data sheet

Date: May –June /2008,

Atomiser device position: *Vertical*

Temperature: 21-25 °C

<i>Test No.</i>	<i>Baffle position from base cover, mm</i>	<i>Air flow rate, Q_a, l/m</i>	<i>Air pressure, P_a, MPa</i>	<i>Waterflow rate, Q_w, l/m</i>	<i>Water pressure, P_w, MPa</i>	<i>Aerosol collected, ml/min</i>	<i>D_{32}, μm</i>	<i>$D_{n0.5}$, μm</i>	<i>Comments</i>
AS-33	80	0.30	0.10	0.001	8	0.0084	5.55	2.64	
AS-34	80	0.35	0.10	0.001	8	0.0165	5.13	2.22	
AS-35	80	0.40	0.10	0.001	8	0.0252	4.73	1.91	
AS-36	80	0.30	0.10	0.001	10	0.0114	5.98	2.17	
AS-37	80	0.35	0.10	0.001	10	0.0081	4.97	1.83	
AS-38	80	0.40	0.10	0.001	10	0.0168	5.72	1.58	
AS-39	80	0.30	0.10	0.001	11	0.0168	5.81	2.10	
AS-40	80	0.35	0.10	0.001	11	0.0200	5.53	1.66	
AS-41	80	0.40	0.10	0.001	11	0.0180	5.33	1.32	
AS-42	80	0.30	0.10	0.001	10	0.0138	6.41	3.27	



Malvern Mastersizer-X results data sheet

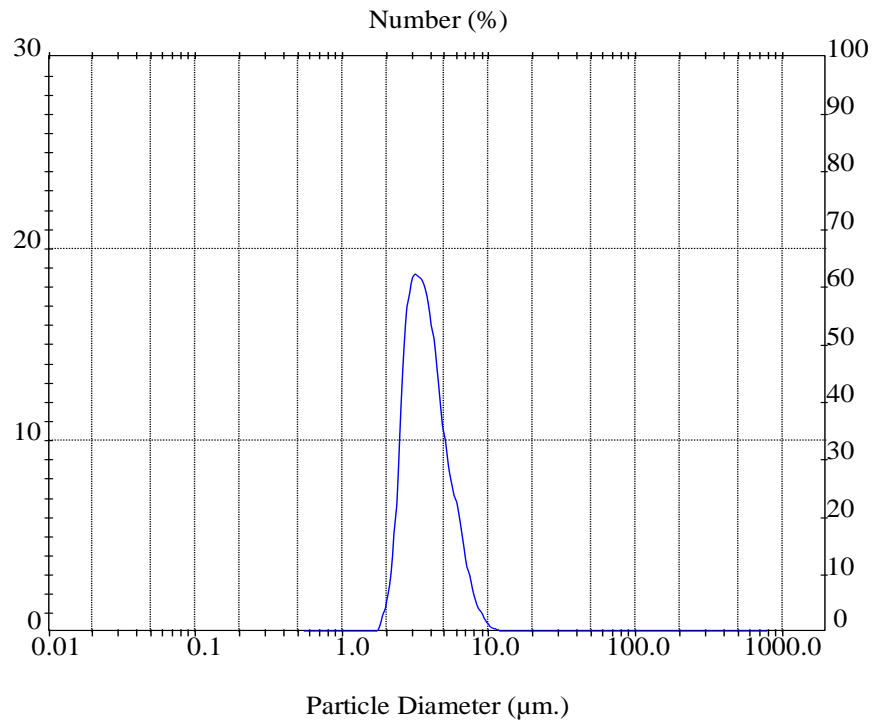
Date: May - June/2008,

Atomiser device position: *Vertical*

Temperature: 21-25 °C

<i>Test No.</i>	<i>Baffle position from base cover, mm</i>	<i>Air flow rate, Q_a, l/m</i>	<i>Air pressure, P_a, MPa</i>	<i>Water flow rate, Q_w, l/m</i>	<i>Water pressure, P_w, MPa</i>	<i>Aerosol collected, ml/min</i>	<i>D_{32}, μm</i>	<i>$D_{n0.5}$, μm</i>	<i>Comments</i>
AS-43	80	0.30	0.1	0.001	10	0.0165	5.19	2.42	
AS-44	80	0.30	0.1	0.001	10	0.0066	5.15	1.72	
AS-45	80	0.30	0.1	0.001	10	0.0153	5.56	2.39	
AS-46	80	0.4	0.1	0.001	10	0.0128	5.89	3.07	
AS-47	80	0.4	0.1	0.001	10	0.0276	4.90	1.58	
AS-48	80	0.4	0.1	0.001	10	0.0220	4.96	1.39	
AS-49	80	0.4	0.1	0.001	10	0.0268	5.97	1.70	

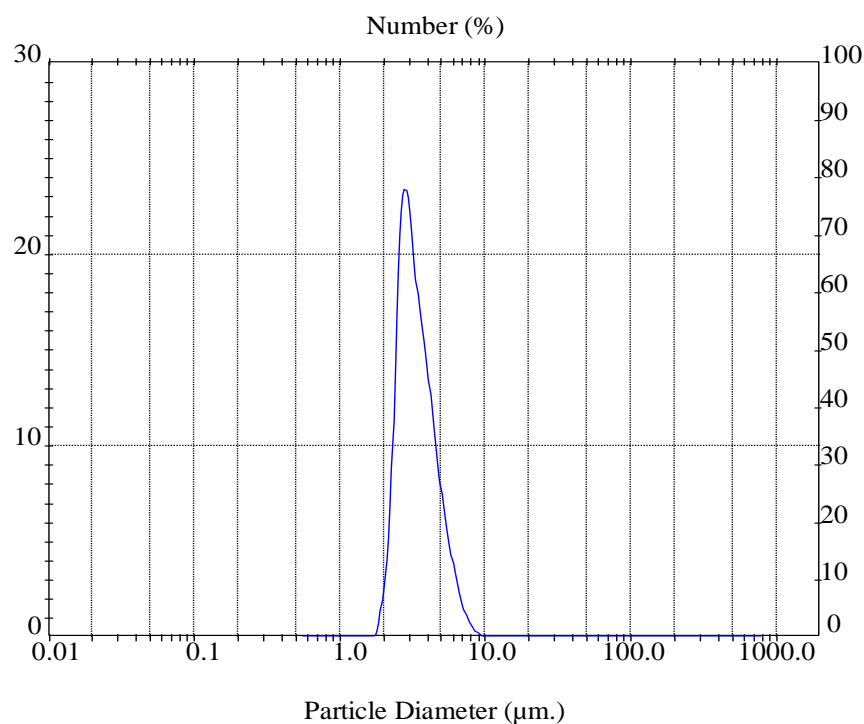
B4: Malvern Mastersizer-X Results



Result: Analysis Table

ID: mizda1		Run No: 8		Measured: 8/5/2008 18:01PM			
File: MUSA		Rec. No: 142		Analysed: 8/5/2008 18:01PM			
Path: C:\SIZERS\DATA\		Source: Analysed					
Range: 300 mm		Beam: 2.40 mm		Sampler: None			
Presentation: 3OHD		Analysis: Polydisperse		Obs': 10.4 %			
Modifications: -				Residual: 1.060 %			
Conc. = 0.0073 %Vol		Density = 1.000 g/cm ³		S.S.A. = 1.1523 m ² /g			
Distribution: Number		D[4,3] = 8.97 µm		D[3,2] = 5.21 µm			
D(n,0.1) = 2.57 µm		D(n,0.5) = 3.63 µm		D(n,0.9) = 5.94 µm			
Span = 9.283E-01		Uniformity = 2.910E-01					
Size (µm)	Number In %	Size (µm)	Number In %	Size (µm)	Number In %	Size (µm)	Number In %
0.49	0.00	3.60	17.10	26.20	0.00	190.80	0.00
0.58	0.00	4.19	13.06	30.53	0.00	222.28	0.00
0.67	0.00	4.88	8.78	35.56	0.00	258.95	0.00
0.78	0.00	5.69	6.36	41.43	0.00	301.68	0.00
0.91	0.00	6.63	3.42	48.27	0.00	351.46	0.00
1.06	0.00	7.72	1.48	56.23	0.00	409.45	0.00
1.24	0.00	9.00	0.55	65.51	0.00	477.01	0.00
1.44	0.03	10.48	0.16	76.32	0.00	555.71	0.00
1.68	0.31	12.21	0.03	88.91	0.00	647.41	0.00
1.95	2.48	14.22	0.00	103.58	0.00	754.23	0.00
2.28	10.11	16.57	0.00	120.67	0.00	878.67	0.00
2.65	17.64	19.31	0.00	140.58	0.00		
3.09	18.50	22.49	0.00	163.77	0.00		
3.60		26.20	0.00	190.80	0.00		

Figure B4-1: Typical spray characteristics; Number (%), particle diameter (µm) and analysis table for test SA -14



Result: Analysis Table

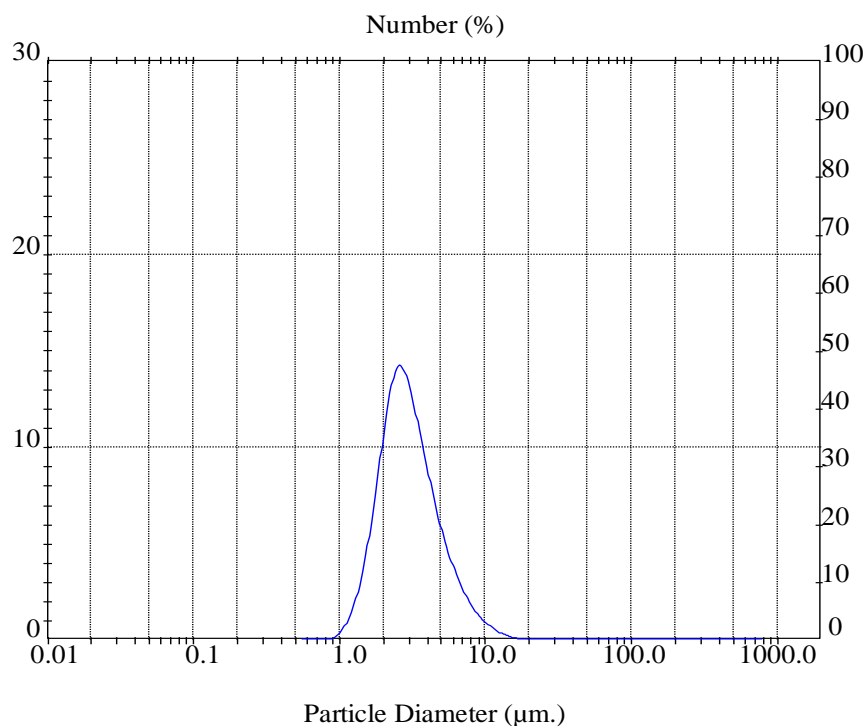
ID:	Run No: 8	Measured: 7/5/2008 19:10PM
File: MUSA	Rec.No: 131	Analysed: 7/5/2008 19:10PM
Path: C:\SIZERS\DATA\		Source: Analysed

Range: 300 mm	Beam: 2.40 mm	Sampler: None	Obs': 11.8 %
Presentation: 3OHD		Analysis: Polydisperse	Residual: 0.948 %
Modifications: -			

Conc. = 0.0068 %Vol	Density = 1.000 g/cm ³	S.S.A.= 1.3876 m ² /g
Distribution: Number	D[4,3] = 4.83 µm	D[3,2] = 4.32 µm
D(n,0.1) = 2.44 µm	D(n,0.5) = 3.22 µm	D(n,0.9) = 5.05 µm
Span = 8.133E-01	Uniformity = 2.583E-01	

Size (µm)	Number In %						
0.49	0.00	3.60	14.85	26.20	0.00	190.80	0.00
0.58	0.00	4.19	10.28	30.53	0.00	222.28	0.00
0.67	0.00	4.88	6.28	35.56	0.00	258.95	0.00
0.78	0.00	5.69	3.45	41.43	0.00	301.68	0.00
0.91	0.00	6.63	1.43	48.27	0.00	351.46	0.00
1.06	0.00	7.72	0.47	56.23	0.00	409.45	0.00
1.24	0.00	9.00	0.06	65.51	0.00	477.01	0.00
1.44	0.03	10.48	0.00	76.32	0.00	555.71	0.00
1.68	0.40	12.21	0.00	88.91	0.00	647.41	0.00
1.95	4.05	14.22	0.00	103.58	0.00	754.23	0.00
2.28	16.77	16.57	0.00	120.67	0.00	878.67	0.00
2.65	23.29	19.31	0.00	140.58	0.00		
3.09	18.64	22.49	0.00	163.77	0.00		
3.60		26.20	0.00	190.80	0.00		

Figure B4-2: Typical spray characteristics; Number (%), particle diameter (µm) and analysis table for test SA -17



Result: Analysis Table

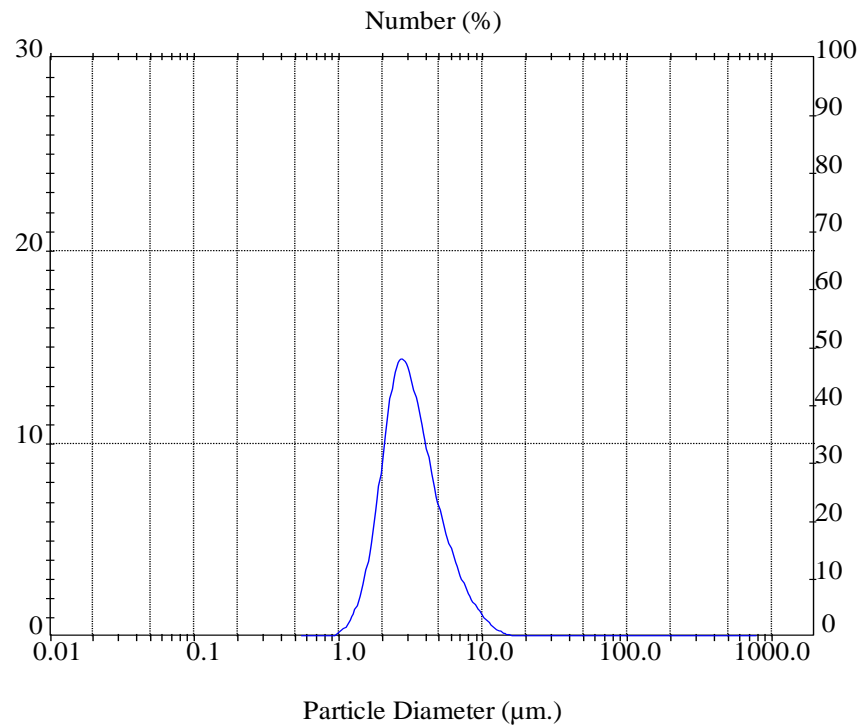
ID:	Run No: 16	Measured: 14/5/2008 13:11PM
File: MUSA	Rec.No: 220	Analysed: 14/5/2008 13:11PM
Path: C:\SIZERS\DATA\		Source: Analysed

Range: 300 mm	Beam: 2.40 mm	Sampler: None	Obs': 1.4 %
Presentation: 3OHD	Analysis: Polydisperse		Residual: 1.576 %
Modifications: -			

Conc. = 0.0012 %Vol	Density = 1.000 g/cm ³	S.S.A.= 0.8782 m ² /g
Distribution: Number	D[4,3] = 21.73 µm	D[3,2] = 6.83 µm
D(n,0.1) = 1.72 µm	D(n,0.5) = 2.86 µm	D(n,0.9) = 5.71 µm
Span = 1.395E+00	Uniformity = 4.459E-01	

Size (µm)	Number In %						
0.49	0.00	3.60	9.38	26.20	0.01	190.80	0.00
0.58	0.00	4.19	7.06	30.53	0.00	222.28	0.00
0.67	0.00	4.88	5.10	35.56	0.00	258.95	0.00
0.78	0.06	5.69	3.66	41.43	0.00	301.68	0.00
0.91	0.34	6.63	2.50	48.27	0.00	351.46	0.00
1.06	1.06	7.72	1.62	56.23	0.00	409.45	0.00
1.24	2.51	9.00	1.02	65.51	0.00	477.01	0.00
1.44	4.89	10.48	0.63	76.32	0.00	555.71	0.00
1.68	8.20	12.21	0.35	88.91	0.00	647.41	0.00
1.95	11.81	14.22	0.18	103.58	0.00	754.23	0.00
2.28	14.07	16.57	0.09	120.67	0.00	878.67	0.00
2.65	13.72	19.31	0.04	140.58	0.00		
3.09	11.70	22.49	0.02	163.77	0.00		
3.60		26.20		190.80			

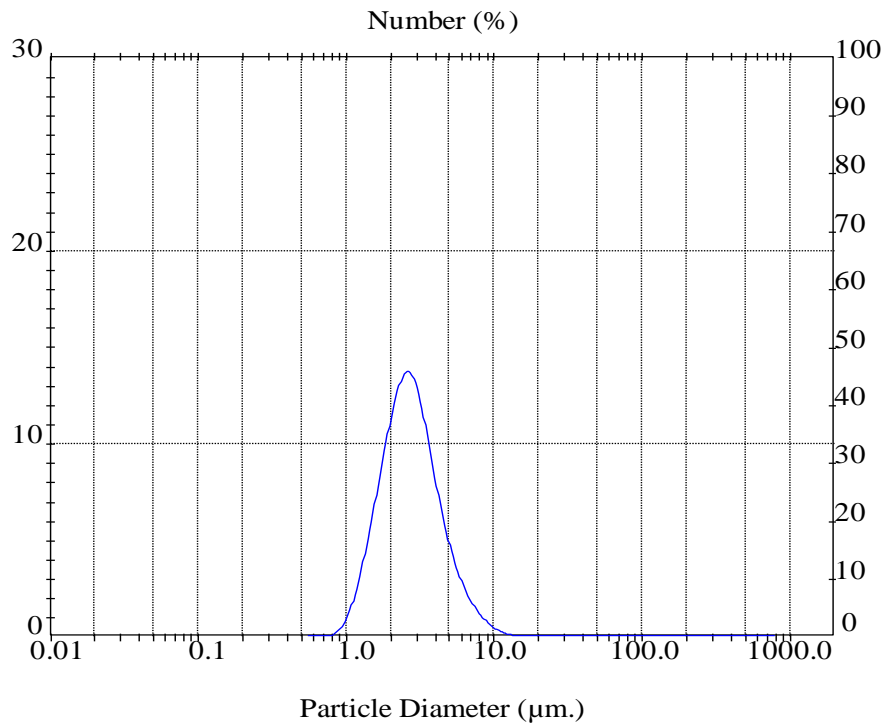
Figure B4-3: Typical spray characteristics; Number (%), particle diameter (µm) and analysis table for test SA -18



Result: Analysis Table

ID: MUSA		Run No: 13		Measured: 13/5/2008 15:51PM			
Path: C:\SIZERS\DATA\		Rec. No: 210		Analysed: 13/5/2008 15:51PM			
Source: Analysed							
Range: 300 nm		Beam: 2.40 mm		Sampler: None			
Presentation: 3OHD		Analysis: Polydisperse		Obs': 0.9 %			
Modifications: -				Residual: 2.949 %			
Conc. = 0.0007 %Vol		Density = 1.000 g/cm³		S.S.A.= 0.9788 m²/g			
Distribution: Number		D[4,3] = 7.94 µm		D[3,2] = 6.13 µm			
D(n,0.1) = 1.86 µm		D(n,0.5) = 3.06 µm		D(n,0.9) = 6.01 µm			
Span = 1.359E+00		Uniformity = 4.305E-01					
Size (µm)	Number In %	Size (µm)	Number In %	Size (µm)	Number In %	Size (µm)	Number In %
0.49	0.00	3.60	10.55	26.20	0.00	190.80	0.00
0.58	0.00	4.19	8.06	30.53	0.00	222.28	0.00
0.67	0.00	4.88	5.94	35.56	0.00	258.95	0.00
0.78	0.04	5.69	4.37	41.43	0.00	301.68	0.00
0.91	0.20	6.63	1.96	48.27	0.00	351.46	0.00
1.06	0.65	7.72	1.26	56.23	0.00	409.45	0.00
1.24	1.64	9.00	0.67	65.51	0.00	477.01	0.00
1.44	3.50	10.48	0.31	76.32	0.00	555.71	0.00
1.68	6.52	12.21	0.13	88.91	0.00	647.41	0.00
1.95	10.46	14.22	0.04	103.58	0.00	754.23	0.00
2.28	13.67	16.57	0.01	120.67	0.00	878.67	0.00
2.65	14.26	19.31	0.00	140.58	0.00		
3.09	12.76	22.49		163.77	0.00		
3.60		26.20		190.80	0.00		

Figure B4-4: Typical spray characteristics; Number (%), particle diameter (µm) and analysis table for test SA -19



Result: Analysis Table

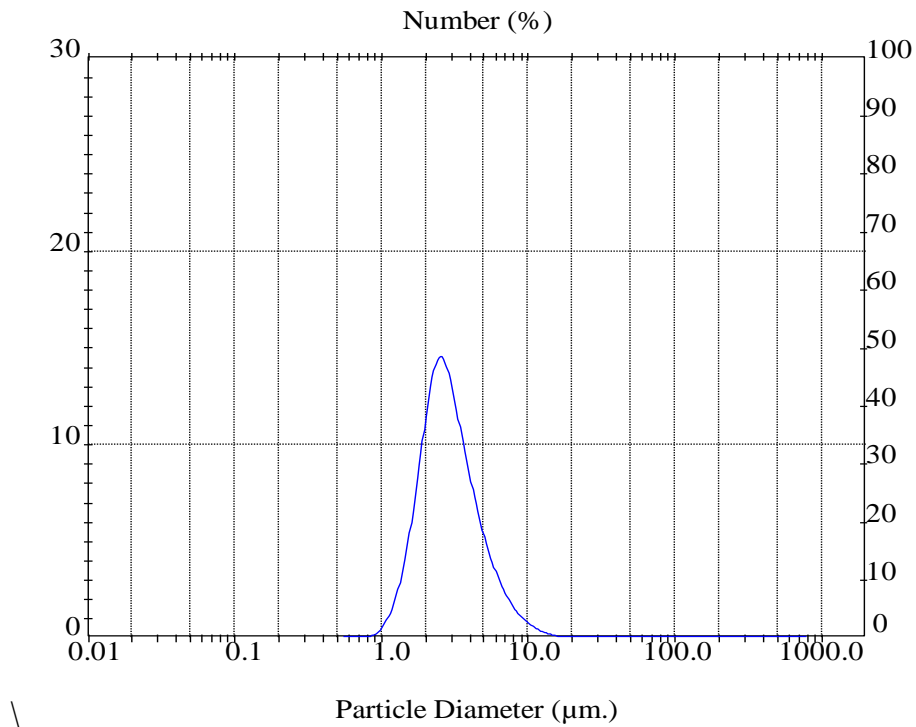
ID:	Run No: 2	Measured: 21/5/2008 10:38PM
File: MUSA	Rec.No: 247	Analysed: 21/5/2008 10:38PM
Path: C:\SIZERS\DATA\		Source: Analysed

Range: 300 mm	Beam: 2.40 mm	Sampler: None	Obs': 7.6 %
Presentation: 3OHD	Analysis: Polydisperse		Residual: 2.067 %
Modifications: -			

Conc. = 0.0052 %Vol	Density = 1.000 g/cm ³	S.S.A.= 1.1513 m ² /g
Distribution: Number	D[4,3] = 6.94 µm	D[3,2] = 5.21 µm
D(n,0.1) = 1.53 µm	D(n,0.5) = 2.66 µm	D(n,0.9) = 4.99 µm
Span = 1.301E+00	Uniformity = 4.184E-01	

Size (µm)	Number In %						
0.49	0.00	3.60	8.68	26.20	0.00	190.80	0.00
0.58	0.00	4.19	6.14	30.53	0.00	222.28	0.00
0.67	0.00	4.88	4.15	35.56	0.00	258.95	0.00
0.78	0.22	5.69	2.73	41.43	0.00	301.68	0.00
0.91	0.85	6.63	1.72	48.27	0.00	351.46	0.00
1.06	2.19	7.72	1.04	56.23	0.00	409.45	0.00
1.24	4.28	9.00	0.56	65.51	0.00	477.01	0.00
1.44	6.90	10.48	0.28	76.32	0.00	555.71	0.00
1.68	9.64	12.21	0.13	88.91	0.00	647.41	0.00
1.95	12.08	14.22	0.05	103.58	0.00	754.23	0.00
2.28	13.58	16.57	0.02	120.67	0.00	878.67	0.00
2.65	13.37	19.31	0.00	140.58	0.00		
3.09	11.39	22.49	0.00	163.77	0.00		
3.60		26.20	0.00	190.80	0.00		

Figure B4-5: Typical spray characteristics; Number (%), particle diameter (µm) and analysis table for test SA -21



Result: Analysis Table

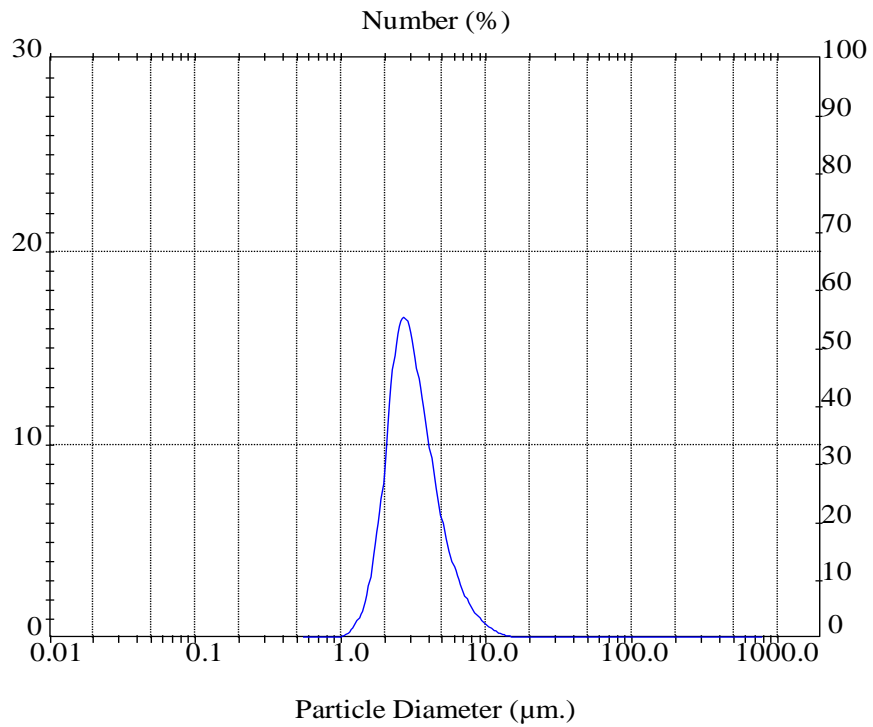
ID:	Run No: 3	Measured: 14/5/2008 10:56PM
File: MUSA	Rec. No: 212	Analysed: 14/5/2008 10:56PM
Path: C:\SIZERS\DATA\		Source: Analysed

Range: 300 mm	Beam: 2.40 mm	Sampler: None	Obs': 1.0 %
Presentation: 3OHD	Analysis: Polydisperse		Residual: 1.927 %
Modifications: -			

Conc. = 0.0008 %Vol	Density = 1.000 g/cm ³	S.S.A.= 0.8858 m ² /g
Distribution: Number	D[4, 3] = 26.72 µm	D[3, 2] = 6.77 µm
D(n, 0.1) = 1.67 µm	D(n, 0.5) = 2.76 µm	D(n, 0.9) = 5.43 µm
Span = 1.362E+00	Uniformity = 4.390E-01	

Size (µm)	Number In %						
0.49	0.00	3.60	8.88	26.20	0.00	190.80	0.00
0.58	0.00	4.19	6.57	30.53	0.00	222.28	0.00
0.67	0.00	4.88	4.66	35.56	0.00	258.95	0.00
0.78	0.11	5.69	3.27	41.43	0.00	301.68	0.00
0.91	0.46	6.63	2.18	48.27	0.00	351.46	0.00
1.06	1.30	7.72	1.39	56.23	0.00	409.45	0.00
1.24	2.90	9.00	0.86	65.51	0.00	477.01	0.00
1.44	5.45	10.48	0.52	76.32	0.00	555.71	0.00
1.68	8.91	12.21	0.28	88.91	0.00	647.41	0.00
1.95	12.52	14.22	0.14	103.58	0.00	754.23	0.00
2.28	14.50	16.57	0.06	120.67	0.00	878.67	0.00
2.65	13.69	19.31	0.03	140.58	0.00		
3.09	11.33	22.49	0.01	163.77	0.00		
3.60		26.20		190.80			

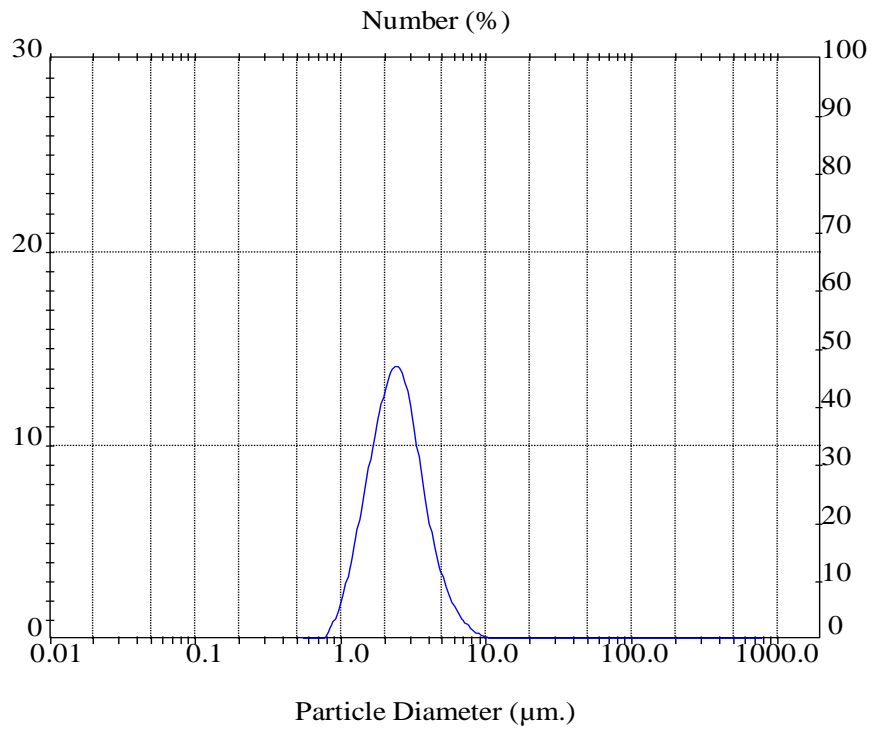
Figure B4-6: Typical spray characteristics; Number (%), particle diameter (µm) and analysis table for test SA -22



Result: Analysis Table

ID: MUSA		Run No: 4		Measured: 16/5/2008 11:51PM			
File: MUSA		Rec.No: 234		Analysed: 16/5/2008 11:51PM			
Path: C:\SIZERS\DATA\		Source: Analysed					
Range: 300 mm		Beam: 2.40 mm		Sampler: None			
Presentation: 3OHD		Analysis: Polydisperse		Obs': 2.8 %			
Modifications: -				Residual: 1.179 %			
Conc. = 0.0023 %Vol		Density = 1.000 g/cm ³		S.S.A.= 0.9684 m ² /g			
Distribution: Number		D[4, 3] = 18.65 µm		D[3, 2] = 6.20 µm			
D(n,0.1) = 1.94 µm		D(n,0.5) = 2.99 µm		D(n,0.9) = 5.46 µm			
Span = 1.176E+00		Uniformity = 3.814E-01					
Size (µm)	Number In %	Size (µm)	Number In %	Size (µm)	Number In %	Size (µm)	Number In %
0.49	0.00	3.60	10.91	26.20	0.00	190.80	0.00
0.58	0.00	4.19	7.76	30.53	0.00	222.28	0.00
0.67	0.00	4.88	5.19	35.56	0.00	258.95	0.00
0.78	0.02	5.69	3.49	41.43	0.00	301.68	0.00
0.91	0.10	6.63	2.24	48.27	0.00	351.46	0.00
1.06	0.38	7.72	1.36	56.23	0.00	409.45	0.00
1.24	1.09	9.00	0.82	65.51	0.00	477.01	0.00
1.44	2.72	10.48	0.44	76.32	0.00	555.71	0.00
1.68	5.98	12.21	0.22	88.91	0.00	647.41	0.00
1.95	11.07	14.22	0.11	103.58	0.00	754.23	0.00
2.28	15.71	16.57	0.05	120.67	0.00	878.67	0.00
2.65	16.37	19.31	0.02	140.58	0.00		
3.09	13.94	22.49	0.01	163.77	0.00		
3.60		26.20		190.80			

Figure B4-7: Typical spray characteristics; Number (%), particle diameter (µm) and analysis table for test SA -23



Result: Analysis Table

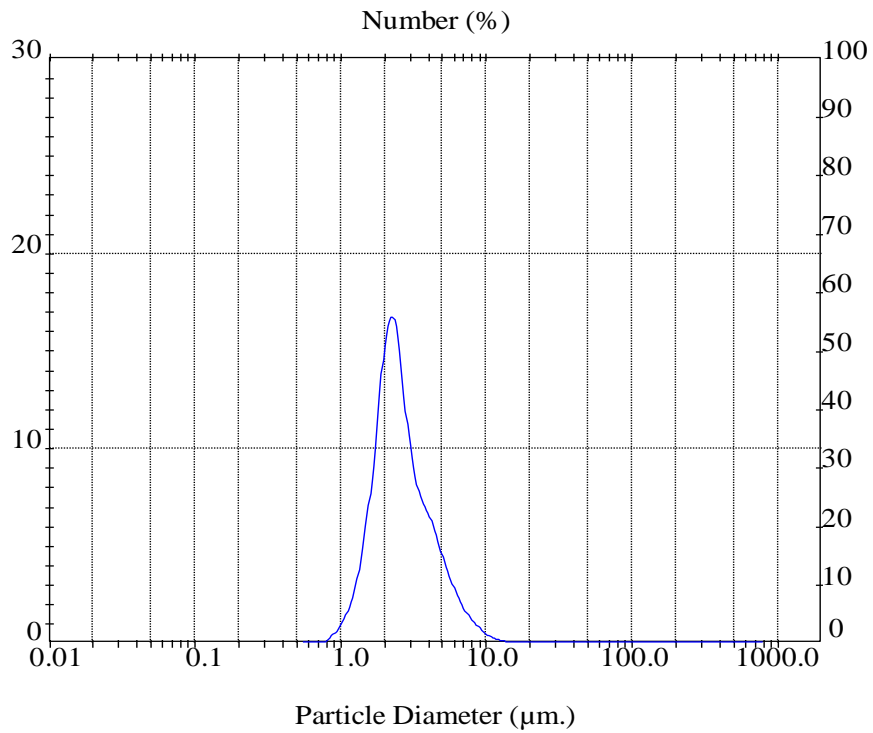
ID:	Run No: 3	Measured: 21/5/2008 10:44PM
File: MUSA	Rec. No: 248	Analysed: 21/5/2008 10:44PM
Path: C:\SIZERS\DATA\		Source: Analysed

Range: 300 nm	Beam: 2.40 nm	Sampler: None	Obs': 8.6 %
Presentation: 3OHD		Analysis: Polydisperse	Residual: 2.256 %
Modifications: -			

Conc. = 0.0047 %Vol	Density = 1.000 g/cm ³	S.S.A = 1.4343 m ² /g
Distribution: Number	D[4,3] = 5.32 µm	D[3,2] = 4.18 µm
D(n,0.1) = 1.38 µm	D(n,0.5) = 2.38 µm	D(n,0.9) = 4.25 µm
Span = 1.205E+00	Uniformity = 3.854E-01	

Size (µm)	Number In %						
0.49	0.00	3.60	6.89	26.20	0.00	190.80	0.00
0.58	0.00	4.19	4.44	30.53	0.00	222.28	0.00
0.67	0.00	4.88	2.74	35.56	0.00	258.95	0.00
0.78	0.60	5.69	1.62	41.43	0.00	301.68	0.00
0.91	1.73	6.63	0.91	48.27	0.00	351.46	0.00
1.06	3.62	7.72	0.44	56.23	0.00	409.45	0.00
1.24	6.13	9.00	0.20	65.51	0.00	477.01	0.00
1.44	8.86	10.48	0.08	76.32	0.00	555.71	0.00
1.68	11.41	12.21	0.03	88.91	0.00	647.41	0.00
1.95	13.37	14.22	0.01	103.58	0.00	754.23	0.00
2.28	14.09	16.57	0.00	120.67	0.00	878.67	0.00
2.65	12.84	19.31	0.00	140.58	0.00		
3.09	9.98	22.49	0.00	163.77	0.00		
3.60		26.20	0.00	190.80	0.00		

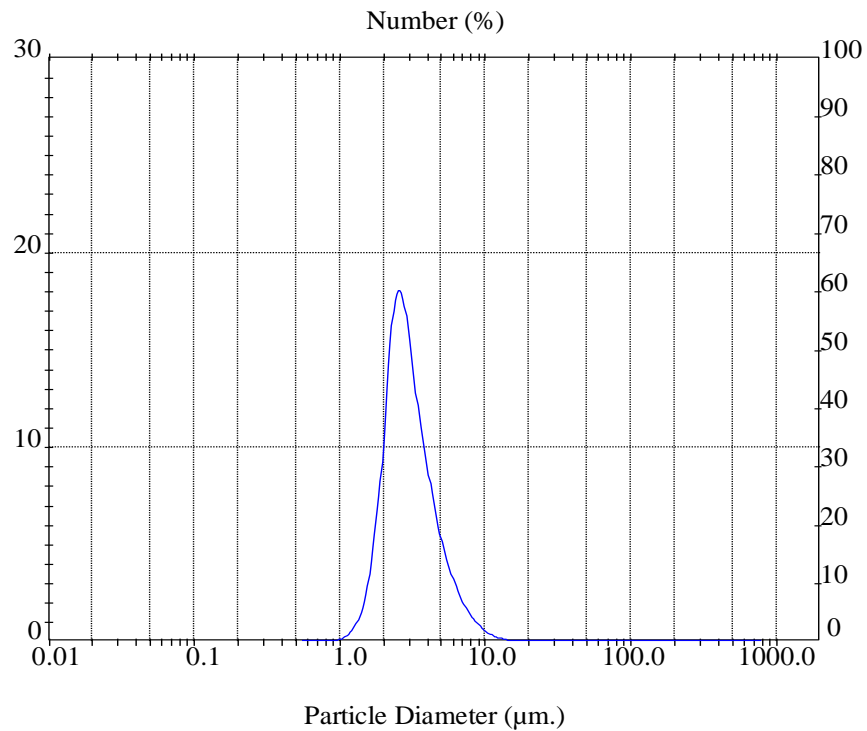
Figure B4-8: Typical spray characteristics; Number (%), particle diameter (µm) and analysis table for test SA -24



Result: Analysis Table

ID: MUSA		Run No: 5		Measured: 30/5/2008 15:32PM			
File: MUSA		Rec.No: 274		Analysed: 30/5/2008 15:32PM			
Path: C:\SIZERS\DATA\				Source: Analysed			
Range: 300 mm		Beam: 2.40 mm		Sampler: None			
Presentation: 3OHD		Analysis: Polydisperse		Obs': 17.3 %			
Modifications: -				Residual: 0.589 %			
Conc. = 0.0129 %Vol		Density = 1.000 g/cm ³		S.S.A. = 1.1122 m ² /g			
Distribution: Number		D[4,3] = 7.77 µm		D[3,2] = 5.39 µm			
D(n,0.1) = 1.55 µm		D(n,0.5) = 2.45 µm		D(n,0.9) = 4.96 µm			
Span = 1.393E+00		Uniformity = 4.332E-01					
Size (µm)	Number In %	Size (µm)	Number In %	Size (µm)	Number In %	Size (µm)	Number In %
0.49	0.00	3.60	6.85	26.20	0.00	190.80	0.00
0.58	0.00	4.19	5.54	30.53	0.00	222.28	0.00
0.67	0.00	4.88	5.54	35.56	0.00	258.95	0.00
0.78	0.00	5.69	3.94	41.43	0.00	301.68	0.00
0.91	0.32	6.63	2.68	48.27	0.00	351.46	0.00
1.06	0.86	7.72	1.71	56.23	0.00	409.45	0.00
1.24	1.90	9.00	1.06	65.51	0.00	477.01	0.00
1.44	3.79	10.48	0.57	76.32	0.00	555.71	0.00
1.68	7.08	12.21	0.28	88.91	0.00	647.41	0.00
1.95	11.91	14.22	0.13	103.58	0.00	754.23	0.00
2.28	16.22	16.57	0.06	120.67	0.00	878.67	0.00
2.65	15.68	19.31	0.02	140.58	0.00		
3.09	11.26	22.49	0.01	163.77	0.00		
3.60	8.12	26.20	0.00	190.80	0.00		

Figure B4-9: Typical spray characteristics; Number (%), particle diameter (µm) and analysis table for test SA -25



Result: Analysis Table

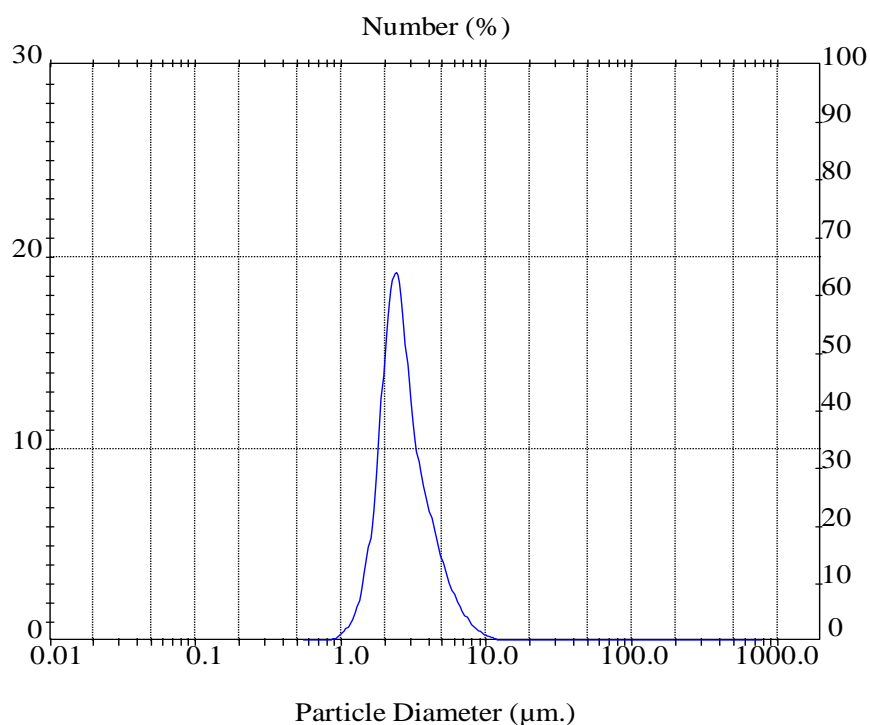
ID:	Run No: 4	Measured: 13/5/2008 12:48PM
File: MUSA	Rec.No: 203	Analysed: 13/5/2008 12:48PM
Path: C:\SIZERS\DATA\		Source: Analysed

Range: 300 mm	Beam: 2.40 mm	Sampler: None	Obs': 4.7 %
Presentation: 3OHD		Analysis: Polydisperse	Residual: 1.111 %
Modifications: -			

Conc. = 0.0034 %Vol	Density = 1.000 g/cm ³	S.S.A.= 1.0840 m ² /g
Distribution: Number	D[4,3] = 10.26 μm	D[3,2] = 5.54 μm
D(n,0.1) = 1.90 μm	D(n,0.5) = 2.84 μm	D(n,0.9) = 5.19 μm
Span = 1.158E+00	Uniformity = 3.691E-01	

Size (um)	Number In %						
0.49	0.00	3.60	9.56	26.20	0.00	190.80	0.00
0.58	0.00	4.19	6.76	30.53	0.00	222.28	0.00
0.67	0.00	4.88	4.53	35.56	0.00	258.95	0.00
0.78	0.03	5.69	3.06	41.43	0.00	301.68	0.00
0.91	0.13	6.63	1.93	48.27	0.00	351.46	0.00
1.06	0.41	7.72	1.18	56.23	0.00	409.45	0.00
1.24	1.14	9.00	0.67	65.51	0.00	477.01	0.00
1.44	2.90	10.48	0.34	76.32	0.00	555.71	0.00
1.68	6.74	12.21	0.17	88.91	0.00	647.41	0.00
1.95	12.98	14.22	0.08	103.58	0.00	754.23	0.00
2.28	17.86	16.57	0.03	120.67	0.00	878.67	0.00
2.65	16.71	19.31	0.01	140.58	0.00		
3.09	12.77	22.49	0.00	163.77	0.00		
3.60		26.20		190.80			

Figure B4-10: Typical spray characteristics; Number (%), particle diameter (μm) and analysis table for test SA-26



Result: Analysis Table

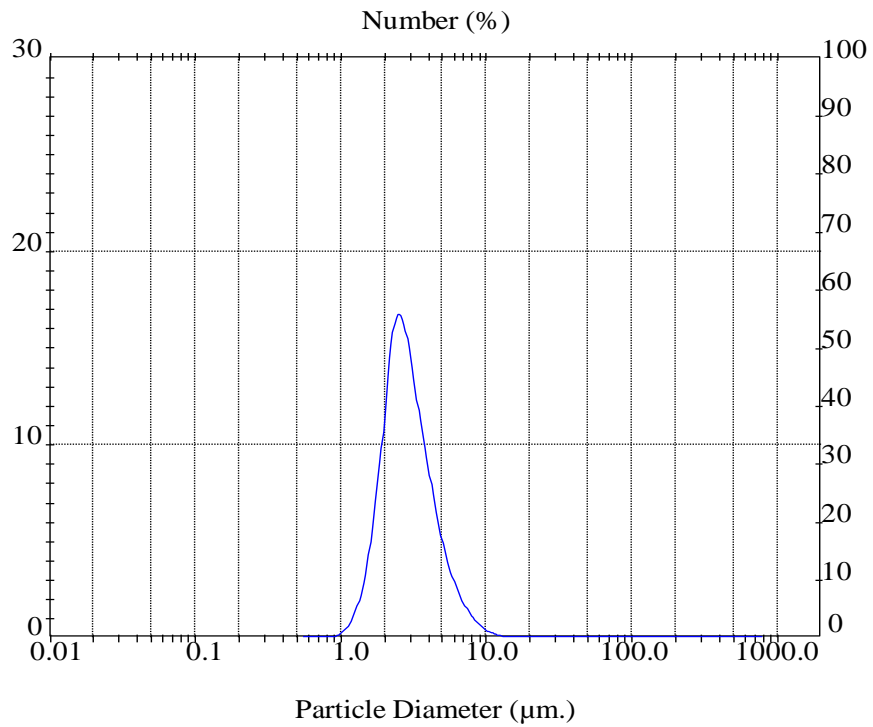
ID:	Run No: 5	Measured: 22/5/2008 13:05PM
File: MUSA	Rec.No: 252	Analysed: 22/5/2008 13:05PM
Path: C:\SIZERS\DATA\		Source: Analysed

Range: 300 mm	Beam: 2.40 mm	Sampler: None	Obs': 2.2 %
Presentation: 3OHD	Analysis: Polydisperse		Residual: 0.796 %
Modifications: -			

Conc. = 0.0014 %Vol	Density = 1.000 g/cm ³	S.S.A.= 1.2149 m ² /g
Distribution: Number	D[4,3]= 9.25 µm	D[3,2]= 4.94 µm
D(n,0.1)= 1.74 µm	D(n,0.5)= 2.56 µm	D(n,0.9)= 4.67 µm
Span = 1.149E+00	Uniformity = 3.652E-01	

Size (µm)	Number In %						
0.49	0.00	3.60	7.41	26.20	0.00	190.80	0.00
0.58	0.00	4.19	5.42	30.53	0.00	222.28	0.00
0.67	0.00	4.88	3.56	35.56	0.00	258.95	0.00
0.78	0.00	5.69	2.27	41.43	0.00	301.68	0.00
0.91	0.10	6.63	1.38	48.27	0.00	351.46	0.00
1.06	0.33	7.72	0.74	56.23	0.00	409.45	0.00
1.24	0.88	9.00	0.38	65.51	0.00	477.01	0.00
1.44	2.14	10.48	0.18	76.32	0.00	555.71	0.00
1.68	4.88	12.21	0.08	88.91	0.00	647.41	0.00
1.95	10.11	14.22	0.03	103.58	0.00	754.23	0.00
2.28	16.82	16.57	0.01	120.67	0.00	878.67	0.00
2.65	18.99	19.31	0.01	140.58	0.00		
3.09	14.43	22.49	0.00	163.77	0.00		
3.60	9.82	26.20		190.80			

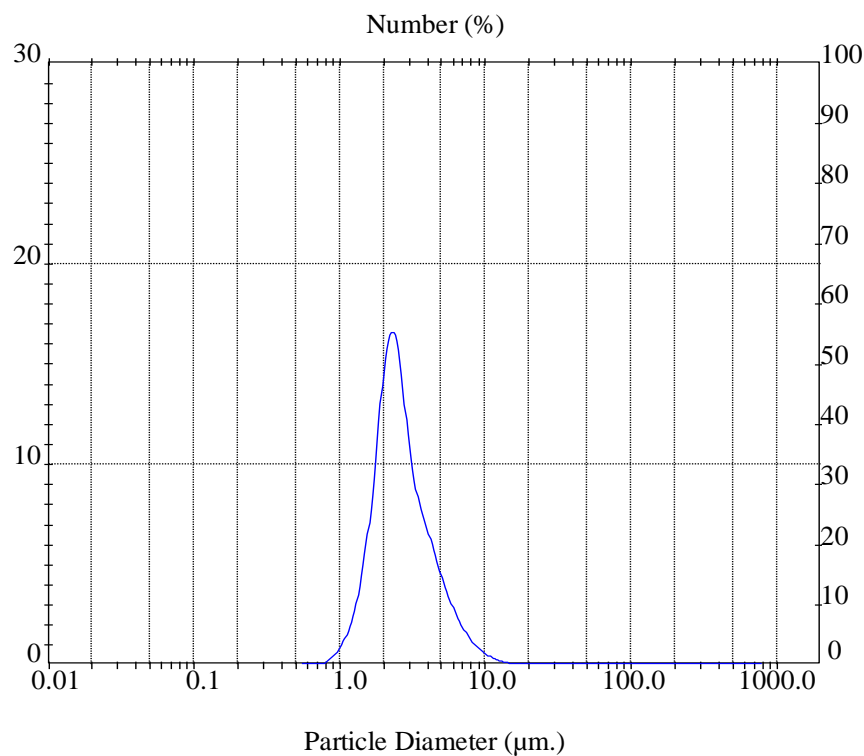
Figure B4-11: Typical spray characteristics; Number (%), particle diameter (µm) and analysis table for test SA-28



Result: Analysis Table

ID:	Run No: 5	Measured: 21/5/2008 10:53PM					
File: MUSA	Rec. No: 250	Analysed: 21/5/2008 10:53PM					
Path: C:\SIZERS\DATA\		Source: Analysed					
Range: 300 nm	Beam: 2.40 nm	Sampler: None	Obs': 3.8 %				
Presentation: 3OHD	Analysis: Polydisperse		Residual: 2.394 %				
Modifications: -							
Conc. = 0.0024 %Vol	Density = 1.000 g/cm ³	S.S.A. = 1.2044 m ² /g					
Distribution: Number	D[4, 3] = 6.50 µm	D[3, 2] = 4.98 µm					
D(n, 0.1) = 1.77 µm	D(n, 0.5) = 2.75 µm	D(n, 0.9) = 4.96 µm					
Span = 1.156E+00	Uniformity = 3.706E-01						
Size (µm)	Number In %	Size (µm)	Number In %	Size (µm)	Number In %	Size (µm)	Number In %
0.49	0.00	3.60	9.35	26.20	0.00	190.80	0.00
0.58	0.00	4.19	6.53	30.53	0.00	222.28	0.00
0.67	0.00	4.88	4.24	35.56	0.00	258.95	0.00
0.78	0.00	5.69	4.24	41.43	0.00	301.68	0.00
0.91	0.05	6.63	2.74	48.27	0.00	351.46	0.00
1.06	0.24	7.72	1.66	56.23	0.00	409.45	0.00
1.24	0.75	9.00	0.96	65.51	0.00	477.01	0.00
1.44	1.94	10.48	0.49	76.32	0.00	555.71	0.00
1.68	4.32	12.21	0.24	88.91	0.00	647.41	0.00
1.95	8.38	14.22	0.11	103.58	0.00	754.23	0.00
2.28	13.54	16.57	0.04	120.67	0.00	878.67	0.00
2.65	16.69	19.31	0.01	140.58	0.00		
3.09	15.44	22.49	0.00	163.77	0.00		
3.60	12.27	26.20	0.00	190.80	0.00		

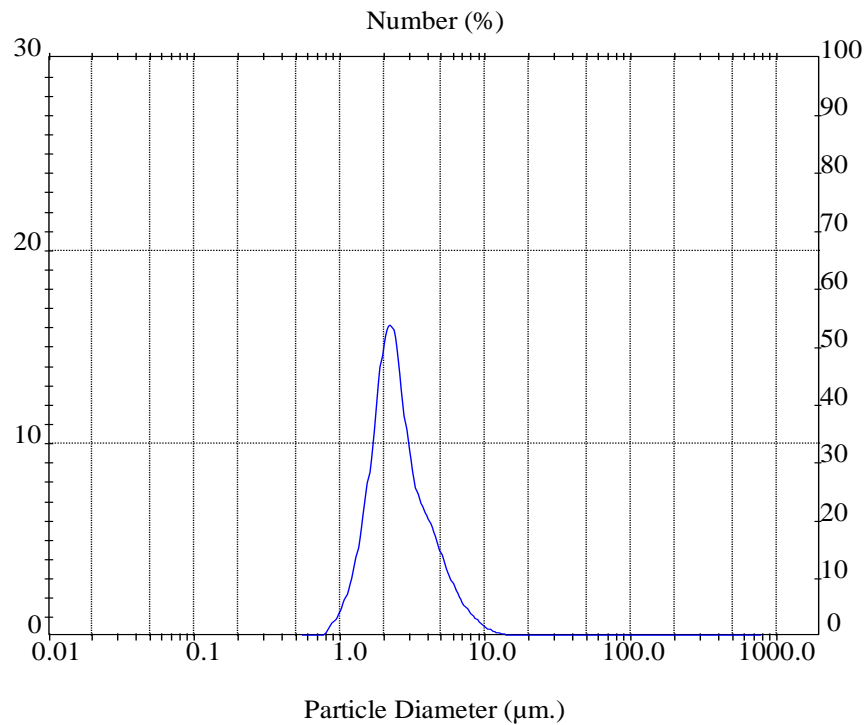
Figure B4-12: Typical spray characteristics; Number (%), particle diameter (µm) and analysis table for test SA-29



Result: Analysis Table

ID: MUSA		Run No: 1		Measured: 30/5/2008 15:18PM			
File: MUSA		Rec.No: 270		Analysed: 30/5/2008 15:18PM			
Path: C:\SIZERS\DATA\		Source: Analysed					
Range: 300 mm		Beam: 2.40 mm		Sampler: None			
Presentation: 3OHD		Analysis: Polydisperse		Obs': 9.3 %			
Modifications: -				Residual: 0.553 %			
Conc. = 0.0071 %Vol		Density = 1.000 g/cm ³		S.S.A.= 1.0414 m ² /g			
Distribution: Number		D[4,3] = 8.59 µm		D[3,2] = 5.76 µm			
D(n,0.1) = 1.58 µm		D(n,0.5) = 2.50 µm		D(n,0.9) = 5.01 µm			
Span = 1.369E+00		Uniformity = 4.335E-01					
Size (µm)	Number In %	Size (µm)	Number In %	Size (µm)	Number In %	Size (µm)	Number In %
0.49	0.00	3.60	7.04	26.20	0.00	190.80	0.00
0.58	0.00	4.19	5.47	30.53	0.00	222.28	0.00
0.67	0.00	4.88	5.47	35.56	0.00	258.95	0.00
0.78	0.00	5.69	3.88	41.43	0.00	301.68	0.00
0.91	0.28	6.63	2.69	48.27	0.00	351.46	0.00
1.06	0.77	7.72	1.74	56.23	0.00	409.45	0.00
1.24	1.72	9.00	1.08	65.51	0.00	477.01	0.00
1.44	3.47	10.48	0.66	76.32	0.00	555.71	0.00
1.68	6.53	12.21	0.36	88.91	0.00	647.41	0.00
1.95	11.15	14.22	0.18	103.58	0.00	754.23	0.00
2.28	15.73	16.57	0.09	120.67	0.00	878.67	0.00
2.65	16.12	19.31	0.04	140.58	0.00		
3.09	12.20	22.49	0.02	163.77	0.00		
3.60	8.78	26.20	0.01	190.80	0.00		

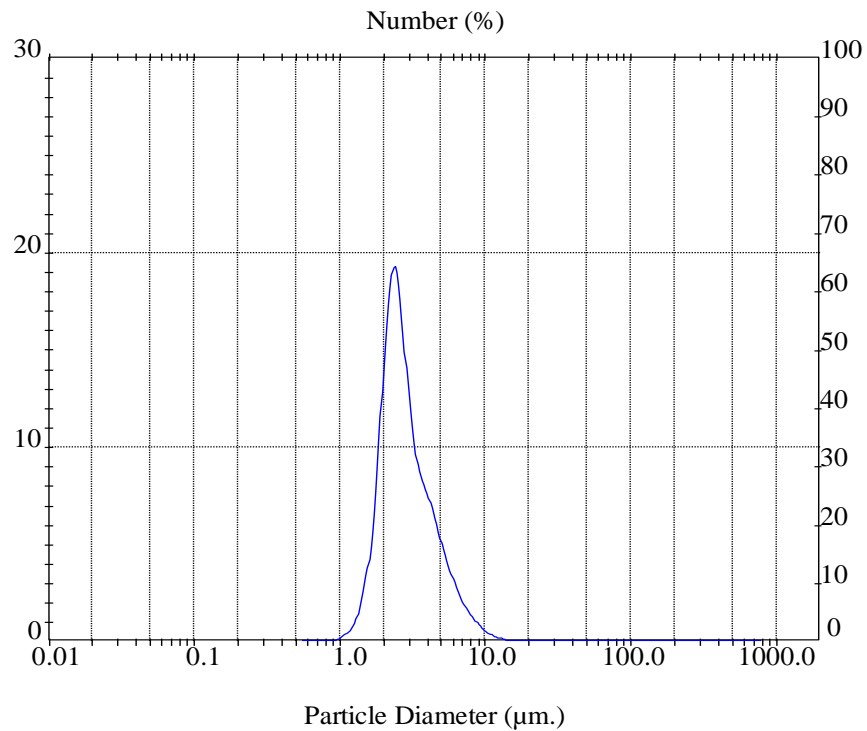
Figure B4-13: Typical spray characteristics; Number (%), particle diameter (µm) and analysis table for test SA-31



Result: Analysis Table

ID: MUSA		Run No: 5		Measured: 5/6/2008 10:40PM			
File: MUSA		Rec. No: 292		Analysed: 5/6/2008 10:40PM			
Path: C:\SIZERS\DATA\		Source: Analysed					
Range: 300 mm		Beam: 2.40 mm		Sampler: None			
Presentation: 3OHD		Analysis: Polydisperse		Obs': 7.1 %			
Modifications: -		Residual: 0.640 %					
Conc. = 0.0051 %Vol		Density = 1.000 g/cm ³		S.S.A.= 1.0785 m ² /g			
Distribution: Number		D[4,3] = 8.52 µm		D[3,2] = 5.56 µm			
D(n,0.1) = 1.48 µm		D(n,0.5) = 2.39 µm		D(n,0.9) = 4.91 µm			
Span = 1.434E+00		Uniformity = 4.488E-01					
Size (µm)	Number In %	Size (µm)	Number In %	Size (µm)	Number In %	Size (µm)	Number In %
0.49	0.00	3.60	6.42	26.20	0.00	190.80	0.00
0.58	0.00	4.19	5.20	30.53	0.00	222.28	0.00
0.67	0.00	4.88	3.74	35.56	0.00	258.95	0.00
0.78	0.47	5.69	2.56	41.43	0.00	301.68	0.00
0.91	1.18	6.63	1.66	48.27	0.00	351.46	0.00
1.06	2.46	7.72	1.05	56.23	0.00	409.45	0.00
1.24	4.58	9.00	0.30	65.51	0.00	477.01	0.00
1.44	7.91	10.48	0.15	76.32	0.00	555.71	0.00
1.68	12.34	12.21	0.07	88.91	0.00	647.41	0.00
1.95	14.95	14.22	0.03	103.58	0.00	754.23	0.00
2.28	10.76	16.57	0.01	120.67	0.00	878.67	0.00
2.65	7.72	19.31	0.00	140.58	0.00		
3.09		22.49		163.77			
3.60		26.20		190.80			

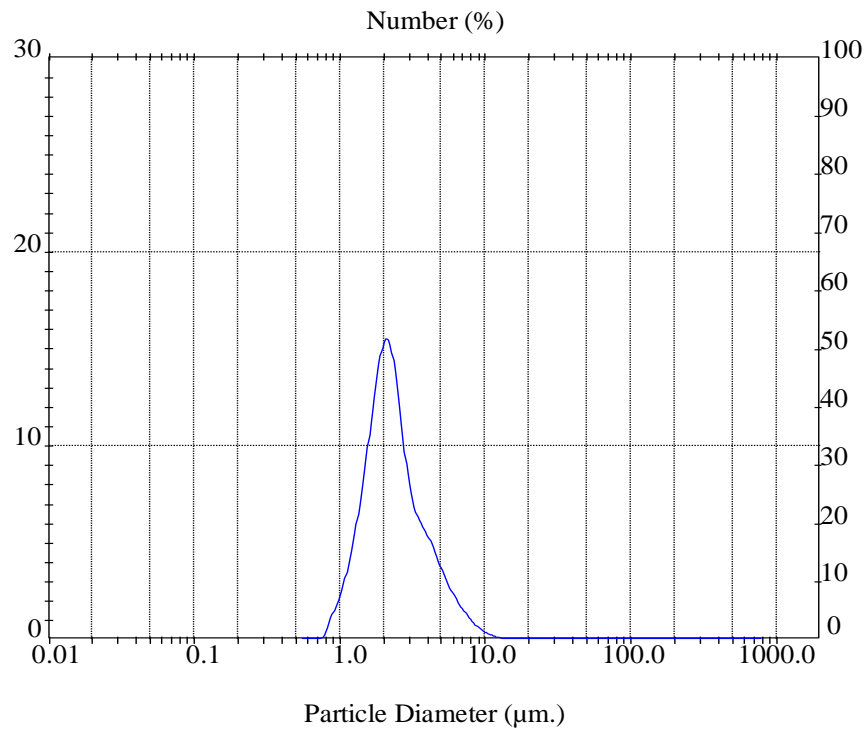
Figure B4-14: Typical spray characteristics; Number (%), particle diameter (µm) and analysis table for test SA-32



Result: Analysis Table

ID: Run No: 8 Measured: 30/5/2008 16:21PM		File: MUSA Rec. No: 275 Analysed: 30/5/2008 16:21PM		Path: C:\SIZERS\DATA\ Source: Analysed			
Range: 300 mm Beamr: 2.40 mm Sampler: None Obs': 4.0 %		Presentation: 3OHD Analysis: Polydisperse Residual: 0.575 %		Modifications: -			
Conc. = 0.0028 %Vol Density = 1.000 g/cm ³ S.S.A.= 1.0813 m ² /g		Distribution: Number D[4, 3]= 7.86 µm D[3, 2]= 5.55 µm		D(n, 0.1)= 1.82 µm D(n, 0.5)= 2.64 µm D(n, 0.9)= 5.18 µm			
Span = 1.268E+00 Uniformity = 4.057E-01							
Size (µm)	Number In %	Size (µm)	Number In %	Size (µm)	Number In %	Size (µm)	Number In %
0.49	0.00	3.60	7.85	26.20	0.00	190.80	0.00
0.58	0.00	4.19	6.31	30.53	0.00	222.28	0.00
0.67	0.00	4.88	4.47	35.56	0.00	258.95	0.00
0.78	0.05	5.69	3.03	41.43	0.00	301.68	0.00
0.91	0.18	6.63	1.93	48.27	0.00	351.46	0.00
1.06	0.54	7.72	1.20	56.23	0.00	409.45	0.00
1.24	1.46	9.00	0.66	65.51	0.00	477.01	0.00
1.44	3.79	10.48	0.34	76.32	0.00	555.71	0.00
1.68	8.94	12.21	0.16	88.91	0.00	647.41	0.00
1.95	16.36	14.22	0.07	103.58	0.00	754.23	0.00
2.28	18.97	16.57	0.03	120.67	0.00	878.67	0.00
2.65	14.04	19.31	0.01	140.58	0.00		
3.09	9.61	22.49	0.00	163.77	0.00		
3.60		26.20		190.80			

Figure B4-15: Typical spray characteristics; Number (%), particle diameter (µm) and analysis table for test SA-33



Result: Analysis Table

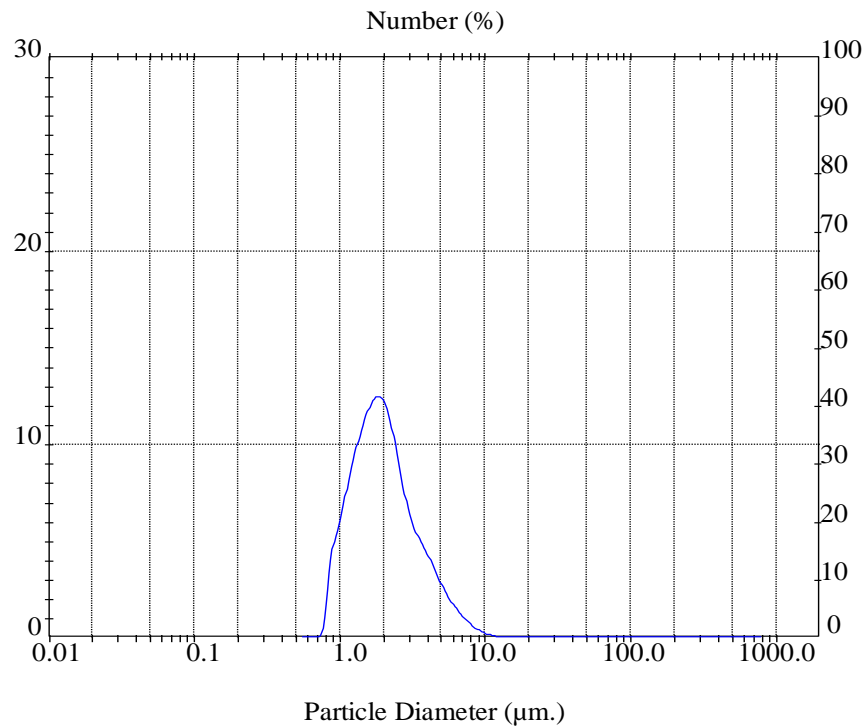
ID:	Run No: 28	Measured: 11/6/2008 17:11PM
File: MUSA	Rec. No: 430	Analysed: 11/6/2008 17:11PM
Path: C:\SIZERS\DATA\		Source: Analysed

Range: 300 mm	Beam: 2.40 mm	Sampler: None	Obs': 7.0 %
Presentation: 3OHD		Analysis: Polydisperse	Residual: 0.624 %
Modifications: -			

Conc. = 0.0047 %Vol	Density = 1.000 g/cm ³	S.S.A. = 1.1699 m ² /g
Distribution: Number	D[4,3] = 7.28 µm	D[3,2] = 5.13 µm
D(n,0.1) = 1.34 µm	D(n,0.5) = 2.22 µm	D(n,0.9) = 4.65 µm
Span = 1.489E+00	Uniformity = 4.613E-01	

Size (µm)	Number In %						
0.49	0.00	3.60	5.59	26.20	0.00	190.80	0.00
0.58	0.00	4.19	4.51	30.53	0.00	222.28	0.00
0.67	0.00	4.88	3.23	35.56	0.00	258.95	0.00
0.78	0.00	5.69	2.25	41.43	0.00	301.68	0.00
0.91	0.90	6.63	1.49	48.27	0.00	351.46	0.00
1.06	2.06	7.72	0.88	56.23	0.00	409.45	0.00
1.24	3.85	9.00	0.47	65.51	0.00	477.01	0.00
1.44	6.44	10.48	0.23	76.32	0.00	555.71	0.00
1.68	9.91	12.21	0.10	88.91	0.00	647.41	0.00
1.95	13.66	14.22	0.04	103.58	0.00	754.23	0.00
2.28	15.51	16.57	0.01	120.67	0.00	878.67	0.00
2.65	13.22	19.31	0.00	140.58	0.00		
3.09	9.06	22.49	0.00	163.77	0.00		
3.60	6.58	26.20	0.00	190.80	0.00		

Figure B4-16: Typical spray characteristics; Number (%), particle diameter (μm) and analysis table for test SA-34



Result: Analysis Table

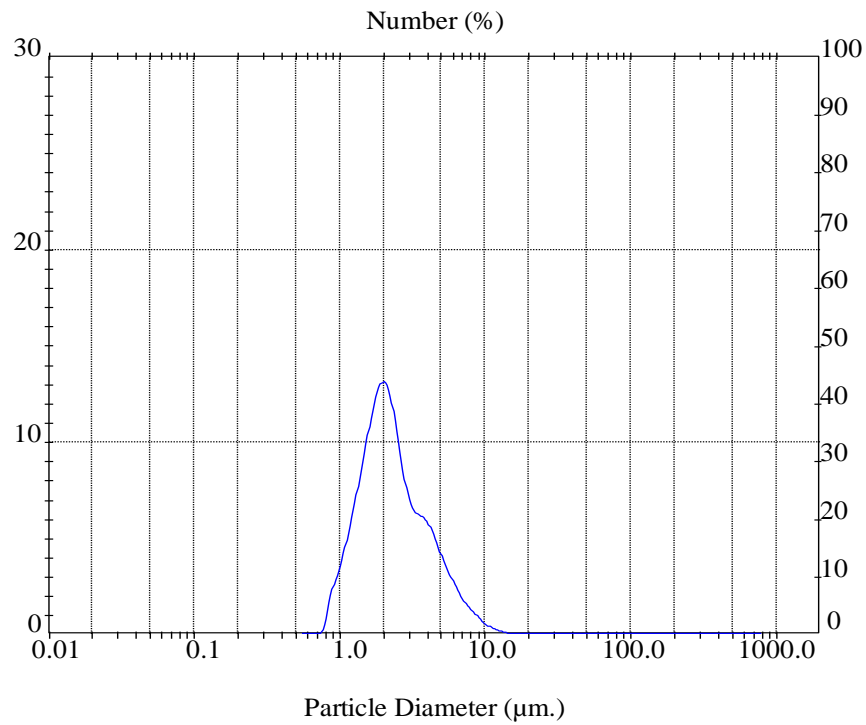
ID:	Run No: 3	Measured: 20/6/2008 19:03PM
File: MUSA	Rec. No: 635	Analysed: 20/6/2008 19:03PM
Path: C:\SIZERS\DATA\		Source: Analysed

Range: 300 nm	Beam: 2.40 nm	Sampler: None	Obs': 10.2 %
Presentation: 3OHD		Analysis: Polydisperse	Residual: 0.488 %
Modifications: -			

Conc. = 0.0063 %Vol	Density = 1.000 g/cm ³	S.S.A.= 1.2687 m ² /g
Distribution: Number	D[4,3] = 6.56 µm	D[3,2] = 4.73 µm
D(n,0.1) = 1.08 µm	D(n,0.5) = 1.91 µm	D(n,0.9) = 4.17 µm
Span = 1.614E+00	Uniformity = 5.041E-01	

Size (µm)	Number In %						
0.49	0.00	3.60	4.54	26.20	0.00	190.80	0.00
0.58	0.00	4.19	3.49	30.53	0.00	222.28	0.00
0.67	0.00	4.88	2.46	35.56	0.00	258.95	0.00
0.78	0.00	5.69	2.46	41.43	0.00	301.68	0.00
0.91	3.35	6.63	1.67	48.27	0.00	351.46	0.00
1.06	5.84	7.72	1.07	56.23	0.00	409.45	0.00
1.24	8.12	9.00	0.61	65.51	0.00	477.01	0.00
1.44	10.14	10.48	0.31	76.32	0.00	555.71	0.00
1.68	11.72	12.21	0.15	88.91	0.00	647.41	0.00
1.95	12.49	14.22	0.06	103.58	0.00	754.23	0.00
2.28	11.82	16.57	0.02	120.67	0.00	878.67	0.00
2.65	9.59	19.31	0.01	140.58	0.00		
3.09	7.07	22.49	0.00	163.77	0.00		
3.60	5.49	26.20	0.00	190.80	0.00		

Figure B4-17: Typical spray characteristics; Number (%), particle diameter (µm) and analysis table for test SA-35

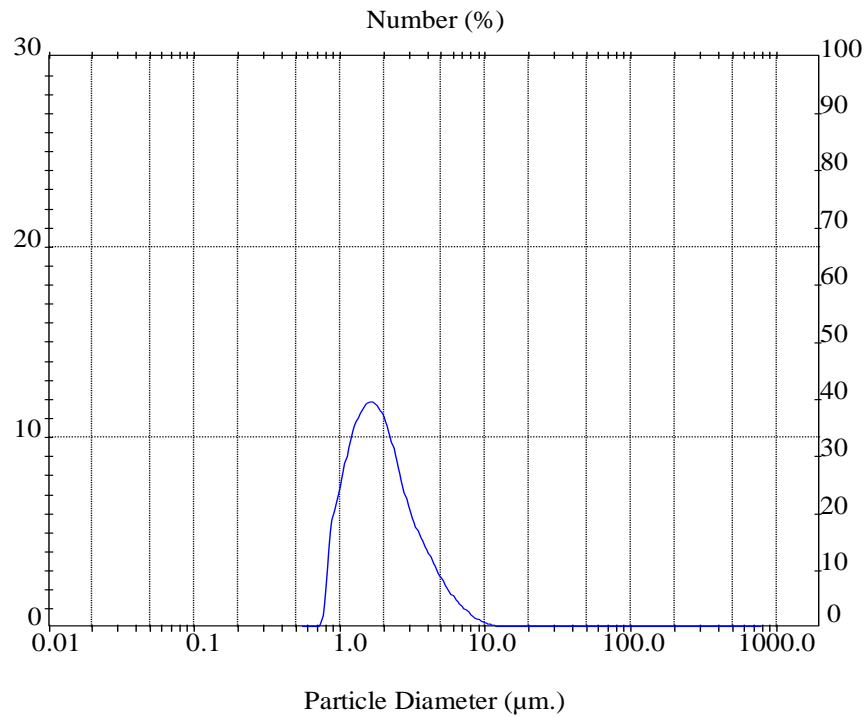


Result: Analysis Table

ID:	Run No: 27	Measured: 12/6/2008 17:18PM	
File: MUSA	Rec. No: 476	Analysed: 12/6/2008 17:18PM	
Path: C:\SIZERS\DATA\		Source: Analysed	
Range: 300 nm	Beam: 2.40 nm	Sampler: None	Obs': 5.0 %
Presentation: 3OHD	Analysis: Polydisperse		Residual: 0.463 %
Modifications: -			
Conc. = 0.0038 %Vol	Density = 1.000 g/cm ³	S.S.A. = 1.0031 m ² /g	
Distribution: Number	D[4, 3] = 16.59 µm	D[3, 2] = 5.98 µm	
D(n, 0.1) = 1.23 µm	D(n, 0.5) = 2.17 µm	D(n, 0.9) = 4.99 µm	
Span = 1.734E+00	Uniformity = 5.423E-01		

Size (µm)	Number In %						
0.49	0.00	3.60	5.99	26.20	0.00	190.80	0.00
0.58	0.00	4.19	4.99	30.53	0.00	222.28	0.00
0.67	0.00	4.88	3.67	35.56	0.00	258.95	0.00
0.78	0.00	5.69	3.67	41.43	0.00	301.68	0.00
0.91	1.68	6.63	2.65	48.27	0.00	351.46	0.00
1.06	3.31	7.72	1.77	56.23	0.00	409.45	0.00
1.24	5.30	9.00	1.18	65.51	0.00	477.01	0.00
1.44	7.69	10.48	0.67	76.32	0.00	555.71	0.00
1.68	10.33	12.21	0.36	88.91	0.00	647.41	0.00
1.95	12.59	14.22	0.18	103.58	0.00	754.23	0.00
2.28	12.94	16.57	0.08	120.67	0.00	878.67	0.00
2.65	10.57	19.31	0.04	140.58	0.00		
3.09	7.66	22.49	0.01	163.77	0.00		
3.60	6.34	26.20	0.00	190.80	0.00		

Figure B4-18: Typical spray characteristics; Number (%), particle diameter (μm) and analysis table for test SA-36



Result: Analysis Table

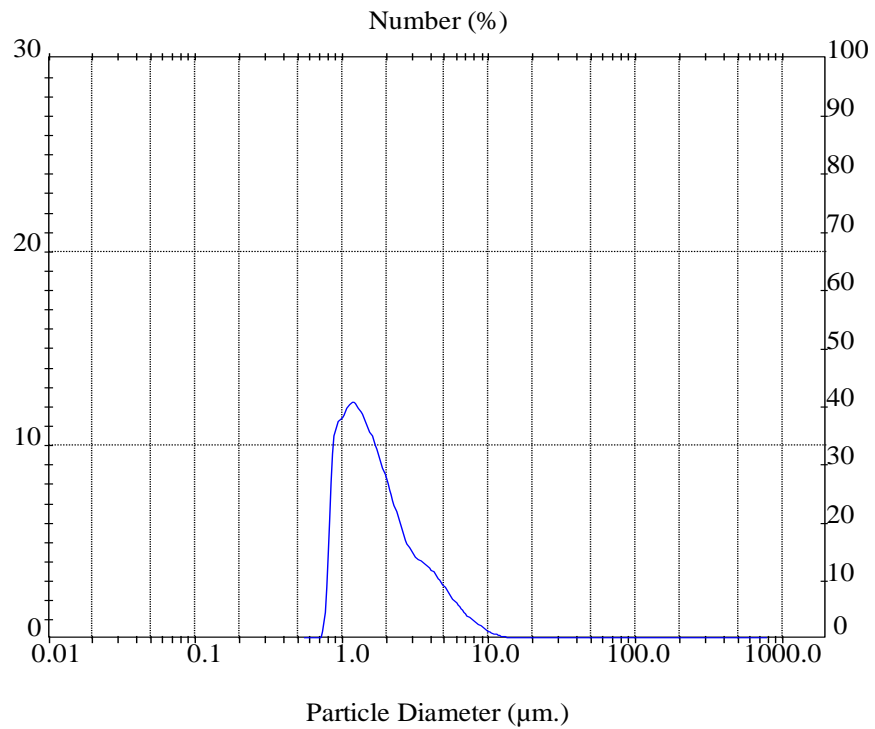
ID:	Run No: 11	Measured: 17/6/2008 14:03PM
File: MUSA	Rec.No: 488	Analysed: 17/6/2008 14:03PM
Path: C:\SIZERS\DATA\		Source: Analysed

Range: 300 mm	Beamr: 2.40 mm	Sampler: None	Obs': 3.6 %
Presentation: 3OHD	Analysis: Polydisperse		Residual: 0.750 %
Modifications: -			

Conc. = 0.0023 %Vol	Density = 1.000 g/cm ³	S.S.A.= 1.2064 m ² /g
Distribution: Number	D[4,3] = 7.97 µm	D[3,2] = 4.97 µm
D(n,0.1) = 1.04 µm	D(n,0.5) = 1.83 µm	D(n,0.9) = 4.08 µm
Span = 1.667E+00	Uniformity = 5.254E-01	

Size (um)	Number In %						
0.49	0.00	3.60	4.25	26.20	0.00	190.80	0.00
0.58	0.00	4.19	3.22	30.53	0.00	222.28	0.00
0.67	0.00	4.88	2.29	35.56	0.00	258.95	0.00
0.78	0.00	5.69	1.57	41.43	0.00	301.68	0.00
0.91	4.17	6.63	1.04	48.27	0.00	351.46	0.00
1.06	7.07	7.72	0.60	56.23	0.00	409.45	0.00
1.24	9.40	9.00	0.32	65.51	0.00	477.01	0.00
1.44	11.01	10.48	0.16	76.32	0.00	555.71	0.00
1.68	11.77	12.21	0.07	88.91	0.00	647.41	0.00
1.95	11.64	14.22	0.03	103.58	0.00	754.23	0.00
2.28	10.58	16.57	0.01	120.67	0.00	878.67	0.00
2.65	8.73	19.31	0.00	140.58	0.00		
3.09	6.76	22.49	0.00	163.77	0.00		
3.60	5.30	26.20	0.00	190.80	0.00		

Figure B4-19: Typical spray characteristics; Number (%), particle diameter (µm) and analysis table for test SA-37



Result: Analysis Table

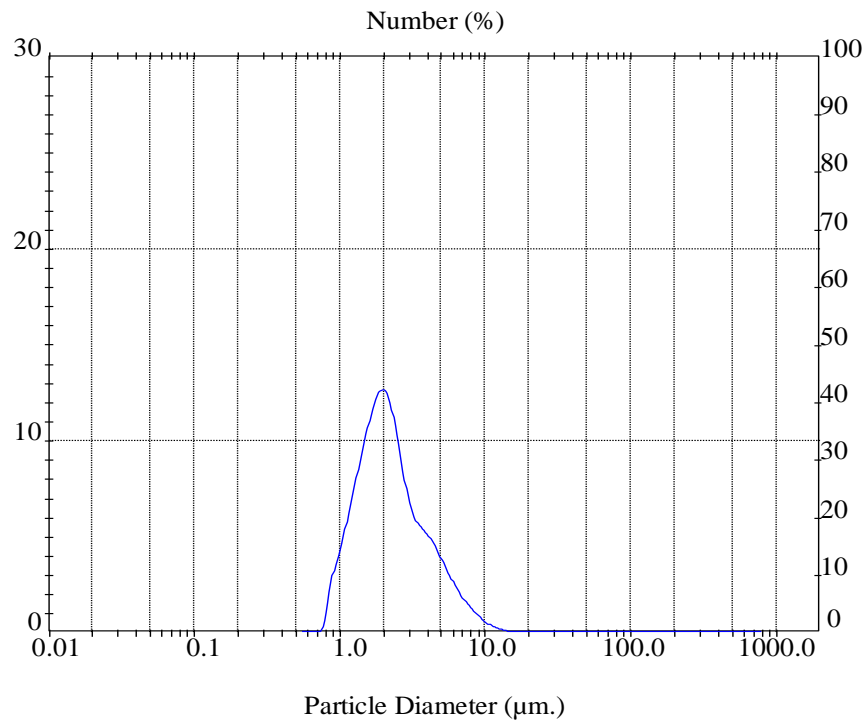
ID:	Run No: 22	Measured: 19/6/2008 15:01PM
File: MUSA	Rec. No: 574	Analysed: 19/6/2008 15:01PM
Path: C:\SIZERS\DATA\		Source: Analysed

Range: 300 mm	Beam: 2.40 mm	Sampler: None	Obs': 5.7 %
Presentation: 3OHD		Analysis: Polydisperse	Residual: 0.663 %
Modifications: -			

Conc. = 0.0042 %Vol	Density = 1.000 g/cm ³	S.S.A. = 1.0485 m ² /g
Distribution: Number	D[4,3] = 8.71 µm	D[3,2] = 5.72 µm
D(n,0.1) = 0.93 µm	D(n,0.5) = 1.58 µm	D(n,0.9) = 4.26 µm
Span = 2.102E+00	Uniformity = 6.485E-01	

Size (µm)	Number In %						
0.49	0.00	3.60	3.74	26.20	0.00	190.80	0.00
0.58	0.00	4.19	3.15	30.53	0.00	222.28	0.00
0.67	0.00	4.88	2.43	35.56	0.00	258.95	0.00
0.78	8.07	5.69	1.79	41.43	0.00	301.68	0.00
0.91	11.32	6.63	1.22	48.27	0.00	351.46	0.00
1.06	12.17	7.72	0.82	56.23	0.00	409.45	0.00
1.24	11.74	9.00	0.47	65.51	0.00	477.01	0.00
1.44	10.66	10.48	0.25	76.32	0.00	555.71	0.00
1.68	9.29	12.21	0.12	88.91	0.00	647.41	0.00
1.95	7.72	14.22	0.06	103.58	0.00	754.23	0.00
2.28	6.07	16.57	0.02	120.67	0.00	878.67	0.00
2.65	4.76	19.31	0.01	140.58	0.00		
3.09	4.10	22.49	0.00	163.77	0.00		
3.60		26.20		190.80			

Figure B4-20: Typical spray characteristics; Number (%), particle diameter (µm) and analysis table for test SA-38



Result: Analysis Table

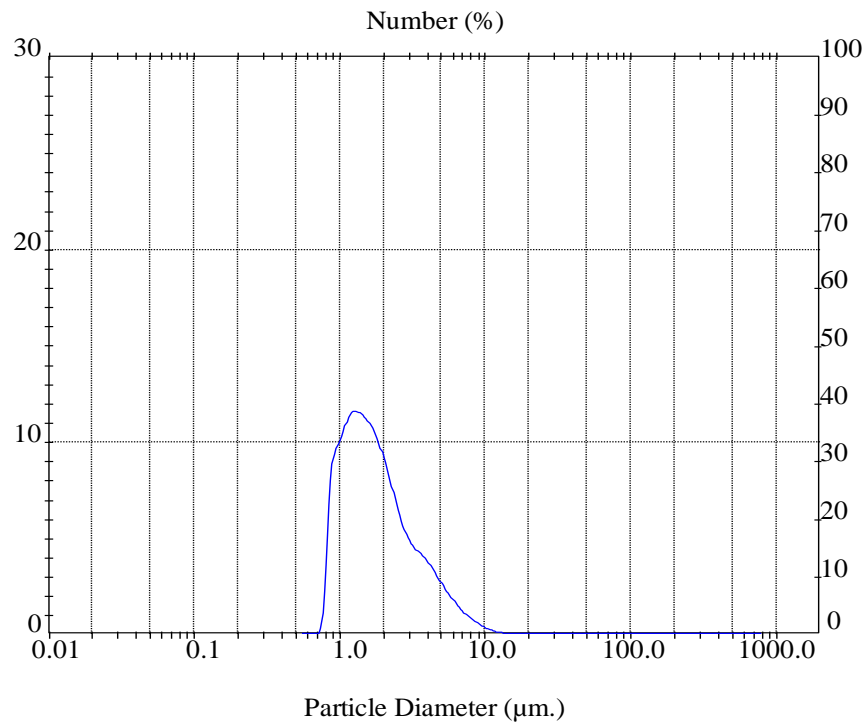
ID:	Run No: 21	Measured: 12/6/2008 16:38PM
File: MUSA	Rec.No: 468	Analysed: 12/6/2008 16:38PM
Path: C:\SIZERS\DATA\		Source: Analysed

Range: 300 mm	Beamr: 2.40 mm	Sampler: None	Obs': 7.3 %
Presentation: 3OHD		Analysis: Polydisperse	Residual: 0.642 %
Modifications: -			

Conc. = 0.0056 %Vol	Density = 1.000 g/cm ³	S.S.A. = 1.0327 m ² /g
Distribution: Number	D[4,3] = 8.17 µm	D[3,2] = 5.81 µm
D(n,0.1) = 1.17 µm	D(n,0.5) = 2.10 µm	D(n,0.9) = 4.93 µm
Span = 1.786E+00	Uniformity = 5.488E-01	

Size (µm)	Number In %						
0.49	0.00	3.60	5.25	26.20	0.00	190.80	0.00
0.58	0.00	4.19	4.51	30.53	0.00	222.28	0.00
0.67	0.00	4.88	3.48	35.56	0.00	258.95	0.00
0.78	2.12	5.69	2.53	41.43	0.00	301.68	0.00
0.91	4.05	6.63	1.74	48.27	0.00	351.46	0.00
1.06	6.19	7.72	1.17	56.23	0.00	409.45	0.00
1.24	8.47	9.00	0.67	65.51	0.00	477.01	0.00
1.44	10.69	10.48	0.35	76.32	0.00	555.71	0.00
1.68	12.35	12.21	0.17	88.91	0.00	647.41	0.00
1.95	12.44	14.22	0.08	103.58	0.00	754.23	0.00
2.28	10.32	16.57	0.03	120.67	0.00	878.67	0.00
2.65	7.50	19.31	0.01	140.58	0.00		
3.09	5.86	22.49	0.00	163.77	0.00		
3.60		26.20		190.80			

Figure B4-21: Typical spray characteristics; Number (%), particle diameter (μm) and analysis table for test SA-39



Result: Analysis Table

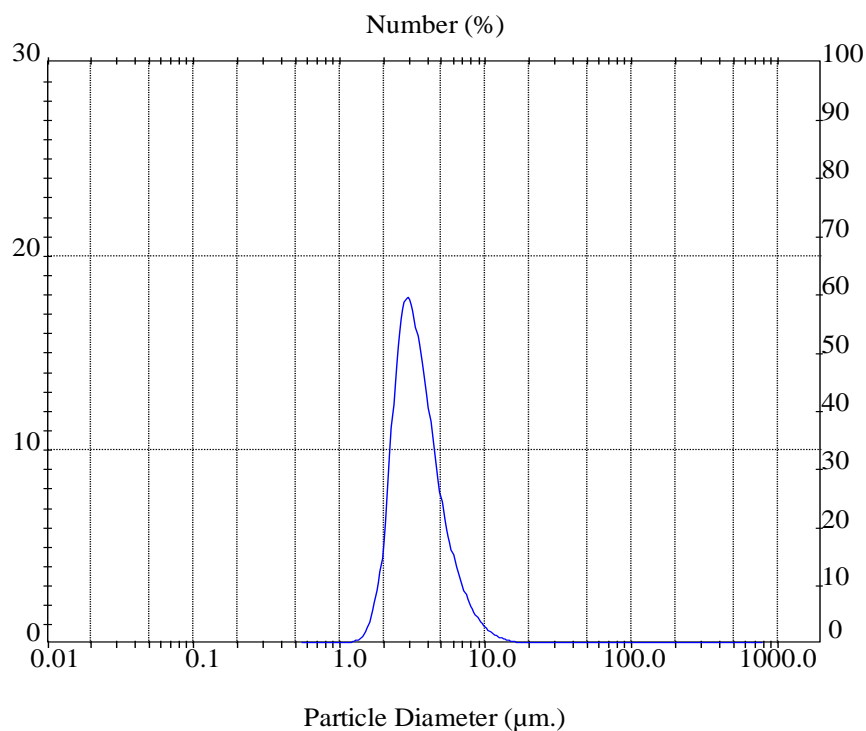
ID:	Run No: 29	Measured: 12/6/2008 17:25PM
File: MUSA	Rec. No: 477	Analysed: 12/6/2008 17:25PM
Path: C:\SIZERS\DATA\		Source: Analysed

Range: 300 mm	Beam: 2.40 mm	Sampler: None	Obs': 7.9 %
Presentation: 3OHD		Analysis: Polydisperse	Residual: 0.568 %
Modifications: -			

Conc. = 0.0057 %Vol	Density = 1.000 g/cm ³	S.S.A.= 1.0847 m ² /g
Distribution: Number	D[4,3] = 8.34 µm	D[3,2] = 5.53 µm
D(n,0.1) = 0.96 µm	D(n,0.5) = 1.66 µm	D(n,0.9) = 4.22 µm
Span = 1.964E+00	Uniformity = 6.133E-01	

Size (µm)	Number In %						
0.49	0.00	3.60	3.97	26.20	0.00	190.80	0.00
0.58	0.00	4.19	3.23	30.53	0.00	222.28	0.00
0.67	0.00	4.88	2.41	35.56	0.00	258.95	0.00
0.78	6.77	5.69	1.74	41.43	0.00	301.68	0.00
0.91	9.91	6.63	1.16	48.27	0.00	351.46	0.00
1.06	11.27	7.72	0.77	56.23	0.00	409.45	0.00
1.24	11.54	9.00	0.44	65.51	0.00	477.01	0.00
1.44	11.11	10.48	0.23	76.32	0.00	555.71	0.00
1.68	10.15	12.21	0.11	88.91	0.00	647.41	0.00
1.95	8.64	14.22	0.05	103.58	0.00	754.23	0.00
2.28	6.78	16.57	0.02	120.67	0.00	878.67	0.00
2.65	5.24	19.31	0.01	140.58	0.00		
3.09	4.44	22.49	0.00	163.77	0.00		
3.60		26.20		190.80			

Figure B4-22: Typical spray characteristics; Number (%), particle diameter (µm) and analysis table for test SA-40



Result: Analysis Table

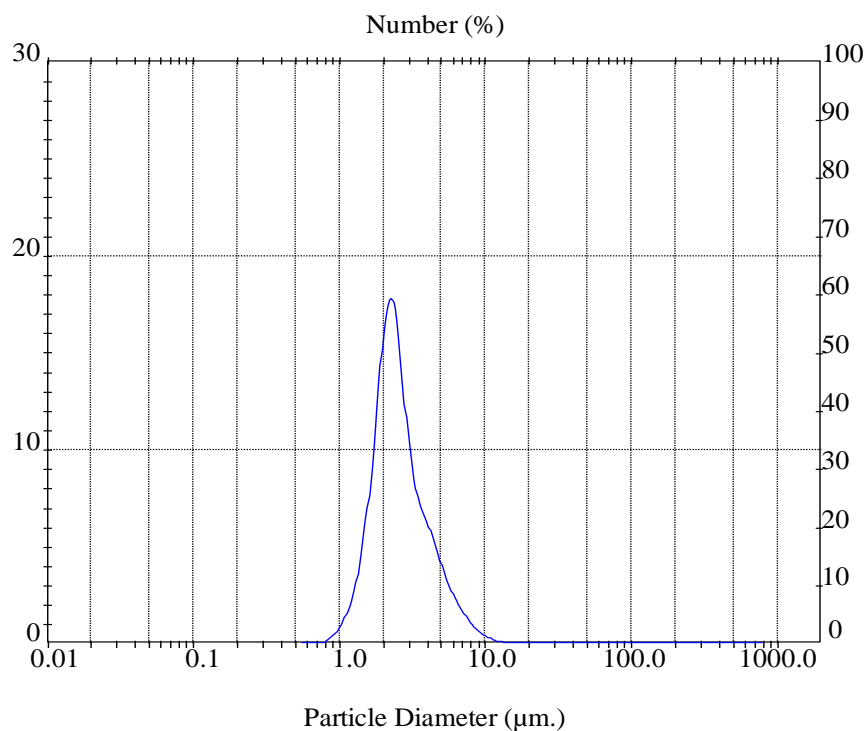
ID:	Run No: 2	Measured: 27/5/2008 13:32PM
File: MUSA	Rec. No: 330	Analysed: 27/5/2008 13:32PM
Path: C:\SIZERS\DATA\		Source: Analysed

Range: 300 mm	Beam: 2.40 mm	Sampler: None	Obs': 5.5 %
Presentation: 3OHD		Analysis: Polydisperse	Residual: 0.855 %
Modifications: -			

Conc. = 0.0046 %Vol	Density = 1.000 g/cm ³	S.S.A.= 0.9363 m ² /g
Distribution: Number	D[4,3] = 11.33 µm	D[3,2] = 6.41 µm
D(n,0.1) = 2.23 µm	D(n,0.5) = 3.27 µm	D(n,0.9) = 5.83 µm
Span = 1.102E+00	Uniformity = 3.576E-01	

Size (µm)	Number In %						
0.49	0.00	3.60	13.33	26.20	0.01	190.80	0.00
0.58	0.00	4.19	9.60	30.53	0.00	222.28	0.00
0.67	0.00	4.88	6.35	35.56	0.00	258.95	0.00
0.78	0.00	5.69	4.29	41.43	0.00	301.68	0.00
0.91	0.01	6.63	2.76	48.27	0.00	351.46	0.00
1.06	0.06	7.72	1.66	56.23	0.00	409.45	0.00
1.24	0.24	9.00	0.98	65.51	0.00	477.01	0.00
1.44	0.86	10.48	0.55	76.32	0.00	555.71	0.00
1.68	2.76	12.21	0.29	88.91	0.00	647.41	0.00
1.95	7.49	14.22	0.15	103.58	0.00	754.23	0.00
2.28	14.39	16.57	0.07	120.67	0.00	878.67	0.00
2.65	17.78	19.31	0.03	140.58	0.00		
3.09	16.31	22.49	0.02	163.77	0.00		
3.60		26.20		190.80	0.00		

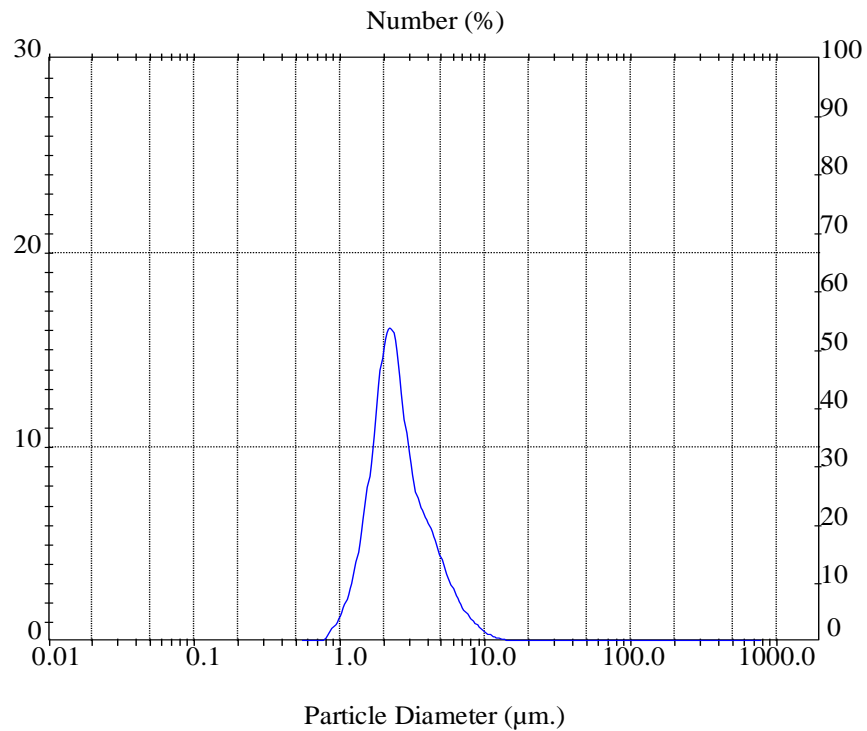
Figure B4-23: Typical spray characteristics; Number (%), particle diameter (µm) and analysis table for test SA-42



Result: Analysis Table

ID: Run No: 8 Measured: 4/6/2008 12:25PM							
File: MUSA Rec. No: 289 Analysed: 4/6/2008 12:25PM							
Path: C:\SIZERS\DATA\ Source: Analysed							
Range: 300 mm	Beam: 2.40 mm	Sampler: None	Obs': 8.1 %				
Presentation: 3OHD	Analysis: Polydisperse		Residual: 0.682 %				
Modifications: -							
Conc. = 0.0055 %Vol		Density = 1.000 g/cm ³	S.S.A.= 1.1562 m ² /g				
Distribution: Number		D[4,3] = 7.44 µm	D[3,2] = 5.19 µm				
D(n,0.1) = 1.57 µm		D(n,0.5) = 2.42 µm	D(n,0.9) = 4.77 µm				
Span = 1.326E+00		Uniformity = 4.125E-01					
Size (µm)	Number In %	Size (µm)	Number In %	Size (µm)	Number In %	Size (µm)	Number In %
0.49	0.00	3.60	6.45	26.20	0.00	190.80	0.00
0.58	0.00	4.19	5.10	30.53	0.00	222.28	0.00
0.67	0.00	4.88	3.56	35.56	0.00	258.95	0.00
0.78	0.28	5.69	2.39	41.43	0.00	301.68	0.00
0.91	0.77	6.63	1.56	48.27	0.00	351.46	0.00
1.06	1.75	7.72	0.90	56.23	0.00	409.45	0.00
1.24	3.64	9.00	0.49	65.51	0.00	477.01	0.00
1.44	7.04	10.48	0.24	76.32	0.00	555.71	0.00
1.68	12.26	12.21	0.11	88.91	0.00	647.41	0.00
1.95	17.12	14.22	0.05	103.58	0.00	754.23	0.00
2.28	16.63	16.57	0.02	120.67	0.00	878.67	0.00
2.65	11.63	19.31	0.01	140.58	0.00		
3.09	7.98	22.49	0.00	163.77	0.00		
3.60		26.20		190.80			

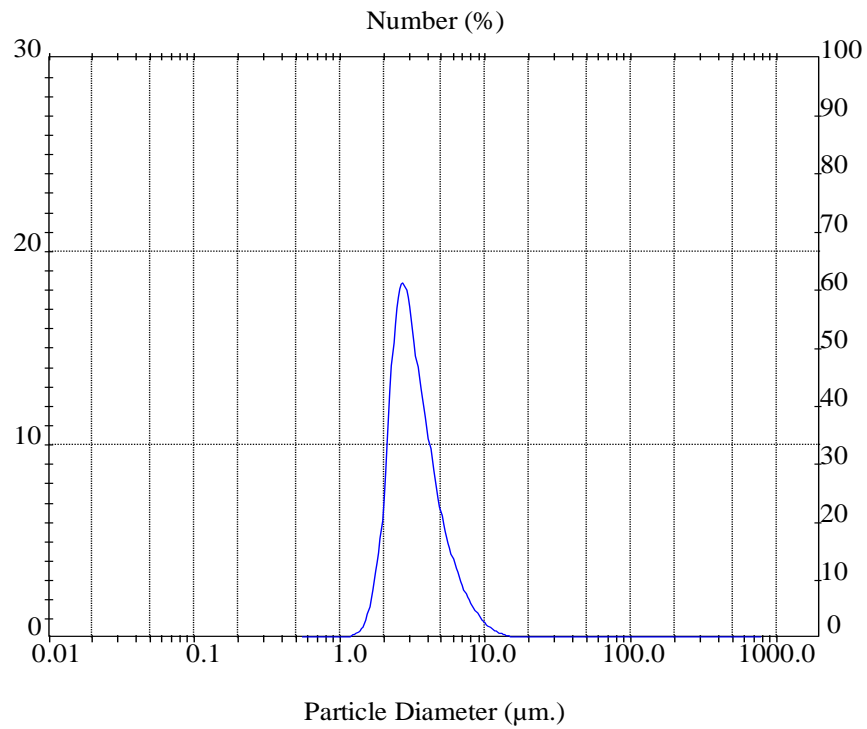
Figure B4-24: Typical spray characteristics; Number (%), particle diameter (µm) and analysis table for test SA-43



Result: Analysis Table

ID: Run No: 5 Measured: 5/6/2008 10:40PM		File: MUSA Rec. No: 298 Analysed: 5/6/2008 10:40PM		Path: C:\SIZERS\DATA\ Source: Analysed			
Range: 300 mm Beam: 2.40 mm Sampler: None Obs: 7.1 %		Presentation: 3OHD Analysis: Polydisperse Residual: 0.640 %		Modifications: -			
Conc. = 0.0051 %Vol Density = 1.000 g/cm ³ S.S.A.= 1.0785 m ² /g		Distribution: Number D[4, 3]= 8.52 µm D[3, 2]= 5.56 µm		D(n, 0.1)= 1.48 µm D(n, 0.5)= 2.39 µm D(n, 0.9)= 4.91 µm			
Span = 1.434E+00 Uniformity = 4.488E-01							
Size (µm)	Number In %	Size (µm)	Number In %	Size (µm)	Number In %	Size (µm)	Number In %
0.49	0.00	3.60	6.42	26.20	0.00	190.80	0.00
0.58	0.00	4.19	5.20	30.53	0.00	222.28	0.00
0.67	0.00	4.88	3.74	35.56	0.00	258.95	0.00
0.78	0.47	5.69	2.56	41.43	0.00	301.68	0.00
0.91	1.18	6.63	1.66	48.27	0.00	351.46	0.00
1.06	2.46	7.72	1.05	56.23	0.00	409.45	0.00
1.24	4.58	9.00	0.58	65.51	0.00	477.01	0.00
1.44	7.91	10.48	0.30	76.32	0.00	555.71	0.00
1.68	12.34	12.21	0.15	88.91	0.00	647.41	0.00
1.95	15.84	14.22	0.07	103.58	0.00	754.23	0.00
2.28	14.95	16.57	0.03	120.67	0.00	878.67	0.00
2.65	10.76	19.31	0.01	140.58	0.00		
3.09	7.72	22.49	0.00	163.77	0.00		
3.60		26.20		190.80			

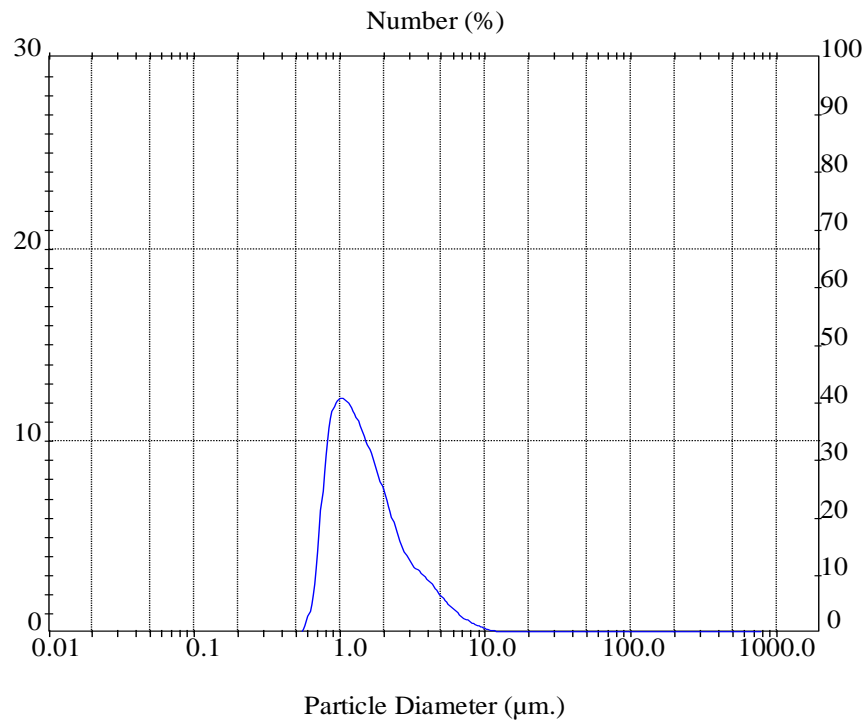
Figure B4-25: Typical spray characteristics; Number (%), particle diameter (µm) and analysis table for test SA-45



Result: Analysis Table

ID: MUSA		Run No: 2		Measured: 3/6/2008 11:32PM			
File: MUSA		Rec. No: 285		Analysed: 3/6/2008 11:32PM			
Path: C:\SIZERS\DATA\				Source: Analysed			
Range: 300 mm		Beam: 2.40 mm		Sampler: None			
Presentation: 3OHD		Analysis: Polydisperse		Obs': 4.2 %			
Modifications: -				Residual: 0.818 %			
Conc. = 0.0032 %Vol		Density = 1.000 g/cm ³		S.S.A.= 1.0192 m ² /g			
Distribution: Number		D[4, 3] = 8.27 µm		D[3, 2] = 5.89 µm			
D(n, 0.1) = 2.12 µm		D(n, 0.5) = 3.07 µm		D(n, 0.9) = 5.64 µm			
Span = 1.145E+00		Uniformity = 3.703E-01					
Size (µm)	Number In %	Size (µm)	Number In %	Size (µm)	Number In %	Size (µm)	Number In %
0.49	0.00	3.60	11.38	26.20	0.00	190.80	0.00
0.58	0.00	4.19	8.18	30.53	0.00	222.28	0.00
0.67	0.00	4.88	5.55	35.56	0.00	258.95	0.00
0.78	0.00	5.69	3.89	41.43	0.00	301.68	0.00
0.91	0.02	6.63	2.52	48.27	0.00	351.46	0.00
1.06	0.10	7.72	1.56	56.23	0.00	409.45	0.00
1.24	0.36	9.00	0.89	65.51	0.00	477.01	0.00
1.44	1.24	10.48	0.47	76.32	0.00	555.71	0.00
1.68	3.89	12.21	0.23	88.91	0.00	647.41	0.00
1.95	9.96	14.22	0.11	103.58	0.00	754.23	0.00
2.28	17.00	16.57	0.05	120.67	0.00	878.67	0.00
2.65	17.96	19.31	0.02	140.58	0.00		
3.09	14.59	22.49	0.01	163.77	0.00		
3.60		26.20		190.80			

Figure B4-26: Typical spray characteristics; Number (%), particle diameter (µm) and analysis table for test SA-46



Result: Analysis Table

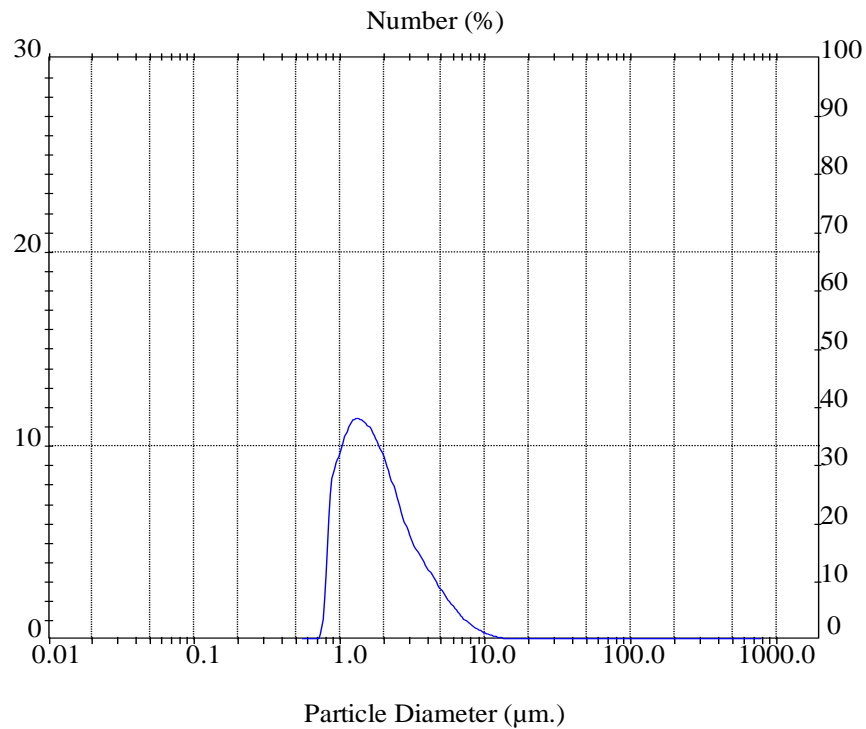
ID:	Run No: 7	Measured: 12/6/2008 12:00PM
File: MUSA	Rec.No: 453	Analysed: 12/6/2008 12:00PM
Path: C:\SIZERS\DATA\		Source: Analysed

Range: 300 mm	Beam: 2.40 mm	Sampler: None	Obs': 8.4 %
Presentation: 3OHD		Analysis: Polydisperse	Residual: 0.526 %
Modifications: -			

Conc. = 0.0055 %Vol	Density = 1.000 g/cm ³	S.S.A = 1.2092 m ² /g
Distribution: Number	D[4, 3] = 7.34 µm	D[3, 2] = 4.96 µm
D(n, 0.1) = 0.83 µm	D(n, 0.5) = 1.39 µm	D(n, 0.9) = 3.60 µm
Span = 1.990E+00	Uniformity = 6.262E-01	

Size (µm)	Number In %						
0.49	0.00	3.60	2.92	26.20	0.00	190.80	0.00
0.58	1.16	4.19	2.33	30.53	0.00	222.28	0.00
0.67	5.29	4.88	1.72	35.56	0.00	258.95	0.00
0.78	10.64	5.69	1.21	41.43	0.00	301.68	0.00
0.91	12.16	6.63	0.79	48.27	0.00	351.46	0.00
1.06	11.96	7.72	0.51	56.23	0.00	409.45	0.00
1.24	11.01	9.00	0.28	65.51	0.00	477.01	0.00
1.44	9.78	10.48	0.14	76.32	0.00	555.71	0.00
1.68	8.40	12.21	0.07	88.91	0.00	647.41	0.00
1.95	6.86	14.22	0.03	103.58	0.00	754.23	0.00
2.28	5.29	16.57	0.01	120.67	0.00	878.67	0.00
2.65	4.06	19.31	0.00	140.58	0.00		
3.09	3.38	22.49	0.00	163.77	0.00		
3.60		26.20	0.00	190.80	0.00		

Figure B4-27: Typical spray characteristics; Number (%), particle diameter (μm) and analysis table for test SA-48



Result: Analysis Table

ID:	Run No: 14	Measured: 12/6/2008 13:46PM
File: MUSA	Rec. No: 463	Analysed: 12/6/2008 13:46PM
Path: C:\SIZERS\DATA\		Source: Analysed

Range: 300 mm	Beam: 2.40 mm	Sampler: None	Obs': 8.5 %
Presentation: 3OHD		Analysis: Polydisperse	Residual: 0.515 %
Modifications: -			

Conc. = 0.0067 %Vol	Density = 1.000 g/cm ³	S.S.A.= 1.0045 m ² /g
Distribution: Number	D[4,3] = 18.16 µm	D[3,2] = 5.97 µm
D(n,0.1) = 0.97 µm	D(n,0.5) = 1.70 µm	D(n,0.9) = 4.15 µm
Span = 1.877E+00	Uniformity = 5.966E-01	

Size (um)	Number In %						
0.49	0.00	3.60	3.89	26.20	0.00	190.80	0.00
0.58	0.00	4.19	3.11	30.53	0.00	222.28	0.00
0.67	0.00	4.88	2.33	35.56	0.00	258.95	0.00
0.78	6.34	5.69	1.66	41.43	0.00	301.68	0.00
0.91	9.44	6.63	1.11	48.27	0.00	351.46	0.00
1.06	10.95	7.72	0.70	56.23	0.00	409.45	0.00
1.24	11.38	9.00	0.42	65.51	0.00	477.01	0.00
1.44	11.05	10.48	0.24	76.32	0.00	555.71	0.00
1.68	10.21	12.21	0.12	88.91	0.00	647.41	0.00
1.95	8.96	14.22	0.06	103.58	0.00	754.23	0.00
2.28	7.41	16.57	0.03	120.67	0.00	878.67	0.00
2.65	5.87	19.31	0.01	140.58	0.00		
3.09	4.72	22.49	0.00	163.77	0.00		
3.60		26.20		190.80			

Figure B4-28: Typical spray characteristics; Number (%), particle diameter (µm) and analysis table for test SA-49

Appendix C: Normalisation Table

Production ID

Plant ID

Carbon quantity
Syngas volume
Hydrogen volume
Carbon Cash Flow
Syngas Cash Flow
Hydrogen Cash Flow

Price ID

Cost ID

Multitubular Membrane Price
Stack Price
Spray Liquid Catalyst Price
Furnace Price
Gas Price
Carbon price
Hydrogen price
Syngas price

Cost ID

Record ID

Spraying Cost
Multitubular Membrane Installation Cost
Furnace Installation Cost
Stack Installation Cost
Spray Equipment Installation Cost
Multitubular Membrane Maintenance Cost
Furnace Maintenance Cost
Spray Equipment Maintenance Cost
Stack Maintenance Cost
Utility Cost

Appendix D: Visual Basic Scripts

Flaring form:

```
PublicClass FlaringGasPlantForm4
'Dim StackPrice, StackInstallationCost, StackMaintenanceCost,totalcost1,
StackUtilityCost, EnvironmentalCost, FlaringAuxiliary As Double
Dim StackFixedCost, StackVariableCost AsDouble

PrivateSub Button1_Click(ByVal sender As System.Object, ByVal e As
System.EventArgs) Handles Button1.Click
    StackFixedCost = StackPrice + StackInstallationCost
    TextBox1.Text = StackFixedCost
    StackVariableCost = StackMaintenanceCost + StackUtilityCost
    TextBox2.Text = StackVariableCost
    totalcost1 = StackFixedCost + StackVariableCost + EnvironmentalCost +
FlaringAuxiliary
    TextBox4.Text = totalcost1
    TextBox3.Text = FlaringAuxiliary
EndSub
```

Syngas recycling form:

```
PublicClass RecyclingGasPlantForm3
'Dim MultitubularMembranePrice, MultitubularMembraneInstallationCost,
MultitubularMembraneMaintenanceCost, SyngasUtilityCost As Double
'dim SyngasVolume, SyngasPrice as double
'Dim SyngasCashFlow, SyngasAuxiliary, totalcost2 As Double
Dim syngasfixedcost, syngasvariablecost AsDouble

PrivateSub Button1_Click(ByVal sender As System.Object, ByVal e As
System.EventArgs) Handles Button1.Click
syngasfixedcost = MultitubularMembranePrice +
MultitubularMembraneInstallationCost
    TextBox1.Text = syngasfixedcost
syngasvariablecost = MultitubularMembraneMaintenanceCost + SyngasUtilityCost
    TextBox2.Text = syngasvariablecost
    SyngasCashFlow = SyngasPrice * SyngasVolume
totalcost2 = syngasfixedcost + syngasvariablecost - SyngasCashFlow +
SyngasAuxiliary
    TextBox4.Text = totalcost2
    TextBox3.Text = SyngasAuxiliary
EndSub
```

Carbonnanotubes recycling form:

```
PublicClass RecyclingGasPlantFormC
'Dim FurnacePrice, FurnaceInstallationCost, FurnaceMaintenanceCost,
SprayingEquipmentPrice, SprayLiquidCatalystPrice, SprayEquipmentInstallationCost
As Double
'Dim SprayEquipmentMaintenanceCost, CabonNanotubesUtilityCost,
CarbonCashFlow, nanotubeAuxiliary, HydrogenCashFlow,
SprayLiquidCatalystVolume, totalcost3 As Double
'dim HydrogenPrice, HydrogenVolume, CarbonPrice, CarbonQuantity as double
Dim carbonanotubesFixedcost, carbonanotubesVariablecost AsDouble
```

```
PrivateSub Button5_Click(ByVal sender As System.Object, ByVal e As
System.EventArgs) Handles Button5.Click
    carbonanotubesFixedcost = FurnacePrice + FurnaceInstallationCost +
SprayingEquipmentPrice + SprayEquipmentInstallationCost
    TextBox1.Text = carbonanotubesFixedcost
    carbonanotubesVariablecost = FurnaceMaintenanceCost +
SprayEquipmentMaintenanceCost + (SprayLiquidCatalystPrice *
SprayLiquidCatalystVolume) + CabonNanotubesUtilityCost
    TextBox2.Text = carbonanotubesVariablecost
    CarbonCashFlow = CarbonQuantity * CarbonPrice
    HydrogenCashFlow = HydrogenVolume * HydrogenPrice
    totalcost3 = carbonanotubesFixedcost + carbonanotubesVariablecost -
CarbonCashFlow - HydrogenCashFlow + nanotubeAuxiliary
    TextBox4.Text = totalcost3
    TextBox3.Text = nanotubeAuxiliary
```

```
PublicClass ComparisonForm2
```

```
PrivateSub Button2_Click(ByVal sender As System.Object, ByVal e As
System.EventArgs)
Me.Hide()
    MainMenuForm1.Show()
EndSub
```

```
PrivateSub Button3_Click(ByVal sender As System.Object, ByVal e As
System.EventArgs)
Me.Hide()
    FlaringGasPlantForm4.Show()
EndSub
```

```
PrivateSub Button1_Click(ByVal sender As System.Object, ByVal e As
System.EventArgs)
Me.Hide()
    RecyclingGasPlantForm3.Show()
EndSub
```

```

PrivateSub Button2_Click_1(ByVal sender As System.Object, ByVal e As
System.EventArgs) Handles Button2.Click
Me.Hide()
    MainMenuForm1.Show()
EndSub

```

```

PrivateSub Button3_Click_1(ByVal sender As System.Object, ByVal e As
System.EventArgs) Handles Button3.Click
Me.Hide()
    RecyclingGasPlantForm3.Show()
EndSub

```

```

PrivateSub Button6_Click(ByVal sender As System.Object, ByVal e As
System.EventArgs) Handles Button6.Click
Me.Hide()
    RecyclingGasPlantFormC.Show()
EndSub

```

```

PrivateSub Button1_Click_1(ByVal sender As System.Object, ByVal e As
System.EventArgs) Handles Button1.Click
Me.Hide()
    FlaringGasPlantForm4.Show()
EndSub

```

```

PrivateSub Button4_Click(ByVal sender As System.Object, ByVal e As
System.EventArgs) Handles Button4.Click
    TextBox1.Text = totalcost1
    TextBox2.Text = totalcost2
    TextBox3.Text = totalcost3
If totalcost1 < totalcost2 And totalcost3 = 0 Then
    Label3.Text = "FLARING IS THE MOST ECONOMIC BUT TRY
RECYCLING TO CARBON NANOTUBES "
ElseIf totalcost1 >= totalcost2 And totalcost3 = 0 Then
    Label3.Text = "RECYCLING TO SYNGAS BY USING MEMBRANE TUBES
IS THE MOST ECONOMIC "
ElseIf totalcost1 = 0 And totalcost2 = 0 And totalcost3 = 0 Then
    Label3.Text = "Sorry, No results, invalid comparison option, please select your
row "
ElseIf totalcost1 < totalcost3 And totalcost2 = 0 Then
    Label3.Text = "FLARING IS THE MOST ECONOMIC BUT TRY
RECYCLING TO SYNGAS BY USING MEMBRANE TUBES "
ElseIf totalcost1 >= totalcost3 And totalcost2 = 0 Then
    Label3.Text = "RECYCLING TO CARBON NANOTUBES IS THE MOST
ECONOMIC "
ElseIf totalcost1 <= totalcost2 And totalcost1 > totalcost3 Then
    Label3.Text = "RECYCLING TO CARBON NANOTUBES IS THE MOST
ECONOMIC "

```

```

ElseIf totalcost1 <= totalcost3 And totalcost1 > totalcost2 Then
    Label3.Text = "RECYCLING TO SYNGAS BY USING MEMBRANE TUBES
IS THE MOST ECONOMIC "
ElseIf totalcost1 > totalcost2 And totalcost1 > totalcost3 And totalcost2 > totalcost3
Then
    Label3.Text = "RECYCLING TO CARBON NANOTUBES IS THE MOST
ECONOMIC "
ElseIf totalcost1 > totalcost2 And totalcost1 > totalcost3 And totalcost3 > totalcost2
Then
    Label3.Text = "RECYCLING TO SYNGAS BY USING MEMBRANE TUBES
IS THE MOST ECONOMIC "
ElseIf totalcost1 > totalcost2 And totalcost1 > totalcost3 And totalcost2 = totalcost3
Then
    Label3.Text = " BOTH OPTIONS OF RECYCLING ARE MORE ECONOMIC
THAN FLARING "
ElseIf totalcost1 < totalcost2 And totalcost1 < totalcost3 And totalcost2 > totalcost3
Then
    Label3.Text = " FLARING BUT RECYCLING CARBON NANOTUBES
METHOD IS MORE ECONOMIC THAN SYNGAS(THINK ABOUT THE
ENVIRONMENT)"
ElseIf totalcost1 < totalcost2 And totalcost1 < totalcost3 And totalcost3 > totalcost2
Then
    Label3.Text = " FLARING BUT RECYCLING SYNGAS IS MORE
ECONOMIC THAN CARBON NANOTUBES(THINK ABOUT THE
ENVIRONMENT) "
ElseIf totalcost1 < totalcost2 And totalcost1 < totalcost3 And totalcost2 = totalcost3
Then
    Label3.Text = " FLARING BUT THINK ABOUT SAVING WITH STORAGE
OPTION "
EndIf
EndSub
EndClass

```

Get data module:

```

Module Data
Public MultitubularMembraneInstallationCost AsSingle
Public FurnaceInstallationCost AsSingle
Public StackInstallationCost AsSingle
Public SprayEquipmentInstallationCost AsSingle
Public MultitubularMembraneMaintenanceCost AsSingle
Public FurnaceMaintenanceCost AsSingle
Public SprayEquipmentMaintenanceCost AsSingle
Public StackMaintenanceCost AsSingle
Public EnvironmentalCost AsSingle
Public StackUtilityCost AsSingle

```

```

Public SyngasUtilityCost AsSingle
Public CabonNanotubesUtilityCost AsSingle
Public PlantType AsSingle
Public PlantLocation AsSingle
Public PlantCapacity AsSingle
Public EquipmentType AsSingle
Public MultitubularMembranePrice AsSingle
Public StackPrice AsSingle
Public SprayingEquipmentPrice AsSingle
Public SprayLiquidCatalystPrice AsSingle
Public FurnacePrice AsSingle
Public FinalProductType AsSingle
Public ProcessType AsSingle
Public SprayLiquidCatalystVolume AsSingle
Public CarbonCashFlow AsSingle
Public SyngasCashFlow AsSingle
Public HydrogenCashFlow AsSingle
Public CarbonQuantity AsSingle
Public CarbonPrice AsSingle
Public HydrogenPrice AsSingle
Public HydrogenVolume AsSingle
Public SyngasVolume AsSingle
Public SyngasPrice AsSingle
Public DateOfRecord AsSingle
Public YearOfCostAssessment AsSingle
Public FlaringFinalCost AsSingle
Public SyngasFinalCost AsSingle
Public CarbonFinalCost AsSingle
Public FlaringAuxiliary AsSingle
Public SyngasAuxiliary AsSingle
Public nanotubeAuxiliary AsSingle
Public totalcost1 AsSingle
Public totalcost2 AsSingle
Public totalcost3 AsSingle
Public con AsNew OleDb.OleDbConnection
Public DS AsNew DataSet
Public DA As OleDb.OleDbDataAdapter
Public Sql AsString
Public maxRows AsInteger
Public INC AsInteger

PublicSub LoadDB()
    con.ConnectionString = "PROVIDER=Microsoft.Jet.OLEDB.4.0;Data Source =
C:\database\FinalProjectDataBase.mdb"
    con.Open()
    MsgBox("A Connection to the Database is now open")
    con.Close()
    MsgBox("The Connection to the Database is now Closed")

```

```
Sql = "SELECT * FROM COST"  
DA = New OleDb.OleDbDataAdapter(Sql, con)  
DA.Fill(DS, "COST")
```

```
Sql = "SELECT * FROM PLANT"  
DA = New OleDb.OleDbDataAdapter(Sql, con)  
DA.Fill(DS, "PLANT")
```

```
Sql = "SELECT * FROM PRICE"  
DA = New OleDb.OleDbDataAdapter(Sql, con)  
DA.Fill(DS, "PRICE")
```

```
Sql = "SELECT * FROM PRODUCTION"  
DA = New OleDb.OleDbDataAdapter(Sql, con)  
DA.Fill(DS, "PRODUCTION")
```

```
Sql = "SELECT * FROM RECORD"  
DA = New OleDb.OleDbDataAdapter(Sql, con)  
DA.Fill(DS, "RECORD")
```

EndSub

PublicSub getData(ByVal x AsInteger)

 x -= 1

OnErrorResumeNext

 MultitubularMembraneInstallationCost =

 DS.Tables("COST").Rows(x).Item("MultitubularMembraneInstallationCost")

 FurnaceInstallationCost =

 DS.Tables("COST").Rows(x).Item("FurnaceInstallationCost")

 StackInstallationCost =

 DS.Tables("COST").Rows(x).Item("StackInstallationCost")

 SprayEquipmentInstallationCost =

 DS.Tables("COST").Rows(x).Item("SprayEquipmentInstallationCost")

 MultitubularMembraneMaintenanceCost =

 DS.Tables("COST").Rows(x).Item("MultitubularMembraneMaintenanceCost")

 FurnaceMaintenanceCost = DS.Tables("COST

").Rows(x).Item("FurnaceMaintenanceCost ")

 SprayEquipmentMaintenanceCost = DS.Tables("COST

").Rows(x).Item("SprayEquipmentMaintenanceCost ")

 StackMaintenanceCost =

 DS.Tables("COST").Rows(x).Item("StackMaintenanceCost")

 EnvironmentalCost = DS.Tables("COST").Rows(x).Item("EnvironmentalCost")

 StackUtilityCost = DS.Tables("COST").Rows(x).Item("StackUtilityCost")

 SyngasUtilityCost = DS.Tables("COST").Rows(x).Item("SyngasUtilityCost")

 CabonNanotubesUtilityCost =

 DS.Tables("COST").Rows(x).Item("CabonNanotubesUtilityCost")

 PlantType = DS.Tables("PLANT").Rows(x).Item("PlantType")

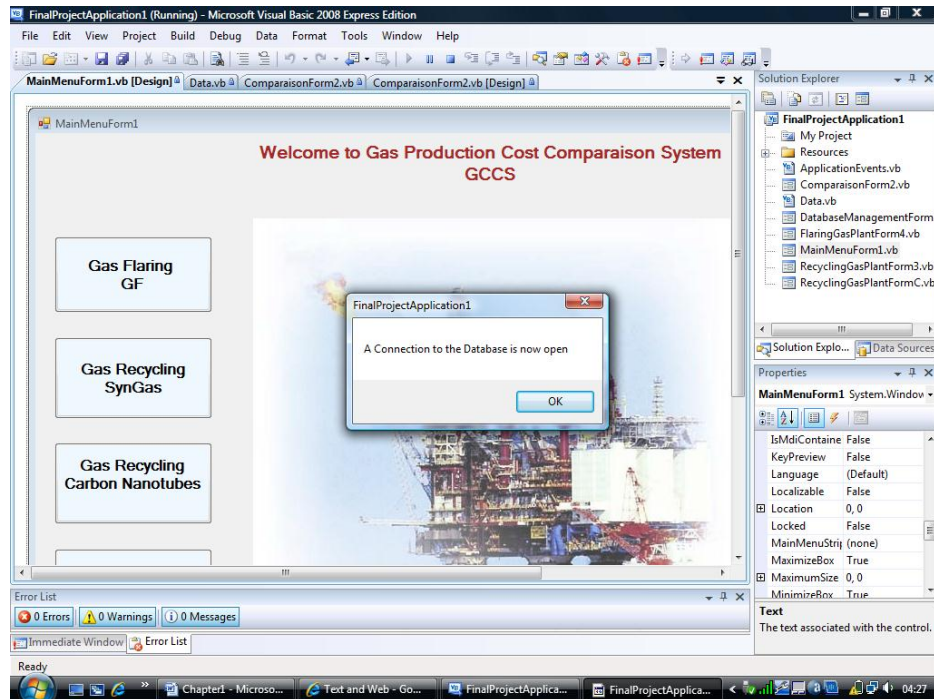
PlantLocation = DS.Tables("PLANT").Rows(x).Item("PlantLocation")
PlantCapacity = DS.Tables("PLANT").Rows(x).Item("PlantCapacity")
EquipmentType = DS.Tables("PLANT").Rows(x).Item("EquipmentType")

MultitubularMembranePrice =
DS.Tables("PRICE").Rows(x).Item("MultitubularMembranePrice")
StackPrice = DS.Tables("PRICE").Rows(x).Item("StackPrice")
SprayingEquipmentPrice =
DS.Tables("PRICE").Rows(x).Item("SprayingEquipmentPrice")
SprayLiquidCatalystPrice =
DS.Tables("PRICE").Rows(x).Item("SprayLiquidCatalystPrice")
FurnacePrice = DS.Tables("PRICE").Rows(x).Item("FurnacePrice")
GasPrice = DS.Tables("PRICE").Rows(x).Item("GasPrice")
SyngasPrice = DS.Tables("PRICE").Rows(x).Item("SyngasPrice")
CarbonPrice = DS.Tables("PRICE").Rows(x).Item("CarbonPrice")
HydrogenPrice = DS.Tables("PRICE").Rows(x).Item("HydrogenPrice")

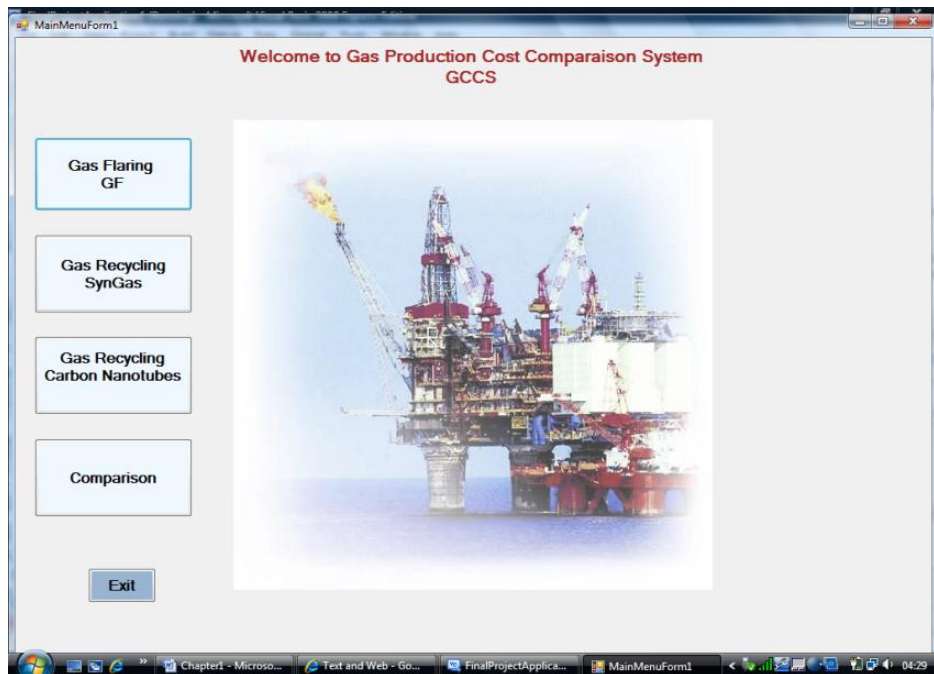
FinalProductType =
DS.Tables("PRODUCTION").Rows(x).Item("FinalProductType")
ProcessType = DS.Tables("PRODUCTION").Rows(x).Item("ProcessType")
SprayLiquidCatalystVolume =
DS.Tables("PRODUCTION").Rows(0).Item("SprayLiquidCatalystVolume")
GasVolume = DS.Tables("PRODUCTION").Rows(x).Item("GasVolume")
CarbonCashFlow =
DS.Tables("PRODUCTION").Rows(x).Item("CarbonCashFlow")
SyngasCashFlow =
DS.Tables("PRODUCTION").Rows(x).Item("SyngasCashFlow")
HydrogenCashFlow =
DS.Tables("PRODUCTION").Rows(x).Item("HydrogenCashFlow")
CarbonQuantity = DS.Tables("PRODUCTION").Rows(x).Item("CarbonQuantity")
SyngasVolume = DS.Tables("PRODUCTION").Rows(x).Item("SyngasVolume")
HydrogenVolume =
DS.Tables("PRODUCTION").Rows(x).Item("HydrogenVolume")
DateOfRecord = DS.Tables("RECORD").Rows(x).Item("DateOfRecord")
YearOfCostAssessment =
DS.Tables("RECORD").Rows(x).Item("YearOfCostAssessment")
FlaringFinalCost = DS.Tables("RECORD").Rows(x).Item("FlaringFinalCost")
SyngasFinalCost = DS.Tables("RECORD").Rows(x).Item("SyngasFinalCost")
CarbonFinalCost = DS.Tables("RECORD").Rows(x).Item("CarbonFinalCost")

EndSub
EndModule

Appendix E: VB programme Testing Results



A message has been clearly displayed to show the connection with the database



The debug has been set on the mainmenu form

FlaringGasPlantForm4

Gas Flaring Plant

Fixed cost 55000

Variable cost 28000

Auxiliaire Cost 0

Please select the appropriate row and press total

1

Total

Your Final cost for Plant1 GFP is 93000

Exit

First form for flaring option

RecyclingGasPlantForm3

Gas Recycling Syngas

Fixed cost 34000

Variable Cost 0

Auxiliaire cost 0

Please select the appropriate row and press total

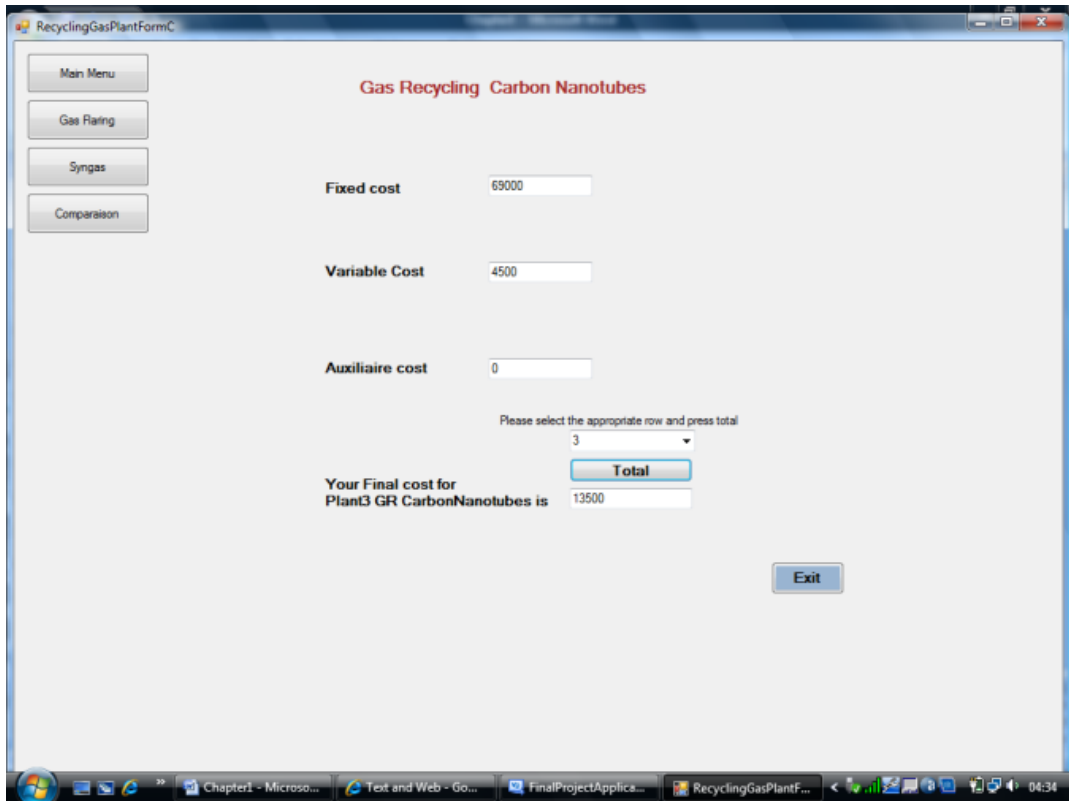
1

Total

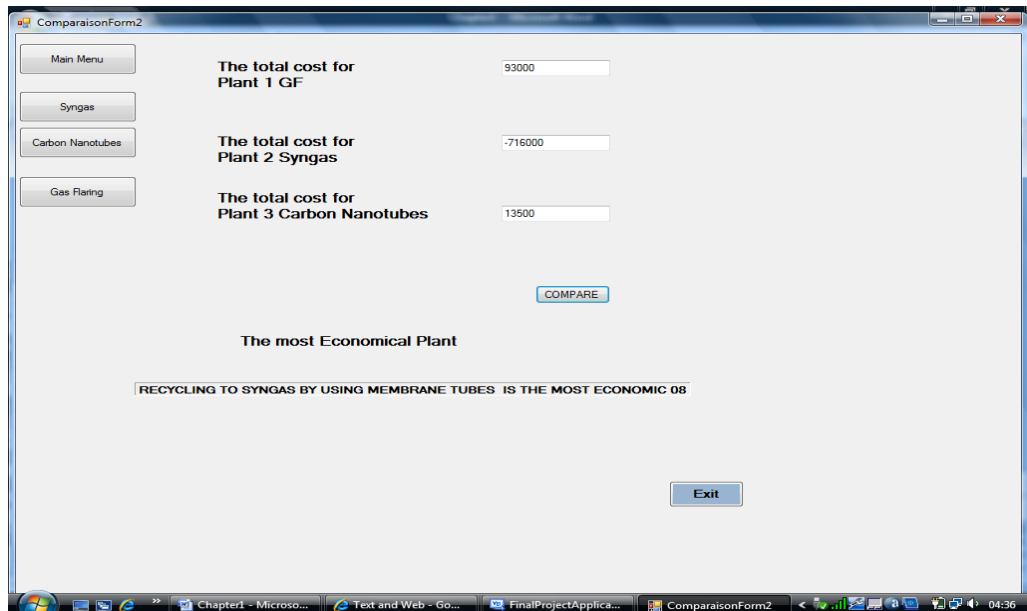
Your Final cost for Plant2 GR Syngas is -716000

Exit

Second form for recycling option1



Third form for recycling option 2



The final form shows the comparison

Appendix F: User Guide for CCS System

F1: Introduction

This manual contains all the information you need to initially install and operate the CCS system and it will help you globally to get started. Some instructions have to be followed before the final installation of the programme.

If this instruction does not give an answer to your problem, consult the last part of this manual, where you can find instructions to solve some of difficulties you could meet while installing or manipulating the programme.

F2: Important information

The software has been specifically designed for gas cost comparisons, and the formulas used are particularly related to the gas economic analysis.

Therefore, any use of the software for another purpose will never give a correct estimation.

The set up of the programme does not necessarily require the visual basic software installation, as the part handed to the user is an executable version of the application.

The programme is directly linked to a database specifically designed to hold the entire information associated to the comparison, so it is imperative to install this database (provided with the programme).

Additionally, this has to be installed in the recommended drive with the correct file name. If not, the database will not be approved by the software and the application will not be activated.

As the CCS system will be used for sensitive purposes, mainly economic analysis, the data holds have to be protected. For that reason, a password has been set up.

F3: Installation

The CCS programme is not complex to set up, as the Visual Basic software does not need to be installed to run the application. Simply save it in the C drive or desktop of your computer.

The database provided needs to be saved in the C Drive with the exact file name.

- i. Insert the CD or the USB Key
- ii. Open the file, you will see a file called **database**
- iii. Save it as document in **C Drive** without changing the name.

The programme and the database are completely linked to each other, but if one of them is unsuccessfully saved the application will not work.

Once both programme and database are installed the whole application is ready for use.

The instructions to utilise the application are detailed in the section how to use the CCS system.

F4: How to use CCS system

F4.1 Database

Before starting to use the programme you have to store your data in the database.

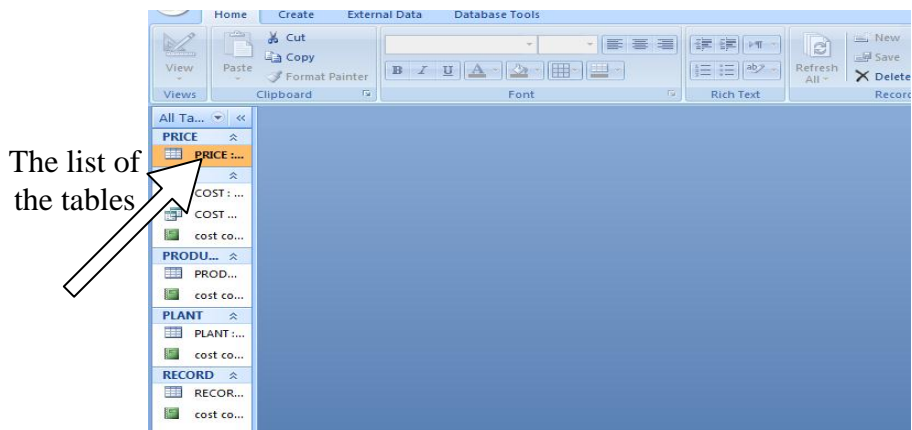
Note that it is necessary to store some data as the calculation depends on them.

This is a list of the data that need to be obligatorily entered in the database to run the programme properly.

- Multitubular Membrane Installation Cost
- Furnace Installation Cost
- Stack Installation Cost
- Spray Equipment Installation Cost
- Multitubular Membrane Maintenance Cost
- Furnace Maintenance Cost
- Spray Equipment Maintenance Cost
- Stack Maintenance Cost
- Environmental Cost
- Stack Utility Cost
- Syngas Utility Cost
- Carbon Nanotubes Utility Cost
- Multitubular Membrane Price
- Stack Price
- Spraying Equipment Price
- Spray Liquid Catalyst Price
- Carbon Cash Flow
- Syngas Cash Flow
- Hydrogen Cash Flow
- Carbon Quantity
- Carbon Price
- Hydrogen Price
- Hydrogen Volume
- Syngas Volume
- Syngas Price
- Flaring Auxiliary
- Syngas Auxiliary
- Nanotube Auxiliary
- Furnace Price
- Spray Liquid Catalyst Volume

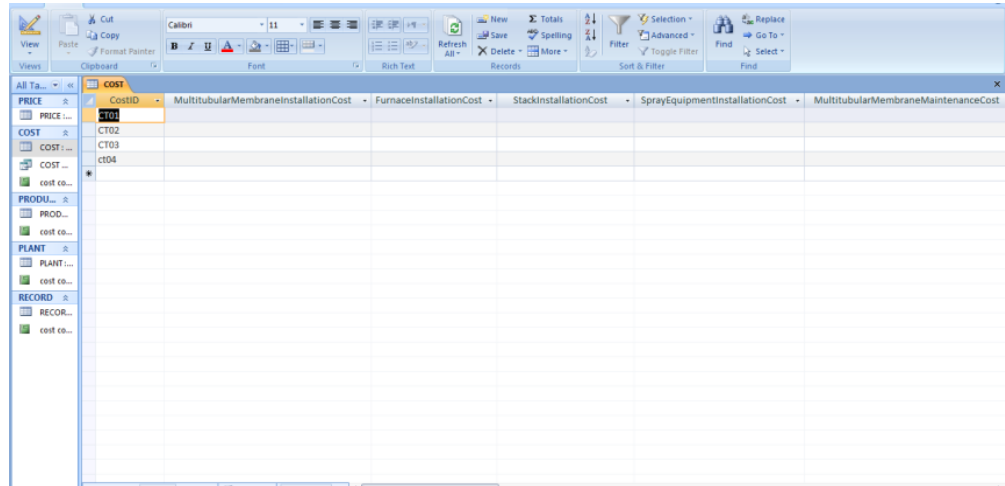
The data have to be stored in order to ensure that they will be selected from the row for the programme.

1. When you double click in the database the following screen will show up:

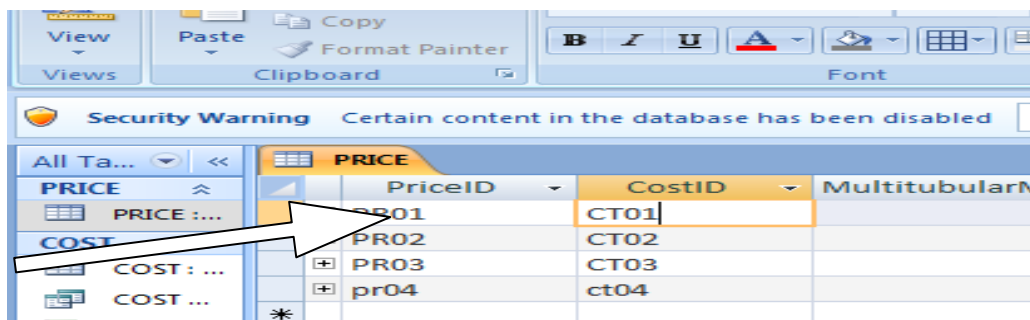


2. On the left hand side of the screen you will see the list of the tables. Simply double click on the titles and you will have the tables ready to fill.

- Each row corresponds to one cost assessment. Just check the title of the column and put in the correspondent data.
- The database sheet looks like this.



- The ID's are important as the user has to give an ID in each row (eg: ID PR01 means ID for production, row number 01).It is the first column of the table. The other ID's present in the same table are taken from tables, which correspond to the same assessment of cost, and means the same row number from another table.

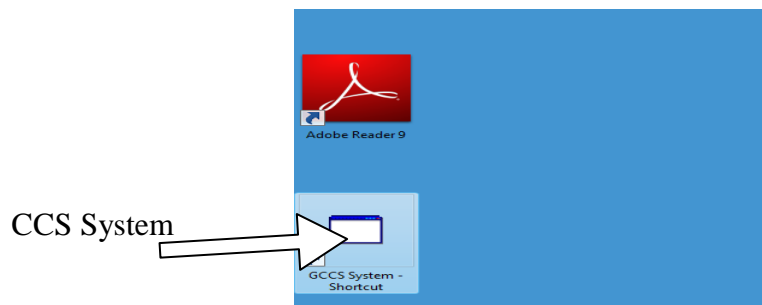


Example: The price ID PR01 shown in the table above is from the price table and CT01 is the cost ID for the same cost assessment, and is brought from the cost table to link the data between the two tables.

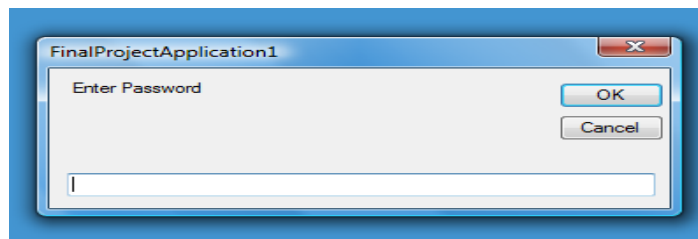
F4.2: CCS programme

The following instructions explain how to run the CCS programme.

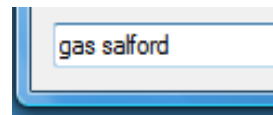
1. Double click on the shortcut entitled “**CCS System**” on the desktop, it should look like this:



2. Then, the following screen will show up:



3. The password that you have to enter is: “gas salford”, you have to type it exactly

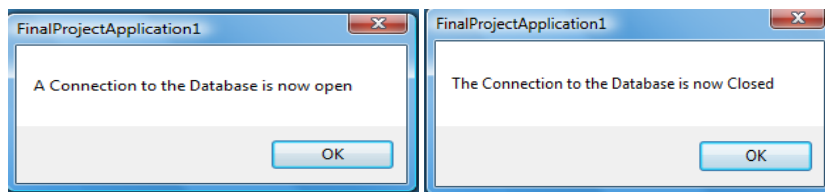


as it appears within the space: and click **OK**. The following form will show up and this will give you access to the system



4. Click on “ please enter the main menu”

You will see two little windows shown in sequence one after the other, so just click **OK**.



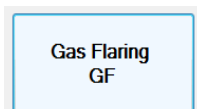
These two windows represent the link with the database, and open and close the connection between the application and the database.

The statement “the connection to the database is now closed” means the connection will be automatically closed at the end of using the application.

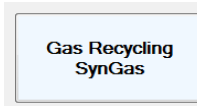
5. The following screen will show up:



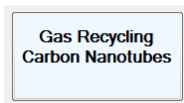
In this window, there are five buttons.



This button gives access to the Gas Flaring form, to assess the cost for the flaring option.



This button gives access to the Gas Recycling to Syngas form, to assess the cost for the recycling to syngas option.



This button gives access to the Gas Recycling Carbon Nanotubes form, to assess the cost for the recycling to carbon Nanotubes option.

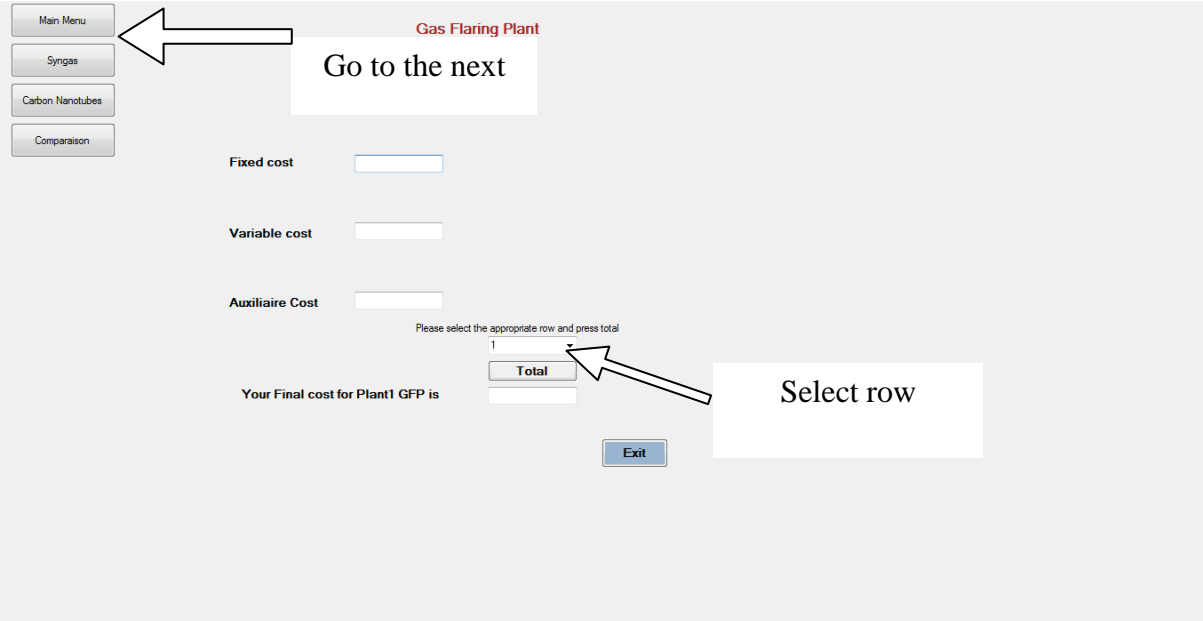


This button gives access to the Comparison form, to make the cost comparison between the three previous options.



This button is for the Exit from the entire system.

- When you access any of the three first forms (gas flaring form, gas recycling to syngas form, gas recycling carbon Nanotubes form), a screen like the following one will show up.



The screenshot shows a web form titled "Gas Flaring Plant". On the left, there is a vertical menu with buttons for "Main Menu", "Syngas", "Carbon Nanotubes", and "Comparison". A white arrow points from the "Main Menu" button to the right. The main content area has a white box with the text "Go to the next" and another white box with "Select row". The form contains three input fields labeled "Fixed cost", "Variable cost", and "Auxiliaire Cost". Below these is a table with a single row containing a "Total" button. A white arrow points from the "Total" button to the right. Below the table is a label "Your Final cost for Plant1 GFP is" followed by an empty input field. At the bottom right, there is an "Exit" button.

All you have to do is to **select the row number** where your information is saved in the database, then click **total**, but do not exit the page as it will exit from the system.

This action will display for you: the fixed cost, the variable cost, any additional cost in auxiliary cost textbox and the final cost for the flaring option. The system will simply extract all the information from the database, apply the corresponding calculations and clearly display the total cost for this option.

The next step is to select your second option that you want to assess and follow exactly the same steps from step (6.). This action has to be applied for the next three options, without exiting the system.

- Once you assess the cost for the three options, just go to the comparison form. Click on the **compare** button, the system will automatically display the three results for the three last options and which option is the most economic. The comparison cannot be done from the beginning, or directly from the main menu access, as the costs have to be calculated in the other forms first.

The total cost for Plant 1 GF	17
The total cost for Plant 2 Syngas	14
The total cost for Plant 3 Carbon Nanotubes	2

The most Economical Plant

RECYCLING TO CARBON NANOTUBES IS THE MOST ECONOMIC

- When you want to proceed to the next comparison, replace the cost results in their textboxes (excluding the total cost) by the value '0', select your new row number again and follow exactly the same steps as previously explained.
- The number of rows is limited to 10, so once all ten rows are completed, you have to store your data in another file for your own record, and clear them from the database to use the rows for new data. You still can save the three final results calculated by the system in the table called **'record'**.
- If the rows are empty the system will automatically pick any option to suggest for the comparison or will display this message:

‘Sorry, No results, invalid comparison option, please select your row’.

Suggestion:

If your installation was successful but the application still does not open, it will be advisable to install Visual Basic software. It is not necessary to have a professional version of Visual Basic: free express version is available to download online.

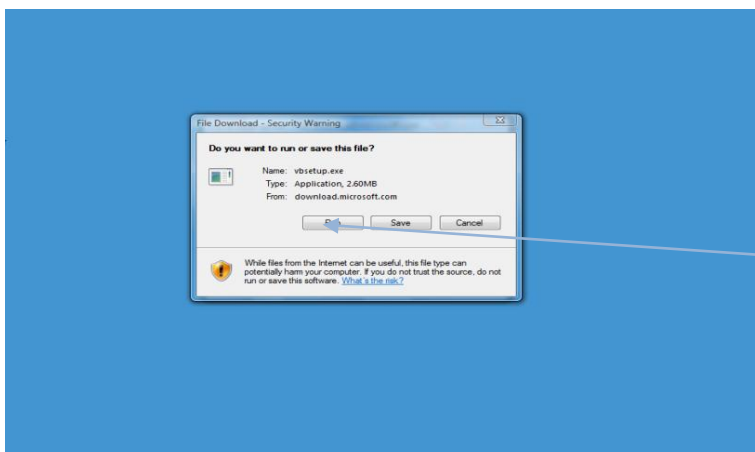
For security reason, the best website to download this version is:

<http://www.microsoft.com/express/vb/Default.aspx>



Select the language and click download

Then, run the file to install it.



Run the file

Once VB is installed, simply save the CCS programme in the **C Drive**, and it will be ready to use.

Note: A registration for the software could be needed to validate the download. A link to the registration section will be proposed, so, just follow the steps. A restart of the computer could be required.

If the access to the system from the desktop gives you a **denied access** message, the VB software installation is the solution and you can open the system from VB.

Appendix G: Comparison and Economic Analysis Results

YEARS	1	2	3	4	5	
Stack Price(K£)	360.000	0	0	0	0	
Stack Installation Costs(K£)	201.780	0	0	0	0	
Stack Fixed Costs(K£)	561.780	0	0	0	0	
Stack Maintenance Costs(K£)	32.552	62.552	62.552	62.552	75.062	
Stack Utility Costs(K£)	8.071	8.071	9.685	9.685	9.685	
Stack Variable Costs(K£)	40.623	70.623	72.237	72.237	84.747	
Environmental Costs(K£)	1800.000	2800.000	3200.000	3200.000	3500.000	
Flaring Auxiliary Costs(K£)	1114.446	130.653	133.638	133.638	156.782	
						Total
Total Costs(K£)	3516.849	3001.276	3405.875	3405.875	3741.529	17071.405

Table G-1: Scenario 1: gas flaring

YEARS	1	2	3	4	5	
Multitubular Membrane Price(K£)	177	0	0	0	0	
Multitubular Membrane Installation Costs(K£)	100.89	0	0	0	0	
Syngas Fixed Costs(K£)	277.89	0	0	0	0	
Multitubular Membrane Maintenance Costs(K£)	31.276	31.276	36.906	36.906	36.906	
Syngas Utility Costs(K£)	4.036	4.036	4.762	4.762	7.476	
Syngas Variable Costs(K£)	35.312	35.312	41.668	41.668	44.382	
Syngas Auxiliary Costs(K£)	579.423	65.326	77.085	77.085	82.107	
Syngas Volume(K£)	420.000	420.000	420.000	560.000	560.000	
Syngas Price(£/m ³)	0.036	0.036	0.036	0.036	0.045	
Syngas Cash Flow(K£)	15.120	15.120	15.120	20.160	25.200	
						Total
Total Costs(K£)	877.504	85.518	103.633	98.593	101.288	1266.536

Table G-2: Scenario 2, option 1: conversion to syngas

YEARS	1	2	3	4	5	
Furnace Price(K£)	141.600	0	0	0	0	
Furnace Installation Costs(K£)	80.712	0	0	0	0	
Spraying Equipment Installation Costs(K£)	53.808	0	0	0	0	
Carbon Nanotubes Fixed Costs(K£)	276.120	0	0	0	0	
Furnace Maintenance Costs(K£)	25.021	25.021	25.021	29.524	29.524	
Spray Equipment Maintenance Costs(K£)	11.219	11.219	11.219	11.219	11.219	
Spray Liquid Catalyst Price(£/m ³)	0.480	0.480	0.480	0.480	0.520	
Spray Liquid Catalyst Volume(Km ³)	15.000	15.000	15.000	18.000	18.000	
Carbon Nanotubes Utility Costs(K£)	3.823	3.823	3.823	7.455	7.455	
Carbon Nanotubes Variable Costs(K£)	47.263	47.263	47.263	56.838	57.558	
Carbon Nanotubes Auxiliary Costs(K£)	598.259	87.437	87.437	105.151	106.483	
Carbon Volume(Km ³)	240.000	240.000	240.000	240.000	240.000	
Carbon Price(£/m ³)	0.220	0.250	0.250	0.250	0.250	
Carbon Cash Flow(K£)	52.800	60.000	60.000	60.000	60.000	
Hydrogen Volume(Km ³)	24.000	24.000	24.000	56.000	62.000	
Hydrogen Price(£/m ³)	0.760	0.760	0.760	0.760	0.840	
Hydrogen Cash Flow(K£)	18.240	18.240	18.240	42.560	52.080	
						Total
Total Costs(K£)	850.602	56.460	56.460	59.430	51.962	1074.914

Table G-3: Scenario 2, option 2: conversion to carbon nanotubes

References

REFERENCES

- Aasberg-Petersen, K., Christensen, T. S., Nielsen, C. S. and Dybkjaer, I. (2003): “*Recent developments in autothermal reforming and pre-reforming for synthesis gas production in GTL applications*”, Fuel Processing Technology, **83**, pp. 253 - 261.
- Abashar M. E. E. (2004): “*Coupling of steam and dry reforming of methane in catalytic fluidised bed membrane reactors*”, International Journal of Hydrogen Energy, Vol. **29**, pp. 799 – 808.
- Abdulkareem, A. S. and Kovo, A. S. (2006): “*Urban air pollution by process industry in Kaduna, Nigeria*”, AU Journal of Technology, Vol. **9** (3), pp. 172 - 174.
- Adegoke, A. A. (2006): “*Utilising the heat content of Gas-to-Liquids by-product streams for commercial power generation*”, MSc Thesis, Texas A & M University.
- Alemagi, D. (2007): “*Towards a comprehensive strategy for the effective and efficient management of industrial pollution along the Atlantic coast of Cameroon*”, PhD Thesis, Faculty of Environmental Sciences and Process Engineering, Brandenburg University of Technology in Cottbus, Germany.
- Almeida, E. L. (2003): “*Creating opportunities for Gas-to-Liquids projects through market organisation*”, Presented at Petroleum and Gas Conference, Brazil, (15th -18th June).
- Ardestani M. and Shafie-Pour, M. (2007): “*Environmentally compatible energy resource production — consumption pattern (case study: Iran)*”, Environment,

Development and Sustainability Journal, Springer Netherlands, ISSN: 1387X, pp. 1573 - 2975.

Armor, J. N. (1992): "*Challenges in membrane catalysis*", Chemtech, Vol. 22, pp. 557 - 563.

Armstrong, P. A., Foster, E. P., Horazak, D. A., Morehead, H. T. and Stein, V. E. (2005): "*Ceramic and coal: ITM oxygen for IGCC*", The 22nd International Pittsburgh Coal Conference, Pittsburgh, Pennsylvania, September 11 - 15.

Asaeda, M. and Yamasaki, S. (2001): "*Separation of inorganic/organic gas mixtures by silica membranes*", Separation and Purification Technology, Vol. 25 (1-3), pp. 151 - 159.

Ashcroft, A. T., Cheetham, A. K., Foord, J. S., Green, M. L. H., Grey, C.P. J., Murrell, A. and Vernon, P. D. F. (1990): "*Selective oxidation of methane to synthesis gas using transition metal catalysis*", Nature, Vol. 344, pp. 319 - 321.

Ayala, L. F. (2006): "*Phase behaviour of hydrocarbon fluids – the key to understanding oil and gas engineering systems*". Business Briefing: Oil and Gas Processing Review Report.

Azzopardi, B. J. (1998): "*Atomisation fundamentals*", 12th UMIST Short Course on Atomiser and Spray Technology, UMIST, UK, 17 - 20 March.

Badwal S.P. and Ciacchi, F.T. (2001): "*Ceramic membrane technologies for oxygen separation*", Advanced Materials, Vol. 13 (12-13), pp. 993 – 996.

Balachandran, U., Dusek, J. T., Maiya, P. S., Ma, B., Mieville, R. L., Kleefisch, M. S. and Udovich, C. A. (1997): “*Ceramic membrane reactor for converting methane to syngas*”, Catalysis Today, Vol. **36**, pp. 265 - 272.

Balachandran, U., Dusek, J. T., Mieville, R. L., Poeppel, R. B., Kleefisch, M. S., Pei, S., Kobylinski, T. P, Udovich, C. A. and Bose, A. C. (1995): “*Dense ceramic membranes for partial oxidation of methane to synthesis gas*”, Applied Catalysis A, Vol. **133**, pp. 19 - 29.

Barbieri G., Violante V., Di Maio F. P., Criscuoli A. and Drioli E. (1997): “*Methane steam reforming analysis in a palladium-based catalytic membrane reactor*”, Industrial and Engineering Chemistry Research, Vol. **36** (8), pp. 3369 - 3374.

Beyvel, L. and Orzechowski, Z. (1993): “*Liquid atomisation*”, Taylor and Francis, Philadelphia PA.

Bhalla, A. S., Guo, R. Y. and Roy, R. (2000): “*The perovskite structure – a review of its role in ceramic science and technology*”, Materials Research Innovations, Vol. **4** (1), pp. 3 - 26.

Bhusham, B. (2006): “*Springer handbook of nano-technology*”, Vol. **2**, 2nd Edition.

Bouwmeester H., (2003): “*Dense ceramic membranes for methane conversion*”, Catalysis Today, Vol. **82** (1 – 4), pp. 141 - 150.

- Burggraaf, A. J. (1992): “*Stuijts memorial lecture 1991: Some new developments in ceramic science and technology*”, Journal of European Ceramic Society, Vol. **9** (4), PP. 245 - 250.
- Chai, S. P., Zein, S. H. S. and Mohamed A. R. (2004): “*Review on carbon nanotubes production via catalytic methane decomposition*”, 1st National Postgraduate Colloquies, NAPCOL 2004, School of Chemical Engineering, USM, Malaysia.
- Chan, S. H. and Wang, H. M. (2000): “*Effect of natural gas composition on autothermal fuel reforming products*”, Fuel Processing Technology, Vol. **64** (1-3), pp. 221 - 239.
- Chen, C. H., Kruidhof, H., Bouwmeester, H. J. and Burggraaf, A. J. (1997): “*Ionic conductivity of perovskite LaCoO_3 measured by oxygen permeation technique*”, Journal of Applied Electrochemistry, Vol. **27** (1), pp. 71 – 75.
- Chen, C., Zhang, Z., Jiang, G. Fan, C. and Liu W. (2001): “*Oxygen permeation through $\text{La}_{0.4}\text{Sr}_{0.6}\text{Co}_{0.2}\text{Fe}_{0.8}\text{O}_{3-\delta}$ membrane*”, Chemistry of Materials, Vol. **13** (9), pp. 2797 - 2800.
- Chen, X., Wu N. J. and Ignatiev, A. (1999): “*Structure and conducting properties of $\text{La}_{1-x}\text{Sr}_x\text{CoO}_{3-\delta}$* ”, Journal of European Ceramic Society, Vol. **19** (6-7) pp.819 - 822.
- Choudhary, V. R., Rajput, A. M. and Prabhakar, B. (1992): “*Low temperature oxidative conversion of methane to syngas over NiO-CaO catalyst*”, Catalysis Letters, Vol. **15**, pp. 363 - 370.

- Christiansen, A. C. and Haugland, F. T. (2001): “*Gas flaring and global public goods*”, FNI Report **20** - (2001). Available at: <http://www.fni.no/doc&pdf/FNI-R2001.pdf>, [01/03/2008].
- Elividge, C. D., Baugh, K. E., Tuttle, B. T. Howard, A. T., Pack, D. W., Milesi, C. and Erwin, E. H. (2007): “*A twelve year record of national and global gas flaring volumes estimated using satellite data*”, Final Report to the World Bank.
- Dahlin J., Spanne M., Karlsson D., Dalene M and Skarping G., (2008): “*Size-separated sampling and analysis of isocyanates in workplace aerosols part-I, denuder-cascade impactor sampler*”, Annals of Occupational Hygiene, Vol. **52** (2), pp. 361-374.
- Dai, H., Rinzler, A. G., Nikolaev, P., Thess, A., Colbert, D. T. and Smalley, R.E. (1996): “*Single-wall carbon nanotubes produced by metal-catalysed disproportionation of carbon monoxide*”, Chem. Phys. Letters, Vol. **260**, pp. 471 - 475.
- Dautzenberg, F. M. and Mukherjee, M. (2001): “*Process in intensification using multifunctional reactors*”, Chemical Engineering Science, Vol. **56** (2), pp. 251 - 267.
- De Groote, A. M., and Froment, G. F. (1996): “*Simulation of the catalytic partial oxidation of methane to synthesis gas*”, Applied Catalysis A: General, Vol. **138**, pp. 245 – 264.

- Devold, H. (2009): "Oil and gas production handbook: an introduction to oil and gas production", 2nd edition, ABB Oil and Gas.
- Diethelm, S., Sfeir, J., Clemens, F., Van Herle, J. and Favrat, D. (2004): "*Planar and tubular perovskite-type membrane reactors for the partial oxidation of methane to syngas*", Solid State Electrochemistry, Vol. **8** (9), pp. 61 - 617.
- Diethelm, S., Vanherle, J., Middleton, P. H. and Favrat, D. (2003): "*Oxygen permeation and stability of $La_{0.4}Ca_{0.6}Fe_{1-x}Co_xO_{3-\delta}$ ($x = 0, 0.25, 0.5$) membranes*", Journal of Power Sources, Vol. **118**, pp.270-275.
- Dijk, W. J. (2006): "*Improved permeation setup for dehydration membranes, in MTO*", Chemical Engineering, University of Twente, Netherlands.
- Dixon, A. G. (2001): "*Analysis of intermediate product yield in distributed-feed nonisothermal tubular membrane reactors*", Catalysis Today, Vol. **67**, pp. 189 - 203.
- Dixon, A. G. (2003): "*Recent research in catalytic inorganic membrane reactors*", International Journal of Chemical Reactor Engineering, Vol. **1**, Review R6, pp. 1 - 35.
- Dixon, A.G. (1999): "*Innovations in catalytic inorganic membrane reactors*", in Spivey, J. J. (ed.), Specialist Periodical Reports: Catalysis, Vol. **14**, Royal Society of Chemistry, London, pp. 40-92.

Djumena, S. T. (2004): “*Reducing gas flaring and venting: how a partnership can help achieve success*”, World Bank/ IFC Oil, Gas, Mining and Chemicals Department.

Donaldson, K., Aitken, R., Tran, L., Stone, V., Duffin, R. Forrest, G and Alexande, A. (2006): “*Carbon nanotubes: a review of their properties in relation to pulmonary toxicology and workplace safety*”, Toxicological Sciences, Vol. **92** (1), pp. 5 - 22.

Dong, H., Shao, Z., Xiong, G. Tong, J. Sheng, S. and Yang, W. (2001): “*Investigation on POM reaction in a new perovskite membrane reactor*”, Catalysis Today, Vol. **67**, pp. 3 – 13.

Dresselhaus, M. S., Dresselhaus, G. and Eklund, P.C. (1996): “*Science of fullerenes and carbon nanotubes*”, Academic Press, San Diego, CA.

Dyer, P. N., Richards, R. E., Russek, S. L. and Taylor, D. M. (2000): “*Ion transport membrane technology for oxygen separation and syngas production*”. Solid State Ionics, Vol. **134** (1-2), pp. 21 - 33.

Ebbesen, T. W. and Ajayan, P. M. (1992): “*Large-scale synthesis of carbon nanotubes*”, Nature, Vol. **358**, pp. 220 - 222,

EIA (2006): “*Natural gas processing: the crucial link between natural gas production and its transportation to market*”, Energy Information Administration, Office of Oil and Gas.

- Eliseev, L. O. (2009): “*Gas-to-Liquid technologies*”, Russian Journal of General Chemistry, Vol. **79**, pp. 2509 - 2519.
- Elvidge, C. D., Ziskin, D., Baugh, K. E., Tuttle, B. T., Ghosh, T., Pack, D. W., Erwin, E. H. and Zhizhin, M. (2009): “*A fifteen year record of global natural gas flaring derived from satellite data*”, Energies, Vol. **2**, pp. 595 - 622.
- Evers, A. A. (2008): “*Actual worldwide hydrogen production*”, Poster presentation, Hannover FAIR Presentation. Available at: <http://www.fair-pr.de/background/worldwide-hydrogen-production-analysis.php>.
[12/05/2009].
- Feng, S. J., Ran, S., Zhu, D. C., Liu, W. and Chen, C. S. (2004): “*Synthesis gas production from methane with $SRFeCo_{0.5}O_y$ membrane reactor*”, Energy & Fuel, Vol. **18**, pp. 385 – 389.
- Gallucci F., Basile A., Iulianelli, A. and Kuipers, H. J. A. M. (2009): “*A review on patents for hydrogen production using membrane reactors*”, Recent Patents on Chemical Engineering, Vol. **2**, pp. 207 - 222.
- Gao, W. and Sammes, N. M. (1999): “*An introduction to electronic materials*”, World Scientific, Singapore.
- Gaudernack B. (1997): “*Natural gas utilisation without CO_2 emissions*”, Energy Conversion and Management, Vol. **38**, Supplement 1, (1997), pp. 165 - 172.

- Geankoplis, C. J. (2003): “*Transport and separation process principle*”, 4th Edition, Pearson Education, New Jersey.
- Gerner, F., Svensson, B. and Djumena, S. (2004): “*Gas flaring and venting: a regulatory frame work and incentives for gas utilisation*”, Public Policy for the World Bank Group Private Sector, Note Number **279**, (Oct. 2004).
- GGFR (2002): “*Report on consultations with stake-holders*”, World Bank (WB) – GGFR Report 1, Washington, D.C.
- GGFR (2004): “*Flared gas utilisation strategy opportunities for small scale uses of gas*”, Global Gas Flaring Reduction Report No. 4, World Bank Group.
- GGFR (2010): “*Global gas flaring reduction: Improving energy efficiency*”, World Bank Issue Brief.
- Golombok, M. and Teunissen, W. (2003): “*A chemical alternative to natural gas flaring*”, Industrial and Engineering Chemistry Research, Vol. **42** (20), pp. 5003 - 5006.
- Gopalan, S. (2002): “*Using ceramic mixed ionic and electronic conductors for gas separation*”, Journal of the Minerals Metals and Materials Society, Vol. **54**, pp. 26 - 29.
- Gue, T., Nikolaev, P., Thess, A., Colbert, D. T., and Smalley, R. E. (1995): “*Catalytic growth of single-walled nanotubes by laser vaporisation*”, Chemical Physics Letters, Vol. **243**, pp. 49 - 54.

- Halvorson, M. (2008): “*Microsoft Visual Basic 2008 - Step by Step*”, Published by Microsoft Press, a Division of Microsoft Corporation.
- Hickman, D. A. and Schmidt, L. D. (1993): “*Production of syngas by direct catalytic oxidation of methane*”, Science, Vol. **259**, pp. 343 - 346.
- Hoang, D. L. and Chan, S. H. (2006): “*Effect of reactor dimensions on the performance of an O₂ pump integrated partial oxidation reformer-a modelling approach*”, International Journal of Hydrogen Energy, Vol. **31**, pp. 1 – 12.
- Hook, V. (1980): “*Methane steam reforming*”, Catalyst Rev. - Sci. Eng., Vol. **21** (1), pp. 1 - 51.
- Horvay, M. and Leukel, W. (1984): “*LDA- measurements of liquid swirl flow in converging swirl chambers with tangential inlets*”, Proceeding 2nd International Symposium on Application of Laser Anemometry to Fluid Mechanics, Lisbon, Portugal, Paper 14.
- Hou, P. X., Xu, S. T., Ying, Q. H., Liu, C. and Cheng, H. M. (2003): “*Hydrogen adsorption/desorption behaviour of multi-walled carbon nanotubes with different diameters*”, Carbon, Vol. **41** (13), pp. 2471-2476.
- Hughes, R. (1992): “*Processing of natural gas offshore*”, A Paper Presented in a Symposium on Production and Processing of Natural Gas, King Saud University, (29th Feb. to 2nd March, 1992).
- Hughes, R. (1996): In “*Industrial membrane separation technology*”, K. Scott and R. Hughes, Eds. Blackie Academic and Professional, London.

- Hwang, S. (2001): “*Inorganic membrane and membrane reactors*”, Featured Review, Korean J. Chem. Eng., Vol. **181** (5), pp. 775 - 787.
- Ibrahim, A. A. (2006): “*Comprehensive study of internal flow field and linear and nonlinear instability of an annular liquid sheet emanating from an atomiser*”, PhD Thesis, University of Cincinnati, Ohio, USA.
- Ibrahim, A. A. and Jog, M. A. (2006): “*Effect of liquid and air swirl strength and relative rotational direction on the instability of an annular liquid sheet*”, Acta Mechanica, Vol. **186** (1-4), pp. 113 - 133.
- Iijima S. (1991): “*Letters to nature*”, Nature, Vol. **354**, pp. 56 - 57.
- Ikeguchi, M., Mimura, T., Sekine, Y., Kikuchi, E. and Matsukata, M. (2005): “*Reaction and oxygen permeation studies in $Sm_{0.4}Ba_{0.6}Co_{0.2}O_{3-\delta}$ membrane reactor for partial oxidation of methane to syngas*”, Applied Catalysis A- General, Vol. **290**, pp. 212 - 220.
- Indriani, G. (2005): “*Gas flaring reduction in the Indonesian oil and gas sector*”, Technical and Economic Potential of Clean Development Mechanism (CDM) Projects, HWWA Report **253**, Hamburg.
- Iwahara, H. Asakura, Y. Katahira, K. and Tanaka, M. (2004): “*Prospect of hydrogen technology using proton-conducting ceramics*”, Solid State Ionics, Vol. **168** (3-4), pp. 299 - 310.
- Jager, B. and Espinoza, R. (1995): “*Advances in low temperature Fischer-Tropsch synthesis*”, Catalysis Today, Vol. **23** (1), pp. 17 - 28.

- Jimenez, J. A. and Madsen, O. S. (2003): “*A simple formula to estimate settling velocity of natural sediments*”, Journal of waterway, Port, Coastal and Ocean Engineering, Vol. **129** (2), pp. 70 - 78.
- Jin, W., Li, S., Huang, P., Xu, N., Shi, J and Lin, Y. S. (2000a): “*Tubular lanthanum cobaltite perovskite-type membrane reactors for partial oxidation of methane to syngas*”, Journal of Membrane Science, Vol. **166**, pp. 13 - 22.
- Jin, W., Gu, X., Li, S., Huang, P., Xu, N. and Shi, J. (2000b): “*Experimental and simulation study on a catalyst packed tubular dense membrane reactor for partial oxidation of methane to syngas*”, Chemical Engineering Science, Vol. **55**, pp. 2617 - 2625.
- Jorio, A., Saito, R., Hafner, J. H., Lieber, C. M., Hunter, M., McClure, T., Dresselhaus, G. and Dresselhaus, M. S. (2001): “*Structural (n,m) determination of isolated single-walled carbon nanotubes by resonant Raman scattering*”, Physical Review Letters, Vol. **86** (6), pp. 1118 - 1121.
- Julbe, A, Farrusseng, D and Guizard, C. (2001): “*Porous ceramic membranes for catalytic reactors- overview and new ideas*”, Journal of Membrane Science, Vol. **181**(1), pp. 3 - 20.
- Kakac, S. and Liu, H. (2002): “*Heat exchangers: selection, rating and thermal design*”, CRC press, Second Edition.
- Kao, Y. K., Lei, L., and Lin, Y. S. (1997): “*A comparative simulation study on the oxidative coupling of methane in fixed-bed and membrane reactors*”, Industrial and Engineering Chemistry Research, Vol.**36**, (9), pp. 3583 - 3593.

- Keshav, T. R. and Basu, S. (2007): “*Gas-to-Liquid technologies: India’s perspective*”, Fuel Processing Technology, Vol. **88**, (5), pp. 493 - 500.
- Khan, M. I. and Islam, M. R. (2007): “*Petroleum engineering handbook*”, Chapter 8, the Membrane Separation, pp. 300 - 340.
- Kharton, V. V., Viskup, A. P., Marozan, I. P. and Naumovich, E. N. (2003): “*Oxygen permeability of perovskite-type $Sr_{0.7}Ce_{0.3}MnO_{3-\delta}$* ”, Materials Letters, Vol. **57**, pp. 3017- 3021.
- Kharton, V. V., Yaremchenko, A. A. Kovalevsky, A. V., Viskup, A. P., Naumovich, E. N. and Kerko, P. F. (1999): “*Perovskite-type oxide for high-temperature oxygen separation membranes*”, Journal of Membrane Science, Vol. **163**, pp. 307- 317.
- Kharton, V. V., Yaremchenko, A. A., Valente, A. A., Sobyenin, V. A., Belyaev, V. D., Semin, G. L. Veniaminov, S. A., Shaula, A. I., Frade, J. R. and Rocha, J. (2005): “*Methane oxidation over Fe-, Co-, Ni- and V-containing mixed conductors*”, Solid State Ionics, Vol. **176** (7-8), pp 781 – 791.
- Khavkin, Y. (2004): “*The theory and practice of swirl atomisers*”, New York, Taylor and Francis.
- Kodas, T. T. and Hampden-Smith, M. J. (1998): “*Aerosol processing of materials*”, Wiley-VCH, Canada.
- Kostiuk, L. and Johnson, M. (2000): “*Flare research project*”, University of Alberta, Interim Report, November 1996 – June 2000, pp. 149.

- Kumar, S., Kumar, S. and Prajapati, J. K. (2009): “*Hydrogen production by partial oxidation of methane: modelling and simulation*”, International Journal of Hydrogen Energy, Vol. **34**, pp. 6655 - 6668.
- Kung, D., Srinivasan, R. Thorogood, R. M. and Edward, E.P. (1996): “*Integrated high temperature method for oxygen production*”, US Patent, 5.616.359.
- Leake, J. and Flynn, C. (2010): “*An elevator into space has moved a step closer with the discovery of super-strong carbon nanotubes*”, Article in Sunday Times, 26/12/2010.
- Lee, K. S., Woo, S. K., Kim, J. W., Ishihara, T. and Kim, D. K. (2003): “*Oxygen-permeating property of LaSrBFeO_3 ($B=\text{Co, Ga}$) perovskite membrane surface modified by LaSrCoO_3* ”, Solid State Ionic, Vol. **158**, pp. 287 - 296.
- Lefebvre, H. (1989): “*Atomisation and sprays*”, CRC publication.
- Li, K., Tan, X. and Liu, Y. (2006): “*Single-step fabrication of ceramic hollow fibres for oxygen permeation*”, Journal of Membrane Science, Vol. **272**, pp.1 - 5.
- Li, K. (2007): “*Ceramic membranes for separation and reaction*”, John Wiley and Sons, UK.
- Li, S., Jin, W., Huang, P., Xu, N., Shi, J., and Lin, Y. S. (2000): “*Tubular lanthanum cobaltite perovskite type membrane for oxygen permeation*”, Journal of Membrane Science, Vol. **166**, (1), pp. 51- 61.

- Li, S., Qi, H., Xu, N., and Shi, J., (1999): “*Tubular dense perovskite type membranes: preparation, sealing, and oxygen permeation properties*” Industrial and Engineering Chemistry Research, Vol. **38**, pp. 5028 - 5033.
- Lieber, C. M., (2001): “*The incredible shrinking circuit*”, Scientific American, Vol. **285** (3), pp. 58 - 65.
- Liu, H. (2000): “*Science and engineering of droplets: fundamentals and applications*”, William Andrew Publishing.
- Liu, T., Temur, H. and Veser, G. (2009): “*Autothermal reforming of methane in a reverse-flow reactor*”, Chem. Eng. Technol. Vol. **32** (9), pp. 1358 - 1366.
- Lu, Y.P., Dixon, A.G., Moser, W.R., Ma Y. H. and Balachandran, U. (2000): “*Oxygen-permeable dense membrane reactor for the oxidative coupling of methane*”, Journal of Membrane Science, Vol. **170**, pp. 27 – 34.
- Luyten, J., Buekenhoudt, A., Adriansens, W., Cooymans, J. Weyten, H. Servaes, F. and Leysen, R. (2000): “*Preparation of LaSrCoFeO_{3-δ} membranes*”, Solid State Ionics, Vol. **135**, pp. 637 - 645.
- Lyons, W. C. and Plisga, C. J. (2005): “*Standard handbook of petroleum and natural gas engineering*”, 2nd edition, Elsevier Inc., pp. 5- 211 - 5-225.
- Ma, B. and Balachandran, U. (1997): “*Oxygen nonstoichiometry in mixed-conducting SrFeCo_{0.5}O_x*”, Solid State Ionics, Vol. **100**, pp. 53 - 62.
- Marongiu-Porcu, M., Wang, X. and Economides, M. J. (2008): “*The economics of compressed natural gas sea transport*”, Presented at the 2008 SPE Russian Oil

& Gas Technical Conference and Exhibition held in Moscow, Russia, 28 – 30 October, SPE 115310.

Marple, V. A and Olson, B. A. (2009): “*Good laboratory practice in particle measurement calibration: cascade impactor*”, KONA Powder and Particle Journal, Vol. 27, pp. 206 - 216.

Meyyappan, M (2005): “*Carbon nanotubes: science and application*”, CRC press.

Miachon, S., Perez, V., Crehan, G., Torp, E., Raeder, H., Bredesen, R., Dalmon, J. A.: (2003) “*Comparison of a contactor catalytic membrane reactor with a conventional reactor: example of wet air oxidation*”, Catalysis Today, Vol. (82), PP. 75–81.

Michel, M. R. (2010): “*Electronic structure study of copper-containing perovskites*”, PhD Thesis, University College London, UK.

Mohitpour, M., Szabo, J. and Hardeveld, T. V. (2005): “*Pipeline operation and maintenance: a practical approach*”, Book Published in New York, American Society of Mechanical Engineers (ASME).

Mokhatab, S., Poe, W. A. and Speight, J. G. (2006): “*Handbook of natural gas transmission and processing*”, Elsevier Inc.

Moulijn, J., Makkee, M., and Van Diepen, A. (2001): “*Chemical process technology*”, John Wiley & Sons Ltd, England, ISBN-10: 0471630624.

- Musculus, M. and Pickett, L. (2005): “*Diagnostic considerations for optical laser-extinction measurements of soot in high pressure transient combustion environments*”, Combustion and Flame, Vol. **141** (4), pp. 371-391.
- NASA (2008): “*Terminal Velocity*”, Glenn Research Centre, at: <http://www.grc.nasa.gov/WWW/K-12/airplane/termv.html>. [02/02/2008].
- Nasr, G.G., Yule, A. J. and Bendig, L. (2002): “*Industrial sprays and atomisation; design, analysis, and applications*”, 1st Edition, Springer Verlag, London.
- OGP (2000): “*Flaring and venting in the oil and gas exploration and production industry: an overview of purpose, quantities, issues, practices and trends*”, International Association of Oil and Gas Producers, Report No. **2.79/288**.
- Oklany, J. S., Hou, K. and Hughes, R. (1998): “*A simulative comparison of dense and microporous membrane reactors for the steam reforming of methane*”, Appl. Catalyst A: General, Vol. **170**, pp. 13-22.
- Olivieri, A. and Veglio, F. (2008): “*Process simulation of natural gas steam reforming: fuel distribution optimisation in the furnace*”, Fuel Processing Technology, Vol. **89**, pp. 622 – 632.
- Paradise, M. and Goswami, T. (2007): “*Carbon nanotubes - production and industrial applications*”, Materials and Design, Vol. **28** (5), pp.1477-1489.
- Park, S. H. (2003): “*The Kyoto protocol: the ethical and economic issues in emission trading*”, Pittsburgh.

- Pena, M. A. and Fierro, J. L. G. (2001): “*Chemical structures and performance of perovskite oxides*”, Chemical Reviews, Vol. 101 (7), pp. 1981– 2018.
- Poettman, F. H. (1983): “*Improved oil recovery*”, Interstate Oil Compact Commission, Oklahoma City.
- Powell, E.S., Orson, J.H., Miller, P.H., Kudsk, P. and Mathiassen, S. (2002): “*Defining the size of target for air induction nozzles*”, Aspects of Applied Biology, International Advances in Pesticide Application, Vol. 66, pp. 65 – 72.
- Pugh, S. (1991): “*Total design, integrated methods for successful product engineering*”, Wokingham, England, Reading, Mass, Addison-Wesley Pub. Co.
- Ravanchi, M. T., Kaghazchi, T. and Kargari, A. (2009): “*Application of membrane separation processes in petrochemical industry: a review*”, Desalination, Vol. 235, pp. 199 - 244.
- Reich, S. Thomson, C. and Maultzsch, J. (2004): “*Carbon nanotubes, basic concepts and physical properties*”, John Welly and sons, UK.
- Reitz R. D. and Bracco, F. V. (1986): “*Mechanism of atomisation of a liquid jet*”, Physics of Fluids, Vol. 25, pp.1730 – 1742.
- Richardson, R. A., Cotton, J. W. and Ormerod, R. M. (2004): “*Influence of synthesis route on the properties of doped lanthanum cobalt and its performance as an electro-chemical reactor for the partial oxidation of natural gas*”, Dalton Trans, the Royal Society of Chemistry J., Vol. 1 (10), pp. 3110-3115.

- Rizk, N. K. and Lefebvre, A. H. (1984): "*Influence of downstream distance on simplex atomiser spray characteristics*", Presented at 1984 ASME Winter Annual Meeting, New Orleans, USA.
- Rostrup - Nielsen, J. R., Sehested, J. and Norskow, J. K. (2002): "*Hydrogen and synthesis gas by steam and CO₂ reforming*", Advances in catalysis, Vol. 47, pp 64-139.
- Ruiz, J. A., Passos, F. B., Bueno, J. M., Souza-Aguiar, E. F., Mattos, L. V. and Noronha, F. B. (2008): "*Syngas production by autothermal reforming of methane on supported platinum catalysts*", Applied Catalysis A: General, Vol. 334, (1-2), pp. 259-267.
- Salman, A. D., Hounslow, M. J. and Seville, J. P. K. (2007): "*Handbook of powder technology*", Granulation, Elsevier Publishing, Amsterdam
- Samal, S. S. and Bal, S. (2008): "*Carbon nanotube reinforced ceramic matrix composites- a review*", Journal of Minerals and Materials; Characterisation and Engineering, Vol. 7 (4), pp. 355-370.
- Santamaria, J., Menendez, M., Pena, J. A. and Barahona, J. I. (1992): "*Methane oxidative coupling in fixed bed catalytic reactors with a distributed oxygen feed; a simulation study*", Catalysis Today, Vol. 13 (2-3), pp. 353-360.
- Schmidt, V. (2007): "*What is new in production?*", Article in World Oil Magazine, Feb. 2007.

- Shaula, A. L., Kharton, V. V. and Marques, F. M. (2004): “*Phase interaction and oxygen transport in $La_{0.8}Sr_{0.2}Fe_{0.8}Co_{0.2}O_3.(La_{0.9}Sr_{0.1})_{0.98}Ga_{0.8}Mg_{0.2}O_3$ composites*”, Journal of the European Ceramic Society, Vol. **24**, pp. 2631 – 2639.
- Shewchuk, S. (2002): “*Gas flaring: a mounting environmental concern in Western Canada*”, Saskatchewan Business Magazine, (June /July 2002), pp. 21.
- Shore, D. (2006): “*A proposed comprehensive model for elevated flare flames and plumes*”, Presented at: American Institute of Chemical Engineers (AIChE) 40th Flare Gas Corporation, Loss Prevention Symposium.
- Sonibare, J. A. and Akeredolu, F. A. (2006): “*Natural gas domestic market development for total elimination of routine flares in Nigeria’s upstream petroleum operations*”, Energy Policy, Vol. **34**, pp. 743–753.
- Spinicci R., Marini, P. De Rossi, S, Faticanti, M. and Porta, P. (2001): “*Oxidative coupling of methane on $LaAlO_3$ perovskite partially substituted with alkali-earth ions*”, Journal of Molecular Catalysis A: Chemical, Vol. **176**, pp. 253 – 265.
- Swithenbank, J., Beer, J. M., Taylor, D. S., Abbot, D. and McCreath, G. C. (1976): “*A laser diagnostic technique for the measurement of droplet and particle size distribution*”, In Acknowledgments Experimental Diagnostics in Gas Phase Combustion, AIAA, **53**, Progress in Astronautics and Aeronautics, B. T. Zinn, Ed.
- Tablet, C., Grubert, G., Wang, H., Schiestel, T., Schroeder, M., Langanke, B. and Caro, J. (2005): “*Oxygen permeation study of perovskite hollow fibre membranes*”, Catalysis Today, Vol. **104**, pp. 126–130.

- Taheri, Z., Nazari, K., Seyed-Matin, N., Safekordi, A. A., Ghanbari, B., Zarrinpashne, S. and Ahmadi, R. (2010): “*Comparison of oxygen permeation through some perovskite membranes synthesised with EDTNAD*”, Reaction Kinetics, Mechanisms and Catalysis, Vol. **100** (2), pp. 459-469.
- Tai, L.W., Nasrallan, M. M., and Anderson, H. U. (1995): “*Thermochemical stability, electrical conductivity, and seebeck coefficient of Sr-doped $\text{LaCo}_{0.2}\text{Fe}_{0.8}\text{O}_{3-\delta}$* ”, Journal of Solid State Chemistry, Vol. **118**, pp.117- 127.
- Tan X. Y. and Li, K. (2006): “*Oxidative coupling of methane in a perovskite hollow-fibre membrane reactor*”, Industrial and Engineering Chemistry Research, Vol. **45**, pp. 142 – 149.
- Tan, X. and Li, K. (2002): “*Modelling of air separation in a LSCF hollow-fibre membrane module*”, AIChE Journal, Vol. **48** (7), pp. 1469-1477.
- Tan, X., Liu, Y. and Li, K. (2005a): “*Preparation of LSCF ceramic hollow fibre membranes for oxygen production by a phase-inversion/sintering technique*”, Industrial and Engineering Chemistry Research, Vol. **44** (1), pp. 61-66.
- Tan, X., Liu, Y. and Li, K. (2005b): “*Mixed conducting ceramic hollow fibre membranes for air separation*”, AIChem. Journal, Vol. **51** (7), pp. 1991-2000.
- Teraoka, Y., Honbe, Y, Ishii, J. Furukawa, H. and Moriguch, I. (2002): “*Catalytic effects in oxygen permeation through mixed-conductive LSCF perovskite membranes*”, Solid State Ionics, Vol. **152-153**, pp. 681-687.

- Teraoka, Y., Zhang, H. M., Furukawa, S., and Yamazoe, N. (1985): “*Oxygen permeation through perovskite-type oxides*”, Chemistry Letters, Vol. **14** (11), pp. 1743-1746.
- Thess, A., Lee, R., Nikolaev, P., Dai, H. J., Petit, P., Robert, J., Xu, C. H., Lee, Y. H., Kim, S. G. and Rinzler, A. G. (1996): “*Crystalline ropes of metallic carbon nanotubes*”, Science, Vol. **273** (5274), pp. 483–487.
- Thursfield, A. and Metcalfe, I. S. (2006): “*Methane oxidation in a mixed ionic-electronic conducting ceramic hollow fibre reactor module*”, Journal of Solid State Electrochemistry, Vol. **10** (8), pp. 604-616.
- Thursfield, A. and Metcalfe, I. S. (2007): “*Air separation using a catalytically modified mixed conducting ceramic hollow fibre membrane module*”, Journal of Membrane Science, Vol. **288** (1-2), pp. 175–187.
- Thursfield, A. and Metcalfe, I.S. (2004): “*The use of dense mixed ionic and electronic conducting membranes for chemical production*”, Journal of Material Chemistry, Vol. **14**, pp. 2475-2485.
- Tokuoka, N., Yamaguchi, Y., Takada, M. and Zhang, F. (1991): “*The spray structure from swirl atomisers (Part 1: general structure of spray)*”, Proceeding of ICLASS-91, NIST, Gaithersburg, MD, USA, pp. 233-240.
- Tsai, C., Dixon A. G., Moser, W. R. and Ma Y. H. (1997): “*Dense perovskite membrane reactors for partial oxidation of methane to syngas*”, AIChE J., Vol. **43**, pp. 2741-2750.

- Tu, H. Y., Takeda, Y., Imanishi, N. and Yamamoto, O. (1999): "*Ln_{0.4}Sr_{0.6}Co_{0.8}Fe_{0.2}O_{3-δ} (Ln=La, Pr, Nd, Sm, Gd) for the electrode in solid oxide fuel cells*". J. Solid State Ionic, Vol. **117**, pp. 277-281.
- Tunney, J.J., M.L. Post, X. Du and D. Yang (2002): "*Temperature dependence and gas-sensing response of conduction for mixed conducting SrFe_yCo_zO_x thin films*", Journal of the Electrochemical Society, Vol. **149** (6), p.H113-H118.
- Uemiya, S. (2004): "*Brief review of steam reforming using a metal membrane reactor*", Topics in Catalysis, Vol. **29** (1-2), pp. 79 - 84.
- Uhlhorn, R. J. R. and Burggraaf, A. J. (1991): "*Inorganic membranes: synthesis, characteristics and applications*", (Ed R. R. Bhawe), Publishers: Chapman and Hall, New York, Chapter 6.
- Van Beurden, P. J. (2004): "*On the catalytic aspects of steam reforming: a literature survey*", Report No. ECN 1-04-003, Energy Research Centre of the Netherlands (ECN), Petten, Netherlands.
- Van Der Haar, L. M. (2001): "*Mixed-conducting perovskite membranes for oxygen separation - Towards the development of a supported thin-film membrane*", PhD Thesis, University of Twente, Netherlands.
- Wang, H., Cong, Y. and Yang, W. (2002): "*Oxygen permeation study in a tubular Ba_{0.5}Sr_{0.5}Co_{0.8}Fe_{0.2}O_{3-δ} oxygen permeable membrane*", Journal of Membrane Science, Vol. **210** (2), pp. 259 - 271.

- Wang, H., Cong, Y. and Yang, W. (2003): “*Investigation on the partial oxidation of methane to syngas in a tubular $Ba_{0.5}Sr_{0.5}Co_{0.8}Fe_{0.2}O_{3-\delta}$ membrane reactor*” Catalysis Today, Vol. **82**, pp. 157-166.
- Wang, H., Tablet, G., Schiestel, T., Werth, S. and Caro, J. (2006): “*Partial oxidation of methane to syngas in a perovskite hollow-fibre membrane reactor*”, Catalyst Communications, Vol.7, pp. 706 - 712.
- Wang, H.H. Tablet, C. Feldhoff A. and Caro, J. (2005): “*A cobalt-free oxygen-permeable membrane based on the perovskite-type oxide $Ba_{0.5}Sr_{0.5}Zn_{0.2}Fe_{0.8}O_{3-\delta}$* ”, Advanced Materials, Vol. **17**, pp. 1785 -1788.
- Wang, Z., Yang, N., Meng, B. and Tan, X. (2009): “*Preparation and oxygen permeation properties of highly asymmetric $La_{0.6}Sr_{0.4}Co_{0.2}Fe_{0.8}O_{3-\alpha}$ (LSCF) perovskite hollow fibre membranes*”, Industrial and Engineering Chemistry Research, Vol. **48**, pp. 510 - 516.
- Wilhelm, D., Simbeck, D., Karp, A. and Dickenson, R. (2001): “*Syngas production for gas-to-liquids applications: technologies, issues and outlook*”, Fuel Proc. Tech., Vol. **71**, pp. 139 - 148.
- Wu, P. K., Tseng, L. K. and Faeth, G. M. (1992): “*Primary breakup in gas/liquid mixing layers for turbulent liquids*”, Atomisation and Sprays, Vol. **2**, pp. 295 - 317.
- Xu, S., and Thomson, W. J. (1998): “*Stability of $La_{0.6}Sr_{0.4}Co_{0.2}Fe_{0.8}O_{3-\delta}$ perovskite membrane in reducing and nonreducing environments*”, Industrial and Engineering Chemistry Research, Vol. **37**, pp. 1290 - 1299.

- Yang, W. S., Wang, H. H., Zhu, X. F. and Lin, L. W. (2005): “*Development and application of oxygen permeable membrane in selective oxidation of light alkanes*”, Topics in Catalyst, Vol. **35**, pp.155 - 167.
- Yin, X., Hong, L. and Liu, Z. L. (2007): “*Asymmetric tubular oxygen-permeable ceramic membrane reactor for partial oxidation of methane*”, Journal of Physical Chemistry C, Vol. **111**, pp. 9194 – 9202.
- York, A. P., Xiano, T. and Green, M. (2003): “*Brief overview of the partial oxidation of methane to synthesis gas*”, Topics in catalyst, Vol. **22** (3-4), pp. 345 - 358.
- Yuji, Y. Shinji, T. and Keizo, Y. (2005): “*Applicability of the electrical low pressure impactor to size determination of aerosols attached to radon decay products*”, Review of Scientific Instruments, Vol. **76** (6), pp. 065102 - 065105.
- Yule, A. and Vamvakoglou, K. (1999): “*Break-up of a liquid sheet adjacent to a single air stream*”, Proc. ILASS-Europe, 99, ONERA, Toulouse.
- Yule, A. J. And Dunkley, J. J. (1994): “*Atomisation of melts for powder production and spray deposition*“, Clarendon press, Oxford.
- Zaman, J. (1999): “*Oxidative processes in natural gas conversion*”, Fuel Processing Technology, Vol. **58** (2-3), pp 61-81.
- Zeng, Y., Tamhankar, S., Ramprasad, N., Fitch, F., Acharya, D. and Wolf, R. (2003): “*A novel cyclic process for synthesis gas production*”, Chemical Engineering Science, Vol. **58**, pp. 577 – 582.

Zhang, F., Yamagauchi, Y., Takada, M and Tokuoka, N. (1991): “*The spray structure from swirl atomisers (Part 2: Effect of injection pressure and atomiser characteristics on spray structure)*”, Proceeding of ICLASS-91, NIST, Gaithersburg, MD, USA, pp. 241 - 248.

<http://www.duesen-schlick.com> [18/02/2008]

http://www.duesen-schlick.de/pcm4_sid2921_downloads/121-123_Hollow_Cone-Nozzles.pdf [18/02/2008]

http://www.malvern.com/LabEng/products/Mastersizer/ms2000/ms2k_datasheet.htm
[19 /02/2008].